University of Cape Town
Division of Biomedical Engineering
Department of Human Biology

Development and Validation of Experimental Protocol and Guidelines for Non-Invasive Superficial and Deep Muscle Electromyography in the Forearm

---

Submitted to the University of Cape Town
In fulfilment of the requirements for the degree

MSc (Med) in Biomedical Engineering

November 2017

Author:	**Yasheen Brijlal**	BSc (Eng) in Electrical Engineering BRJYAS001
Supervisors:	**Dr Yumna Albertus**	Senior Lecturer Division of Exercise Science and Sports Medicine
	Dr Kylie de Jager	Honorary Research Affiliate Division of Biomedical Engineering
	Prof Thomas Franz	Head of Division Division of Biomedical Engineering

Abstract

The present study investigated a novel non-invasive superficial and deep surface electromyography (sdEMG) technique to detect and isolate extrinsic muscles of the hand with the aim of developing experimental guidelines to aid future studies. The sdEMG technique comprises of two or more surface electrode arrays encircling the limb under investigation set up in a monopolar EMG recording modality and a blind source separation (BSS) algorithm to decompose the recorded mixed monopolar EMG signals into their constituent components, which is proposed to reflect the underlying EMG activity of each muscle. Three experimental parameters linked to the finger movement protocol (MP) were investigated that varied the effects of timing, randomisation and movement anticipation on the ability of the sdEMG technique to detect and isolate the superficial muscles flexor digitorum superficialis (FDS) and extensor digitorum (ED), and the deep muscles extensor indicis (EI), extensor pollicis longus (EPL), flexor digitorum profundus (FDP) and flexor pollicis longus (FPL). FDS and FDP were split into FDS-Index, FDS-Ring, FDP-Index and FDP-Ring bands resulting in a total of eight muscles investigated.

A standard movement protocol consisting of 12 dynamic movements was designed to target the activation of the investigated muscles during each experimental run. The Timing experiments varied the movement window duration to 3, 5 and 7 seconds using the standard MP sequence. The Randomisation experiment consisted of a randomised MP sequence. The Anticipation experiment presented participants with the current, and next movement instruction in the standard MP sequence.

The developed sdEMG system implemented 64 custom-made surface electrodes arranged in three bands positioned around the distal third of the forearm. An *OT Bioelettronica® EMG-USB2* 256-channel biopotential amplifier was used, set up in a referenced monopolar EMG configuration. Contraction detection apparatus was built consisting of finger exoskeletons and flex sensors to record when finger movements occurred. A forearm testing platform was built to secure the participant's forearm during experimental testing and a visual participant instruction system was developed to convey the timed movement instructions.

Five healthy, right-hand dominant male participants (mean ± SD; age: 24 ± 3 years) without any history of neuromuscular diseases or disabilities were recruited for the study. Each participant completed five experimental runs of the five MP variations while the EMG and flex sensor data was recorded. Independent Component Analysis (ICA) was used as the BSS algorithm and the EMG recordings were decomposed into Independent Components (ICs) which were further processed with a windowed 250ms root mean square (RMS) smoothing filter as well as signal normalisation. The flex sensor data was used to generate synchronised literature-informed predicted EMG (pEMG) waveforms, representing the ideal EMG activation signals for each muscle. The muscle-specific pEMG waveforms were also processed with a 250ms RMS filter and signal normalisation before signal comparisons were made using Pearson's correlation against all pICs. In each experimental run, the pIC with the highest calculated Pearson's correlation coefficient (r) value for each pEMG waveform was initially selected as the representative IC (rIC) for that muscle. A rIC selection algorithm was also developed which reassigned pICs that were selected to represent multiple muscles to ensure each muscle was assigned a unique rIC.

A case study was conducted to evaluate the effects of the investigated movement protocol parameters upon which experimental guidelines were formed. Fisher-corrected mean population correlation coefficients (ρ) and 95% confidence intervals were calculated to evaluate the effects of timing, randomisation and anticipation of movements. Using an amalgamated population of all the experiments and experimental runs combined, the eight muscles investigated were isolated with ρ values greater than 0.65 indicating moderate

isolation (defined as $0.60 \leq \rho < 0.80$), with the exception FDS-Index Band which was poorly isolated ($\rho < 0.60$) with a ρ value of 0.59. The data did, however, show high variability in all experiments indicating that the sample population was too small and was possibly influenced by poor performing participants.

The *Timing*, *Randomisation* and *Anticipation* experiments showed no discernible effects across all participants on the ability of the sdEMG technique to detect and isolate the deep and superficial forearm muscles investigated. The Anticipation experiment also showed that participant reaction delays on average increased steadily during each experimental run suggesting the anticipated visual cues were too complex and potentially confused participants.

Concise experimental sdEMG guidelines were developed in which the sdEMG technique was found to be robust to variations of the three movement protocol parameters investigated.

Declaration

I, ***Yasheen Brijlal***, hereby declare that the work on which this dissertation is based is my original work (except where acknowledgements indicate otherwise) and that neither the whole work nor any part of it has been, is being, or is to be submitted for another degree in this or any other university.

I empower the university to reproduce for the purpose of research either the whole or any portion of the contents in any manner whatsoever.

Signature: Signed by candidate

Date: 27 November 2017

Acknowledgements

I would like to thank my parents, Savitha and Bimal Brijlal, and my sister, Larissa Mahadew for their continuous hard-work to provide me with the very best opportunities in life. They have constantly supported my career ambitions and their tireless efforts, unwavering love, encouragement and support have made it possible for me to complete this degree.

I would especially like to thank my supervisors; Dr Kylie de Jager for her absolute compassion, kindness and invaluable assistance as a supervisor and close friend; Dr Yumna Albertus who provided a much-needed clinical perspective on the research and her constant support and encouragement; and Prof Thomas Franz for his understanding and willingness to support this research to completion.

I would also like to thank my academic advisors; Dr Lester John for providing the platform upon which the research was based and for his involvement in the development of the project; Prof Tania Douglas for her kindness and understanding throughout my degree; and Prof Sudesh Sivarasu for his encouragement.

I am truly grateful for the constant support, encouragement and guidance I received from my close friend and colleague, Cara Mills. I would also like to thank my close friends, Chrey Sookha, Giancarlo Beukes, Anastasia Doyle, Jerry Sam, Neha Awasthi and Ameen Bardien who have supported and continuously motivated me throughout this long journey. To all the biomedical engineering students who have passed through the Flow Studies and the Medical Devices Labs, thank you for all the new friendships formed, the many coffee and lunch breaks had, as well as the numerous office debates and conversations enjoyed.

To my psychiatrist Dr Unita Chetty and psychologist Ms Michelle Foulds, I am forever grateful.

I would also like to acknowledge the financial assistance provided by the National Research Foundation of South Africa.

~ Dedicated to Savitha and Bimal Brijlal ~

Table of Contents

List of Abbreviations

α-MN	Alpha-motoneuron
ABS	Acrylonitrile Butadiene Styrene (plastic)
AC	Alternating current
ADC	Analog-to-digital converter
AP	Action potential
APL	Abductor pollicis longus
ATM	Activation timing mask
ATP	Adenosine triphosphate
AUX	Auxiliary (input)
BSS	Blind Source Separation (algorithm)
CH	Channel
CNS	Central nervous system
COR	Centre of rotation
DC	Direct current
DIP	Distal interphalangeal (joint)
DPx	Distal phalanx
DRL	Driven Right-Leg (circuit)
ECG	Electrocardiography
ED	Extensor digitorum
EI	Extensor indicis
EMG	Electromyography
EMI	Electromagnetic interference
EPB	Extensor pollicis brevis
EPL	Extensor pollicis longus
Ex	Extension
FDP	Flexor digitorum profundus
FDS	Flexor digitorum superficialis
FEx	Full extension
FFx	Full flexion
FPL	Flexor pollicis longus
FS	Flex sensor
Fx	Flexion
GRP	Group (2^{nd} to 5^{th} digits)
GUI	Graphical User Interface
HMI	Human-Machine Interface
HPF	High-pass filter
IC	Independent Component
ICA	Independent Component Analysis
IED	Inter-electrode distance
IND	Index (finger)

IP	Interphalangeal (joint)
LPF	Low-pass filter
MCP	Metacarpophalangeal (joint)
MFAP	Muscle fibre action potential
MN	Motoneuron
MP	Movement protocol
MPx	Middle phalanx
MU	Motor unit
MUAP	Motor unit action potential
MVC	Maximum voluntary contraction
PDF	Probability density function
pEMG	Literature-informed, predicted EMG waveforms
PEx	PIP extension
PFx	PIP flexion
pIC	Processed IC
PIP	Proximal interphalangeal (joint)
PPx	Proximal phalanx
rIC	Representative IC
RMS	Root-mean-square (Moving RMS filter)
RNG	Ring Group (2rd to 5^{th} digits)
ROI	Region of interest
sdEMG	Superficial and deep muscle electromyography
sEMG	Surface electromyography
SENIAM	Surface ElectroMyoGraphy for the Non-Invasive Assessment of Muscles
THB	Thumb
TP	Tibialis posterior

List of Variables

CI	Confidence interval
fa	Full activation
IQR	Interquartile range
N	Sample size
pa	Partial activation
r	Pearson's correlation coefficient
SD	Standard deviation
SE	Standard error
z	Fisher-corrected *r* value
ρ	Mean population correlation coefficient
σ	Standard deviation

List of Figures

List of Tables

Part A – Overview

Part A provides an overview of the contents of the present study and contextualises the concepts of the sdEMG technique. The theoretical framework for the sdEMG technique as well as a review of previous works and the study outline is presented in Chapter 1. The fundamental principles and recording techniques of electromyography are then outlined in Chapter 2.

Chapter 1 - Introduction

Electromyography (EMG) is a well-established technique that is able to provide insight into the neuromuscular functionality of skeletal muscles by measuring the myoelectric signals emanating from muscle fibres. In particular, surface electromyography (sEMG) is able to detect and evaluate muscle functionality *non-invasively* at the skin surface making it popular in both research and clinical fields. The biggest drawback of surface EMG is that *only superficial muscle* (muscles directly below the skin) activity can be detected, while the only clinically accepted technique for measuring *deep muscle* (muscles lying below superficial muscles) activity is *invasive intramuscular EMG* using needle or fine-wire electrodes. A large portion of all skeletal muscles lie in the deep muscle layers and thus are often neglected in EMG research due to the risks involved with intramuscular EMG as well as the need for a trained clinician to safely, and accurately insert the electrodes into the deep muscles.

A method to measure deep muscle EMG activity using surface electrodes is a highly sought after technology for research and rehabilitation purposes. Several techniques have been tested however currently no definitive method has been developed that can accurately measure deep muscle activity from the skin surface. A novel method to *non-invasively* detect and isolate superficial *and* deep muscle activity using surface electrodes and a statistical signal separation algorithm was developed by Dr Lester John (2010)[1] in the Division of Biomedical Engineering at the University of Cape Town, known as the *sdEMG technique*. The present study sought to expand upon the sdEMG technique by addressing experimental parameters and procedures that have been assumed or overlooked in previous studies with the intention of developing experimental guidelines for future sdEMG research. The sdEMG technique attempts to separate deep and superficial EMG however without concurrent invasive recording it is difficult to validate and verify the results.

A pilot study investigating the extrinsic muscles of the hand was conducted on five healthy male participants to determine the feasibility of detecting deep and superficial muscles activity in the forearm. Additionally, the effects of *timing*, *randomisation* and *anticipation of movements* in the developed movement protocol were investigated. The ability to detect deep and superficial muscle activity has numerous research and clinical applications and the present study aspires to provide insight into the underlying factors influencing the performance of the current implementation of the sdEMG technique.

This chapter presents an overview of the sdEMG technique in Section 1.1, followed by a detailed review of previous works in Section 1.2 and concludes with the present study overview in Section 1.3.

1.1 Non-Invasive Superficial and Deep Muscle Electromyography

Through timed targeted muscle contractions, the non-invasive superficial and deep muscle electromyography (sdEMG) technique proposes that with an appropriate *monopolar*[2] *EMG* recording configuration, and a suitable statistical signal separation algorithm, superficial and deep muscle activity can be detected and isolated. The current implementation of the sdEMG technique has been successfully applied to the upper arm, forearm and lower leg. The sdEMG methodology is described pictorially in Figure 1.1 where *Independent Component Analysis (ICA)* was used as the statistical signal separation algorithm.

[1] The sdEMG technique is patented, priority date: July 2009. Patents: WIPO South Africa (ZA201109253 B); USA (US 20120184838 A1); Europe (EP 2459062 A1); China (CN 102573620 A/B); Japan (JP2013500108 A, JP5662443 B2).

[2] Monopolar surface EMG refers to an EMG recording configuration where the measured skin voltages at each electrode are referenced to a single resting skin potential. EMG recording modalities will be discussed in Section 2.1.4.

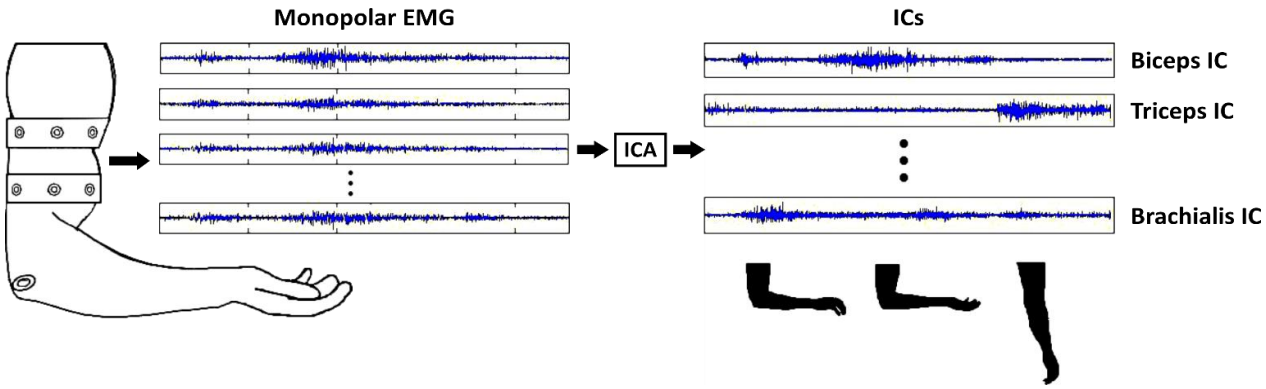

Figure 1.1 – Illustration of the sdEMG technique methodology using monopolar EMG and Independent Component Analysis (ICA).

ICA – Independent Component Analysis, IC – Independent Component. Two electrode arrays are placed around the upper arm as well as a reference electrode on the olecranon (bony protrusion at the elbow) indicating the monopolar surface EMG electrode configuration used.

Image reproduced and adapted from Moroaswi & John (2010).

The *Independent Components (ICs)* shown reflect the *compound EMG* source signals that were best-selected to approximate the underlying muscle sources. *Compound EMG* refers to the spatio-temporal summation of all motor unit action potential (MUAPs[3]) detected within the recording electrode pick-up area originating from a *single muscle.* For the purposes of the present study, compound EMG is considered to represent the EMG activity from a *single muscle source*. These concepts will be discussed further in the Previous Works (Section 1.2) and the theoretical basis for the sdEMG technique is presented first.

1.1.1 sdEMG Theory

The technique comprises of the application of surface electrodes arranged in one or more arrays that encircle the limb under investigation, set up in a monopolar EMG recording configuration. In this configuration, the measured EMG signals at each electrode constitute a mix of the compound EMG activity from *all muscles* within the vicinity of the electrode pick-up area. The sdEMG technique rests on the assumption that the measured surface EMG signals reflect a *linear mix of compound EMG signals* from both the superficial and deep muscles. This assumption is supported by the spatial summation effect of volume conduction on MUAPs from deep and superficial motor units propagating towards the skin surface which is described in Section 2.1.5. It is also assumed using a large[4] quantity of electrodes allows for sufficient EMG activity to be measured from all the activated muscles.

The sdEMG technique further proposes that the linearly mixed EMG signals can be decomposed into their constituent sources using a suitable un-mixing technique such as, but not limited to, Independent Component Analysis. The constituent sources reflecting compound EMG signals are assumed to be *statistically independent or unrelated from each other* due to the unique muscle activation characteristics during targeted contractions, unique innervation characteristics as well as anatomical variation. ICA is implemented as the un-mixing technique in the present study and the following will be a discussion on the assumptions, requirements and limitations of ICA when applied to EMG signals.

[3] A MUAP is a bioelectrical signal produced by a single motor unit which is discussed further in Section 2.1.2.

[4] Previous studies have implemented at least double the number of electrodes as there are muscles in the limb under investigation. The rationale for this minimum quantity will be discussed in Section 1.2.

1.1.2 Application of Independent Component Analysis to EMG Signals

Independent Component Analysis (ICA) is a statistical signal separation algorithm which attempts to decompose a set of linearly mixed signals into their *statistically independent* source components. ICA is a blind source separation (BSS) algorithm that requires no prior information regarding the spatial locations of sensors, signal characteristics, or the processes generating the observed signals making it a suitable un-mixing algorithm for the sdEMG technique.

Assuming a linear mixing process, the ICA mathematical model can be represented in matrix notation as:

$$\boldsymbol{x} = \boldsymbol{A}\boldsymbol{s} \qquad \textbf{Equation 1-1}$$

Where, $\boldsymbol{x} = [x_1(t), \dots, x_n(t)]$ denotes the observed mixtures, $\boldsymbol{s} = [s_1(t), \dots, s_n(t)]$ represents the latent statistical independent source signals and $\boldsymbol{A}$ is the unknown $[n \times n]$ linear mixing matrix. The aim of ICA is to determine an inverse de-mixing matrix, $\boldsymbol{W} = \boldsymbol{A}^{-1}$, which maximises the statistical independence between the estimated sources $\hat{\boldsymbol{s}}$, which can be determined from the observed mixture $\boldsymbol{x}$, using Equation 1-2.

$$\hat{\boldsymbol{s}} = \boldsymbol{W}\boldsymbol{x} \qquad \textbf{Equation 1-2}$$

When applied to electromyography, the ICA mathematical model denoted by Equation 1-1 can be described pictorially as shown in Figure 1.2, where $\boldsymbol{x}$ denotes the measured EMG signals, $\boldsymbol{A}$ represents the underlying myoelectric signal generation model, $\boldsymbol{s}$ denotes the independent muscle sources, and $\hat{\boldsymbol{s}}$ denotes the estimated EMG source components.

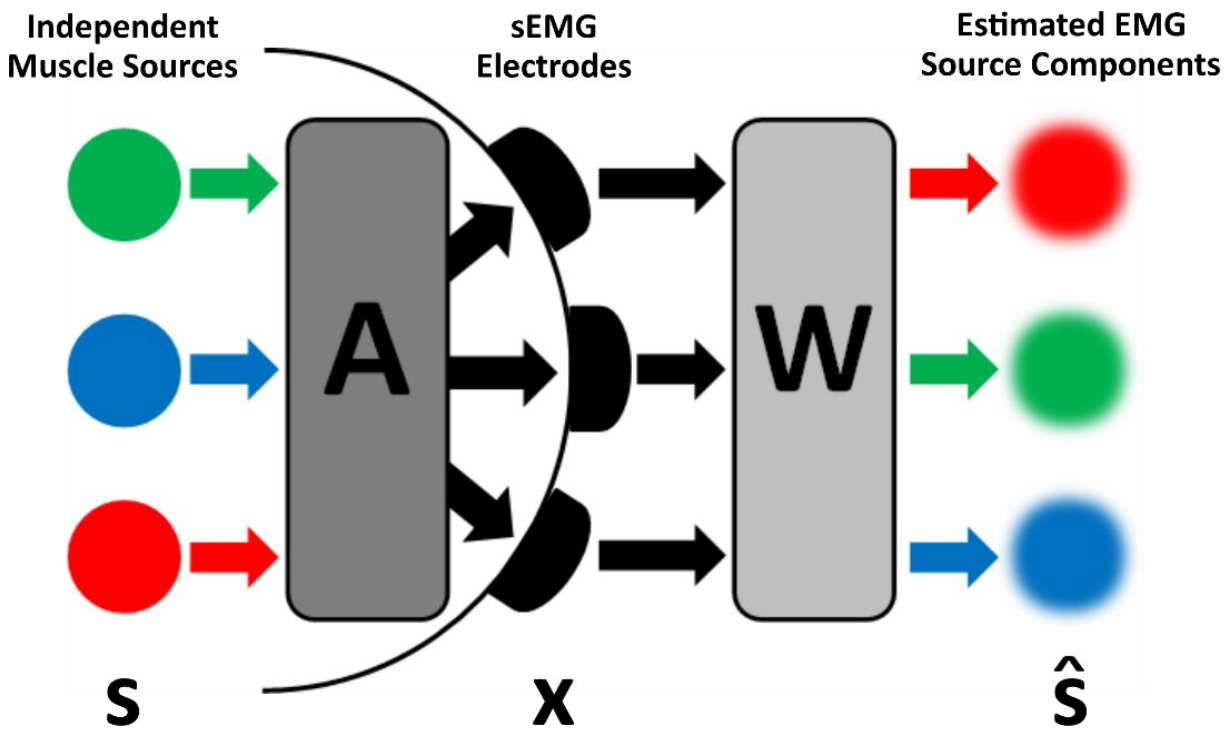

Figure 1.2 – Illustration of the Independent Component Analysis model applied to EMG.

$\boldsymbol{s}$ – Independent muscle sources (solid coloured circles), $\boldsymbol{A}$ – Linear mixing matrix, $\boldsymbol{x}$ – Measured EMG signals, $\boldsymbol{W}$ – De-mixing matrix, $\hat{\boldsymbol{s}}$ – Unordered estimated EMG source components (blurred coloured circles). Image reproduced and adapted from Swanepoel (2017).

An extensive review of ICA literature[5] was conducted by Swanepoel (2017) and a summarised list of the ICA assumptions and requirements found included:

I. **Statistically independent sources**

The source signals are mutually independent and generated by random processes.

II. **Independent components have non-Gaussian distributions**

ICA separates sources based on their non-Gaussianity, that being how dissimilar the probability density function (PDF) of each component is from a Gaussian (Normal) distribution. The Central Limit Theorem establishes that the sum of two independent random variables has a distribution closer to a Gaussian distribution than either of the original variables (Makino, 2003). The same is true for variables with non-Gaussian distributions, thus ICA attempts to estimate the independent components by searching for non-Gaussian sources.

III. **Linearly mixed sources**

The measured signals are assumed to be linear summations of the source components as described by the linear mixing matrix $\boldsymbol{A}$ in Equation 1-1.

IV. **Square mixing matrix**

ICA requires there to be at least an equal number of recording sensors as there are independent sources, therefore, the linear mixing matrix $\boldsymbol{A}$ is assumed to be square, i.e. $[n \times n]$. Square inverse matrices are more computationally efficient thus ICA algorithms assume the number of input signals is equal to the number of independent source signals present.

V. **Spatially stationary sources**

The sources are assumed to remain spatially stationary with time relative to the recording sensors, thus maintaining the fixed linear mixing matrix model $\boldsymbol{A}$.

VI. **Noiseless mixing**

The signals are assumed to be free from external noise.

VII. **Negligible transmission delays**

It is assumed there are no signal transmission delays from the sources to the recording sensors and that all signals arrive at the recording sensors simultaneously.

The assumptions and requirements of ICA are satisfied in the sdEMG technique according to the following adapted arguments put forward by Swanepoel (2017):

I. **Statistically independent sources**

Delorme, Sejnowski, & Makeig (2007); James & Hesse (2005); Jung et al. (2001); Naik & Kumar (2011).

The statistical independence of MUAPs along with the unique muscle activation characteristics during specific contractions, unique innervation characteristics as well as the anatomical variations support the assumption that muscles can be considered statistically independent sources.

[5] The reviewed literature consisted of works by: Delorme (2002); Delorme et al. (2007); Djuwari et al. (2005); Hyvärinen & Oja (2000); James & Hesse (2005); Jung et al. (2001); Naik & Kumar (2011); Naik, Yina Guo, & Hung Nguyen (2013).

II. Independent components have non-Gaussian distributions

Delorme et al. (2007); Djuwari, Kumar, & Palaniswami (2005); Hyvärinen & Oja (2000); James & Hesse (2005); Jung et al. (2001); Naik & Kumar (2011); Nazarpour, Al-Timemy, Bugmann, & Jackson (2013).

A study conducted by Nazarpour et al. (2013) investigated the PDFs from EMG signals at various MVC levels. Their findings showed that at low MVC values the monopolar EMG signal distributions were super-Gaussian and that the peakedness (kurtosis) of the PDF increased as the MVC level decreased. See Appendix A (Figure A-1) for the resultant PDFs plots at various levels of contraction for abductor pollicis brevis.

The present study investigates dynamic finger movements in which the contraction forces are near the minimum[6] required to produce finger movement, effectively *'no-load'* conditions. These conditions would correspond to very low MVC values and it is assumed the super-Gaussian distribution of the monopolar EMG signals, as well as the peakedness observed at low MVC levels, would sufficiently satisfy the non-Gaussian requirement.

III. Linearly mixed sources

Delorme et al. (2007); Djuwari et al. (2005); James & Hesse (2005); Jung et al. (2001); Naik & Kumar (2011); Roeleveld, Stegeman, Vingerhoets, & Oosterom (1997).

The assumption that the recorded monopolar EMG signals are a linear summation of the muscle source signals is reasonable since it is well-established that surface EMG signals are the spatio-temporal summation of all the MUAPs detected within the electrode pick-up area.

IV. Square mixing matrix

Djuwari et al. (2005); James & Hesse (2005); Naik & Kumar (2011).

This assumption is fulfilled by ensuring there is at least the same number of recording sensors (electrodes) as there are independent sources (muscles) within the investigated limb. All sdEMG studies oversubscribe the required number of recording sensors by at least a factor of two, therefore ICA will compute a square matrix in which the estimated source components will exceed the number of muscle sources. It is expected that the excess independent components will reflect noise and artefact signals that are embedded in the observed mixtures, which can be discarded prior to further analysis.

V. Spatially stationary sources

Since the electrodes are placed around the distal half of the forearm and low resistance dynamic movements are tested in the present study, very little electrode movement is expected. Furthermore, the muscles in the forearm are elongated and low force contractions do not cause the underlying muscles to bulge as much as larger muscles like biceps brachii do. Biceps brachii was included in the initial dynamic sdEMG Brachialis study (Moroaswi & John, 2010) with promising results, therefore it is expected the electrodes in the present study can be considered spatially stationary.

[6] Without MVC level testing the percentage could not be determined in the present study however previous sdEMG studies implementing static movements used 30-40% MVC levels which showed sufficiently peaked PDFs. See Appendix A (Figure A-2) for a typical PDF found for a raw monopolar EMG signal at ~40% MVC in the study by Swanepoel (2017).

VI. **Noiseless mixing**

Completely noiseless surface EMG signals are unlikely due to general electrical noise present in the testing environment as well as electromagnetic interference from the recording equipment. The effects of environmental noise can be reduced with good skin preparation, shortened electrode cabling, removal of external noise sources as well as an efficient equipment setup.

VII. **Negligible transmission delays**

Through volume conduction, the induced electric currents from MUAPs spread almost instantaneously to the recording electrodes, therefore no significant time delays are experienced.

The present study implements the MATLAB® *fastICA* package (Gävert, Hurri, Särelä, & Hyvärinen, 2005) which includes pre-processing steps that simplify the ICA decomposition process. The pre-processing steps are *signal centring* which subtracts the mean resulting in zero-mean signals, and *signal whitening* which transforms the signals to be uncorrelated having unit variance through the application of Principal Component Analysis.

There are two main limitations associated with ICA:

I. The amplitude of the ICs cannot be determined.
II. The output order of the ICs is arbitrary.

These limitations are mainly due to signal whitening which removes the link between sensor location and the estimated source components. The process also removes amplitude scaling, however, the *fastICA* algorithm does maintain the *relative amplitudes* between the *dimensionless ICs*.

It should be noted that these limitations do not negatively impact the sdEMG technique as the ICs are normalised to allow for comparison across multiple experimental runs (shortened to *runs*). The technique also includes an IC selection algorithm to attribute ICs to specific muscles, therefore the output order of the ICs is irrelevant.

1.2 Previous Works

The non-invasive sdEMG technique has been applied to the upper and lower limbs with promising results which have strengthened the applicability in the field of deep muscle electromyography. A review of previous sdEMG works was conducted to identify commonalities, improvements, limitations and aspects of the experimental procedures that have been assumed or overlooked. A brief summary of the successive development of the technique is presented in Table 1-1 highlighting the deep muscles investigated in each study. Each study is outlined and a deeper assessment of the forearm study by Pitman (2015) was conducted as it is most applicable to the present forearm study.

Table 1-1: Summary of the previous non-invasive superficial and deep muscle electromyography studies indicating the deep muscles investigated.

Authors	Body region	Deep muscles
Moroaswi & John (2010)	Upper arm	Brachialis
Sayed, Albertus-Kajee, Schwellnus, & John (2012)	Lower leg	Tibialis posterior
Mulligan (2014)	Upper arm	Brachialis
Pitman (2015)	Forearm	Flexor pollicis longus, Extensor pollicis longus, Extensor pollicis brevis, Abductor pollicis longus
Swanepoel (2017)	Lower leg	Flexor digitorum longus, Flexor hallucis longus, Extensor hallucis longus, Tibialis posterior

Several conventions have been maintained in previous sdEMG studies with favourable results and were therefore also maintained in the present study as summarised below.

- Independent Component Analysis was used as the statistical signal separation algorithm. The MATLAB® *fastICA* package has been implemented producing favourable results to decompose the monopolar EMG signals to into statistically independent components representing compound EMG source signals.
- The number of monopolar surface electrodes used was at least double the number of muscles in the region investigated which was needed to ensure that ICA assumption (IV) in Section 1.1.2 was met. This has led to a successive increase in electrodes (12, 20, 30, 40) implemented.
- Electrodes were arranged in arrays and strategically placed to detect MUAPs on both sides of muscle innervation zones as they propagate towards the tendons – described further in Section 2.1.1. Since the sdEMG technique aims to isolate EMG activity from multiple superficial and deep muscles, the electrode band placement locations were estimated using literature to best suit the underlying anatomy. Literature considered included kinesiological EMG works, SENIAM[7] recommendations for the superficial muscles as well as intramuscular EMG studies identifying deep muscle innervation zones.

While these reflect the fundamental commonalities between previous sdEMG studies, there have been successive improvements to the sdEMG technique that are discussed next in the review of each study.

1.2.1 Deep Brachialis Studies

The initial proof of concept sdEMG study was conducted by Moroaswi & John (2010) to identify deep muscle activity from the brachialis muscle in the upper arm. The study implemented two bands of six electrodes each positioned around the upper arm and a reference electrode placed on the olecranon as illustrated in Figure 1.3 (a). The electrodes were evenly spaced around the upper arm and the bands were aligned to match the SENIAM recommended electrode positions for biceps [brachii]. This was considered a suitable arrangement to also detect muscle activity from the deep brachialis muscle which lies below biceps, as well as triceps [brachii] on the posterior side of the upper arm.

[7] The SENIAM project (Surface Electromyography for the Non-Invasive Assessment of Muscles) defines a standard set of European recommendations for sEMG experimental protocols and data reporting (Hermens et al., 1999). Details available at http://www.seniam.org/.

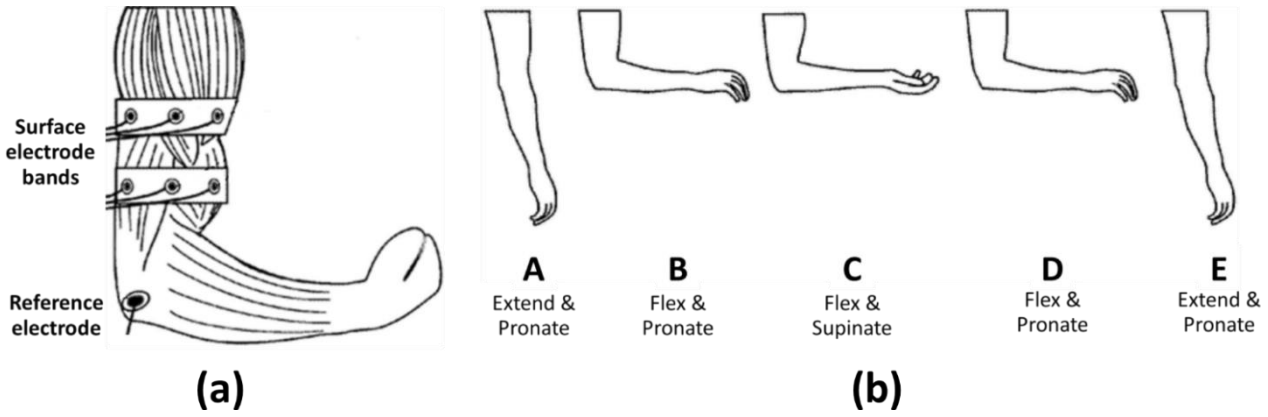

Figure 1.3 – Surface electrode placements on the upper arm (a) and the dynamic movement protocol (b) used in the initial brachialis sdEMG study (Moroaswi & John, 2010).

Images reproduced and adapted from Moroaswi & John (2010).

Anatomically it is not possible to target brachialis independently from the actions of biceps, therefore the initial challenge for the researchers was to devise a *dynamic movement protocol (MP)*[8] that would allow for both muscles to be isolated individually. After studying the functional anatomy and biomechanics of the upper arm, a movement protocol consisting of five movements was developed as illustrated in Figure 1.3 (b).

The MP aimed to isolate the actions of brachialis from biceps by comparing the muscle activations during pronation and supination while in the flexed position as indicated in Figure 1.3 (b)(B, C, D). Additionally, triceps was isolated during arm extension from the pronated position shown in Figure 1.3 (b)(A, E).

Table 1-2 shows the corresponding muscle-movement mappings which indicate the *relative muscle activation contributions* during the arm movements implemented in the developed movement protocol. The concept of relative muscle activation contributions as well as the definitions of *full activation* and *partial activation* will be discussed in Section 3.1. At this stage, the relative muscle activation contributions provide a means to differentiate biceps muscle activity from brachialis.

Table 1-2: Anticipated muscle activation contributions from each muscle in the developed movement protocol implemented in the Brachialis study.

Muscle	Arm movement				
	Extend & Pronate	Flex & Pronate	Flex & Supinate	Flex & Pronate	Extend & Pronate
Biceps		+	++	+	
Brachialis		++	+	++	
Triceps	++				++

'++' indicates full muscle activation and '+' indicates partial muscle activation.

The ability to isolate a muscle using the sdEMG technique centres on having known muscle-movement mappings which are needed to attribute an IC to a muscle that best aligns with the anticipated muscle

[8] A movement protocol is defined as a timed sequence of unique static or dynamic movements interleaved with rest periods to be performed by the participant during testing. The brachialis studies did not include rest periods however it has become standard practice in all subsequent sdEMG studies. Further information is presented in Section 3.2.

activations. In this study, brachialis was expected to be *fully active* during arm pronation Figure 1.3 (b)(B, D) while *partially active* during arm supination Figure 1.3 (b)(C) in which biceps was expected to be *fully active*.

A sample set of results from the initial Brachialis study is presented in Figure 1.4 showing six ICs and the muscles assigned to them. From the ICs presented, IC 5 was selected to best represent brachialis in which full muscle activation was observed during pronation (highlighted in green rectangles), and partial muscle activation was observed during supination (highlighted in the red rectangle).

The preliminary unpublished results provided sufficient evidence to investigate the sdEMG technique further. Mulligan (2014) conducted a follow-up sdEMG study investigating brachialis on 20 healthy participants using the same MP and experimental protocol with an increased electrode count of 30. The study also aimed to develop a genetic algorithm to be implemented on top of the ICA algorithm to determine the minimum number of electrodes required to isolate brachialis as well as the optimal electrode placements. While the results presented focused on the genetic algorithm, the study did indicate that activity from the deep brachialis muscle was successfully detected and isolated using the sdEMG technique. This provided the foundation for future studies to investigate other deep muscles in the lower leg and forearm.

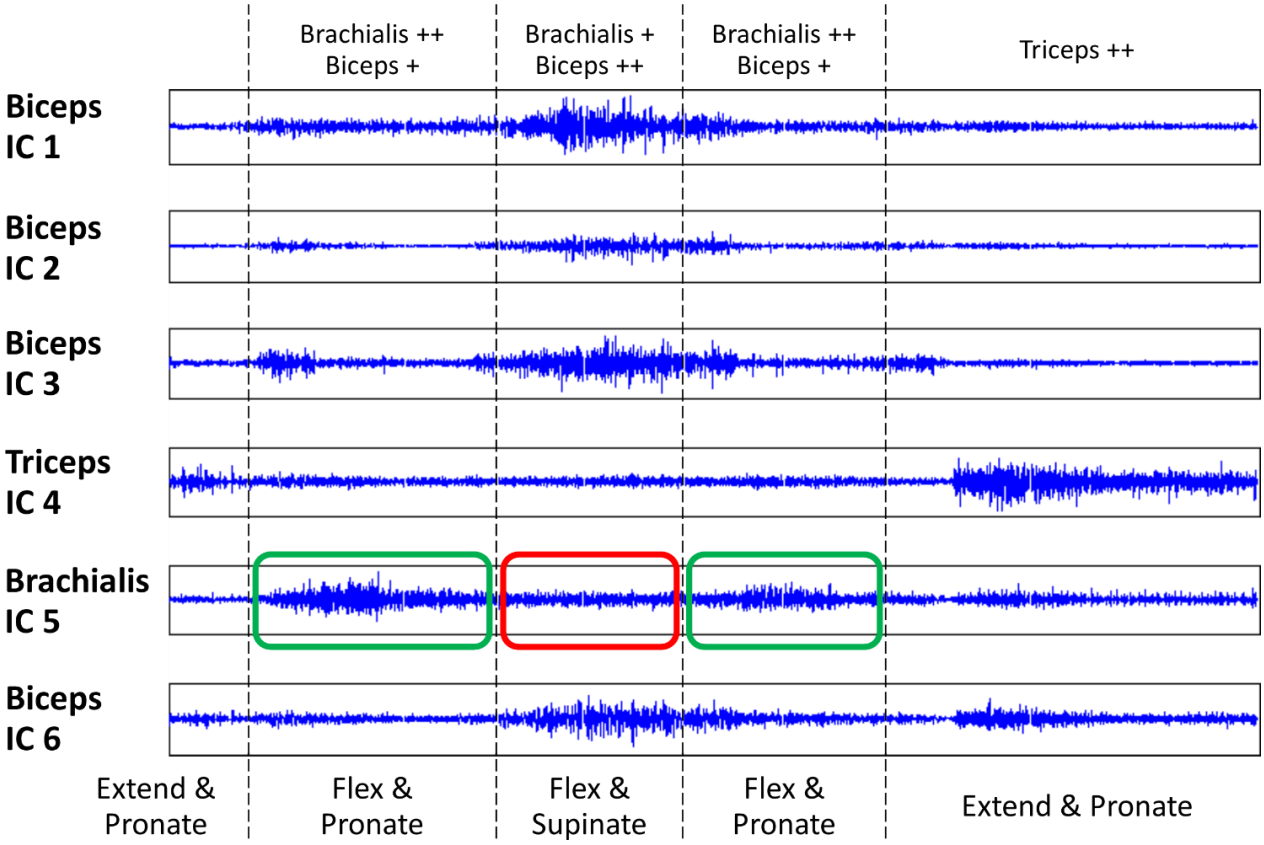

Figure 1.4 – Preliminary results from the initial Brachialis study Moroaswi & John (2010).

For each movement window, the relative muscle activation contributions are listed at the top, where '++' indicates full muscle activation and '+' indicates partial muscle activation.

IC 5 was selected to best represent brachialis where the green rectangles indicate full muscle activation during pronation and red rectangles indicate partial activation during supination.

Note the IC numbering is arbitrary and does not reflect muscle isolation performances.

Image redrawn and adapted from Moroaswi & John (2010).

1.2.2 Deep Tibialis Posterior Study

The preliminary lower leg sdEMG study was investigated by Sayed et al. (2012) to detect and isolate the deep tibialis posterior (TP) muscle in the calf region of the lower leg. One of the key research questions was whether the sdEMG technique was transferable from the upper arm consisting of a few large muscles, to the densely populated lower leg consisting of many smaller muscles. The study implemented a modified experimental methodology from the previous brachialis studies in order to account for the unique underlying anatomy and the biomechanics of the foot.

Tibialis posterior is a deep muscle in the posterior region of the calf which is active during *plantar flexion* (extension of the foot about the ankle joint) of the subtalar joint as well as *foot inversion* (tilting of the foot inwards towards the midline of the body) about the ankle joint. In addition to the two movements associated with TP, many other muscles[9] are activated during plantar flexion and foot inversion, increasing the complexity of the movement protocol required to isolate TP. The study implemented a *static movement protocol* consisting of six[10] isometric contractions interleaved with rest periods which proved to be more repeatable between experimental runs compared to the dynamic brachialis movement protocol. The movement protocol used 5 second contraction and rest windows which was *assumed* to be a sufficient duration to activate the muscles.

The experimental setup implemented two arrays of 10 electrodes each positioned around the lower leg spaced 20mm apart halfway between the tibial tuberosity and the medial malleolus. The electrode placement was deemed acceptable to detect sufficient monopolar EMG measurements from all the underlying deep and superficial muscles investigated. The study introduced an adjustable three degree of freedom foot apparatus to confine the foot and measure the various applied forces during the six static foot movements. The developed foot apparatus shown in Figure 1.5 enabled researchers to measure the applied forces during isometric contractions as well as provide a means to determine the exact onset and offset times of each contraction.

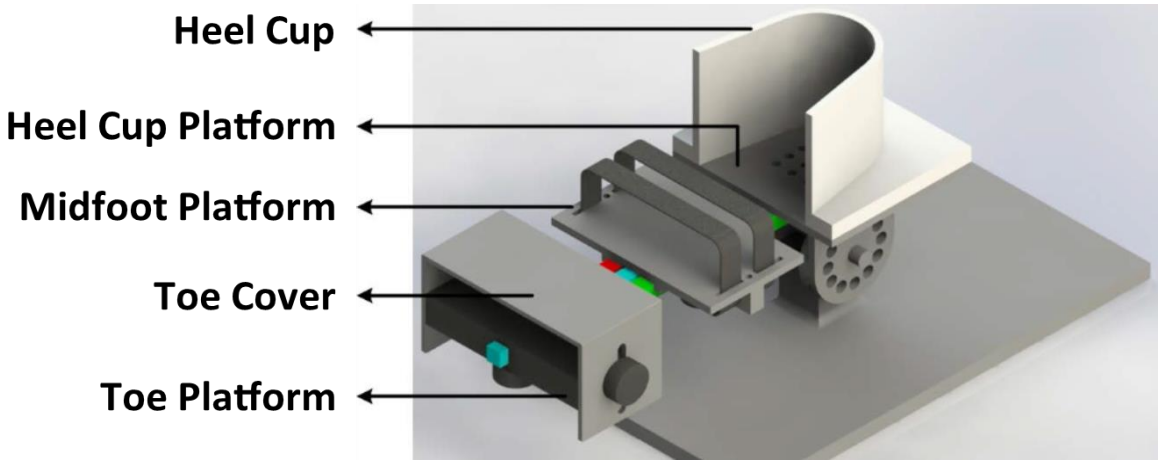

Figure 1.5 – Foot apparatus developed to measure the various isometric contraction forces during testing (rendered in Solidworks® 2014).

The original foot apparatus was developed by Sayed et al. (2012) and manufactured by Mr C Harris (UCT). The modified foot apparatus is shown from the expansion study by Swanepoel (2017).

[9] Plantar flexion activates tibialis posterior, flexor digitorum longus, flexor hallucis longus, triceps surae and peroneus longus. Foot inversion activates tibialis posterior, flexor digitorum longus, flexor hallucis longus and tibialis anterior.

[10] The six static movements were plantar flexion, dorsiflexion, inversion, eversion, toe flexion and extension.

Preliminary unpublished results from the tibialis posterior study are presented in Figure 1.6 showing good conformity between the *processed IC* (red line) and the *predicted EMG waveform* (blue line). A *processed IC* is defined as a normalised IC (output of the *fastICA* algorithm) that has been filtered using a 250ms moving window root-mean-square (RMS) filter. A *predicted EMG waveform* is a reference signal reflecting the idealised anticipated EMG for a specific muscle during the MP. These concepts are described further in Chapter 6. The preliminary results suggested that the sdEMG technique was transferrable to the lower leg and that deep muscle activity from TP was detected and isolated, paving the way for further development of the technique.

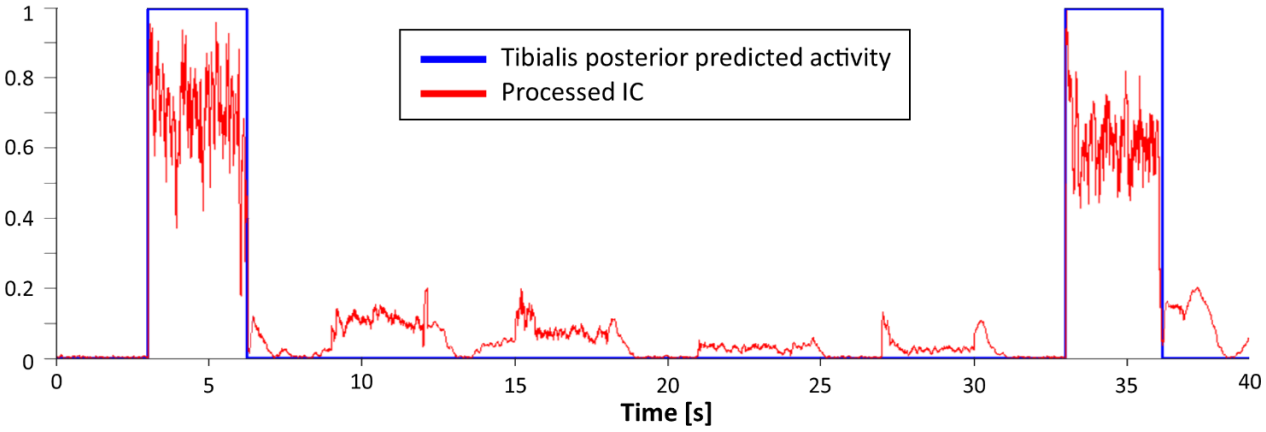

Figure 1.6 – Preliminary unpublished results from the Tibialis Posterior study by Sayed et al. (2012).

Increased EMG activity is present during plantar flexion at 5s and foot inversion at 35s which corresponds to the anticipated EMG activity for tibialis posterior in the implemented movement protocol.

Image redrawn from Sayed et al. (2012).

1.2.3 Extrinsic Thumb Muscles Study

The sdEMG technique was further developed by Pitman (2015) who investigated the extrinsic muscles of the thumb which are located in the forearm. From the previous upper arm and lower leg preliminary results it was hypothesised that the technique would also be transferable to the forearm. The study was conducted on 15 healthy male participants with 10 experimental runs each. The deep muscles investigated were flexor pollicis longus (FPL), extensor pollicis longus (EPL), extensor pollicis brevis (EPB) and abductor pollicis longus (APL), as well as the superficial muscles flexor digitorum[11] (FD) and extensor digitorum (ED). A static movement protocol consisting of six isometric contractions interleaved with rest periods and a 5 second movement window duration was implemented as illustrated in Table 1-3.

[11] Flexor digitorum superficialis (superficial) and flexor digitorum profundus (deep) were grouped together as "flexor digitorum".

Table 1-3: Movement protocol developed for the Extrinsic Thumb Muscles study (Pitman, 2015).

Time [s]		0	5	10	15	20	25	30	35	40	45	50	55	60
Isometric Contraction	Rest													
	Thumb flexion (TFl)													
	Thumb extension (TEx)													
	Thumb abduction (TAb)													
	Thumb adduction (TAd)													
	Index finger flexion (IFFl)													
	Index finger extension (IFEx)													

The study used 40 custom-made surface electrodes arranged in two elasticised bands as well as a reference electrode placed on the olecranon. The increased electrode count was needed to satisfy the convention of using at least double the number of electrodes as there are muscles in the region being investigated. The study indicated a two electrode array layout however in line with previous sdEMG conventions it is considered a four electrode array layout since there is a large 20mm spacing between the rows as shown in Figure 1.7 (a).

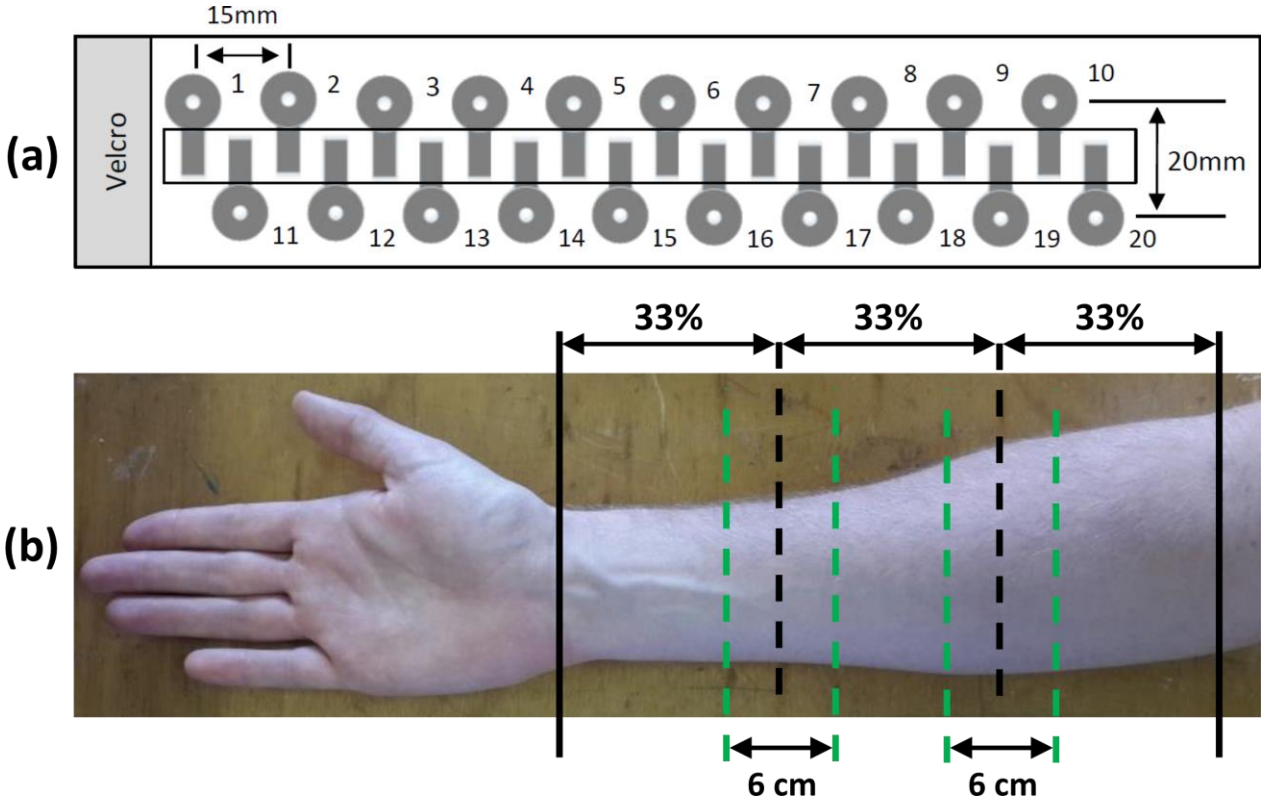

Figure 1.7 – Schematic of the designed electrode bands (a) and forearm band placements (b) implemented by Pitman (2015).

The green dashed lines indicate the placement of the elasticised electrode bands which were approximately 6 cm wide.

Image reproduced and adapted from Pitman (2015).

The purpose of the spacing was to allow for equivalent bipolar calculations[12] to be done on the monopolar EMG recordings to compare the processed superficial ICs for FD and ED to their bipolar equivalent waveforms. This arrangement also provided a larger EMG detection area and therefore it was assumed this would not negatively impact the outcomes of the study. The electrode bands were placed around the distal and proximal thirds of the forearm as measured from the olecranon to the styloid process on the ulna as shown in Figure 1.7 (b).

Similar to the Tibialis Posterior study, a testing rig consisting of an adjustable two degree of freedom thumb dynamometer (axial force measurement device) and a moulded forearm splint was developed as shown in Figure 1.8 (a, b, c). The forearm splint in conjunction with adjustable hand and wrist supports served to prevent unwanted finger, hand and wrist movements during testing. A finger load cell was also developed to measure index finger flexion and extension forces during testing as shown in Figure 1.8 (d).

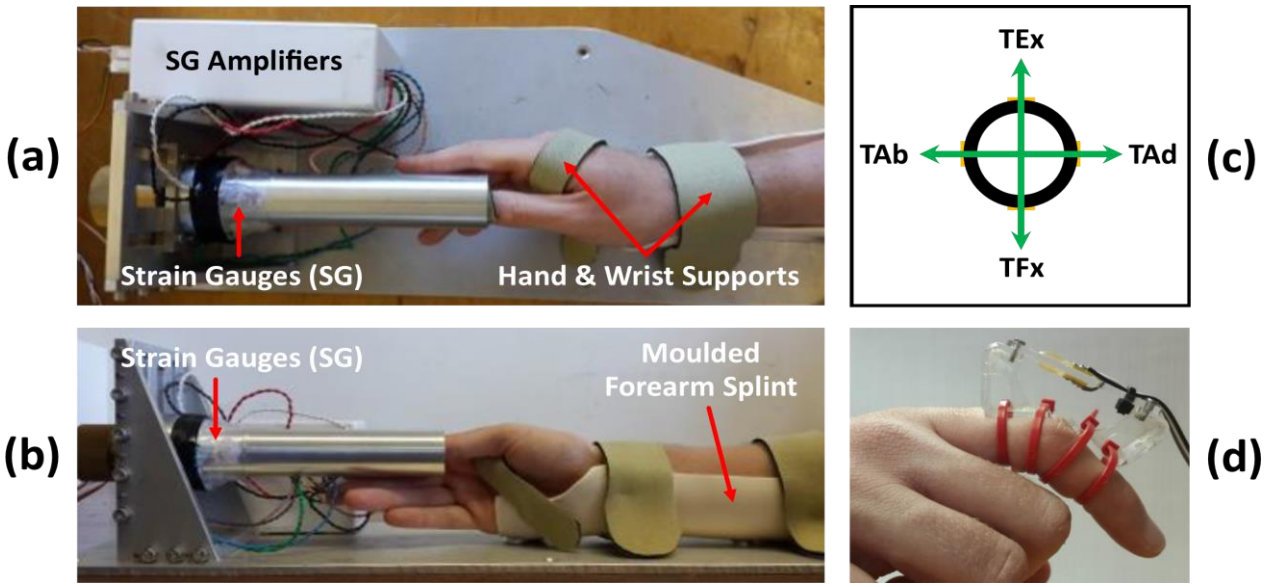

Figure 1.8 – Developed testing rig, dynamometer and finger load cell used by Pitman (2015).

SG – Strain gauge, TFl – Thumb flexion, TEx – Thumb extension, TAb – Thumb abduction, TAd – Thumb adduction.

***(a)** Top view of the testing rig and dynamometer showing vertical strain gauges as well as the hand and wrist supports.*

***(b)** Left side view of the testing rig and dynamometer showing horizontal strain gauges and the forearm splint.*

***(c)** Cross-sectional front view of the dynamometer tube indicating the thumb movement directions.*

***(d)** Index finger load cell apparatus used to measure index flexion and extension forces.*

Images reproduced and adapted from Pitman (2015).

The thumb dynamometer and finger load cell apparatus served the same functions as the foot apparatus developed in the Tibialis Posterior study, namely *contraction force measurement* and *contraction time detection*. Prior to testing, participants were instructed to contract at their maximum voluntary contraction (MVC) level for each static movement in the MP while the applied forces were measured. The MVC levels were used to calibrate the force feedback system which would later instruct participants to maintain a standardised 30% MVC level for each contraction during testing. It was assumed based PDF findings from (Nazarpour et al., 2013), 30% MVC levels would be low enough to fulfil the non-Gaussian ICA requirement.

[12] The locations of the electrodes on the forearm were noted during testing so that the bipolar pairs could be used to calculate the bipolar equivalent waveforms for the superficial muscles. Bipolar EMG will be outlined in Section 2.1.4.

Pitman (2015) in collaboration with Swanepoel (2017) made several important improvements to the sdEMG experimental procedure as well as the data processing and performance evaluation analysis. Some of the key improvements made in the experimental procedure include the implementation of a Graphical User Interface (GUI) to deliver visual instructions to participants, force feedback gauges to aid participants in maintaining isometric contraction levels, randomisation of contraction sequences in the MP and contraction time synchronisation of the predicted EMG waveforms. Additionally, Pearson's correlation coefficient (*r*) was implemented as a measure of *conformity* between processed ICs and predicted EMG waveforms which enabled researchers to quantitatively assess the level of muscle isolation. The implementation of Pearson's correlation also served as a method to autonomously to select *representative ICs (rICs)* which reflected the pIC that most likely represented the EMG activity from a specific muscle.

A snippet from the GUI developed by Pitman (2015) is shown in Figure 1.9 which indicates the contraction prompt image for *thumb flexion* and the three force feedback gauges. For the thumb flexion instruction, the green region of the *vertical gauge* indicates the -30% ± 10% target effort level to be maintained while the horizontal and index finger gauges show the rest positions (0% ± 10%).

	Visual feedback			
Contraction	Contraction prompt Image	Effort level gauges		
		Vertical	Horizontal	Index finger
Thumb Flexion	THUMB DOWN 	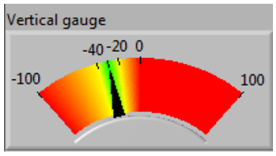	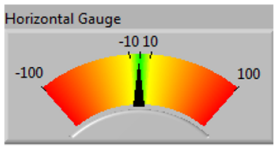	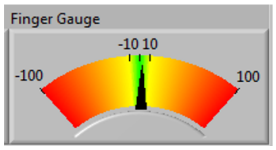

Figure 1.9 – Visual instruction for thumb flexion and force feedback gauges shown to participants in the GUI developed by Pitman (2015).

The force feedback gauges were calibrated to each participants MVC levels prior to testing.

Images reproduced and adapted from Pitman (2015).

A sample set of results from the study are presented in Figure 1.10 showing high levels of correlation between the rICs and the pEMGs for the deep muscles ($r > 0.83$), however very poor correlation was seen for the superficial muscles (*r* values of 0.14 and 0.23). While high *r* values were found for the deep muscles, there were several mismatches between the rICs and pEMG waveforms as highlighted with red rectangles in Figure 1.10. For instance, rIC 2 was assigned to represent muscle activity from flexor pollicis longus, however, two distinct bursts of unexpected EMG activity was present during thumb adduction and thumb extension. Proposed explanations for this phenomenon were the inability of ICA to fully decompose the EMG signals into their independent sources, co-contracting muscles, participant contraction errors and inaccurate pEMG waveforms.

The mean population correlation values (ρ) were calculated for each muscle across 150 experimental runs. The ρ values reported for the deep muscles were 0.81 for FPL, 0.88 for EPL, 0.92 for EPB and 0.83 for APL, while the superficial muscles were 0.38 for FD and 0.36 for ED. These results indicate that the sdEMG technique was transferrable to the forearm and activity from the deep extrinsic muscles of the thumb were non-invasively detected and isolated.

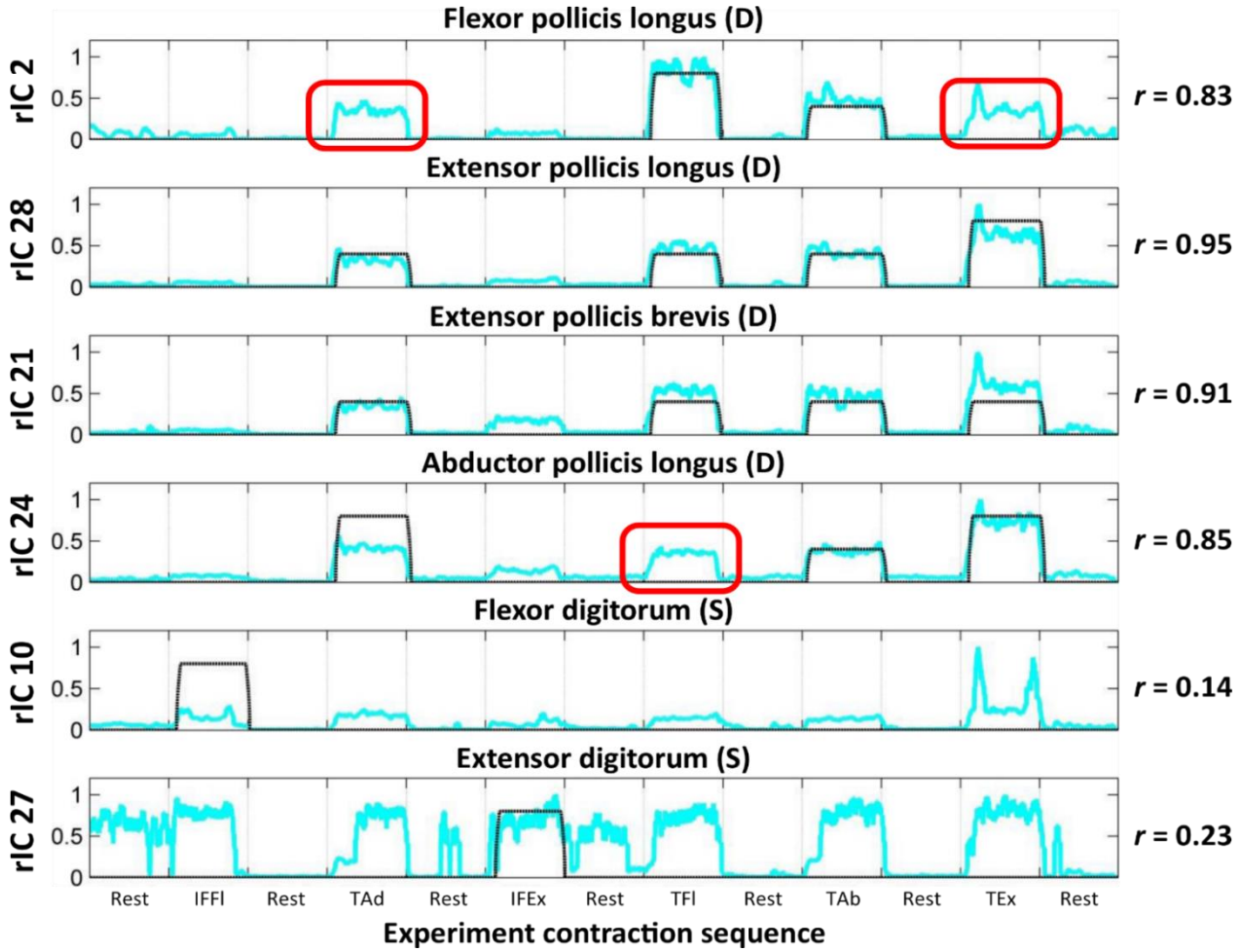

Figure 1.10 – Sample set of results for the Extrinsic Thumb Muscles study by Pitman (2015).

Representative ICs – Cyan waveforms, Predicted EMG – Black waveforms. D – Deep muscle, S – Superficial muscle, TFl – Thumb flexion, TEx – Thumb extension, TAb – Thumb abduction, TAd – Thumb adduction, IFFl – Index finger flexion, IFEx – Index finger extension.

The red rectangles highlight selected mismatches between rICs and pEMG waveforms.

Image reproduced and adapted from Pitman (2015).

1.2.4 Extrinsic Foot Muscles Study

Swanepoel (2017) expanded upon the Tibialis Posterior study by Sayed et al. (2012) to include the extrinsic foot muscles activated during the gait cycle. The study was conducted on 17 healthy male participants at two knee positions (flexed at 90° and fully extended) with 10 experimental runs each resulting in a data pool of 340 experimental runs. The improved experimental procedures developed in conjunction with Pitman (2015) were implemented to investigate deep muscle activity from flexor digitorum longus, flexor hallucis longus, extensor hallucis longus and tibialis posterior. Additionally, the superficial muscles triceps surae, tibialis anterior, peroneus longus and extensor digitorum longus were considered.

The movement protocol and foot apparatus developed in the Tibialis Posterior study was used (see Figure 1.5), in conjunction with an interactive GUI including three force feedback gauges, similar to that of the Extrinsic Thumb Muscles study. A standardised 40% ± 10% of MVC level was required to be performed by participants that provided sufficient EMG activity while satisfying the non-Gaussian ICA source requirement discussed in Section 1.1.2 (II). The study reported high mean population correlation values greater than 0.70 for all the deep and superficial muscles in both knee positions with little variation between the two positions

across all muscles. A sample set of results from a high performing participant is presented in Figure 1.11 showing correlation values greater than 0.80 for all muscles.

While the correlation values shown in Figure 1.11 are considered very high, it should be noted that several mismatches between the rICs and the pEMG waveforms were visible (highlighted in dashed red rectangles). For instance, rIC 5 was assigned to represent muscle activity from the triceps surae, however, two distinct bursts of unexpected EMG activity were present during toe flexion and foot inversion. Similar occurrences were seen in results in the Extrinsic Thumb Muscles study and this phenomenon appears to be a limitation in the current implementation of the sdEMG technique.

The results indicated the sdEMG technique was successfully applied to the lower leg and was able to detect and isolate the deep and superficial extrinsic muscles of the foot non-invasively. Furthermore, Pearson's correlation coefficient was shown to be an effective quantitative tool to rank and select rICs to represent muscle activity and was thus maintained in the present study.

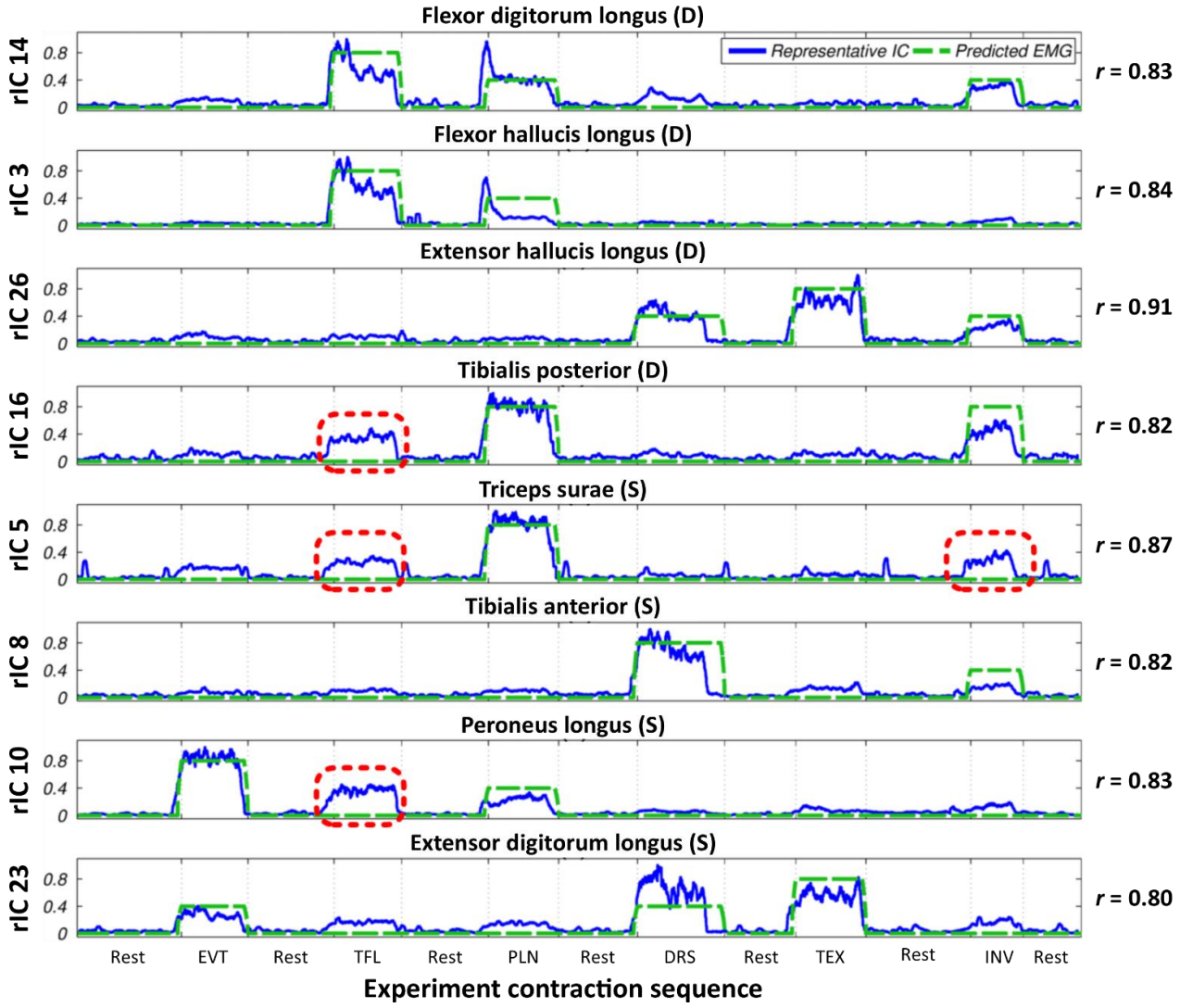

Figure 1.11 – Sample set of results for the Extrinsic Foot Muscles study by Swanepoel (2017).

Representative ICs – Blue waveforms, Predicted EMG – Dashed green waveforms. D – Deep muscle, S – Superficial muscle, EVT – Eversion, TFL – Toe flexion, PLN – Plantar flexion, DRS – Dorsiflexion, TEX – Toe extension, INV – Inversion.

The dashed red rectangles highlight selected mismatches between the rICs and pEMG waveforms.

Image reproduced and adapted from Swanepoel (2017).

1.3 Study Overview

1.3.1 Research Rationale and Significance

The sdEMG technique has many applications in both diagnostic and kinesiological EMG research as an alternative to invasive intramuscular EMG. The ability to detect deep muscle activity *non-invasively* can provide diagnostic information that can be used as a *precursor* to performing *invasive* intramuscular diagnostic EMG in patients with suspected neuromuscular abnormalities. The technique also allows for *compound deep muscle EMG* to be isolated which is absent in intramuscular EMG. Compound deep muscle EMG has many applications including muscle performance monitoring, neuromuscular rehabilitation, gait analysis, fine motor myoelectric control of prostheses and augmented reality control.

Previous sdEMG studies have transferred the technique to the forearm and lower leg from the initial upper arm Brachialis study and in doing so also improved the experimental procedures. The present study focused on expanding the technique by investigating underlying *experimental parameters* that have been assumed or overlooked in previous studies. In doing so, the present study will guide future sdEMG research with a greater understanding of the underlying experimental parameters that can be adjusted to better suit the experiments, apparatus and movement protocol development, as well as the experimental procedures to be conducted.

As a step to expand upon the findings of Pitman (2015), the extrinsic muscles of the hand were selected for the present study, similar to the successive step made by Swanepoel (2017) on the extrinsic muscles of the foot from the Tibialis Posterior pilot study Sayed et al. (2012).

1.3.2 Research Aims and Objectives

The aim of the present study was to develop a set of guidelines from experimental observations for the non-invasive superficial and deep muscle electromyography technique.

In order to achieve this aim the following research objectives were established:

1. Develop a dynamic movement protocol that sufficiently isolates the activation of the extrinsic hand muscles limited to the superficial muscles flexor digitorum superficialis (FDS) and extensor digitorum (ED), and the deep muscles extensor indicis (EI), extensor pollicis longus (EPL), flexor digitorum profundus (FDP) and flexor pollicis longus (FPL).

2. Develop an sdEMG system to detect and isolate EMG activity from the extrinsic hand muscles.

   Sub-objectives:

   a. Design and manufacture 64 reusable surface electrodes, electrode holders and elasticised bands.

   b. Develop a contraction detection system consisting of finger exoskeletons and flex sensors.

   c. Design and manufacture an ergonomic testing platform including a moulded forearm splint.

   d. Develop a participant instruction system consisting of a display and a Graphical User Interface.

3. Design and conduct three experiments on healthy participants investigating the effects of varying the movement protocol parameters: *timing*, *randomisation* and *movement anticipation*.

4. Develop an sdEMG data processing pipeline to determine representative ICs for each muscle across all experimental runs.

   Sub-objectives:

   a. Develop an activation time detection algorithm to determine the precise onset and offset times of each contraction using the flex sensor data from the contraction detection system.

   b. Develop an algorithm to generate time-adjusted predicted EMG waveforms from the flex sensor data for each muscle and experimental run.

   c. Develop an algorithm to select unique representative ICs that best represent the activity of the extrinsic hand muscles for each experimental run.

5. Perform a case study to determine the effects of the three movement protocol parameters investigated on the ability of the sdEMG technique to detect and isolate deep and superficial muscle activity non-invasively.

1.3.3 Scope of the Study

The present study performed experimental testing procedures on five healthy, right-hand dominant male participants (mean ± SD; age: 24 ± 3 years) without any history of neuromuscular diseases or disabilities. A group of five participants was deemed sufficient to determine the feasibility of using the sdEMG to capture EMG recordings for the extrinsic muscles of the hand and to identify trends from which preliminary experimental guidelines could be developed.

1.3.4 Plan of Development

Part A provides an overview of the contents of the present study and contextualises the concepts of the sdEMG technique. The theoretical framework for the sdEMG technique as well as a review of previous works and the study outline is presented in Chapter 1. The fundamental principles and recording techniques of electromyography are then outlined in Chapter 2.

Part B details the design and development of the sdEMG system used in the present study. Chapter 3 describes the formation of the movement protocol for the musculature investigated and Chapter 4 outlines the design and development of the experimental apparatus built for the present study.

Part C outlines the implementation of the sdEMG technique in the detection and isolation of the extrinsic muscles of the hand. The experimental procedures taken to acquire the data from participants are described in Chapter 5 and the data processing steps are detailed in Chapter 6.

Part D presents a case study exploring the experimental results. Chapter 7 primarily discusses the effects of the three movement protocol parameters investigated on the ability of the sdEMG technique to detect and isolate the extrinsic muscles of the hand. The global muscle performances are quantified and participant reaction delays are also explored.

Part E presents the main findings and discusses the non-ideal observations identified throughout the analyses in Chapter 8. Proposed future work is outlined in Chapter 9 and a list of concise sdEMG guidelines is presented in Chapter 10.

Chapter 2 - Background

2.1 Electromyography

Electromyography (EMG) is a well-established technique used to measure and analyse bioelectrical signals emanating from muscle fibre membranes duration muscle contractions. Electromyography can be applied in two contexts, *Diagnostic EMG* and *Kinesiological EMG*. Diagnostic EMG (also known as *Clinical* or *Neurological EMG)* can be viewed as a microscopic application analysing motor unit action potentials (MUAPs) to assess neuromuscular functionality by observing signal characteristics such as the motor unit firing frequency, MUAP conduction velocities, timings and amplitudes to name a few. Conversely, Kinesiological EMG provides a macroscopic view on muscle activity as seen by compound EMG signals used to assess muscle performance by considering the signal timings and amplitudes, as well as the resultant movement and force production.

The underlying physiological processes involved in the activation of muscles are presented to provide the theoretical framework necessary for the formation of EMG signals. The methods for detecting and recording EMG signals are outlined with a focus on *Kinesiological monopolar surface EMG practices* that are implemented in the sdEMG technique.

2.1.1 Muscle Electrophysiology

Skeletal or voluntary muscles are composed of muscle bundles known as *fascicles* which are further subdivided into *muscle cells* known as *muscle fibres* as illustrated in Figure 2.1. Muscle fibres are able to produce force in response to neurological excitation from the central nervous system (CNS) or muscle reflex. Skeletal muscles below the neck are electrically excited from the spinal column via peripheral motor nerves which forms part of the CNS. The smallest functional unit of a muscle is known as a *motor unit (MU)* which is comprised of a *single alpha-motoneuron (α-MN)* originating at the spinal column, and *all* the muscle fibres it innervates as illustrated in Figure 2.1 showing two MUs (purple and red groups). An alpha-motoneuron consists of a cell body and dendrites that originate in the anterior horn of the spinal grey matter, axons enclosed in nerves and the motor endplates (neuromuscular junctions) that innervate the muscle fibres as shown in Figure 2.1 and Figure 2.2.

An *action potential (AP)* is bioelectrical impulse signal that is generated when there is a change in the electrical potential across cellular membranes as a result of the sudden flow of ionic charges across the cell membrane. The electrophysiology of muscle fibres is complex, and for brevity, the Hodgkin & Huxley (1952) model of the nerve cell is used as an approximation for muscle fibres to provide a simplified understanding of the generation of action potentials, which is the basis of EMG signals. Nerve and muscle cells have a resting membrane potential of approximately -80 to -90 mV (intracellular potential being negative with respect to the extracellular fluid) that is sensitive to changes in the ionic balance across the membrane. Muscle fibre membranes are most permeable to sodium $[Na^+]$, potassium $[K^+]$ and chlorine $[Cl^-]$ ions which maintain the resting potential and are responsible for fluctuations of the membrane potential needed to form an action potential. The muscle fibre membrane is known as the sarcolemma which is embedded with sodium-

potassium active[13] ion pumps, and voltage-gated[14] sodium and potassium ion channels that allow selective ion flow in response to neurological activation.

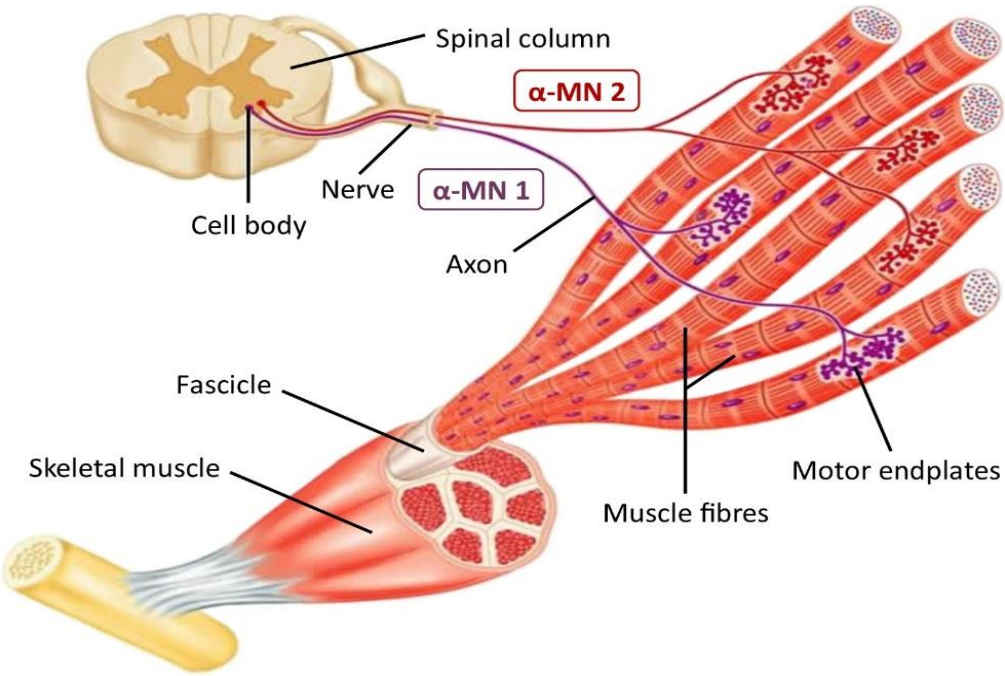

Figure 2.1 – Skeletal muscle histology identifying alpha-motoneurons (α-MN) and the formation of motor units (MU).

An alpha-motoneuron consists of the neuron cell body, dendrites, axons and motor endplates.

A motor unit consists of a single α-MN and all the muscle fibres it innervates. Two MUs are shown with purple and red α-MNs and the fibres they innervate.

Image adapted from Marieb (2001).

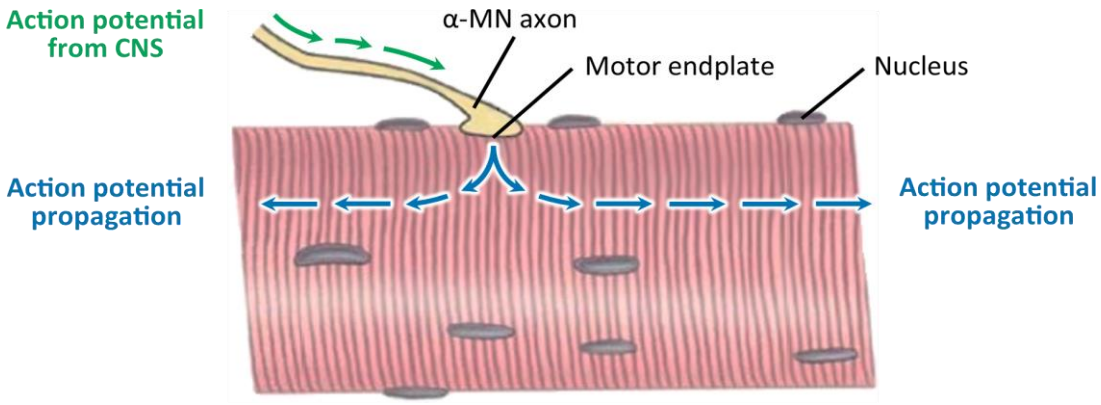

Figure 2.2 – Single motor unit structure indicating action potential (AP) propagation within a muscle fibre.

The AP propagates throughout the muscle fibre in opposite directions originating in the innervation zone where the motor endplates synapse to the muscle fibre.

Image adapted from Guyton & Hall (2006).

[13] Active ion pumps are transmembrane proteins that require energy in the form of adenosine triphosphate (ATP) to selectively transport ions across cell membranes against ionic concentration gradients.

[14] Voltage-gated ion channels are transmembrane proteins that allow selective ion flow across cell membranes in response to changes in the membrane potential within the vicinity of the channel.

The formation of an action potential, also known as the *depolarisation-repolarisation cycle*, consists of four stages which are described pictorially in Figure 2.3. The underlying muscle fibre ion transport mechanisms that are activated in response to neuromuscular excitation are illustrated in Figure 2.3 (a), while the formation of the bioelectrical signal response is shown in Figure 2.3 (b).

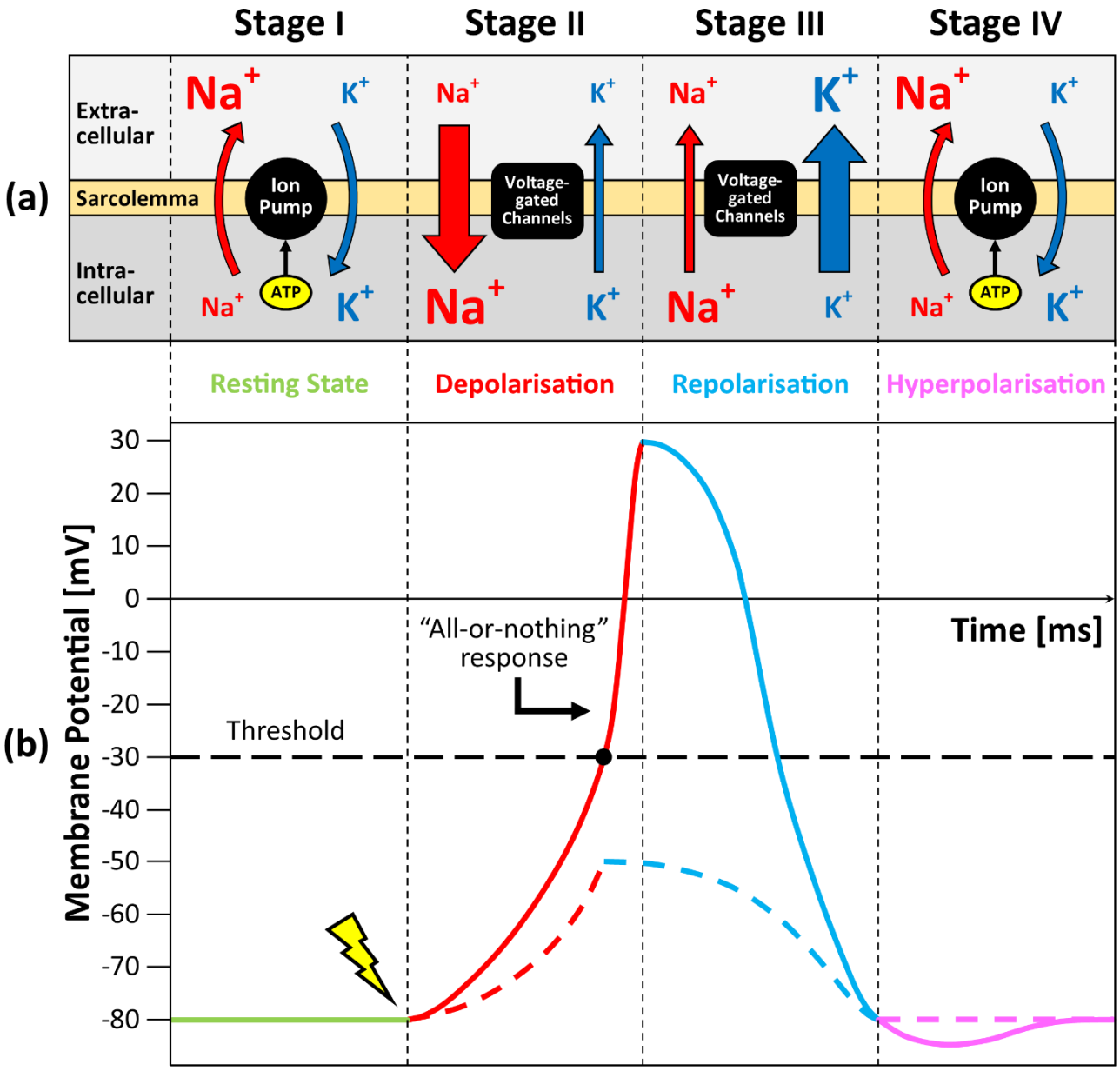

Figure 2.3 – Formation of a muscle fibre action potential (MFAP) in response to neuromuscular excitation.

(a) *Illustration of the ion concentrations and the primary ion transportation mechanisms across the sarcolemma during each stage of the depolarisation-repolarisation cycle. The sodium and potassium ion concentrations are shown by the relative font sizes and the flow of ions are shown by the arrows where the relative arrow size indicates the relative rate of flow during each stage of the depolarisation-repolarisation cycle.*

(b) *Illustration of the membrane potential signal during muscle fibre excitation. The yellow lightning bolt symbol indicates the time of neuromuscular excitation. The solid lines indicate the successful formation of an action potential and the dashed lines indicate a failed activation that did not cross the threshold value (-30 mV) needed to trigger a muscle fibre action potential.*

Diagram redrawn and adapted from Swanepoel (2017). Additional information derived from Guyton & Hall (2011); Seeley, Stephens, & Tate (2007).

Stage I – Resting State

Prior to muscle activation, the natural resting membrane potential is maintained at approximately -80mV (green line in Figure 2.3 (b)(Stage I)) through active transport of ions against the ionic concentration gradients by sodium-potassium ion pumps as shown in Figure 2.3 (a)(Stage I).

Stage II – Depolarisation

The activation of an alpha-motoneuron (α-MN) from the CNS or due to muscle reflex results in the release of the neurotransmitter *acetylcholine* at the motor endplates within the synaptic cleft from the α-MN axon. These molecules bind to their receptor sites on the *ligand-gated*[15] *sodium ion channels*. The binding activates these channels and permits sodium ions to flow into the cell causing a small localised depolarisation zone resulting in an increase of the membrane potential (more positive with respect to the intercellular fluid). The steady depolarisation (increasing of membrane potential) of the muscle fibre activates the *voltage-gated sodium channels* resulting in an influx of sodium ions into the cell thereby increasing the membrane potential as shown in Figure 2.3 (a)(Stage II) (Guyton & Hall, 2011).

If the muscle fibre membrane potential exceeds the activation threshold (-30mV), the cell depolarises further as more voltage-gated sodium channels open. The muscle fibre elicits the *'all-or-nothing' response* that causes a *rapid* influx of sodium ions within a fraction of a millisecond as shown by the steep gradient of the solid red curve in Figure 2.3 (b)(Stage II). The rapid depolarisation results in a peak membrane potential of approximately 30mV at which point the cell is saturated with sodium ions. This bioelectrical impulse signal reflects the peak action potential of the excited muscle fibre.

If the muscle fibre membrane potential does not exceed the activation threshold (-30mV) as shown by the dashed red curves in Figure 2.3 (b)(Stage II), the sodium-potassium pumps activate to restore the resting membrane potential through the backward exchange of ions during the repolarisation stage as shown by the dashed blue curves in Figure 2.3 (b)(Stage III).

Stage III – Repolarisation

Within fractions of a millisecond after the voltage-gated sodium ion channels open, the increased membrane potential activates the inactivation gates of the same voltage-gated sodium ion channel to close. Simultaneously the voltage-gated potassium ion channels are activated which open more than normal to repolarise the membrane by allowing positive potassium ions out of the cell resulting in a decreasing membrane potential as shown by Figure 2.3 (a)(Stage III). The potassium ion channels activate slower than the sodium ion channels, therefore the membrane potential decreases at a lower rate since the sodium ions are trapped in the cell, and at this stage, only the potassium ions are responsible for repolarising the cell. The sodium ion channels only begin to reopen when the membrane potential is near the resting potential at which point the sodium ions within the cell begin to slowly exit the cell.

Stage IV – Hyperpolarisation

As the membrane potential returns to the resting potential, the potassium ion channel inactivation gates begin to close however this process is slow and thus the cell hyperpolarises below the resting potential by allowing an excess of potassium ions out of the cell as shown by the pink curve in Figure 2.3 (b)(Stage

[15] Ligand-gated ion channels are transmembrane proteins that selectively activate when bound to specific neurotransmitters.

IV). As the potassium ion channel inactivation gates close, the near-resting membrane potential reactivates the sodium ion channels to release sodium outwards, and the sodium-potassium active ion pumps begin to restore the ionic concentrations to resting state, primarily by transporting the surplus of sodium ions out of the cell. The cell membrane potential returns to the resting state and is capable of initiating the formation of another action potential in response to further neuromuscular excitation.

The successful formation of an action potential at the α-MN innervation point sparks a chain reaction within the muscle fibre. The AP begins to propagate in both directions along the muscle fibre towards the muscle tendons due to fluctuations in the ion charge distribution between adjacent membrane patches of the muscle fibre. Figure 2.4 illustrates the AP propagation through the muscle fibre from the α-MN innervation point.

Figure 2.4 (a) shows the polarised muscle fibre during resting conditions and the location of the α-MN axon synapse (yellow lightning bolt symbol) where the muscle fibre is excited. After the muscle fibre is excited, the localised depolarisation results in the membrane potential becoming *positive* with respect to the intercellular fluid as shown in Figure 2.4 (b). The adjacent patches of the muscle fibre are still in the polarised resting state with a *negative* membrane potential thus there are adjacent patches of opposite charge polarities at the depolarisation front, indicated by the edges of the shaded area in Figure 2.4 (b).

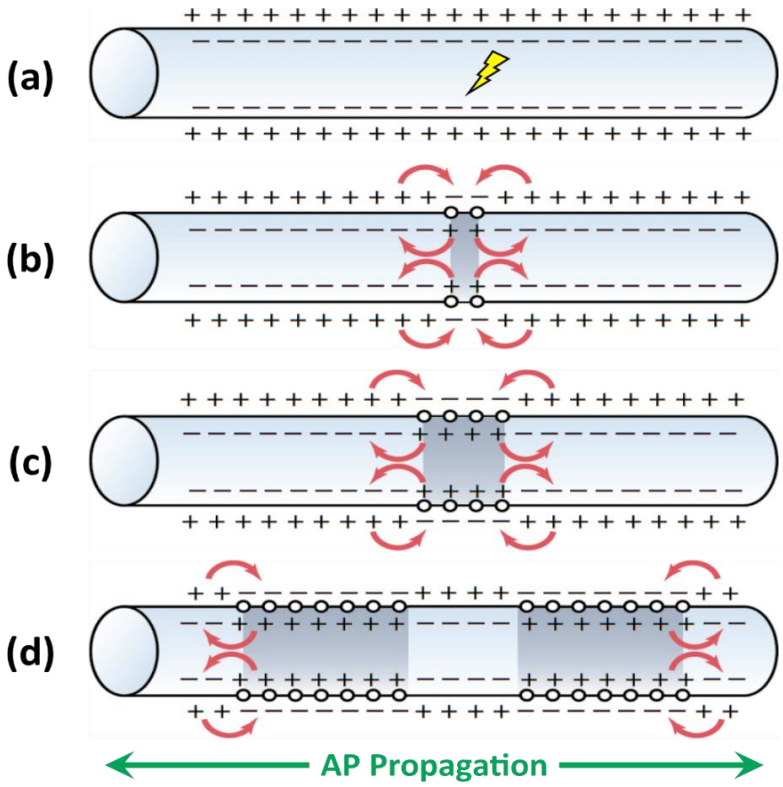

Figure 2.4 – Fluctuations in the muscle fibre ion charge distributions leading to the outward propagation of the action potential.

(a) *Polarised muscle fibre ion charge distribution during rest. The lightning bolt indicates the axon synapse point.*

(b) *Localised depolarisation at the axon synapse forming bioelectric dipoles between adjacent patches of positive and negative potentials. The generated localised ionic currents are shown by red arrows.*

(c) *Expansion of the depolarisation front along the muscle fibre.*

(d) *Further propagation of the depolarisation-repolarisation front away from the axon synapse. The original stimulated region has repolarised to the resting membrane potential and ion charge distributions.*

Images adapted from Guyton & Hall (2011).

The combination of opposite charge polarities and the distances separating them is representative of bioelectric dipoles. These dipoles generate a potential difference between excited and non-excited regions of the muscle fibre allowing localised ionic currents to flow in the intercellular and extracellular regions. As these ionic currents flow, they change the membrane potential of the adjacent non-excited regions thus activating voltage-gated sodium ion channels in the non-excited regions that lead to further depolarisation along the muscle fibre causing the AP to propagate outwards as shown in Figure 2.4 (c). The depolarisation-repolarisation front propagates throughout the muscle fibre as shown in Figure 2.4 (d) and this propagation is known as the *muscle fibre action potential (MFAP)*.

2.1.2 EMG Signal Detection

In practice, it is not feasible to detect and measure muscle fibre action potentials (MFAP) in terms of membrane potential changes at an intercellular level as this would require microscopic electrodes embedded into individual muscle fibres. Instead, electromyography techniques aim to provide researchers with a global view of muscle activity at either the motor unit level (MUAP signal decomposition), or the compound EMG level (EMG signals proportional to force and movement production). To achieve this, electromyograms (EMG signals) are measured using either intramuscular electrodes (needle or fine-wire) inserted directly into the muscle bellies, or surface electrodes placed on the skin above the muscle being investigated.

Most physiological tissues surrounding skeletal muscles are electrically conductive allowing the generated ionic currents during the intracellular muscle fibre action potential propagation (shown in Figure 2.4) to generate an electric field within the surrounding extracellular volume. With a characteristic known as *volume conduction* (discussed in Section 2.1.5), the induced potential changes (representative of the MFAP) can be measured by detection electrodes placed within the generated electric field (either in the extracellular volume or at the skin surface). The detected measurements are causally related to the muscle fibre activations and thus are considered representative of MFAPs.

A bipolar[16] surface EMG configuration is presented in Figure 2.5 to describe the detection of an EMG signal using surface electrodes, a differential amplifier and a signal display. For simplicity, a single muscle fibre is considered with the intracellular and extracellular polarities indicated in Figure 2.5 (a) using *'+'* and *'-'* symbols. The propagating AP is highlighted in red at discrete time instances *t0* to *t6*. The propagating front and the generated dipole is shown travelling from left to right in Figure 2.5 (a) and the measured EMG signal (potential difference between the inputs of the differential amplifier) in millivolts is shown in Figure 2.5 (b).

The following discussion is made with reference to Figure 2.5 with figure cross-references removed for clarity.

At *t0* the muscle fibre is at rest with the same potential present at both electrodes which are cancelled out by the differential amplifier. At *t1* the AP is generated, but has not propagated within the detection region under the negative electrode (negative amplifier input) thus the differential output remains at 0mV. As the dipole propagates closer to the left edge of the negative electrode between *t1* and *t2* there is a potential difference measured between the electrodes. As the dipole passes an increasing output signal is generated, shown in (b) at *t2*, which reaches a maximum amplitude when the dipole is directly below the negative electrode. Likewise between *t2* and *t3* the signal decreases and returns to 0mV when the dipole is equidistant between the electrodes, therefore the same potential is measured at both electrodes. The dipole continues

[16] Bipolar surface EMG refers to an EMG recording configuration where the measured signal is the difference in potentials between two surface electrodes. EMG recording modalities will be discussed in Section 2.1.4.

to pass underneath the positive electrode (positive amplifier input) and the potential difference measured decreases below 0mV and reaches a minimum amplitude at *t4*. As the dipole passes the right edge of the positive electrode the potential difference measured increases back to the 0mV at *t5* and remains at 0mV at *t6* since the dipole has propagated passed the detection range. The resultant EMG signal at *t6* is a *biphasic MFAP* recorded from surface electrodes.

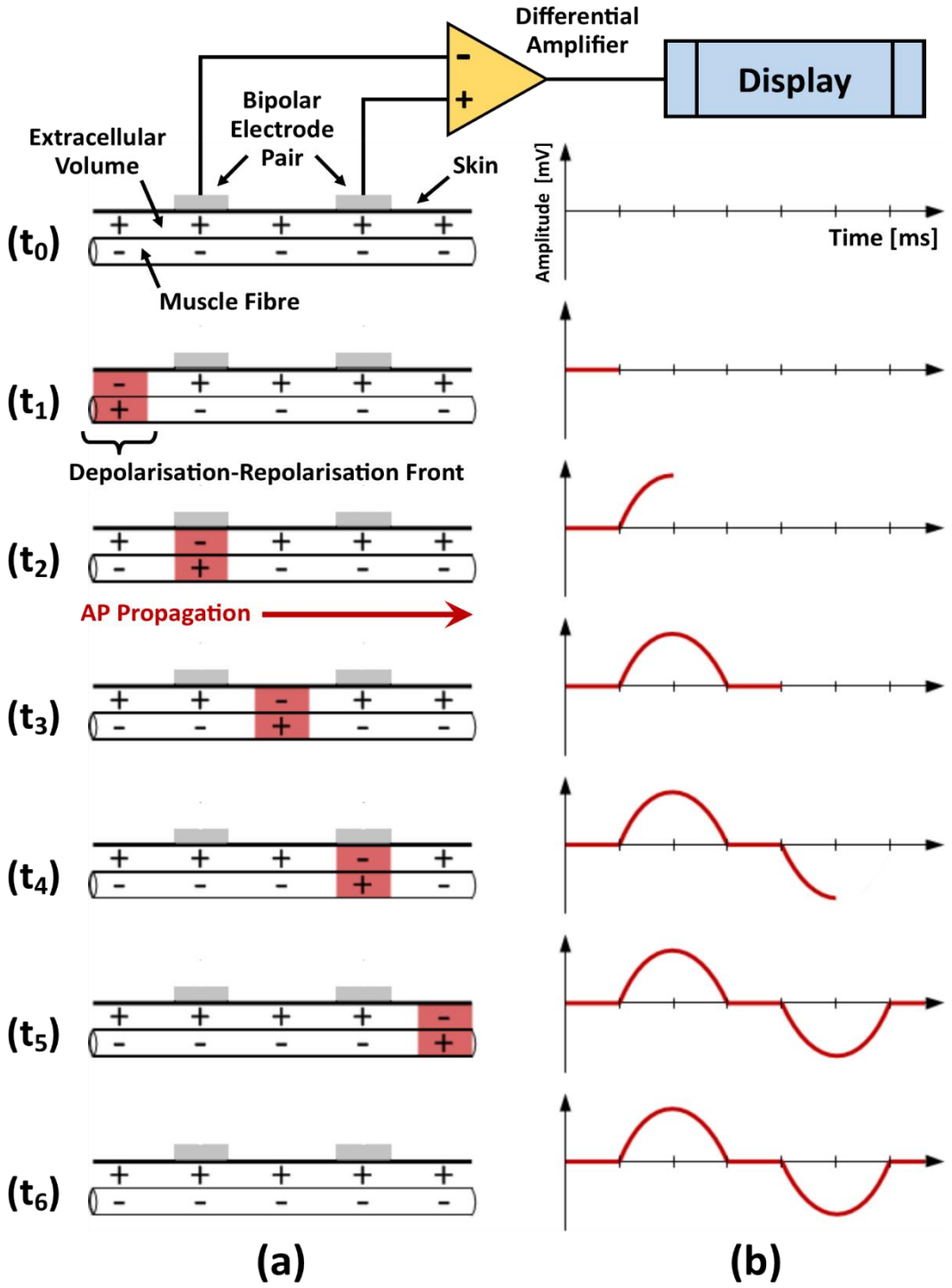

Figure 2.5 – Bipolar EMG recording setup illustrating the detection of the EMG signal from the extracellular volume as the depolarisation-repolarisation front propagates in one direction.

(a) *Propagation of an action potential along a single muscle fibre in relation to the electrode placements.*

(b) *Detected EMG signal shown at discrete time instances t_0 to t_6.*

Diagram reproduced and modified from Swanepoel (2017). Originally adapted from Kumar & Mital (1996).

The *spatio-temporal summation* of the MFAPs generated by all the muscle fibres innervated by a single motor unit (MU) is known as the *motor unit action potential (MUAP)*. MUAPs form the smallest functional EMG signal that is typically monophasic, biphasic, triphasic or quadriphasic, where polyphasic (> 4 phases) MUAPs are rare but do occur in abnormal muscle tissue (De Luca & Basmajian, 1985). The EMG signal developed in Figure 2.5 (b) at *t6* is equivalent to a *biphasic MUAP* from a motor unit consisting of a *single* muscle fibre.

Since compound EMG is the spatio-temporal summation of all the *MUAPs* within the electrode detection region originating from a single muscle, the relative locations of motor endplates (innervation zones), as well as the location and orientation of the electrodes, result in complex signals known as EMG interference patterns. An example of EMG signal formation is presented in Figure 2.6 where three biphasic MUAP trains with different firing frequencies are summed together.

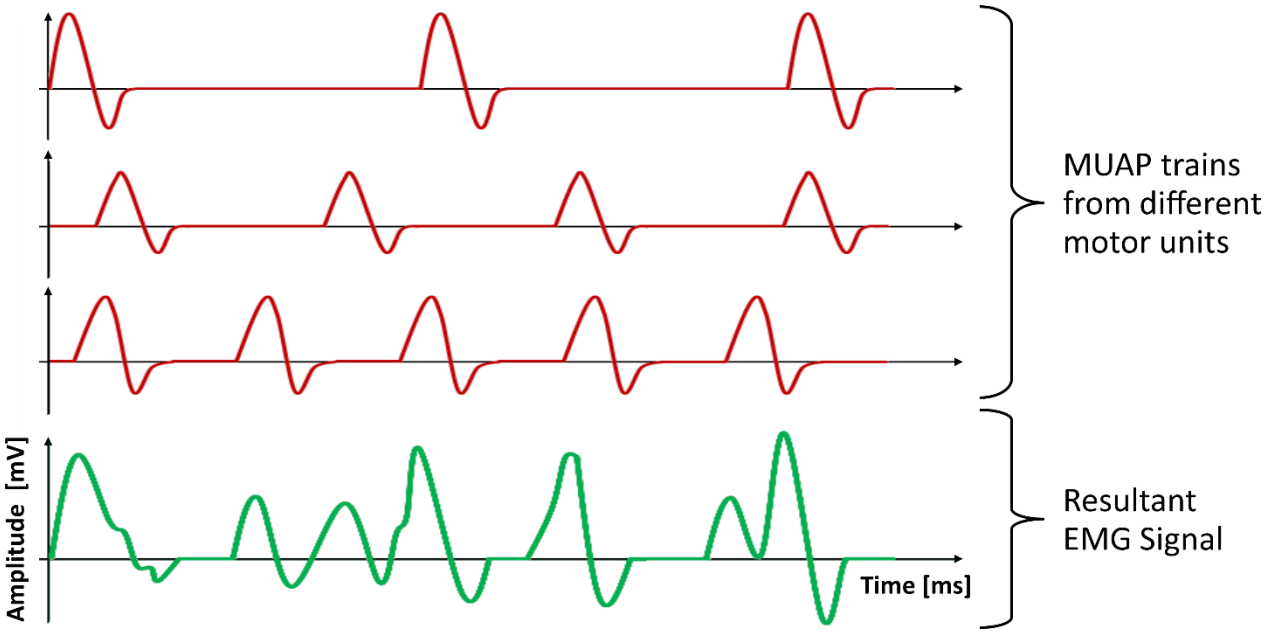

Figure 2.6 – Resultant EMG signal formed from the spatio-temporal summation of three MUAP trains with different firing frequencies.

Diagram reproduced and adapted from Swanepoel (2017). Originally adapted from Kumar & Mital (1996).

2.1.3 EMG Detection Techniques

EMG detection is broadly divided into *surface electromyography* and *intramuscular electromyography*. Both detection techniques implement electrodes connected to biopotential amplifiers needed to amplify the detected EMG signals from the microvolt level to a suitably higher voltage range that can be digitalised for offline signal processing. A brief description of the key advantages, fundamental detection differences and application limitations are presented.

Surface Electromyography

Surface electromyography (sEMG), as the name suggests is a *non-invasive* method that uses surface electrodes to measure skin surface voltages which are most representative of compound EMG from the underlying *superficial muscle(s)*. Due to the large[17] surface electrode pick-up areas, the detected signals are susceptible to signal crosstalk from adjacent muscles and to decrease this phenomenon, surface electrodes need to be carefully placed above the superficial muscle belly under investigation. Similarly, due to the large electrode surface areas, sEMG is also susceptible to environmental electrical noise which reduces the accuracy of the detected muscle activity. The large electrodes are however less affected by minor shifts in electrode positions making sEMG robust to most dynamic movements and allow for reproducible recordings over multiple experimental repetitions.

It is generally accepted that sEMG is unable to adequately measure deep muscle EMG activity. Some deep muscles such as abductor pollicis longus can be detected at the surface as the muscle is partially accessible at the skin surface, however, this does not provide adequate muscle exposure to detect an accurate EMG signal that sufficiently represents the *global* muscle activity.

Due to the non-invasive nature of sEMG, this technique is widely used for research and clinical purposes in both Diagnostic EMG and Kinesiological EMG applications. Surface EMG is a robust technique that can provide accurate insight into superficial muscle activity when good experimental procedures are followed.

Intramuscular Electromyography

Intramuscular electromyography is an *invasive* procedure that allows for the local electrical activity from *a few muscle fibres* of deep *or* superficial muscles to be measured. The technique uses needle or fine-wire electrodes inserted directly into the muscle bellies that are less than a millimetre in diameter. The electrodes are placed within the extracellular environment of the muscle fibres resulting in more direct MUAP measurements with nearly no muscle crosstalk and very little environmental electrical noise.

While intramuscular EMG results in high-quality signals compared to sEMG, it is inherently limited to very small detection sites thus the resultant EMG signals are specific to *a few muscle fibres* which may not necessarily reflect the *global activity* of the muscle investigated which is seen in sEMG. Intramuscular EMG is also an invasive procedure that requires qualified clinicians to safely insert and remove the electrodes limiting the applicability to mainly clinical research applications which do not permit dynamic movements. There are also several safety concerns with intramuscular EMG such as potential infection, electrode breakages and discomfort to the patient (Daube & Rubin, 2009; Strommen & Daube, 2001).

Currently, intramuscular EMG is the only clinically accepted method for measuring deep muscle activity, albeit at a microscopic level. Given the invasive nature and the limited EMG pick-up area, intramuscular EMG is generally only applicable to Diagnostic EMG studies that are focused on neuromuscular abnormalities that are identifiable at the muscle fibre level.

The sdEMG technique attempts to detect and isolate deep muscle activity non-invasively using sEMG practices as an alternative intramuscular EMG techniques.

[17] A commonly used circular surface electrode has a diameter of 10mm which is significantly larger than the alternative fine-wire or needle electrodes used in intramuscular EMG.

2.1.4 EMG Recording Modalities

EMG recording is broadly divided into two modalities, *bipolar EMG* and *monopolar EMG*. The fundamental difference is the manner in which the electrodes are configured in either a *bipolar* or a *monopolar* recording configuration. Both electrode configurations apply to surface and intramuscular EMG detection techniques. Since the present study implements sEMG techniques, the recording modalities are described with reference to surface electrodes.

Bipolar EMG

Most EMG studies implement the bipolar electrode configuration which consists of two detection electrodes placed in line with the muscle length above the muscle belly separated by a small distance known as the inter-electrode distance (typically 20mm). An additional amplifier reference electrode is placed further away on an electrically inert area, typically a bony prominence such as the olecranon at the elbow for upper arm studies. The detection electrodes ('positive' and 'negative') are connected to a differential amplifier that subtracts the common-mode signal present on both detection electrodes resulting in an EMG signal that reflects only the *changes in EMG activity*. With this configuration, common potentials coupled to both electrodes possibly including crosstalk, electrocardiography (ECG) interference and external interference such as 50/60Hz AC power line noise are removed (in the ideal case) making bipolar EMG favourable in most applications.

Monopolar EMG

The monopolar electrode configuration is less commonly used which consists of a single detection electrode placed above the muscle belly and a reference electrode placed on an electrically inert area away from the muscle as described in the bipolar configuration. A differential amplifier is also used where the detection electrode is connected to the 'positive' input and the reference electrode or 'ground' voltage (fixed amplifier reference voltage, typically 0V) is connected to the 'negative' input. The resultant EMG signal is a compound signal of all the measured potentials at the detection site which possibly includes muscle crosstalk and other common-mode interferences as described in the bipolar configuration. While the monopolar configuration tends to be less intuitive for applications requiring a simple binary output (Is the muscle active or inactive?), there are applications typically investigating the decomposition of compound EMG to analyse MUAPs or crosstalk that require the common-mode signals retained in monopolar EMG.

The present study implemented the monopolar EMG recording modality as the sdEMG technique requires the common-mode signals to extract information regarding deep and superficial muscle activity.

2.1.5 Volume Conduction

Volume conduction in the context of EMG is the ability of action potentials to propagate away from their source generators (muscle fibres) through electrically conductive physiological tissues surrounding the muscle towards the detection electrodes (Rutkove, 2007). The volume conductor is commonly modelled as a cylinder[18] consisting of three concentric layers representing muscle, fat and skin (Merletti & Parker, 2004). Each layer has different electrical characteristics that influence MUAP propagation in the volume conductor

[18] A cylindrical model is typically used for upper or lower limb EMG studies.

which gives rise to signal distortions in the measured EMG at both the intramuscular and skin surface levels. The volume conductor primarily applies a spatial low-pass filtering ('blurring') effect to propagating MUAPs that intensifies as the detection electrode is placed further away from the source (Merletti & Parker, 2004).

The volume conduction filtering effect is most pronounced in surface EMG where the radial distance between the muscle fibres and surface electrodes is greatest, as illustrated in Figure 2.7. Figure 2.7 highlights the 'flattening' of the MUAP shape as a result of the volume conductor's low-pass filter effect where the high-frequency triphasic MUAP quickly attenuates[19] in amplitude as the radial distance away from the MU increases. An adverse effect of volume conduction is seen at the 25mm radial depth where the EMG signal has distorted from a triphasic MUAP to a biphasic MUAP that has also attenuated from the microvolt to the nanovolt level.

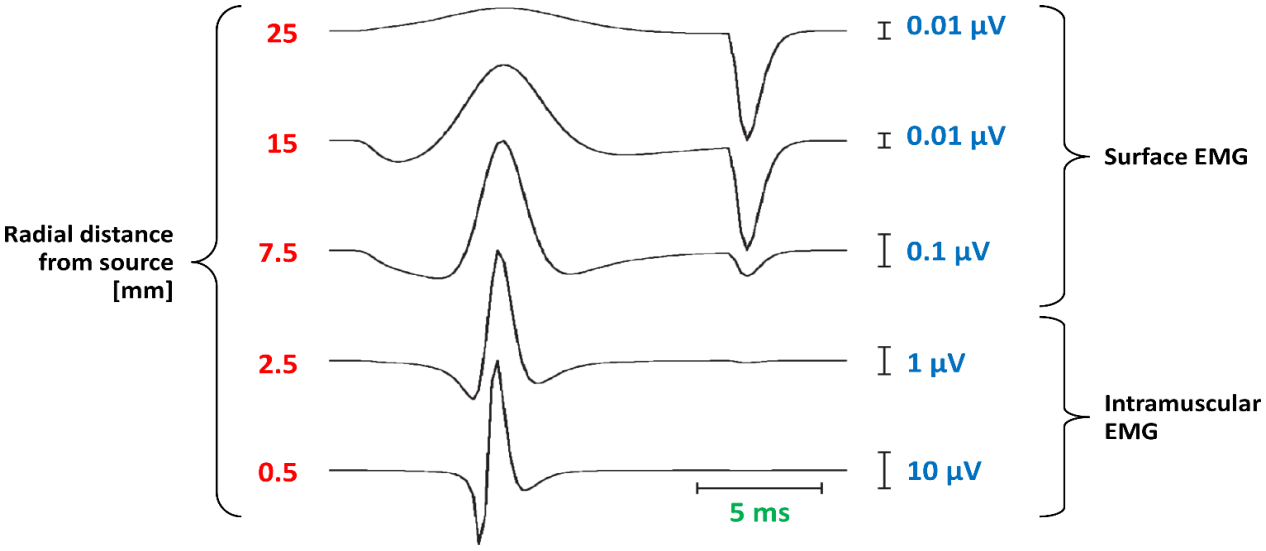

Figure 2.7 – The observed spatial filtering effect due to volume conduction on a single triphasic MUAP at various radial depths away from the source muscle fibre.

Image reproduced and adapted from Blok, Stegeman, & van Oosterom (2002).

A clinical study by Roeleveld, Stegeman, Vingerhoets, & Oosterom (1997) investigated the effects of volume conduction on sEMG potentials from individual MUs at various depths for both monopolar and bipolar EMG recordings. The study implemented a 36-channel EMG recording system consisting of two rows of 18 electrodes spread evenly over the anterior semi-circumference of the biceps brachii muscle. The experimental setup also included two intramuscular electrodes inserted in the recording area to implement a novel *"intramuscular scanning EMG"* technique to determine the MU position and radial depth to the surface electrodes. Nine participants were tested and 52 MUs at various radial depths were measured with a total of 42 sessions (experimental repetitions).

The study reported that the surface monopolar and bipolar EMG recordings indicated that the MUAP amplitudes were attenuated differently by volume conduction and that the degree of signal attenuation was proportional to the radial distance from the MU to the surface electrodes. Figure 2.8 shows four sets of results illustrated as cross-sectional representations of the biceps brachii muscle for monopolar recordings (a, b) and bipolar recordings (c, d) at two different MU depths, and the superficial MUs are shown in (a, c) and the deep MUs are shown in (b, d). The principal result of the study was that MUAP amplitudes at the

[19] Signal attenuation is the opposite of amplification, effectively amplification with a fractional gain value.

surface were attenuated by the volume conductor. Several other observations were made with respect to the EMG recording configurations (monopolar or bipolar) as well as the MU depth which is synonymous with the muscle layer (deep or superficial).

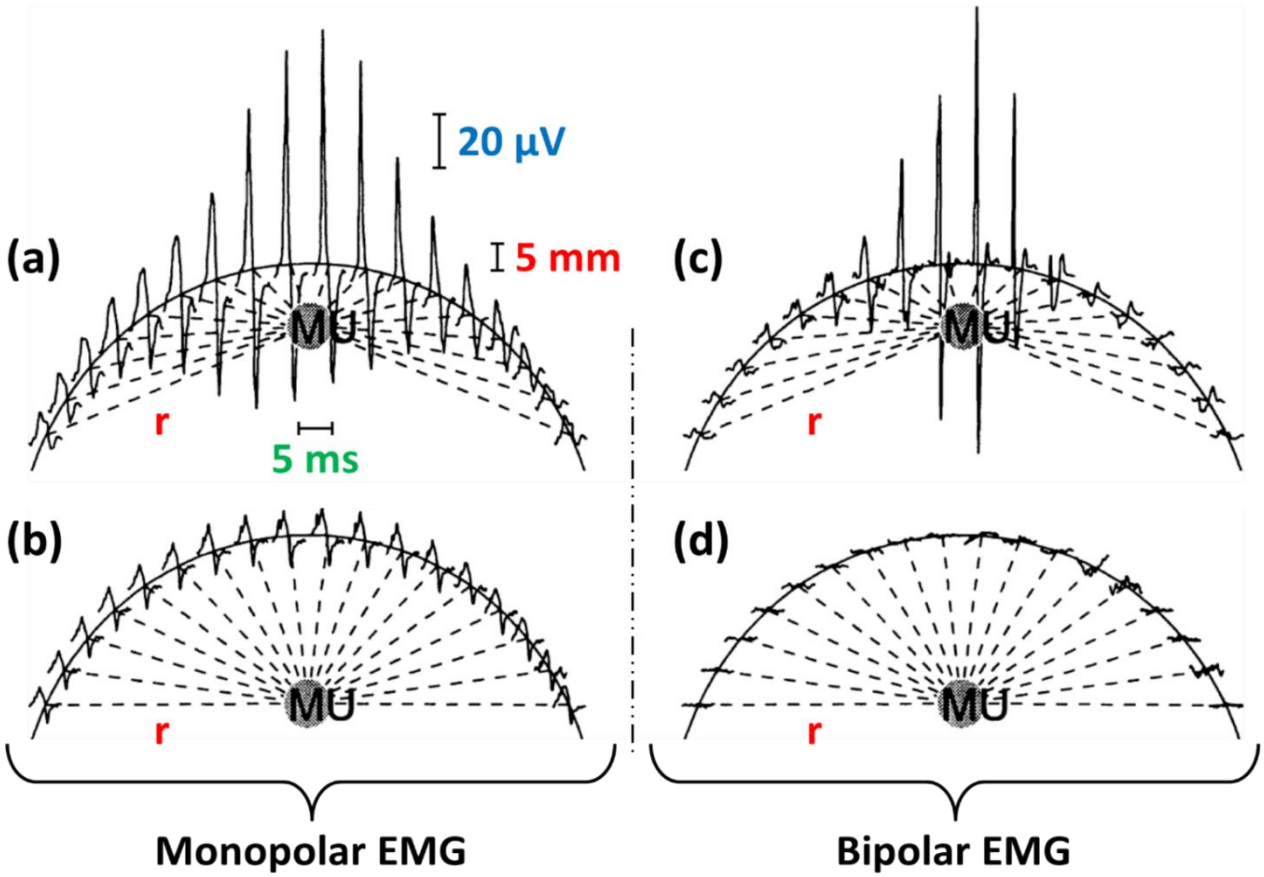

Figure 2.8 – Cross-sectional representation of the biceps brachii muscle indicating the MU location and the recorded MUAPs at the skin surface.

MUAPs were recorded at 18 locations on the skin surface with varying distances (r) between the source MU and the recording electrodes. MU depth was obtained using a novel "intramuscular scanning EMG" technique.

***(a)** Superficial MU monopolar EMG MUAP distribution.*

***(b)** Deep MU monopolar EMG MUAP distribution.*

***(c)** Superficial MU bipolar EMG MUAP distribution.*

***(d)** Deep MU bipolar EMG MUAP distribution.*

Image reproduced and adapted from Roeleveld et al. (1997).

The bipolar EMG recordings presented in Figure 2.8 (c, d) show faster MUAP signal attenuation as the radial distances increases when compared to the monopolar recordings shown in Figure 2.8 (a, b). This result agrees with the understanding that the volume conductor broadens the distributions of the surface potentials from deep MUs more than the superficial MUs since the MUAPs have a further radial distance to propagate. The broadened distribution of the surface potentials from deep MUs also results in greater spatial signal overlap across adjacent electrodes since the radial distances are similar. The overlapping potentials appear as common-mode signals at the surface electrodes which are present in the monopolar EMG recordings as illustrated in Figure 2.8 (b). Conversely, since bipolar EMG removes the common-mode potentials, the measured EMG signals are effectively cancelled out as shown by the nearly fully attenuated signals in Figure 2.8 (d).

The volume conductor also affects the spatio-temporal summation of MUAPs in relation to the distances from *multiple sources (motor units)*, which can occur at different depths. The sdEMG technique relies on the assumption that the monopolar EMG recordings taken from multiple electrodes encircling the volume conductor are a linear mixture of MUAPs from different muscles in *both* the deep and superficial layers. Since monopolar EMG retains all potentials within the electrode pick-up area, the measured signals are expected to contain muscle activity from deep muscles, albeit at smaller signal amplitudes. While the measured potentials in Figure 2.8 (b) at a depth of ∼25mm are slightly lower than 20µV (peak-to-peak) for a deep MU, it is expected that the effects of the volume conductor on the sdEMG technique will be of a similar amplitude level for the present forearm study. Additionally, the sdEMG technique implements a large number of surface electrodes that encircle the entire limb, therefore it is expected the potentials measured at all electrodes will provide sufficient information to isolate both deep and superficial muscle activity.

Part B – Development of an sdEMG System

Part B details the design and development of the sdEMG system used in the present study. Chapter 3 describes the formation of the movement protocol for the musculature investigated and Chapter 4 outlines the design and development of the experimental apparatus built for the present study.

Chapter 3 - Musculature Investigated

The development of an sdEMG system begins by selecting the limb and musculature to be investigated. It is critical that the limb studied allows for EMG activity from individual muscles to be isolated through protocols that target specific muscle contractions. The present study investigated the extrinsic muscles of the hand as a successive step to the previous forearm study (Pitman, 2015). This chapter describes the procedures followed to develop a dynamic movement protocol needed to isolate the extrinsic muscles of the hand.

3.1 Muscle Selection

The present study investigated the superficial *flexor digitorum superficialis (FDS)* and *extensor digitorum (ED)* muscles, and the deep *extensor indicis (EI)*, *extensor pollicis longus (EPL)*, *flexor digitorum profundus (FDP)* and *flexor pollicis longus (FPL)* muscles which are shown in Figure 3.1 and Figure 3.2. The gross motor functions of each muscle are to fully flex or extend the finger digit(s) it inserts onto, including movement of the metacarpophalangeal (MCP) joints. The fine motor functions of these muscles are outlined in Table 3-1 highlighting the functional commonality of the 2nd to 5th digits which poses a muscle isolation dilemma.

Table 3-1: Fine motor functions of the investigated muscles (Gilroy, MacPherson, & Ross, 2012).

Digits	Muscle	Muscle layer	Fine motor function
1	Extensor pollicis longus (EPL)	Deep	Thumb IP joint extension
1	Flexor pollicis longus (FPL)	Deep	Thumb IP joint flexion
2	Extensor indicis (EI)	Deep	Index PIP joint extension
2-5	Extensor digitorum (ED)	Superficial	Semi-independent† PIP joint extension
2-5	Flexor digitorum superficialis (FDS)	Superficial*	Semi-independent† PIP joint flexion
2-5	Flexor digitorum profundus (FDP)	Deep	Semi-independent† DIP joint flexion

IP – Interphalangeal, PIP – Proximal interphalangeal, DIP – Distal interphalangeal.

** FDS lies in the intermediate muscle layer, however, it is considered a superficial muscle in the present study.*

† Hand dexterity varies among people, some are able to perform fully independent movement of each digit.

The dynamic movements investigated in the present study and the corresponding muscle activations are outlined in Table 3-2. Two finger groupings were defined to enable isolation of FDS from FDP, and EI from ED. The 2nd to 5th digits acting as a single unit was defined as *'Group'*, and the 3rd to 5th digits acting as a single unit was defined as the *'Ring Group'*. The purpose of these groupings will be outlined in Sections 3.2.1 and 3.2.2.

In an sdEMG study, ideal muscle isolation occurs when there is a *one-to-one muscle-movement* mapping, however in practice it is possible for a single movement to map to multiple muscles, which poses an independent muscle isolation problem. For example, thumb IP flexion only activates FPL while concurrent flexion of the 2nd to 5th digits activate FDS and FDP simultaneously. It should be noted that the corollary of this, *one-to-one movement-muscle* mapping, does not provide the same information needed to independently isolate that muscle. For example, concurrent extension of the 3rd to 5th digits activate ED as indicated in Table 3-2, however, this does not imply ED can be isolated using *only* this movement as there are other movements that also activate ED, such as index extension.

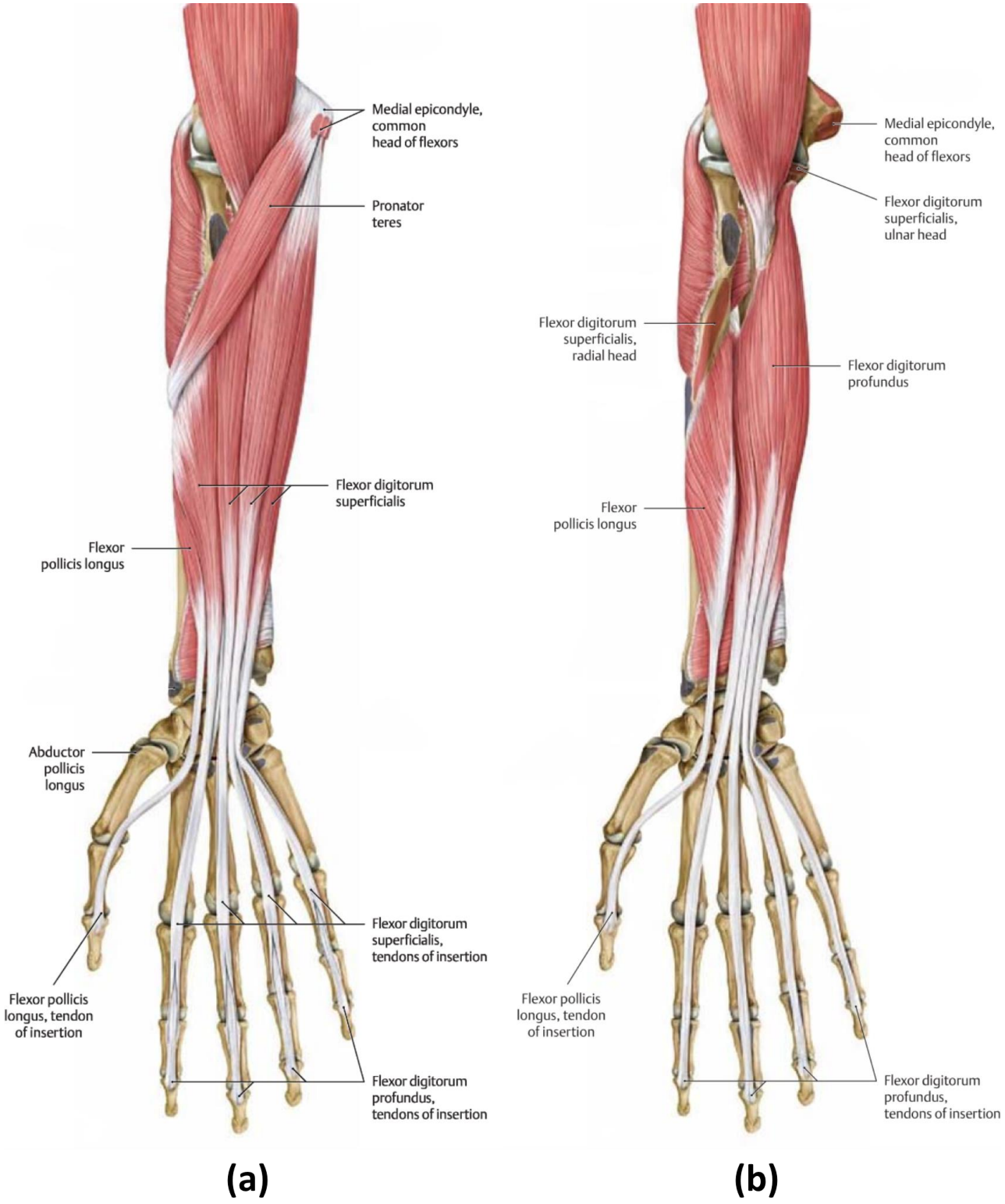

Figure 3.1 – Anterior view of the muscles in the right forearm.

(a) *Intermediate muscle layer*

(b) *Deep muscle layer*

Images adapted from Schuenke, Schulte, & Schumacher (2010).

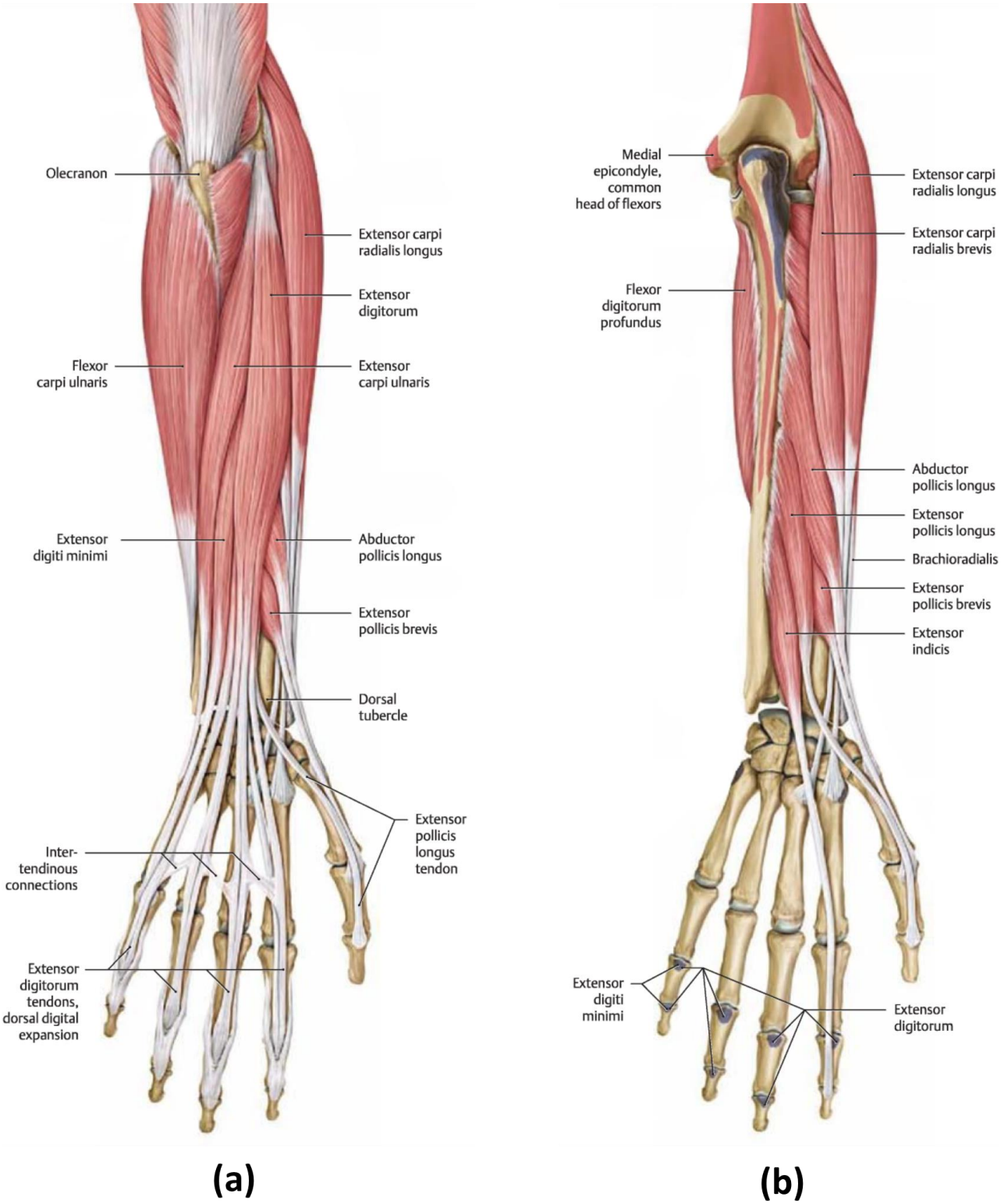

Figure 3.2 – Posterior view of the muscles in the right forearm.

(a) *Superficial muscle layer*

(b) *Deep muscle layer*

Images adapted from Schuenke, Schulte, & Schumacher (2010).

Table 3-2: Forearm muscle activations during fine motor finger movements (Gilroy et al., 2012).

		Forearm target muscles					
Dynamic movements	**Digits**	**ED**	**EI**	**EPL***	**FDP**	**FDS**	**FPL***
Thumb IP flexion	1						✓
Thumb IP extension	1			✓			
Index full flexion	2				✓	✓	
Index full extension	2	✓	✓				
Index PIP flexion	2				✓	✓	
Index PIP extension	2	✓	✓				
Group† flexion	2-5				✓	✓	
Group† extension	2-5	✓	✓				
Group† PIP flexion	2-5				✓	✓	
Group† PIP extension	2-5	✓	✓				
Ring‡ Group flexion	3-5				✓	✓	
Ring‡ Group extension	3-5	✓					

IP – Interphalangeal, PIP – Proximal interphalangeal, DIP – Distal interphalangeal, ED – Extensor digitorum, EI – Extensor indicis, EPL – Extensor pollicis, longus, FDP – Flexor digitorum profundus, FDS – Flexor digitorum superficialis, FPL – Flexor pollicis longus.

** Single muscle, single movement mappings.*

† 'Group' consists of the 2nd to 5th digits acting as a single unit.

‡ 'Ring Group' consists of the 3rd to 5th digits acting as a single unit (strapped together during testing).

Table 3-2 also highlights that all movements except thumb IP flexion, thumb IP extension and Ring Group extension activate multiple muscles during movements resulting in co-contractions. Since the sdEMG technique requires unique isolation of each muscle, the targeted muscle contractions implemented in the present study needed to differentiate co-contracting muscles by comparing their *relative muscle activation contributions*.

Relative muscle activation contribution was defined as the relative proportion of the measured EMG activity between co-contracting muscles, as determined by the EMG signal amplitudes. While the actual contributions are not precisely known, it was assumed that there will be a noticeable difference in the measured EMG signals to differentiate between two muscles which were activated simultaneously. By further analysing the fine motor functions of each muscle, unique muscle-movement activation contribution mappings were derived to isolate the individual muscles, which will be discussed further in Section 6.3.

After the forearm anatomy was investigated and the muscles of interest were selected, the next step in the development of an sdEMG system was to derive a *movement protocol* to ensure isolated EMG activity.

3.2 Movement Protocol

A *movement protocol (MP)* is defined as a timed sequence of unique static or dynamic movements interleaved with rest periods to be performed by the participant during testing. While the term infers physical movement, it refers to both static movements (isometric contractions) and dynamic movements (isotonic contractions). The purpose of a movement protocol is to time-code movements in a known sequence which isolates unique muscle-movement mappings needed to select decomposed source signals to represent specific muscles.

In the present study, *full and partial finger movements* were required in the developed MP to isolate FDS from FDP, and EI from ED. These muscle pairs have common insertion points, therefore the finger joint(s) are activated simultaneously, however with different muscle activation contributions. *Full finger movement* was defined as flexion or extension that activates the *MCP, PIP and DIP joints* simultaneously as illustrated in Figure 3.3. *Partial finger movement* was defined as flexion or extension that only activates the *PIP and DIP joints* while maintaining the MCP joint in a rest position, as illustrated in Figure 3.4. Due to anatomical variation, most people are unable to independently control their DIP finger joints, therefore *partial finger movements* are also referred to as *PIP flexion* or *PIP extension*.

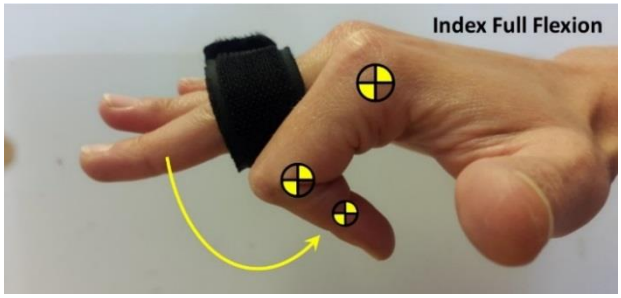

Figure 3.3 – Independent full index finger flexion.

Three centre-of-rotation markers are shown located on the index MCP, PIP and DIP joints which are activated simultaneously during independent full index finger flexion while the Ring Group remains in the natural rest position.

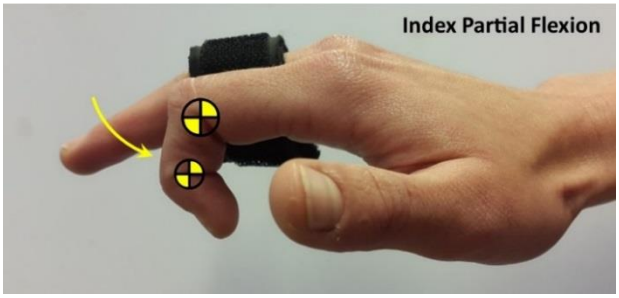

Figure 3.4 – Independent partial index finger flexion.

Two centre-of-rotation markers are shown located on the index PIP and DIP joints which are activated simultaneously during independent partial index finger flexion while the Ring Group remains in the natural rest position.

In the present study, the *rest position* was defined as a state where the fingers were returned to a *natural semi-flexed position* with little to no muscle activity present. This rest position differs from the *anatomical hand position* where all fingers are *extended* and lie on the same plane as the palm. It should be noted that the *full and partial extension* movements are not the same as returning to *rest* – extension returns fingers to the *anatomical hand position* while moving to the rest position returns the fingers to a *natural semi-flexed position*.

A movement protocol was designed with 12 unique finger movements that enabled individual isolation of the investigated forearm muscles in the present study. The formation of the movement protocol is described in Table 3-3, derived from the forearm musculature discussed in Section 3.1 as well as the muscle activations

presented in Table 3-2. Previous sdEMG studies have successfully isolated superficial and deep muscle EMG activity using 5 second *movement windows*[20], therefore this was selected for the initial movement protocol.

In general, each movement (red blocks) is followed by a rest period (green blocks). There are however two exceptions where movements are consecutive without a rest period (blue blocks); *Group PIP* flexion and extension and *Index PIP* flexion and extension. The reason for this can be explained by considering the functions of FDS and FDP, as well as ED and EI, discussed next.

Table 3-3: Movement protocol developed for isolating ED, FDS, EI, EPL, FPD and FPL.

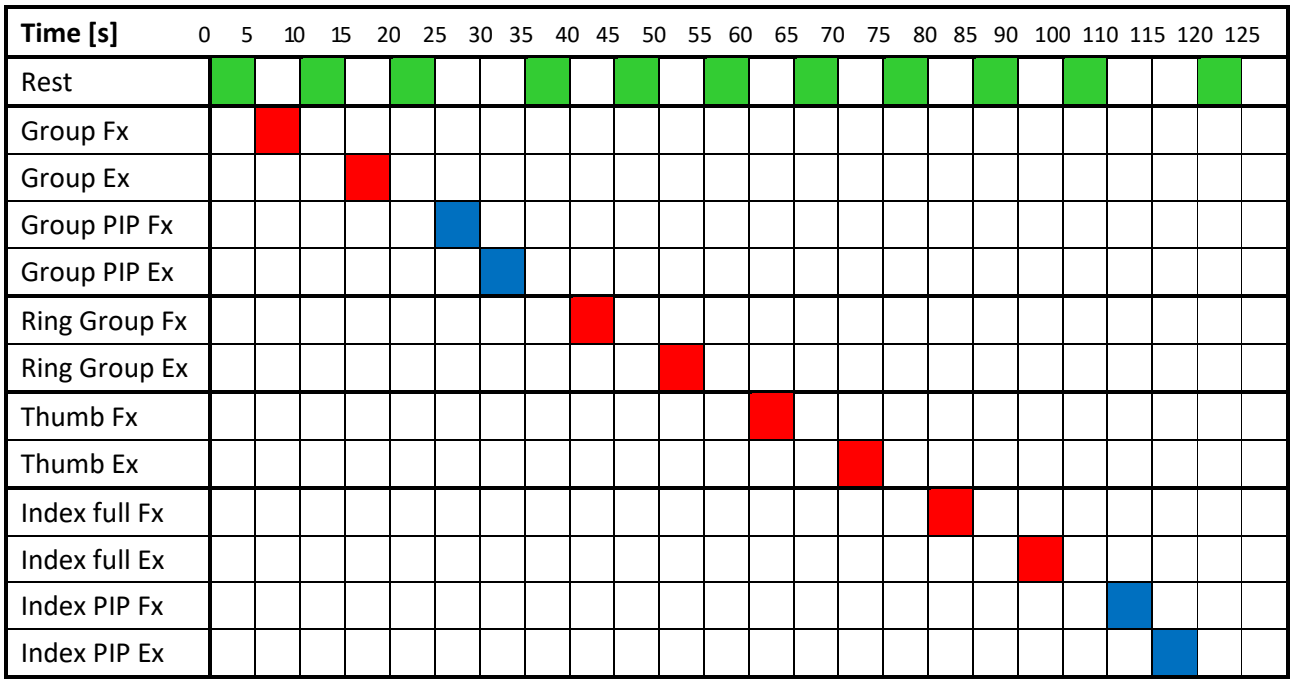

Fx – Flexion, Ex – Extension, PIP – Proximal interphalangeal.

3.2.1 Isolating FDS from FDP

Flexor digitorum superficialis (FDS) originates as a single muscle and then branches into four large and distinct muscle and tendon bundles inserting on the anterior distal aspect of the middle phalanges of the 2nd to 5th digits as shown in Figure 3.1 (a). These distinct muscle bundles are able to function as independent muscles for fine motor movements, thus providing independent[21] flexion of the MCP and PIP finger joints.

Likewise, flexor digitorum profundus (FDP) originates as a single muscle which branches into four small and distinct muscle and tendon bundles inserting on the anterior distal aspect of the distal phalanges of the 2nd to 5th digits as shown in Figure 3.1 (b). While these muscle bundles aren't as pronounced as FDS, they do allow semi-independent[22] flexion of the DIP joint.

[20] A movement window is a time interval for which a muscle contraction is sustained to maintain a finger position.

[21] Due to anatomical variation some people are able to flex their PIP finger joints independently. In general, most people have semi-independent control of their PIP and MCP joints due to the large distinct muscle bundles of FDS.

[22] Due to anatomical variation some people are able to flex their DIP finger joints independently. In general, most people have semi-independent control of their DIP joints due to co-contraction of FDS resulting in concurrent DIP and PIP flexion.

Consequently, it is challenging to isolate FDS from FDP during Group full flexion (Figure 3.5) as both muscles will be activated, albeit with different muscle activation contributions. To address this problem, the relative muscle activation contributions needed to be considered. FDS (all bundles acting as one muscle) was assumed to be fully active during Group PIP flexion (Figure 3.6) and FDP was assumed to be partially active.

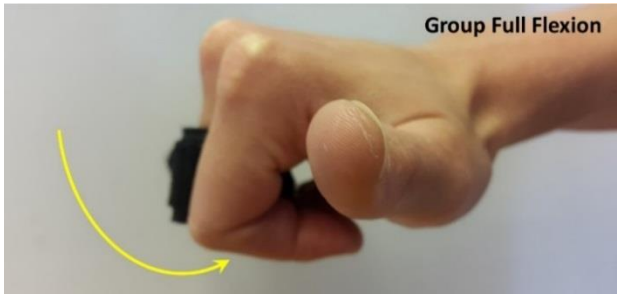

Figure 3.5 – Group full flexion.

During Group full flexion both FDS and FDP are fully active.

Figure 3.6 – Group PIP flexion.

During Group PIP flexion FDS is assumed to be fully active while FDP is assumed to be partially active.

Group PIP flexion can be achieved by starting at the rest position and returning to the rest position, however, Group PIP extension was another movement included in the movement protocol (needed to isolate EI from ED), therefore the flexion-extension pair was performed consecutively without a rest period.

To achieve this, the following movement sequence was required for activation:

Rest → Group PIP flexion → Group PIP extension → Rest.

3.2.2 Isolating EI from ED

Extensor indicis (EI) is a small muscle that inserts on to the index finger at the proximal aspect of the middle and distal phalanges as shown in Figure 3.2 (b) and Figure 3.7. For simplicity, EI is considered to act independently[23] to ED for fine extension of the PIP and DIP finger joints. EI also contributes to Group extension in conjunction with ED.

Extensor digitorum (ED) originates as a single muscle which branches into four small muscle and tendon bundles, as shown in Figure 3.2 (a), which insert onto the posterior proximal aspect of the *dorsal digital expansion* shown in Figure 3.8, on the 2nd to 5th digits. These bundles are not as distinct as FDS and FDP, however, they do allow for some individual finger extension. The *dorsal digital expansion* extends from the proximal aspect of the middle phalanx to the proximal aspect of the distal phalanx. While ED has individual muscle and tendon bundles, it does not allow for the *full* independent extension of the 2nd to 5th digits due to the inter-tendinous connections linking the four tendons in the dorsum of the hand shown in Figure 3.8.

Consequently, it is challenging to isolate EI from ED during independent full index extension (Figure 3.9) as both muscles will be activated, albeit with different muscle activation contributions. To address this problem, the relative muscle activation contributions needed to be considered. EI was assumed to be fully activate during independent index PIP extension, provided the Ring Group did not extend[24] as shown in Figure 3.10.

[23] Due to the common insertion point of EI on the index finger, there will be some concurrent activation of ED while EI is fully active thus EI acts semi-independently to ED.

[24] This is an ideal case, due to the inter-tendinous connections of ED there will be some concurrent Ring Group extension.

In order to perform partial index extension to achieve these muscle isolations, the index finger needed to be in a partially flexed position thus a consecutive movement was required without a rest period.

To achieve this, the following movement sequence was required for activation:

Rest → Index full flexion → Index PIP extension → Rest.

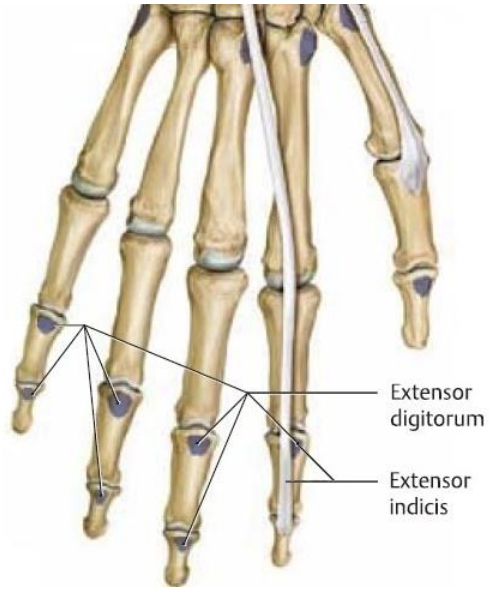

Figure 3.7 – Right dorsal view of the hand (a).

The ED tendon insertion locations are shown on the proximal aspects of the middle and distal phalanges.

The EI tendon insertion locations are shown on the proximal aspects of the middle and distal phalanges.

These locations refer to the effective point where the pulling force is exerted.

Image adapted from Schuenke et al. (2010).

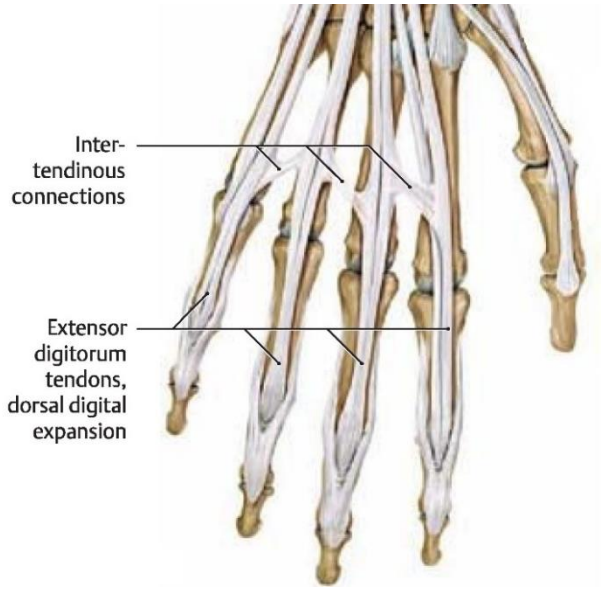

Figure 3.8 – Right dorsal view of the hand (b).

The ED tendon insertions on the dorsal digital expansions are shown indicating the closely linked DIP and PIP finger extension movements.

The inter-tendinous connections are shown which prevents full independent finger extension.

Image adapted from Schuenke et al. (2010).

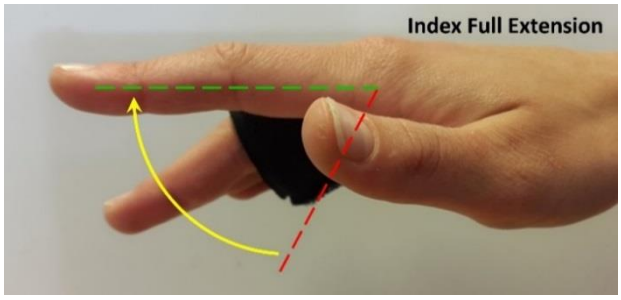

Figure 3.9 – Independent full index finger extension.

Independent index full finger extension is shown with the Ring Group (3rd to 5th digits) in the natural rest position. During index full flexion both ED and EI are fully active.

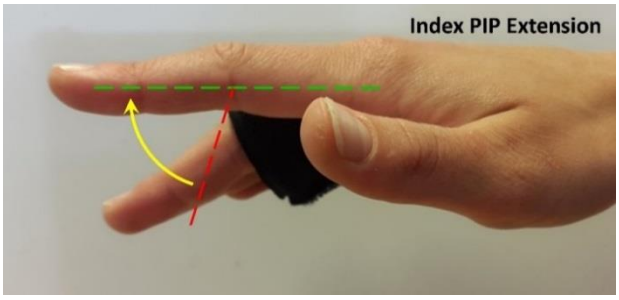

Figure 3.10 – Independent index PIP finger extension.

Independent index PIP finger extension is shown with the Ring Group (3rd to 5th digits) in the natural rest position. This ensures that EI is fully activate, while ED is partially active.

Chapter 4 - Data Acquisition System

An overview of the experimental apparatus required to conduct an sdEMG study is presented in Figure 4.1. All sdEMG studies require an *EMG Acquisition System*, *Testing Apparatus* and a *Participant Instruction System*. This chapter discusses these three main system components with an emphasis on design considerations for setting up a dynamic forearm study.

The Data Acquisition System design considerations are presented as generic outlines for all sdEMG systems followed by a detailed description of the apparatus built to conduct the present forearm study. The Data Acquisition System outputs three databases: *raw EMG signals*, t*iming data* that reflects exact muscle contraction times, and the *MP sequences* that indicate the order in which movements were executed during each experimental run.

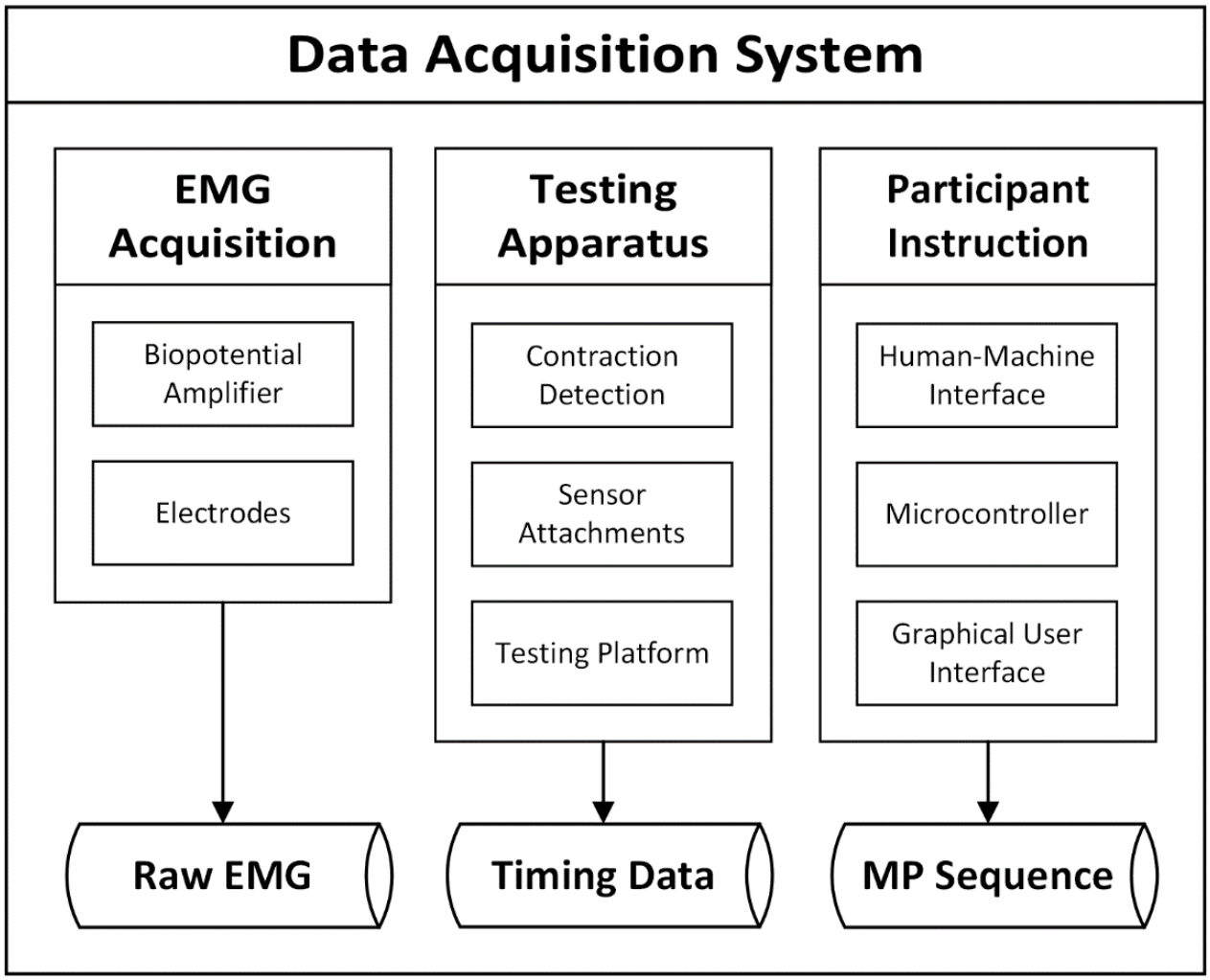

Figure 4.1 – Data Acquisition System overview highlighting the requirements for the EMG Acquisition, Testing Apparatus and Participant Instruction sub-systems.

4.1 EMG Acquisition

EMG acquisition systems consist of a biopotential amplifier and electrodes set up in either a bipolar or monopolar recording modality as described in Section 2.1.4. The specific requirements of these components will be discussed in the context of the developed sdEMG system for the present study.

4.1.1 Biopotential Amplifier

An sdEMG system requires a multichannel biopotential amplifier capable of recording *monopolar EMG* activity as well as sensor and trigger signals. The auxiliary sensor and trigger signals are needed to synchronise the recorded EMG data with the performed movements. In lieu with the sdEMG conventions followed in previous sdEMG works (Section 1.2), the number of electrodes was oversubscribed by at least a factor of two which sets the minimum number of recording channels needed from the biopotential amplifier.

The forearm contains 20 muscles, therefore a minimum of 40 monopolar EMG channels was required in the present study. As described in Section 2.1.5, volume conduction leads to higher attenuation of deep muscle MUAPs compared to superficial muscles, therefore it was hypothesised recording sEMG from *more locations* than required (> 40) would result in ample compound EMG activity to detect the smaller deep FPL, EPL and EI muscles during the developed *low resistance* dynamic MP. It was assumed 64 electrodes would be a suitable quantity for the underlying musculature which conveniently matched the recording system's input configurations – the available 256 input EMG channels were grouped into four 64-channel blocks.

An *OT Bioelettronica® EMG-USB2* 256-channel biopotential amplifier was used which features sufficient EMG and auxiliary channels needed for the present study. The device recording settings selected are indicated in Table 5-2 and the device hardware specifications can be found in Appendix B. The system supports *Referenced Monopolar EMG* recording and includes a Driven Right-Leg (DRL)[25] circuit to suppress AC power line noise (50 Hz in South Africa).

4.1.2 Electrodes

Commercially available sEMG electrodes are commonly made of silver [Ag] or silver-chloride [AgCl] which are available in disposable or reusable types. Disposable electrodes are usually pre-gelled with conductive and adhesive paste while dry reusable Ag or AgCl electrodes can be attached directly to the skin, however, the use of conductive paste is recommended. The paste serves to reduce the effective electrode-skin impedance and improve electrical conductivity in the tissue by providing dissociated chlorine ions needed to form the ionic transfer bridge to the electrode (Day, 2002).

Due to the large quantity of electrodes used in an sdEMG system, reusable individual electrodes are preferred. Commercially available electrode arrays have fixed inter-electrode distances (IED) therefore for participants with large forearm diameters the arrays may not always be able to *fully* encircle the limb which is required in the sdEMG technique. Since ICA does not require any prior information about the source spatial locations, except for the requirement of the sources not moving relative to the sensors (electrodes), the IED spacing is not crucial and can be variable. Consequently, previous studies have used custom-made electrodes fitted to elasticised bands to accommodate a variety of participant limb diameters.

In the context of the present study, the *forearm window* was defined as a 60mm wide region of the forearm, the midline of which was offset proximally by ~50mm from the styloid process of the ulna as shown in Figure 4.2. This region falls roughly in the distal third of the forearm as measured from styloid process of the ulna to the olecranon at the elbow. The present study implemented 64 reusable electrodes that encircled the limb

[25] The human body is susceptible to electromagnetic interference (EMI) due to the presence of parasitic capacitances between the body and electromagnetic sources including 50/60 Hz AC power lines. Power line noise is more prevalent in monopolar EMG as these signals retains the common-mode EMG potentials. A Driven Right-Leg circuit (DRL) is implemented to remove excessive noise by injecting an averaged, inverted current into the body thus actively reducing the common-mode potential and removing most of the 50/60 Hz power line noise.

within the *forearm window*. Commercially available disposable individual electrodes were found to be too large to fit 64 electrodes within the forearm window, therefore custom-made reusable electrodes were built.

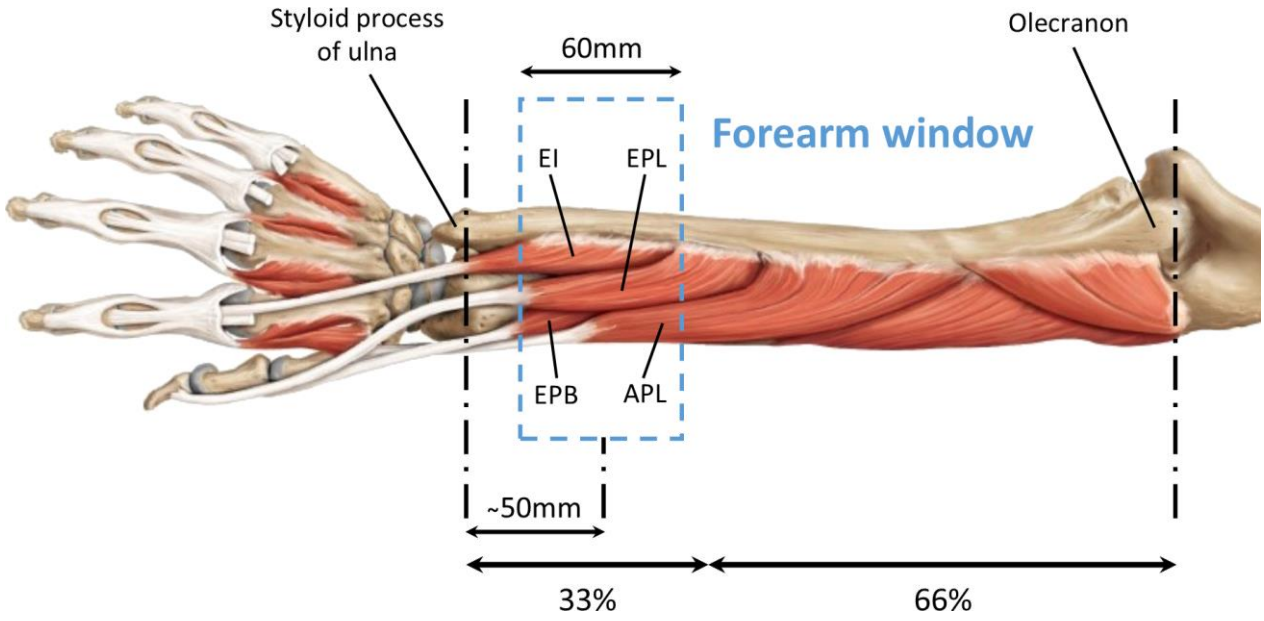

Figure 4.2 – Posterior view of the deep muscle compartment indicating the location of the forearm window in relation to the underlying forearm musculature.

EI – Extensor indicis, EPL – Extensor pollicis longus, EPB – Extensor pollicis brevis, APL – Abductor pollicis longus.

The forearm window encircles three of the deep muscles under investigation: EI, EPL and FPL. FPL is not visible as it is located in the anterior intermediate compartment of the forearm.

Image adapted from Schuenke et al. (2010).

Figure 4.2 shows that extensor pollicis brevis (EPB) and abductor pollicis longus (APL) also lie within the forearm window which does not form part of the muscles under investigation. These neighbouring muscles were considered in the development of movement protocol (Section 3.2) as well as in the design of the testing platform (Section 4.2.3) to ensure they remained *inactive* during participant testing.

The reusable electrodes were made from a 0.5mm sterling silver plate (92.5% Ag) that was cut into 10×3mm (L×W) rectangular pieces where the electrode length was placed parallel to the muscle fibres in accordance with SENIAM guidelines for sEMG electrodes (Hermens et al., 1999).

Perspex® electrode holders were designed to house the electrodes as shown in Figure 4.3 and the assembled electrode bands are presented in Figure 4.4 and Figure 4.5. The electrode holders incorporated a conductive paste reservoir (~0.5mm deep) and a slot for the elastic strap used to form the electrode bands as shown in Figure 4.3 (b). Each electrode plate was soldered onto a gold-plated male header pin which mates with the wire leads via female crimp connectors as shown in Figure 4.3 (a) and Figure 4.4. This connection type was preferred over direct 'wire-to-board' soldering as it allowed for the electrodes to be individually removed, cleaned and replaced if necessary.

The 64 electrodes were divided into three bands consisting of 20, 22 and 22 electrodes shown in Figure 4.5. The electrode band groupings were experimentally verified to fit comfortably within the forearm window for the smallest (170mm) and largest (215mm) participant circumferences tested in the present study.

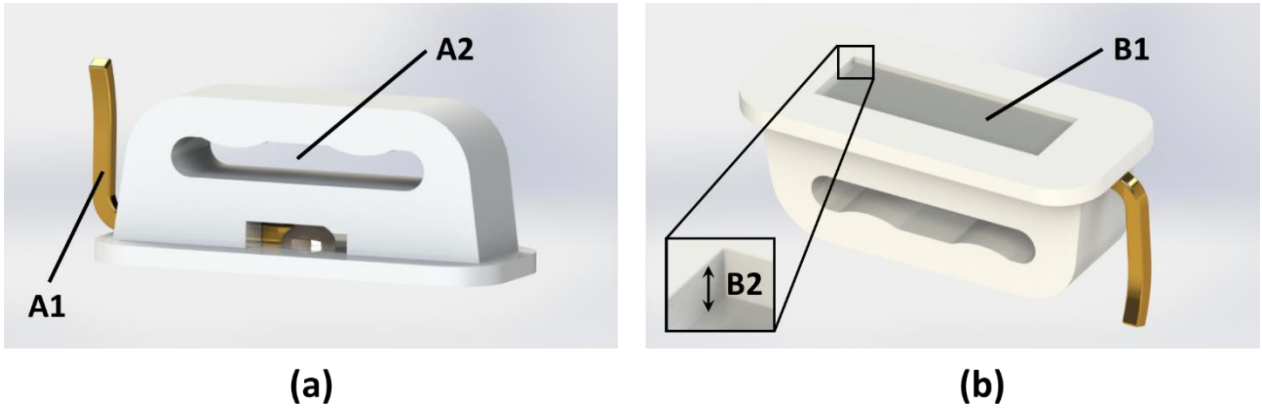

Figure 4.3 – Electrode holders (rendered in Solidworks® 2014).

(a) *Front oblique view showing the gold-plated male header pin connector (A1) with a bent vertical shaft used to friction lock wire leads to the electrodes. The elastic strap slot (A2) is also shown with friction extrusions along the top slot surface.*

(b) *Bottom oblique view showing the sterling silver electrode plate (B1) and conductive paste reservoir (B2).*

Figure 4.4 – Assembled electrode band highlighting the crimp connections used for the lead wires.

The crimped wire connectors were insulated with black heat-shrink and friction-locked to the electrode pin headers.

Figure 4.5 – Final assembled electrode bands consisting of 20, 22 and 22 electrodes each.

The 20 electrode band was attached to the distal end of the forearm window which had the smallest circumference.

The inter-electrode distances could be adjusted to match each participant's forearm circumferences ensuring the electrodes fully encircled the limb.

4.2 Testing Apparatus

Muscle contractions in an sdEMG study can either be isometric (static movements) or isotonic (dynamic movements) which lead to different apparatus design considerations. Timed movement protocols are defined with a fixed movement window duration (e.g. 5 seconds), however, in practice participants are unable to perform movements at the exact contraction onset and offset times. To ensure the *processed ICs* and the *predicted EMG waveforms* are synchronised, muscle activation time detection was required using electronic sensors. The processed ICs and predicted EMGs will be defined and discussed in Chapter 6.

The implementation of these sensors requires apparatus that attaches to the participant as well as a testing platform to prevent unwanted movements during testing. The following will be a discussion of the experimental equipment requirements as well as the details of the developed testing apparatus.

4.2.1 Contraction Detection

In the context of an sdEMG study, a static movement protocol (isometric contractions) requires force measurements and a dynamic movement protocol (isotonic contractions) requires position measurements (linear or rotational) to determine muscle activation timings.

Previous sdEMG studies implemented strain gauges to measure the exerted force during static movement protocols in order to detect when muscle activation occurs. In contrast, dynamic movement protocols require position measurements using sensors that are able to elongate further than strain gauges, which typically have a maximum translation of 10% relative to the gauge length (typically 5 to 15mm long).

Dynamic movements can be linear, rotational or a combination of both. Linear movements can be measured using, but not limited to, capacitive sensors or linear-to-rotational linkages connected to a potentiometer or optical encoder. Rotational movements can be measured using, but not limited to, flex sensors, potentiometers or optical encoders. These are a few easy to integrate sensor options however there are more complex sensors such as accelerometers which could be considered, however, they require additional signal processing to obtain the synchronisation markers needed for the sdEMG technique.

Once the appropriate sensor has been selected, operational circuitry may need to be developed. Sensors may operate at a different voltage level than the EMG data recording system and subsequently will require signal conditioning through additional circuitry, possibly including an amplification or attenuation stage.

The present study used four *Spectra Symbol®* 2.2” flex sensors, shown in Figure 4.6 (a), to measure finger joint rotation about the thumb IP, index finger MCP & PIP and ring finger MCP joints. These sensors work on the same principle as strain gauges, elongation (due to bending) of the sensor results in resistance changes that can be measured using an appropriate resistor network circuit with voltage amplification.

Flex sensors are more robust than strain gauges thus an adjustable resistor divider circuit with high output impedance buffer was sufficient signal conditioning as shown in Figure 4.7. The finger joint rest positions and the nominal resistance of the flex sensors were variable therefore a 100kΩ potentiometer was included in the circuit to allow for individual sensor calibration. Due to the large deflection (10-100kΩ) of the flex sensors during finger flexion (see Figure 4.6 (b)), the measured output range was greater than 1V for all sensors when referenced to a 0-5V supply. The *OT Bioelettronica® EMG-USB2* biopotential amplifier has a 1.22mV ADC resolution (12-bit) on the auxiliary channels, therefore a 1V deviation (820 increments) was deemed

sufficient to obtain accurate synchronisation signals without external amplification. The circuit diagram implemented is presented in Figure 4.7 and the built circuitry is shown in Figure 4.14.

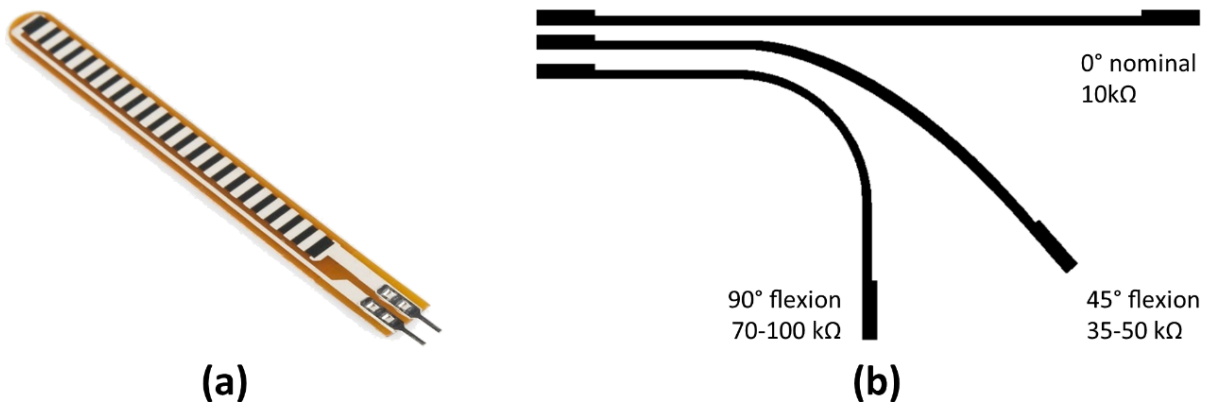

Figure 4.6 – Spectra Symbol® flex sensor (a) and typical resistance values during flexion (b).

Image credit (a): www.sparkfun.com. Image (b) adapted from Syed et al. (2012).

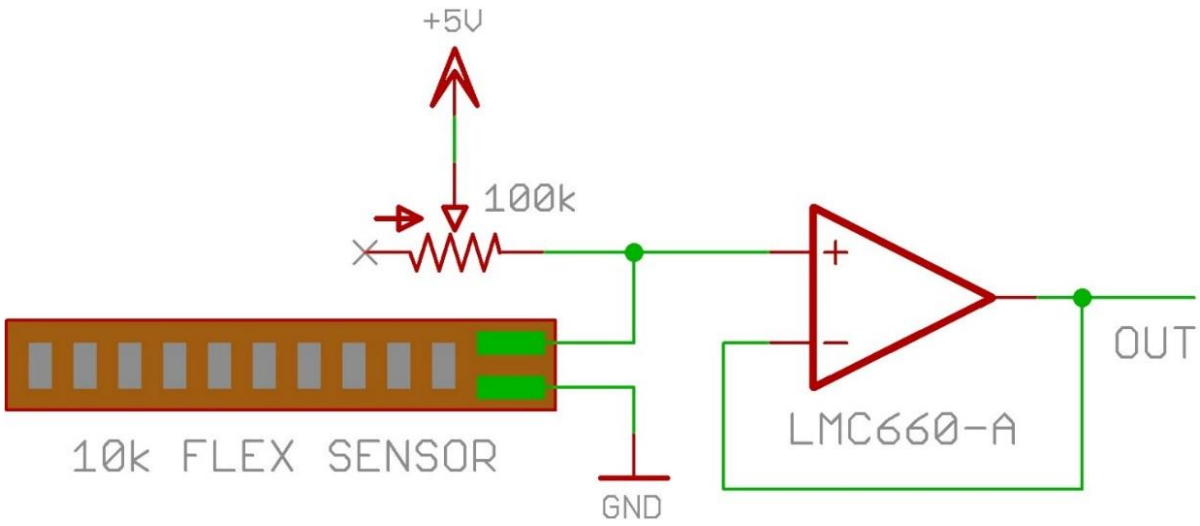

Figure 4.7 – Adjustable flex sensor amplifier circuit diagram.

The voltage divider stage was set up so that an increase in flexion resulted in an increase in output voltage. An input-output and rail-to-rail LMC660 operational amplifier was used for the impedance buffer stage to ensure the low impedance resistor divider did not overload the auxiliary inputs of the biopotential amplifier.

4.2.2 Sensor Attachments

After the appropriate sensors are selected for contraction detection, suitable sensor attachments are required to fit the sensors onto the participant. It is essential that the attachment apparatus is well placed to measure the force or position changes due to the targeted contractions in the movement protocol. The attachments should also be comfortable and not restrict blood flow to the limb.

Finger movements were tested in the present study which required flex sensors to be placed around the various finger joints. The flex sensors were placed on the dorsal side of the phalanges for the PIP joints, and on the dorsum for the MCP joints. With this type of sensor placement, there was a radial offset from the finger joint centre-of-rotation (COR) and the arc formed by the flex sensor during finger flexion as illustrated

in Figure 4.8. As a result of the radial offset, the flex sensor slides along the top of the finger during flexion and extension, therefore, it could not be fixed directly on to the phalanges on either side of the joint.

A representative kinematic diagram for a finger joint is presented in Figure 4.8 highlighting the flex sensor translation effect. The flex sensor is fixed to the top of the proximal phalanx (right finger segment) and is shown horizontally at 0° with a nominal 55mm length, and also at a 45° bend while maintaining the same nominal 55mm length. In the horizontal position (0°) the flex sensor endpoint is set at a 40mm radial distance from the fixed COR. This point on the dorsal phalanx (left finger segment) translated by 6.68mm when flexed to the 45° position.

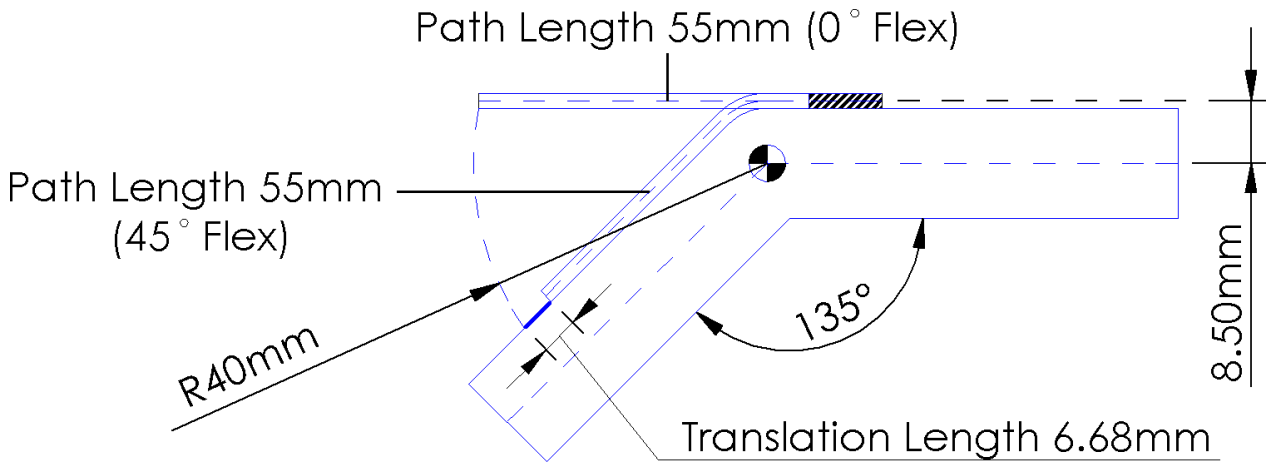

Figure 4.8 – Representative kinematic diagram for a finger highlighting the flex sensor translation effect experienced during flexion.

Translation occurs due to the offset between the finger dorsal surface and the joint centre-of-rotation which introduces an increase in arc length at the joint apex during flexion. Strictly speaking the flex sensor increases in length due to plastic deformation, however, this is minuscule in comparison to the sensor length.

The translation effect is due to the dorsal surface being situated at an 8.5mm radial offset from the joint COR which introduces an increase in arc length at the joint apex during flexion. The translation distance is considered large enough to prevent natural flexion if the sensor was fixed on both phalanges. To account for the translation, finger exoskeletons were built to fix the flex sensor to the proximal side of the joint and allow the flex sensor to slide within a slot embedded in the distal segment as shown in Figure 4.9 and further illustrated in Figure 4.10. The finger exoskeleton segments were designed for the thumb proximal and distal phalanges, index proximal and middle phalanges as well as the ring proximal phalanx.

A cross-sectional view of the index finger sensor attachments is presented in Figure 4.10 highlighting the flex sensor placements. For participant testing the PIP joint flex sensor was fixed to the proximal phalanx while the MCP joint flex sensor was fixed to the dorsum of the hand. The PIP joint flex sensors were fixed using friction locks between the sensor slot and the heat-shrink insulation around the wire connection terminals. The MCP joint flex sensors were fixed using adhesive tape and further secured using a *Velcro®* strap wrapped around the hand.

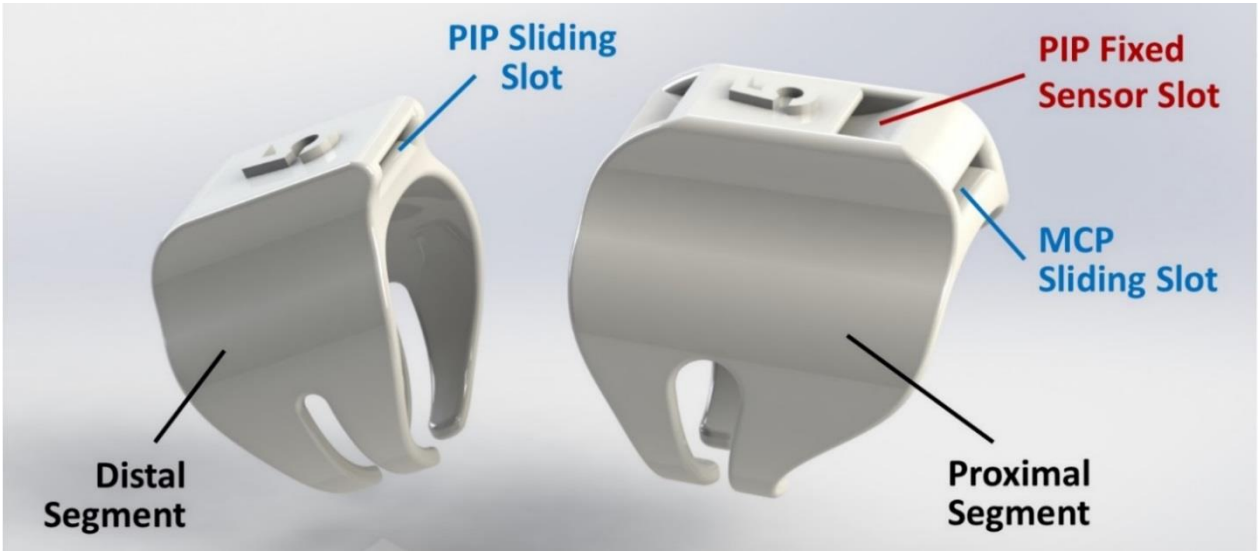

Figure 4.9 – Index finger exoskeleton segments outlining their design and core features.

Finger exoskeleton segments are shown where the proximal segment attaches to the index proximal phalanx and the distal segment attaches to the index middle phalanx.

The finger exoskeleton segments have four prongs that wrap around the finger which provides a flexible and comfortable attachment mechanism.

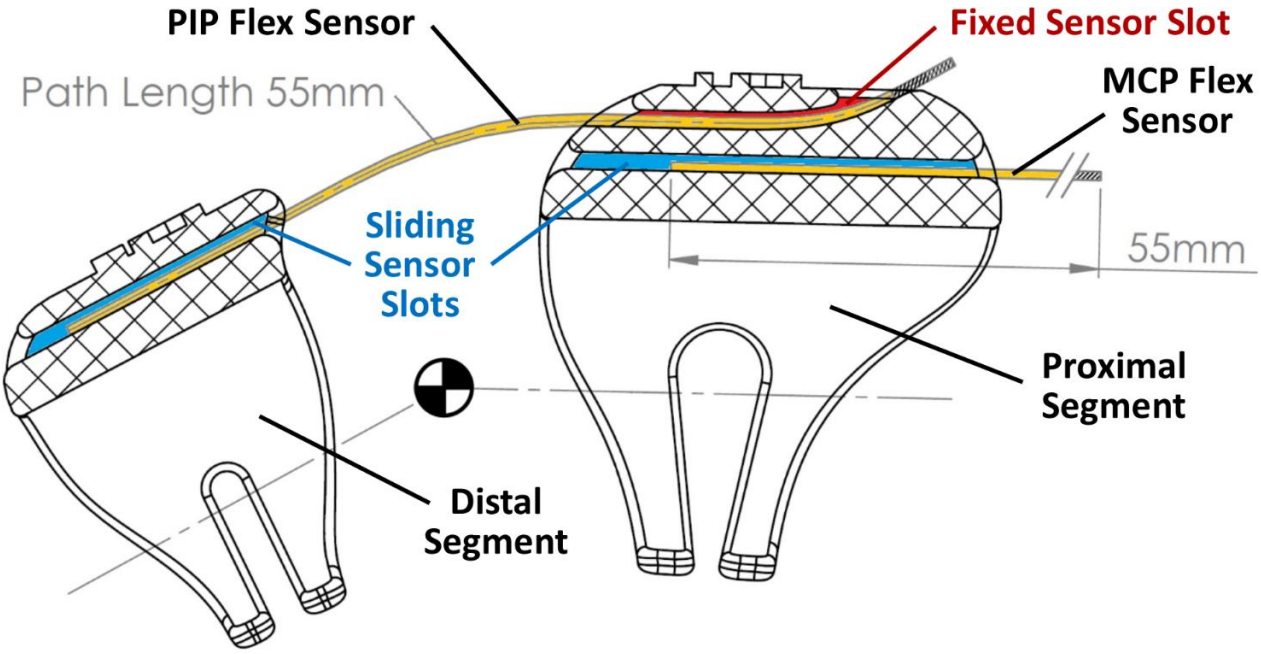

Figure 4.10 – Cross-sectional view of the index finger exoskeleton segments with flex sensors inserted.

The bending region of the flex sensor is shown above the joint COR, however, there is a minor bend at the entrance of the fixed sensor slot. This bend stays constant thus it would not influence the measurements during flexion and extension.

The five finger segments were modelled on the Author's hand and scaled smaller and larger resulting in ten different sizes of each segment to account for a wide range of participant finger sizes. The segments were 3D printed in Acrylonitrile Butadiene Styrene (ABS) plastic. The segments were sandpapered and treated with acetone vapour resulting in a smooth finish to make the attachments comfortable as shown in Figure 4.11.

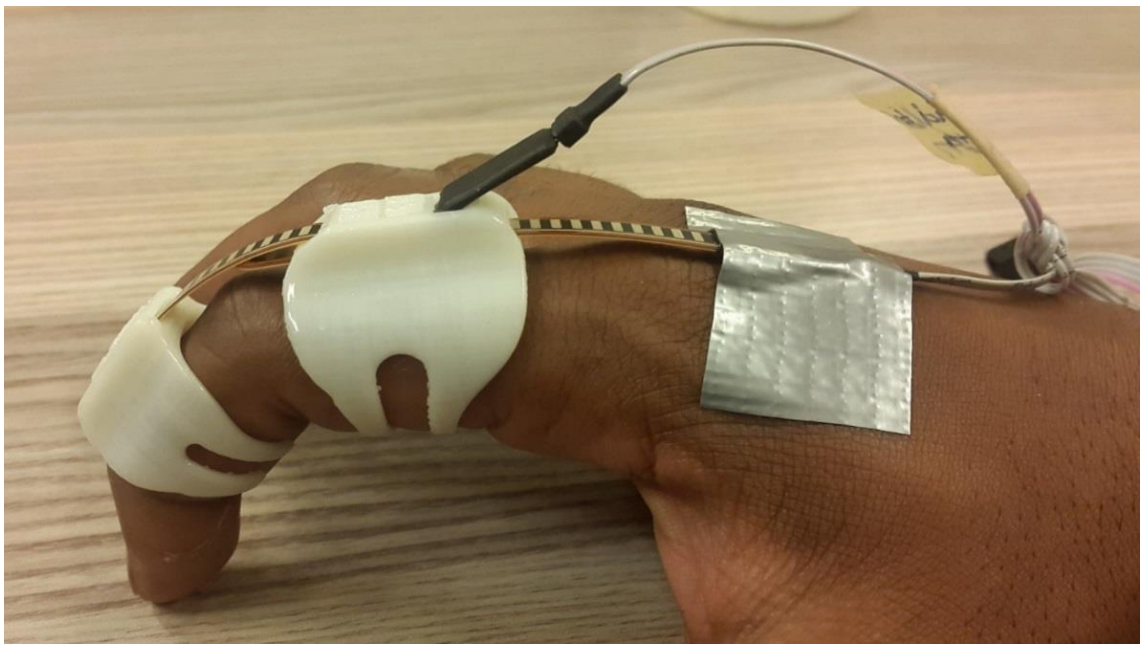

Figure 4.11 – Index finger exoskeleton segments attached to right hand.

4.2.3 Testing Platform

The sdEMG technique relies heavily on the crosstalk phenomenon in the recorded monopolar EMG signals to comprise of EMG activity from the muscles activated during the MP, therefore it was crucial to minimise unwanted contractions from neighbouring muscles not pertaining to the instructed movement. To assist with this task a suitable testing platform was built with movement restriction components.

In the present forearm study, upper arm contractions were not tested therefore this region was supported in a rest position to ensure minimal muscle activity during testing. The finger joints that were not activated in the MP were kept in a state of rest using a moulded forearm splint and *Velcro®* straps. While the restraints implemented may have inhibited *dynamic movements,* unintended *isometric contractions* (static muscle contractions *without* skeletal movement) may have occurred. For example, semi-independent flexion of any of the 2nd to 5th digits will activate the common FDS and FDP muscles in spite of any applied restraints on the other digits.

In Figure 4.2, EPB and APL were identified to also lie within the forearm window which could result in the recording of unintended contractions. To reduce activation of these muscles, the designed testing platform restricted thumb MCP extension (the function of EPB) and thumb abduction (the function of APL). The purpose of the restricted setup was to provide the participant with a structure that supported the weight of the hand and arm which assisted the participant in maintaining the rest position during testing.

In the present study, the forearm was required to be in a pronated position with only the interphalangeal and metacarpophalangeal finger joints free to move. The designed forearm testing platform is presented in Figure 4.12 consisting of a wooden base, an extended forearm splint and *Velcro®* straps.

The Author's forearm was moulded using thermoplastic splint material by Ms Hannarie le Roux – an Occupational Therapist at Groote Schuur Hospital. During testing, the arm platform was positioned to ensure the upper arm was perpendicular to the forearm and at a comfortable distance from a participant's body. This orientation enabled the participant to relax the upper arm muscles during testing. Further details regarding the testing apparatus setup will be discussed in Section 5.2.

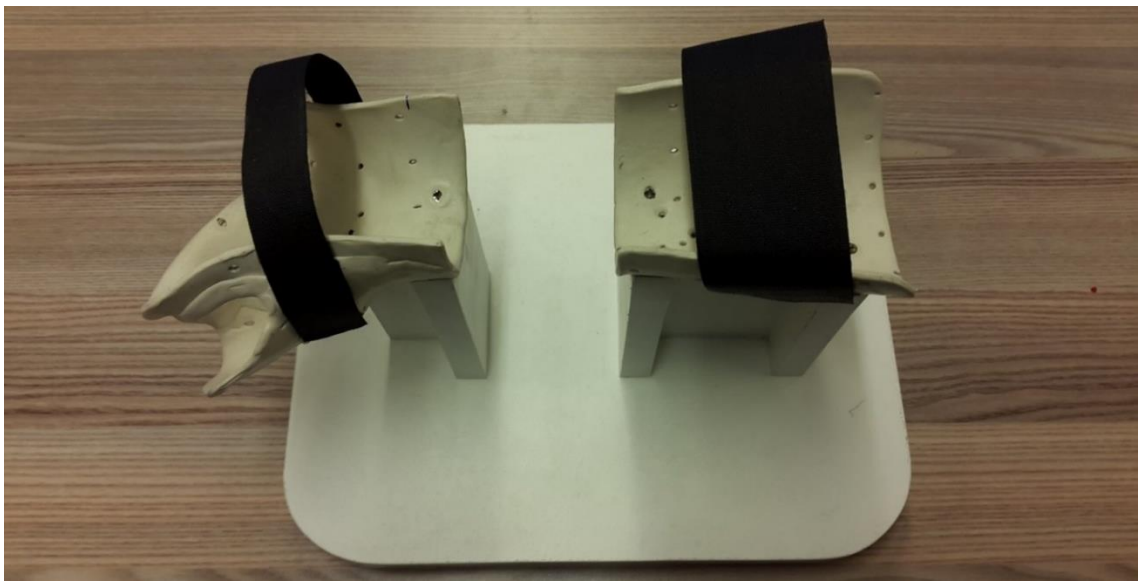

Figure 4.12 – Forearm testing platform built to restrict unwanted movements during testing.

The splint has a gap in the forearm window region to accommodate the electrode bands that encircle the forearm. The thermoplastic used was semi-flexible and able to bend to match the contours of each participant's forearm.

4.3 Participant Instruction

During testing, participants need to be instructed on when to start and stop specific contractions in the movement protocol. While auditory cues are an option, this would require participants to memorise the movements which is an unrealistic task and may result in mistakes during testing. Furthermore, it would be difficult for participants to complete a randomised movement protocol based solely on auditory cues.

Visual instructions are intuitive and can be implemented using a Human-Machine Interface such as a computer monitor or standalone display paired with a Graphical User Interface. Depending on the complexity of the study, text instructions may suffice however images indicating the movements to be performed are preferred. Additionally, feedback mechanisms can be implemented such as force and angle readings to ensure sustained contractions, as well as to verify that the correct movements are being executed.

4.3.1 Human-Machine Interface

A Human-Machine Interface (HMI) display device is required to present visual instructions to the participant during testing. It is essential that the display device and EMG recording system be synchronised, which can be achieved using a start trigger signal. The ideal contraction onset and offset markers needed for contraction synchronisation can then be calculated using the predetermined movement window duration (e.g. 5).

In an sdEMG system, it is convenient to use a standalone display device so that the output trigger signal can be recorded as an auxiliary signal on the EMG recording system resulting in a single data file containing synchronised EMG and sensor signals.

The participant instruction system developed for the present study used a standalone *ITEAD Nextion® 7" HMI* touchscreen display controlled by a custom-built microcontroller development board which synchronised the movement instructions with the EMG and auxiliary data acquisition. The display was mounted on a wooden base with 3D printed holders set at a comfortable 75° viewing angle as shown in Figure 4.13 and the developed electronics are shown in Figure 4.14.

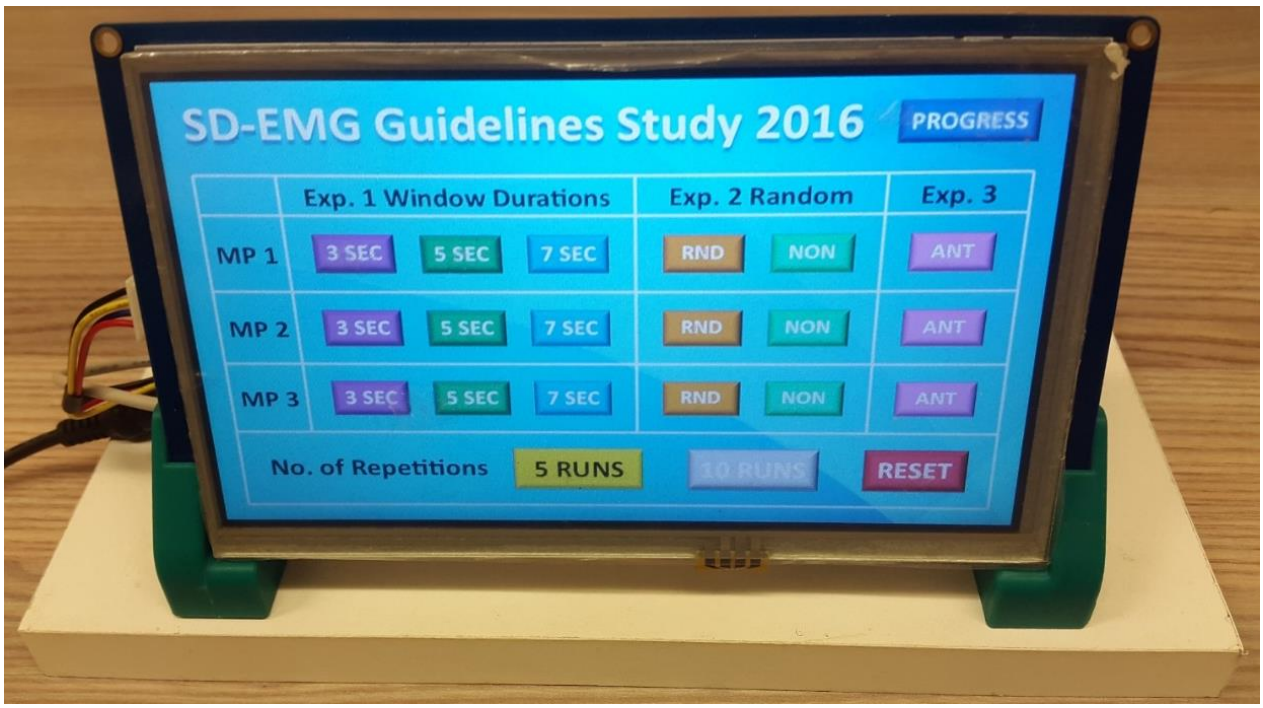

Figure 4.13 – ITEAD Nextion® 7” HMI touchscreen display showing the developed GUI.

The home screen of the developed GUI is shown presenting the experiment and test options. The GUI is controlled by a microcontroller and the touchscreen was used for user input and test selection.

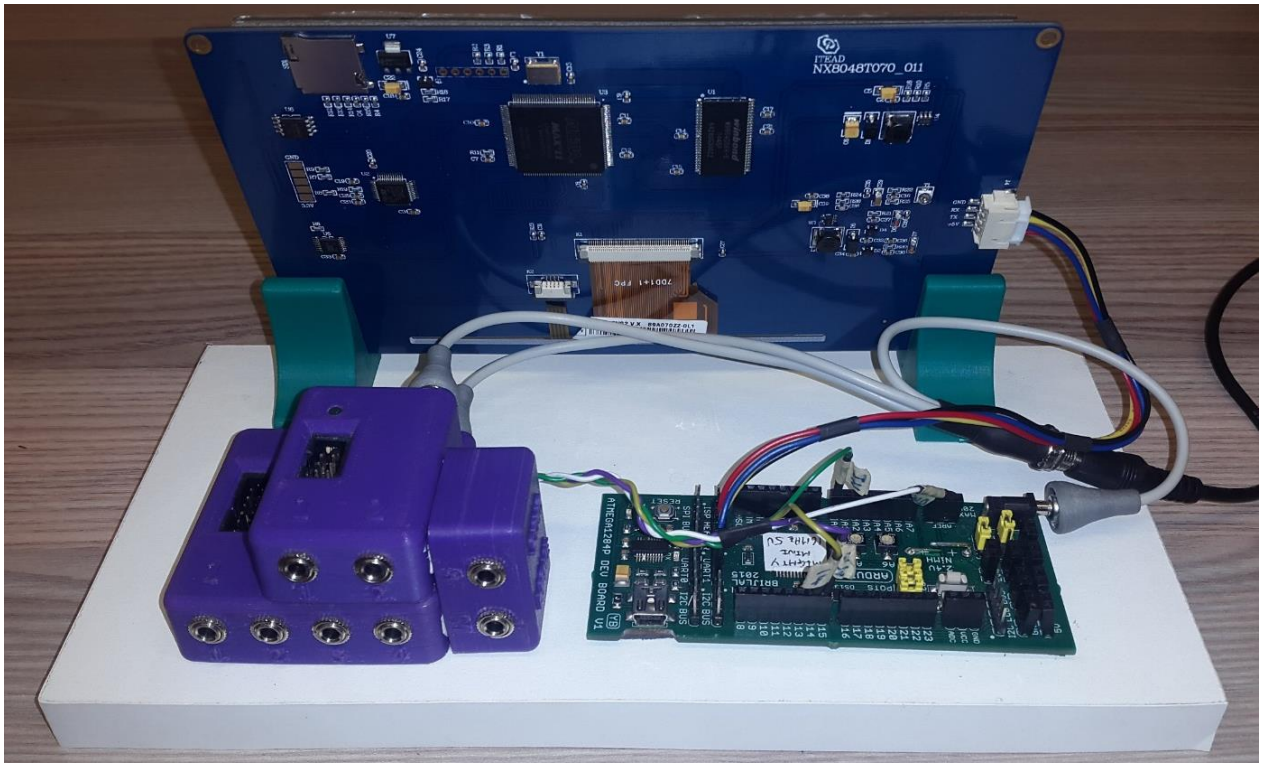

Figure 4.14 – HMI and flex sensor electronics developed for the Participant Instruction System.

Adjustable flex sensor amplifiers and synchronisation buffer circuitry are shown on the left, housed in purple ABS plastic boxes. The buffered outputs are connected to the auxiliary input channels of the biopotential amplifier via 3.5mm mono audio jacks to BNC connector cables (not shown).

The custom-built microcontroller development board is shown on the right, which controls the display, loads the required test images to the HMI and outputs the synchronisation signals to the buffer circuitry.

4.3.2 Graphical User Interface

Within the context of an sdEMG study, a Graphical User Interface (GUI) is required to *'playback'* a timed slideshow of the movement protocol from an image database in a specific sequence. The images presented should provide clear instructions on how to perform the movements without distracting the participant. In a randomised movement protocol, the controlling device (computer or microcontroller) would need to send the randomised contraction sequence to the GUI program which would change the 'playback' order of the images accordingly.

A robust GUI was developed that featured multiple experiment modes including three different movement protocols options, as shown in Figure 4.13. One movement protocol was used in the present study however the additional functionality was included for future studies.

As an example, the visual movement instructions for Group flexion as displayed on the HMI during participant testing is shown in Figure 4.15. Prior to the displayed Group flexion image, a rest image was displayed for 3 seconds which was selected as the movement window duration for this experimental run. The participant was instructed to complete and hold the Group flexion position for 3 seconds thereafter another rest image was shown. This process was continued for all the movements in the MP and repeated for the desired number of experimental runs.

Similar visual instructions were used for the other movements implemented in the MP and the complete set of the visual cues implemented in the present study can be found in Appendix C.

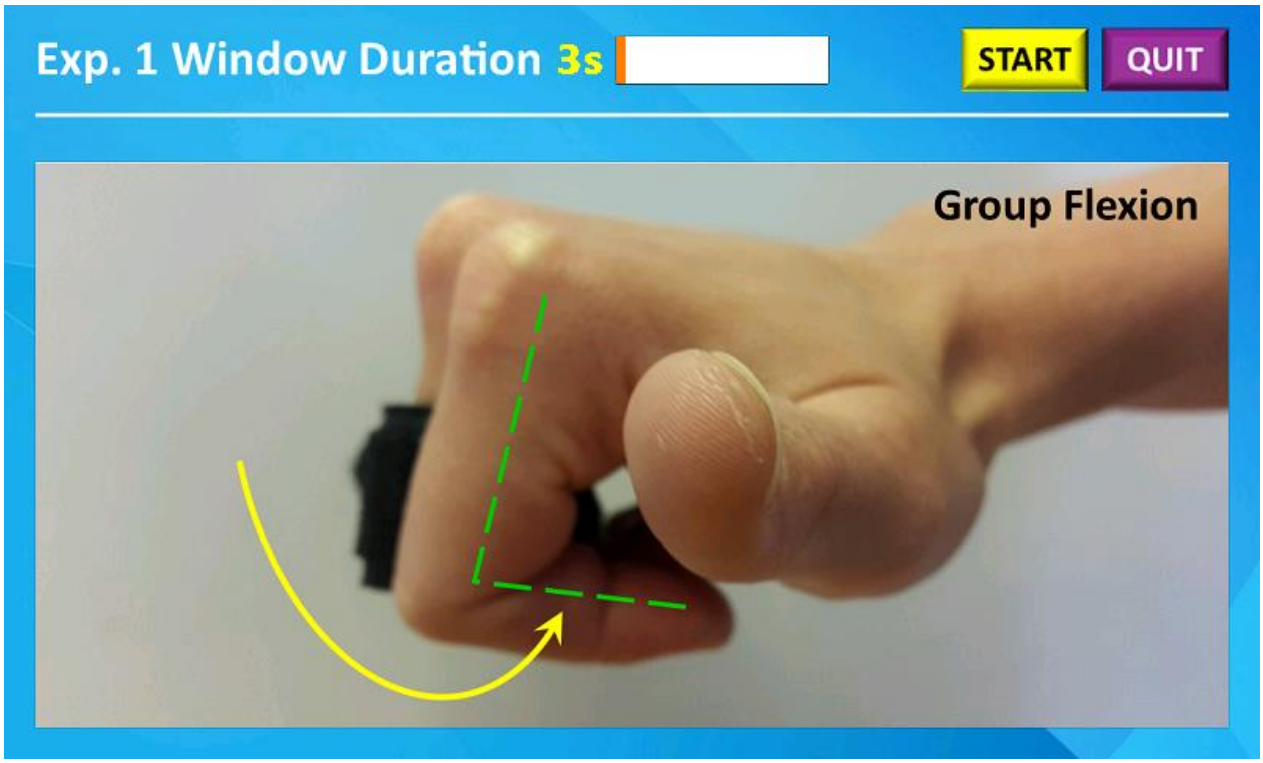

Figure 4.15 – GUI screenshot of the participant instruction for the Group flexion movement.

The yellow arrow indicates the finger movement required from the natural semi-flexed rest position. The green dashed line indicates the final position that muscle be held for 3 seconds.

An orange progress bar for the current test run is shown as well as the start/stop and quit buttons which were operated by the researcher. The start/stop button allowed for test runs to be reset if there were any participant mistakes or data recording errors.

Part C – Implementation of an sdEMG System

Part C outlines the implementation of the sdEMG technique in the detection and isolation of the extrinsic muscles of the hand. The experimental procedures taken to acquire the data from participants are described in Chapter 5 and the data processing steps are detailed in Chapter 6.

Chapter 5 - Data Recording

This chapter outlines the experimental procedures followed in the present study to conduct participant testing. Ethics approval for the testing was granted by the University of Cape Town's Research Ethics Committee (HREC Reference Number: 846/2014) for the study titled: *Identifying Extrinsic Muscles of the Hand Using Non-invasive Deep Muscle Electromyography.* Informed consent was obtained from all participants and the experimental testing procedures were conducted in accordance with the Declaration of Helsinki (WMA, 2013), ICH Good Clinical Practice (ICH, 2015) and the laws of South Africa.

5.1 Participants

Five healthy, right-hand dominant male participants (mean ± SD; age: 24 ± 3 years) without any history of neuromuscular diseases or disabilities were recruited for the study. A group of five participants was deemed sufficient to determine the feasibility of using the sdEMG technique to detect and isolate the extrinsic hand muscles and to identify trends from which preliminary experimental guidelines could be developed.

Anthropometric measurements were taken before participant testing as they were needed to customise the experimental apparatus (described in Section 5.1.2). The anthropometric data for the participant population are summarised in Table 5-1.

Table 5-1: Participant population anthropometric characteristics.

Physical measurements	Mean ± SD	Units
Age	24 ± 3	years
Height	179 ± 5	cm
Weight	75.8 ± 5.9	kg
Distance from styloid process of ulna to olecranon	268 ± 11	mm
Distance from styloid process of ulna to Electrode Band 1	34 ± 9	mm
Distance from styloid process of ulna to Electrode Band 2	54 ± 10	mm
Distance from styloid process of ulna to Electrode Band 3	69 ± 8	mm
Forearm circumference of Electrode Band 1	180 ± 11	mm
Forearm circumference of Electrode Band 2	190 ± 11	mm
Forearm circumference of Electrode Band 3	205 ± 10	mm

5.1.1 Skin Preparation

Skin preparation is required in surface EMG acquisition to reduce the skin impedance due to dead skin cells and ensure stable electrode placement by removing dirt and sweat (Hermens, Freriks, Disselhorst-Klug, & Rau, 2000). Each participant's forearm was cleaned thoroughly using *Spes Medica® Everi* abrasive paste and dried with a clean towel. Their wrists were cleaned to attach the conductive *DRL Out* (left wrist) and *DRL In* (right wrist) straps. Their right elbow was also cleaned to attach the *Amplifier Reference* and *Patient Reference* electrodes on the olecranon. These connections and placements will be further discussed in Section 5.2.1.

5.1.2 Apparatus Customisation

A number of measurements were recorded from each participant which were used to customise the experimental apparatus to match the forearm anatomy of each participant.

Electrode Band Customisation

The electrode bands were modified based on the measured forearm circumferences, in order to maximise the EMG pick-up region within the *forearm window*. The 64 electrodes were divided into three bands of 20, 22 and 22 electrodes fastened to elastic straps. As discussed in Section 4.1.2, ICA does not require any prior information about the source (electrodes) locations, therefore the inter-electrode distance (IED) spacing was not crucial and could be variable. Participant forearm circumferences ranged between 170mm and 215mm, therefore the individual electrodes were spread out regularly along the elastic straps to ensure the electrode arrays fully encircled each participant's forearm in accordance with the sdEMG requirements described in Section 1.1.1.

A customised electrode band is shown in Figure 5.1 consisting of 20 electrodes for a participant with a 170mm distal forearm circumference. The IED was modified to allow for an approximate 15mm offset between the last electrode and the circumference length point (170mm) to allow the band to be stretched tightly when strapped to the participant. This offset also ensured for the last electrode was positioned close to the first electrode (adjacent to the elastic band buckle) when stretched, thereby fully encircling the forearm with electrodes.

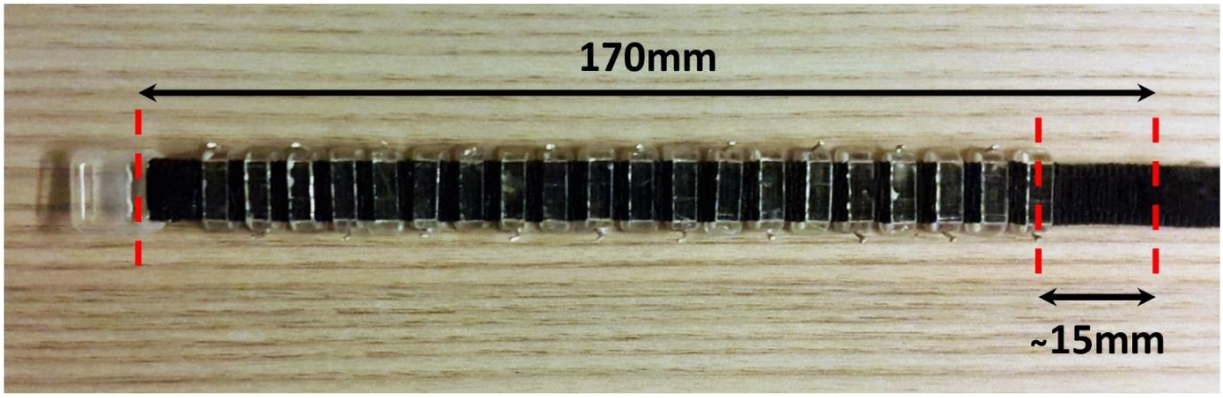

Figure 5.1 – Customised electrode band with variable inter-electrode distances also indicating the offset required to fully encircle the forearm with electrodes.

The diagram is not to scale.

Sensor Attachment Customisation

The sensor attachments were selected to ensure the contraction detection sensors remained in place during testing. Prior to setup, participants were provided finger exoskeleton segments that attached firmly to the; thumb proximal and distal, index finger proximal and middle, and ring finger proximal phalanges. These finger exoskeleton segments housed the flex sensors that allowed for joint finger movements to be measured during testing. An example of the contraction detection apparatus fitted on a participant is shown in Figure 5.2. The *Ring Group* defined in Section 3.1 was formed by strapping the proximal phalanges of the 3rd to 5th digits together using a *Velcro®* strap.

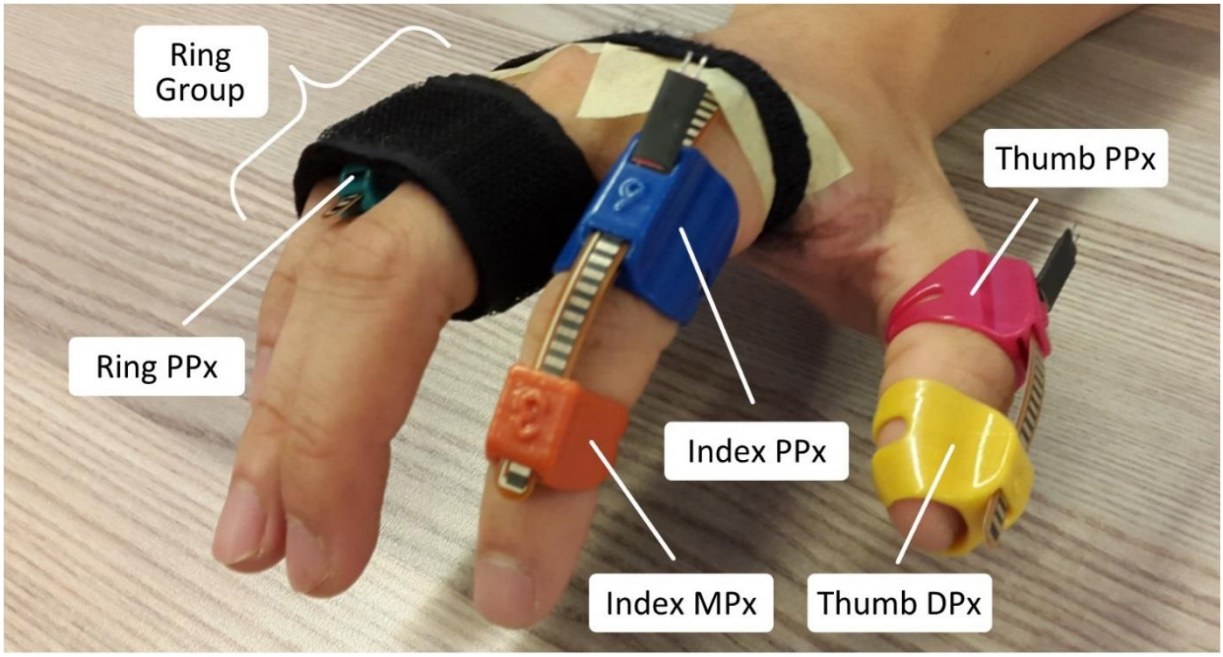

Figure 5.2 – Customised finger exoskeleton and flex sensor configuration on a participant.

PPx – Proximal phalanx, MPx – Middle phalanx, DPx – Distal phalanx.

The numbers on the finger exoskeleton segments indicate the different segment sizes used to realise the custom exoskeleton set.

5.1.3 Electrode Preparation

The testing platform was designed to accommodate various participant forearm diameters. It was important to standardise the placement of the electrodes bands across participants to allow for comparable results. The SENIAM electrode placement guidelines (Hermens et al., 1999) are typically used for this purpose however they do not include the deep FPL, EPL and EI muscles investigated in the present study. Instead, the *forearm window* was defined to standardise the location of the electrode bands to ensure the deep FPL, EPL and EI muscles were well encircled as illustrated in Figure 4.2.

The electrodes were polished using a wire brush to remove surface corrosion and cleaned using surgical alcohol before each participant was tested. The electrodes were coated with a thin layer of *Spes Medica® AC cream* – a commercial sEMG adhesive and conductive paste. The paste filled the reservoirs of the electrode holders shown in Figure 4.3 (b) and protruded ~1mm out to ensure firm contact with the skin.

After the paste was applied to the electrodes, the electrode-wire connectors were checked for loose connections by gently tugging on each lead. If a connection was found to be loose, the electrode header pin was bent to create a tighter friction lock. Broken electrode leads or electrode header pins were *not* repaired during testing. If found, they were noted in the participant testing notes and were repaired or replaced for the next participant testing session. During data processing at most two *'dead'* channels[26] were found in some datasets which were later removed as outliers – discussed further in Section 6.1.1.

[26] Dead channels refer to constant baseline signals with no signal activity, typically due to disconnected electrode leads.

5.2 Apparatus Setup

The EMG recording system was set up away from electrical noise sources such as AC power sockets and connected to a laptop for data acquisition using *OT BioLab®.* The test platform, HMI and the participant's seat were arranged ergonomically while allowing for the electrical connections to be made between the test equipment. The following sub-sections discuss the detailed setup of the test equipment as well as modifications required for the present study.

5.2.1 EMG Recording System

The EMG and auxiliary sensor data were recorded using an *OT Bioelettronica® (OTB) EMG-USB2* 256-channel biopotential signal amplifier. The EMG recording system was set up in *Referenced Monopolar* modality with the *Driven Right-Leg (DRL)* feature enabled as recommended in the system User Manual (Merlo, 2011). The EMG input channels also included a pre-amplification stage via four 16-channel monopolar active adapters (AD1x16SM5). Each active adapter had a separate *Amplifier Reference* connection and so the four reference connections were daisy-chained together to ensure *all* 64 EMG channels had the *same* voltage reference.

The OTB recommended 16-channel Referenced Monopolar EMG recording setup is presented in Figure 5.3 indicating the placements of the *Patient Reference*, *Amplifier Reference*, *DRL In* and *DRL out* electrode straps for sEMG measurements on the right arm.

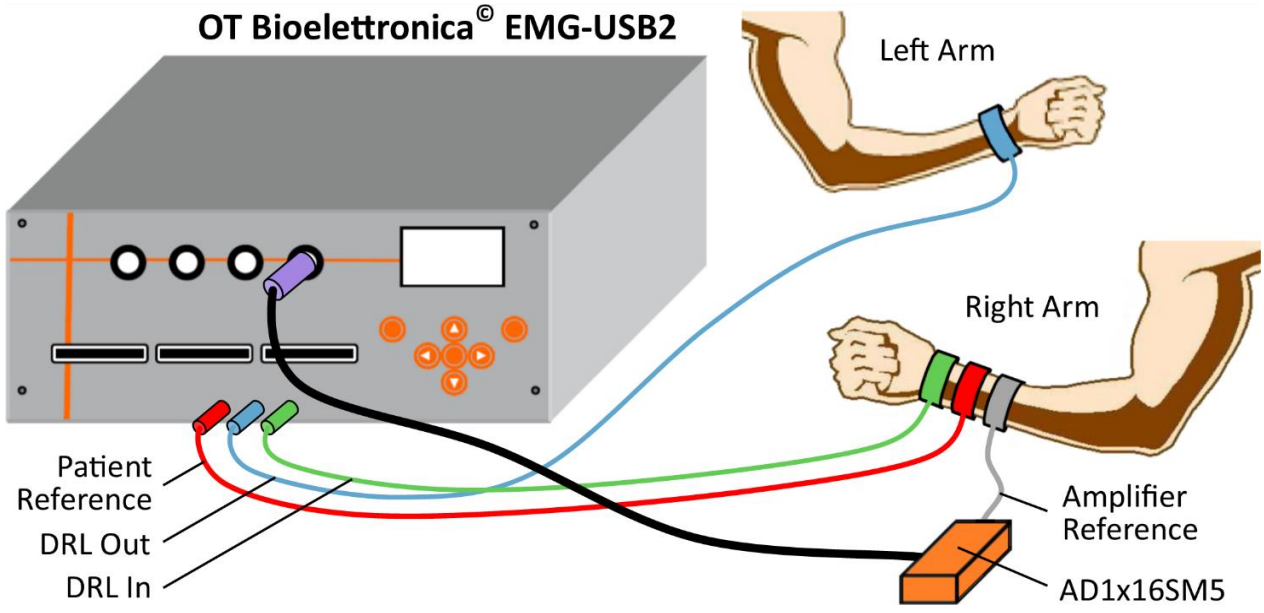

Figure 5.3 – OT Bioelettronica's recommended Referenced Monopolar EMG recording setup.

AD1x16SM5 – OTB 16-channel monopolar active adapter.

Image adapted from EMG-USB2 User Manual (Merlo, 2011).

The recommended recording setup presented in Figure 5.3 shows that the *Patient Reference*, *DRL In* and *Amplifier Reference* electrode straps occupy a large portion of the distal right forearm and would obstruct the placement of the electrode bands within the *forearm window*. Furthermore, this setup would also lead to the *DRL In* and *Amplifier Reference* electrode straps encircling the EI, EPL and FPL muscles as illustrated in Figure 5.4. These muscles are activated in the MP, therefore this arrangement was unacceptable since the *DRL In* and *Amplifier Reference* electrode straps needed to be placed on bioelectrically *inactive* regions.

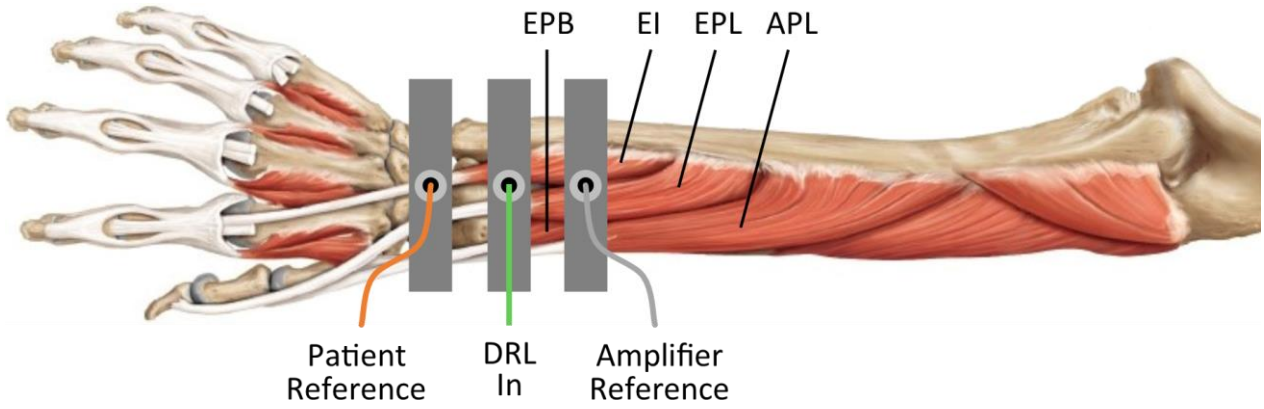

Figure 5.4 – OT Bioelettronica's recommended Patient Reference, DRL In and Amplifier Reference placements on the forearm.

EPB – Extensor pollicis brevis, EI – Extensor indicis, Extensor pollicis longus, APL – Abductor pollicis longus.
Image adapted from Schuenke et al. (2010).

Given the recording setup requirements for the present study, the *Patient Reference*, *Amplifier Reference* and *DRL In* straps were carefully repositioned away from the forearm window. The *Patient Reference* and *Amplifier Reference* connections were placed on the olecranon via disposable pre-gelled electrodes while the *DRL In* remained on the wrist as illustrated in Figure 5.5 and Figure 5.6.

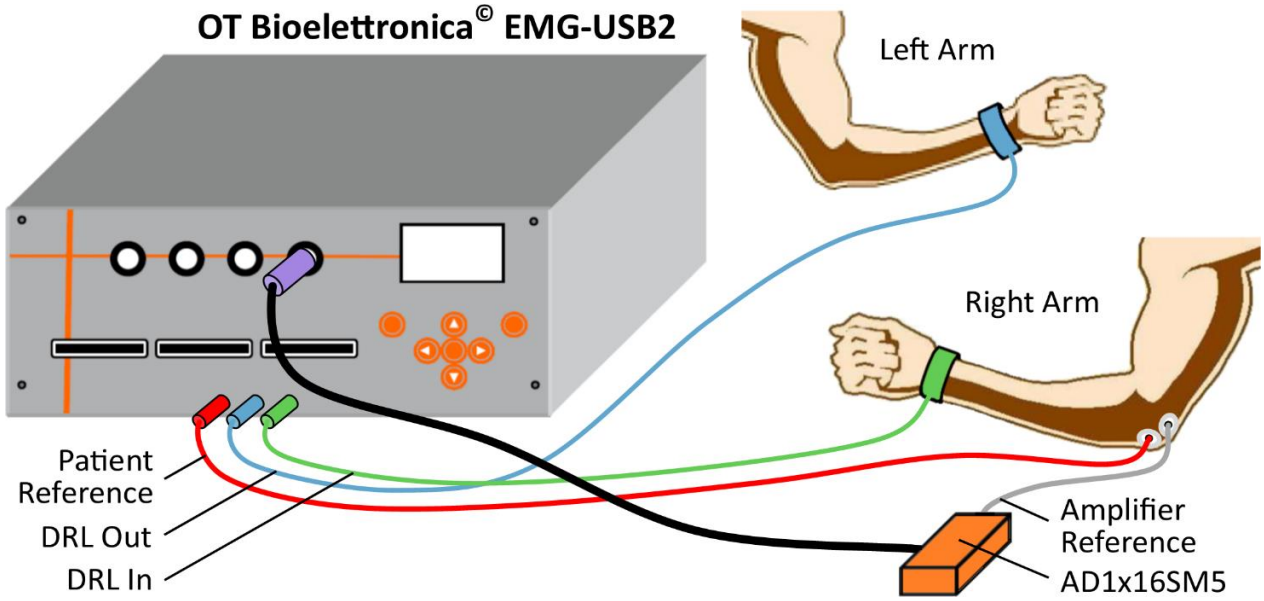

Figure 5.5 – Modified Referenced Monopolar EMG recording setup.

AD1x16SM5 – OTB 16-channel monopolar active adapter.
Image adapted from EMG-USB2 User Manual (Merlo, 2011).

The modified Referenced Monopolar EMG recording setup ensured that the *Amplifier Reference* and *DRL In* connections were on bioelectrically inactive areas without overlapping into the forearm window in which the electrode bands were placed as illustrated in Figure 5.6.

After the hardware was set up, the hardware and software settings indicated in Table 5-2 were applied and the complete EMG recording system was verified prior to participant testing.

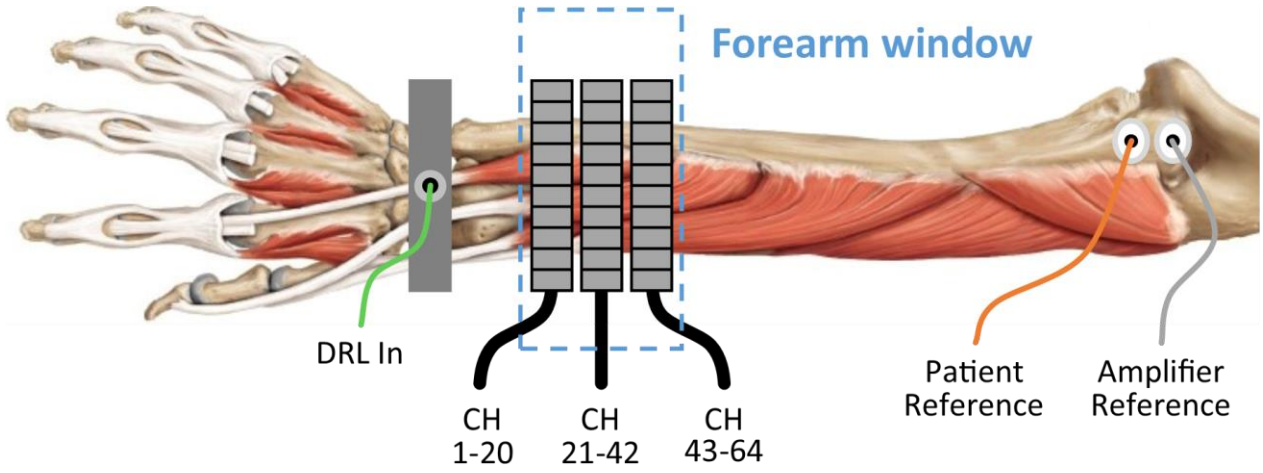

Figure 5.6 – Modified Patient Reference, DRL In and Amplifier Reference connection placements needed to accommodate the placement of the electrode bands within the forearm window.

Image adapted from Schuenke et al. (2010).

Table 5-2: Settings used for the OT Bioelettronica® EMG-USB2 recording system.

Setting	Selection	Comments
Recording mode	Referenced Monopolar	DRL connection required
Recording resolution	12-bit ADC	Equivalent to 4096 increments
Input channel mode	64 + 16	IN 1-4 and AUX IN
EMG inputs	IN 1-4	4 x 16-channel AD1x16SM5 adapters
Auxiliary inputs	AUX IN 1-5	Flex sensors and trigger signal
Sampling frequency	5,120 Hz	The standard 1,000 Hz was unavailable
Bandwidth	3-500 Hz	Separate high pass and low pass analog filters
EMG input gain	10,000 [V/V]	Applies to IN 1-4 and includes pre-amplifier gain (x5)
Auxiliary input gain	0.5 [V/V]	Applies to AUX 1-16

5.2.2 Graphical User Interface

Participants were instructed to execute the movements displayed on the GUI developed in Section 4.3.2. The experiments varying the movement protocol parameters were conducted as described below and will be expanded upon in Section 7.1.

- The *Timing experiments* investigated the effect of the MP movement window duration (3, 5 and 7 seconds).
- The *Randomisation experiment* investigated the effect of randomising the MP sequence.
- The *Anticipation experiment* investigated the effect of participants anticipating the next movement in the MP sequence.

As an example, a set of movement instruction images displayed on the GUI are shown in Table 5-3 for a fixed (non-randomised) movement protocol consisting of Group flexion, Group Extension, Group PIP flexion and Group PIP extension.

Table 5-3: First seven visual cues displayed on the GUI for a fixed movement protocol sequence.

Timing & Randomisation* Experiments		Anticipation Experiment	
A		H	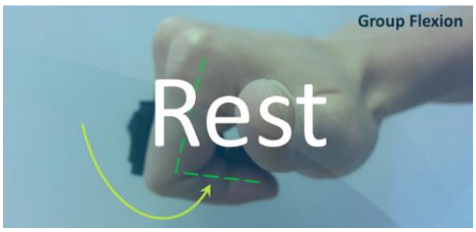
B	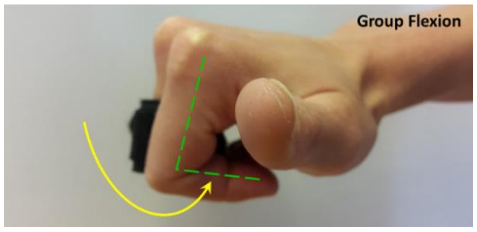	I	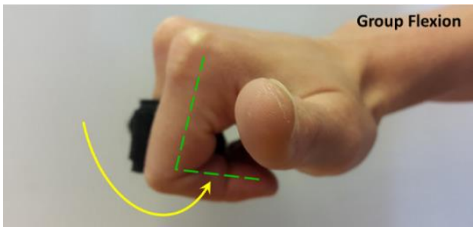
C		J	
D	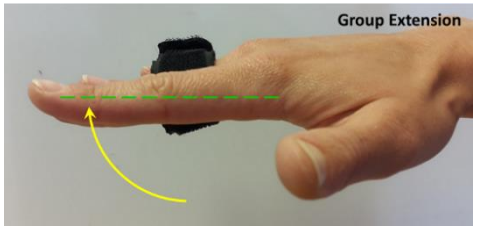	K	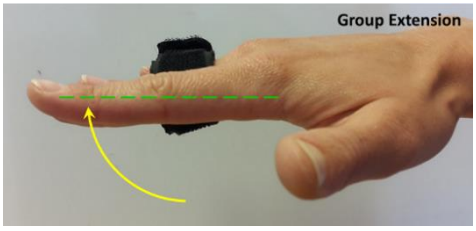
E		L	
F	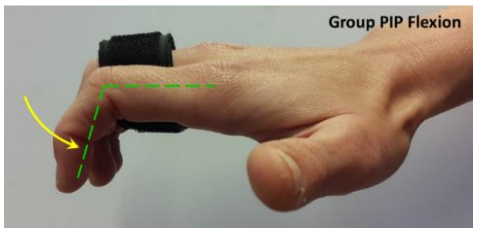	M	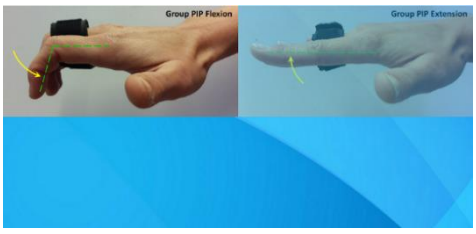
G	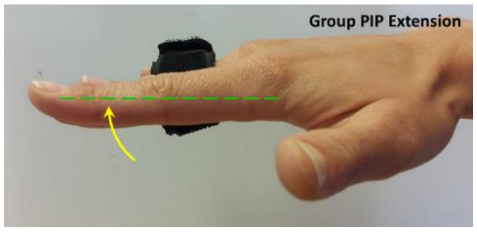	N	

Each row represents a sustained contraction corresponding to the selected movement window duration (e.g. 5 seconds).

** The Randomisation experiment uses the same images as the Timing experiment, however, the images are displayed in a randomised sequence. The anticipated images indicate the current movement to be performed in the foreground, and the next movement to be performed in the background (watermarked image). For example, image H instructs rest and informs the next movement to be performed is Group flexion.*

The visual cues used for the Timing & Randomisation experiments are shown by images A-G (column 1) and the visual cues used for the Anticipation experiment are shown by images H-N (column 2). Each image instructs a sustained contraction for the selected movement window duration (e.g. 5 seconds).

As shown in Table 5-3, the Anticipation experiment displays the movement that follows the current one as a watermarked background image, thus allowing for the anticipation effect to be investigated. Full-size images were used for all movements except Group PIP, and Index PIP flexion and extension. These consecutive movements were arranged in quadrants as illustrated in images L, M and N. The full set of visual cues used is presented in Appendix C, Table C-1 (Timing and Randomisation) and Table C-2 (Anticipation).

5.3 Participant Setup

After a participant's skin was prepared they were seated with their right forearm strapped into the testing platform, situated on a raised platform beside the seat. The seat height was adjusted to ensure their arms were aligned to an ergonomic 90° during testing. The HMI device was placed on a desk at a comfortable viewing height and distance in front of the participant. The electrodes and sensors were connected to the participant followed by a system verification procedure before experimental testing began as outlined below.

5.3.1 Electrode Placement

The electrode connection procedure began by attaching wet electrode straps for the *DRL In* on the right wrist and *DRL Out* on the left wrist. The *Patient Reference*, *Amplifier Reference* and electrodes were attached to the participant as indicated in Figure 5.6. The first and last electrodes of each band were placed on the anterior side of the forearm above the tendon pathways. The electrode bands were tightened to ensure the electrodes made good contact with the skin without causing discomfort to the participant. The electrode placements across the forearm, as well as the contraction detection apparatus, are shown in Figure 5.7.

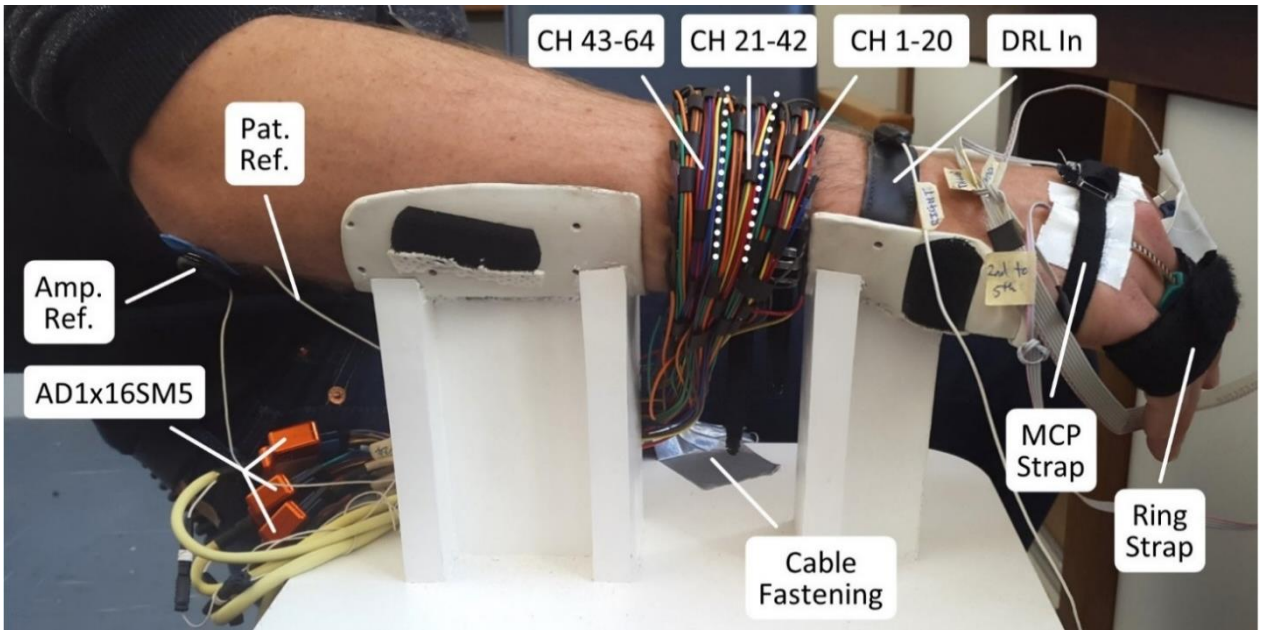

Figure 5.7 – Participant setup indicating electrode bands and reference electrode placements.

Amp. Ref – Amplifier Reference, Pat. Ref. – Patient Reference, AD1x16SM5 – OTB 16-channel monopolar active adapter, CH – Channels, DRL – Driven Right-Leg (circuit), MCP – Metacarpophalangeal (joint).

The electrode bands were connected to the EMG recording system via *AD1x16SM5* pre-amplifiers where the channel numbering began from the distal electrode band (20 electrodes). The *Patient Reference* and *DRL* leads were connected directly to the EMG recording system. All cables were fastened tightly to the testing platform using adhesive tape (see *Cable Fastening* in Figure 5.7) where possible, to limit cable movements during testing, thereby reducing the presence of movement artefacts in the EMG recordings.

5.3.2 Sensor Connections

The customised finger exoskeleton segments and flex sensors were attached to the participant as illustrated in Figure 5.2. The thumb IP and index PIP sensors were further secured to the *fixed sensor slots* (see Figure 4.9) using adhesive tape. The index MCP and Ring Group MCP sensors were stuck to the dorsum of the hand using adhesive tape and were further secured using an elastic strap (*MCP Strap*) wrapped around the hand. Each flex sensor was adjusted using the buffer circuitry developed in Section 4.2.1 to maximise the output voltage range over the participant's full range of motion for each finger joint. The customised finger exoskeleton segments, fastening straps and flex sensor connections are also shown in Figure 5.7.

5.4 Testing Procedure

The participant testing procedure began with a system verification check to ensure the experimental apparatus was functioning correctly. Participants were given practice time to learn the 12 unique movements in the movement protocol. During the practice session, the real-time EMG signal acquisition display was monitored to ensure the EMG recording setup was capturing acceptable EMG and auxiliary signals. The system verification steps and participant experimental testing procedure is outlined below.

5.4.1 System Verification

In order to consider the sdEMG system setup acceptable for participant testing, the hardware parameters were required to be functioning correctly and the real-time signals acquired needed to be characteristic of EMG, as described in EMG literature. The essential sdEMG system parameters monitored during the practice sessions and the corresponding corrective measures implemented are outlined in Table 5-4.

Table 5-4: sdEMG system verification conditions and corrective measures implemented.

System parameter	Acceptable conditions	Corrective measures
Input channels	Minimum of 60 active channels	Repeat electrode preparation procedure
Channel clipping	No signal clipping permitted	Decrease amplifier gains
Flex sensor channels	Minimum 1V signal deviation	Adjust flex sensor buffer circuitry
Trigger signal	0V to 2.5V step signal	Reconnect or replace trigger output cable

After the hardware parameters were functioning correctly, the real-time EMG signal characteristics were examined to ensure acceptable EMG signal acquisition. It was essential that the EMG signals were inspected during experimental testing to ensure the data recorded was indeed characteristic of EMG. While this was a subjective process that depended heavily on the experience of the researcher, there were several essential EMG signal characteristics that needed to be present as indicated in EMG literature.

EMG signals should have the following essential characteristics (Konrad, 2005):

- Sufficiently amplified without signal clipping.
- Distinctive EMG bursts that return to baseline within a few milliseconds of contraction termination.
- A constant mean baseline, typically 0V.
- Low resting baseline noise levels.

While these do not represent all EMG signal characteristics, these were easy to check and implement corrective measures during experimental testing. Corrective measures included reducing amplifier gains, fastening cable connections, adjusting the location of the EMG system away from electrical noise sources and demonstrating the execution of the movements to the participant.

The present study used 69 input signal channels (64 EMG and 5 auxiliary) which made it impossible to continuously monitor each channel throughout participant testing. Instead, signal clipping was tested for prior to testing by instructing the participant to form a full hand grip at their maximum voluntary contraction (MVC) level to ensure that the recorded EMG signals were within the amplifier input voltage ranges. Resting baseline amplitude and noise levels were observed at the start of each experimental run and monitored for baseline shifts or noise fluctuations periodically on different channels during data acquisition.

A screenshot of the real-time signal acquisition monitor is presented in Figure 5.8 which shows an *acceptable* EMG recording setup for a practice Group flexion test. This dataset shows clean and constant baselines during the *Rest windows* and distinctive EMG bursts that returned to the baseline quickly during the *Group flexion window*, which were characteristic of EMG signals.

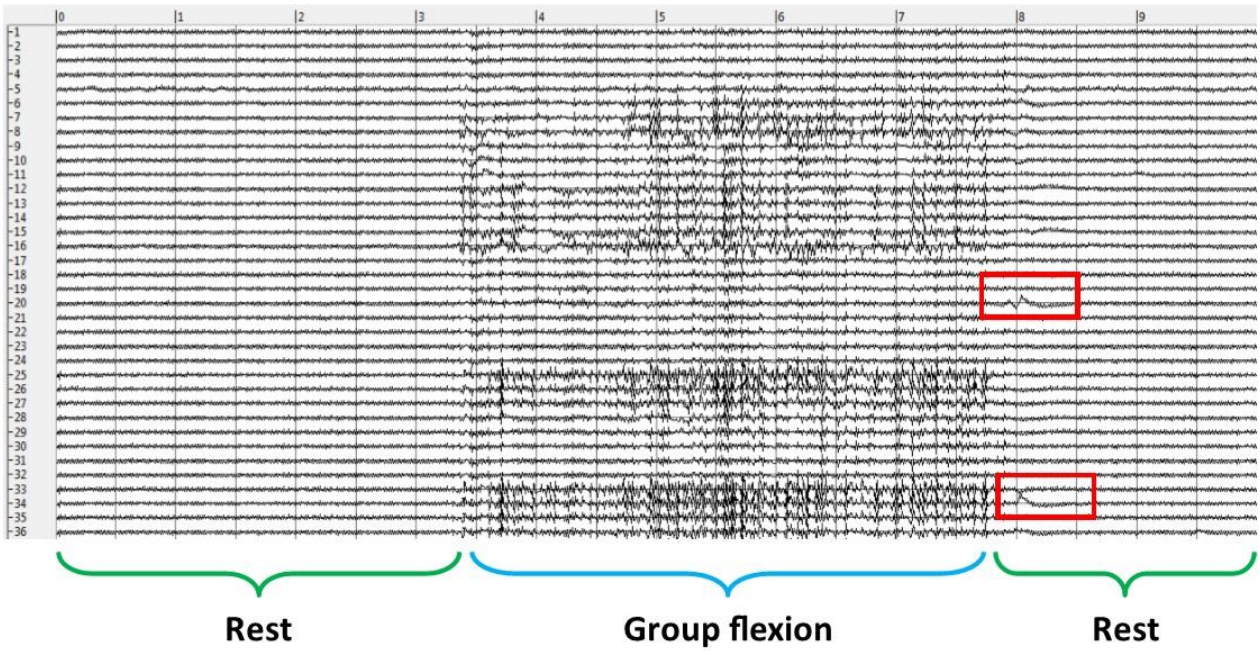

Figure 5.8 – Screenshot of the real-time signal acquisition (EMG channels 1-36) taken during a practice test indicating an acceptable recording setup.

The red blocks highlight cable or electrode movement signal artefacts during rest regions, however, these were deemed acceptable as it is impossible to achieve perfect signals due to the expansion of the forearm during contractions which inevitably leads to minor movement of the electrodes and subsequently the cables.

There were, however, two visible *signal artefacts*[27] highlighted with red boxes in Figure 5.8 that occur at the transition from Group flexion to Rest at ~8s. These were considered *movement signal artefacts* which were difficult to avoid since the forearm inevitably expands during the contractions implemented in the *dynamic MP*. It is speculated that the expansion of the electrode bands led to minor electrode and cable movements that resulted in these signal artefacts. Nevertheless, the recordings were deemed acceptable since only two channels contained signal artefacts and the remaining channels were characteristic of EMG signals.

In contrast, a screenshot of the real-time signal acquisition monitor is presented Figure 5.9 showing an *unacceptable* EMG recording setup for another Group flexion practice test. Several prominent signal artefacts were present across multiple channels as highlighted with the coloured boxes in Figure 5.9. Two artefacts at the start of the Group flexion contraction (at ~0.5s) were assumed to be cable movement artefacts from the participant twitching slightly to stabilise the contraction as highlighted with the red boxes. Similarly, two sets of artefacts occur at the transition from contraction to rest (at ~5s) highlighted with orange boxes which were considered *contraction-specific* movement artefacts. There was also a continuous signal artefact that extended across the entire rest window highlighted in the green box which was indicative of a *'dead'* channel due to a disconnection of the electrode from either the skin surface or from the cable. The pink box shows steady, but noisy signal baselines on channels 1-4 across the contraction and rest windows suggesting common EMI noise was coupled to the channels. In addition to the signal artefacts and noise observed, the blue box shows unexpected EMG activity during the rest period indicating the participant may not have fully relaxed their muscles during the rest period.

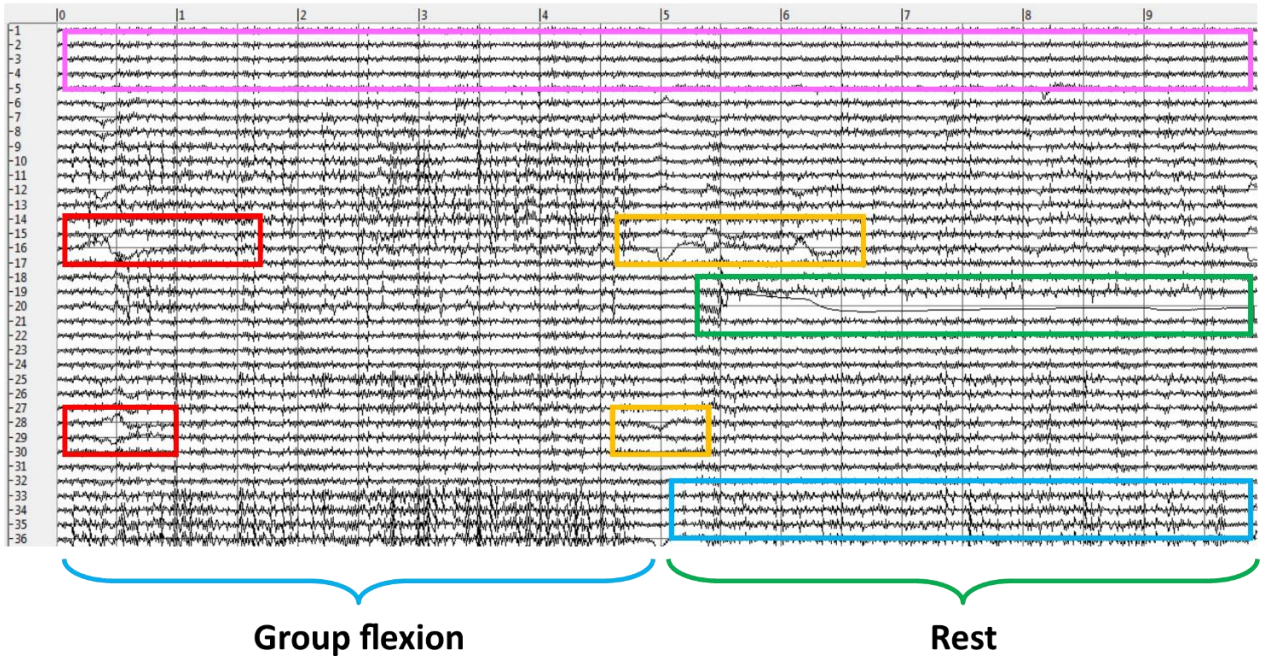

Figure 5.9 – Screenshot of the real-time signal acquisition (EMG channels 1-36) taken during a practice test indicating an unacceptable recording setup.

The red and orange boxes highlight possible cable or electrode movement artefacts. The pink box highlights consistent EMI noise throughout the recordings. The green box highlights an electrode disconnection from either the skin surface or from the cable. The blue box highlights unexpected EMG activity during the rest period.

[27] For EMG signals, artefacts are typically considered time shifts greater than 5ms (Konrad, 2005). Time shifts are characterised by a signal segment that deviates from the baseline and returns to the baseline after a 'long' period relative to the resting baseline average frequency which is ideally 0 Hz (flat signal). The period of time that the signal segment remains above or below the resting baseline before returning is the effective time shift.

Given the extent of signal artefacts and noise present on the channels shown in Figure 5.9, the EMG recording setup was deemed unacceptable and corrective measures (as described previously) were taken before commencing with further testing. The real-time visual inspection process described above was also conducted throughout the participant testing procedures and corrective measures were implemented when needed.

The system verification served as an iterative process that also provided the participant with additional practice time to learn the movements, whilst also ensuring all aspects of the experimental apparatus and EMG signal acquisition system was functioning correctly.

5.4.2 Experimental Testing

Once the sdEMG recording setup was complete and the system was verified, participants were taught how to execute the movement protocols for the five sub-experiments defined in Section 5.2.2. Participants were then allowed to practice executing the different movement protocols, after which experimental testing began.

Due to memory limitations on the *Nextion® HMI* device, the GUI software was separated into two programs, one for the Timing and Randomisation experiments and another for the Anticipation experiment. The microcontroller and HMI were uploaded with the software programs as required for randomised execution of the experiments.

Upon visual instructions, participants performed five experimental runs of each movement protocol variation. Participants were monitored during testing to ensure the correct movements were executed and experimental runs were restarted if mistakes were made. Participants were given breaks between runs to reduce the effects of fatigue. Throughout testing the equipment was monitored, if any technical failures arose during testing, the equipment was corrected to meet the system requirements presented in Sections 5.2 and 5.3.

The EMG and auxiliary signals were recorded for each experimental run using the system recording settings provided in Table 5-2 and the data was saved in the *OT BioLab®* file format (**.otb*) for offline data processing. Participant-specific log text files for each experimental run were saved on the microcontroller's SD-Card and subsequently collated with the recorded EMG and auxiliary signal datasets.

A total of 25 datasets were saved for each participant resulting in a total of 125 data files for participant testing population. The recorded data files served as the inputs for the offline data processing discussed in Chapter 6.

Chapter 6 - Data Processing

The implementation of the sdEMG technique in the present study aimed to determine *representative ICs (rICs)* for the deep and superficial investigated muscles by applying a standardised sdEMG data processing pipeline which is outlined in Figure 6.1.

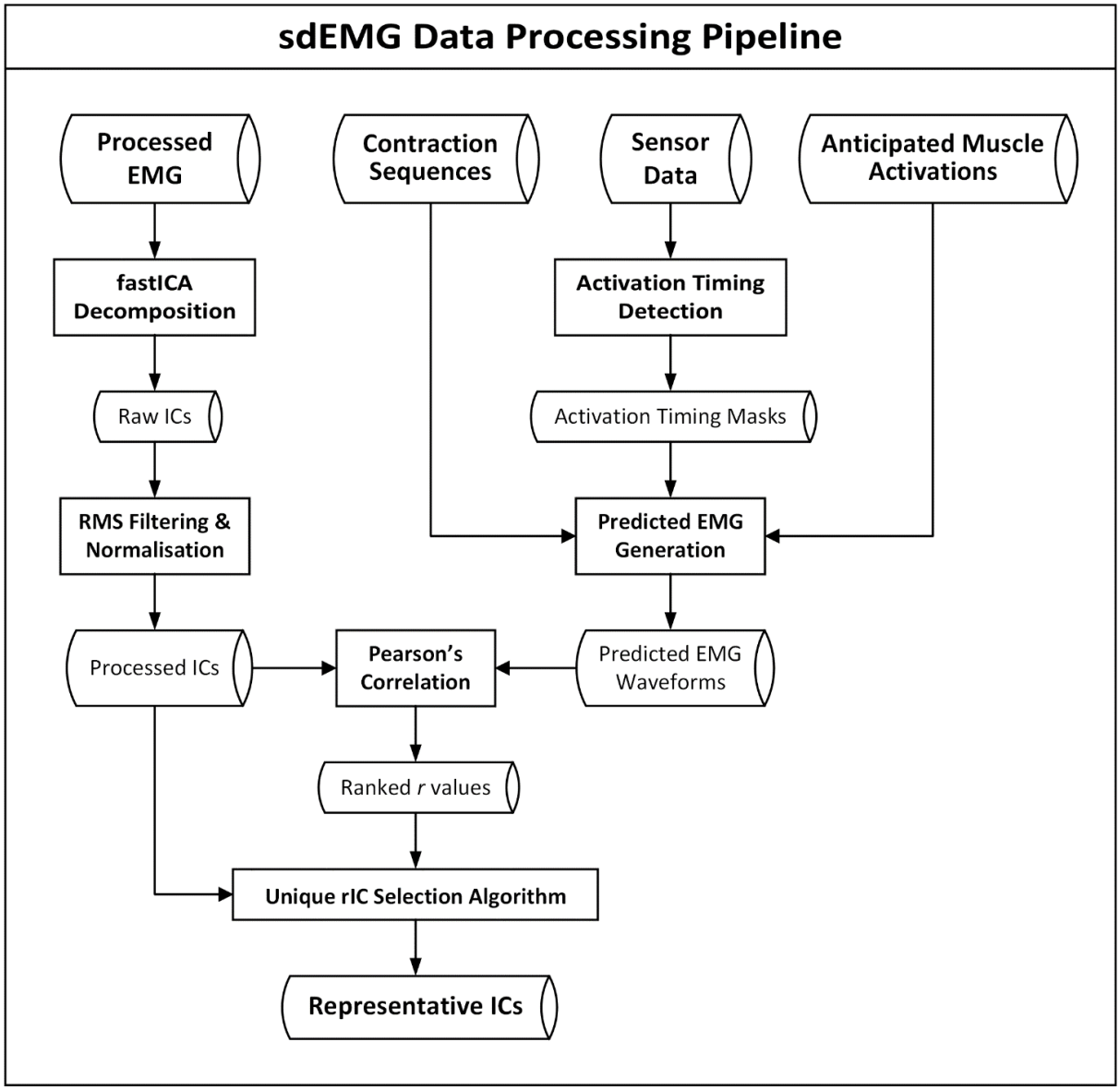

Figure 6.1 – Flowchart of the standardised sdEMG data processing pipeline.

The recorded raw monopolar EMG signals were decomposed using ICA and processed using standard EMG techniques to produce *processed Independent Components (pICs)* that best estimated the individual muscle sources. Subsequently, *predicted EMG (pEMG)* waveforms reflecting the *anticipated or expected EMG activity* for each muscle were generated to provide reference signals for *representative* IC selection. To this end, Pearson's correlation coefficient (*r*) was used as the measure of signal conformity between pICs and pEMGs, and subsequently, the pICs for each muscle were ranked based on their *r* values. A unique rIC selection algorithm was developed to select rICs based on their pIC *r* values to best represent the isolated EMG activity for each muscle. This chapter discusses the rationale and details of each processing step presented in Figure 6.1 using the recorded datasets.

6.1 EMG Processing

Standard EMG processing techniques begin with a visual inspection of the raw EMG signals during and after data acquisition. This process provides the researcher with a holistic view as to the validity of the raw data and the performance of the recording system during participant testing. The following will be a discussion on the standard EMG processing steps implemented in the present study.

6.1.1 Raw Data Visual Inspection

Due to the sheer volume[28] of data recorded in an sdEMG system, software memory failures are common resulting in incomplete or corrupted files. As a global inspection, the recorded datasets were individually checked to ensure the files contain all required signals (64 EMG and 5 auxiliary) for the entire test duration. Three out of the expected 125 files were found to be incomplete and had to be discarded from the study.

Since an sdEMG system oversubscribes the number of recording channels required, researchers are able to remove potential outlier channels that do not resemble typical EMG signals, as described in Section 5.4.1. As an initial processing step, the raw EMG signals were visually inspected to identify potential outlier channels to be excluded from the datasets. Examples of raw EMG recordings are presented in Figure 6.2 indicating signal artefacts on channels 13 and 14, while channels 15 and 16 resemble typical EMG signals.

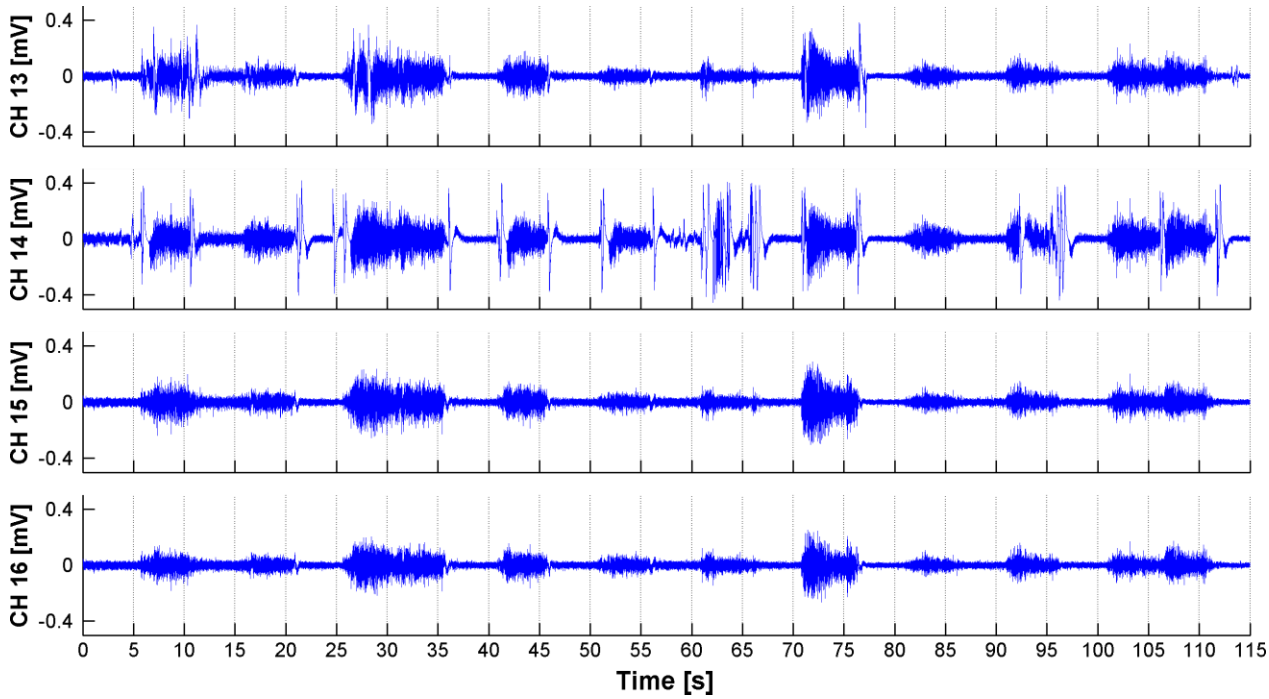

Figure 6.2 – Sample set of raw EMG recordings indicating potential outlier channels.

This sample dataset is from Participant 3, Timing 5s experiment, run 5 showing raw EMG channels 13-16. This contraction sequence follows the fixed MP with the movement name labels left out for brevity.

In Figure 6.2, channel 13 showed signs of movement artefacts at approximately: 11, 27, 28, 71 and 77 seconds. These artefacts are not as pronounced as those in channel 14, however, to be cautious this channel

[28] In the present study large data files were acquired due to the high: channel count (69), test durations (up to 161s), high sampling frequency (5,120Hz) and data the recording system's signal resolution (12-bit).

was flagged as a potential outlier. Only 40 channels were required in the present study as discussed in Section 4.1.1, therefore it was expected a reduced channel count would not negatively impact the outcome of the ICA algorithm. By contrast, channel 14 was clearly an outlier with numerous signal artefacts (large atypical spikes and slow signal settling times) present. These artefacts were most likely due to cable or electrode movements since they generally appeared at the onset and offset times of the contraction windows which is when the forearm would have expanded the most.

Further justification for selecting channels 13 and 14 as outliers are made apparent in Figure 6.3 where the corresponding normalised EMG envelopes[29] are shown. From the raw EMG recordings presented in Figure 6.2, channel 13 was cautiously flagged as a potential outlier due to the presence of a few signal artefacts. The corresponding enveloped EMG signal presented in Figure 6.3 highlights the adverse effects of these artefacts, which erroneously materialised as potential EMG bursts in the envelope signal.

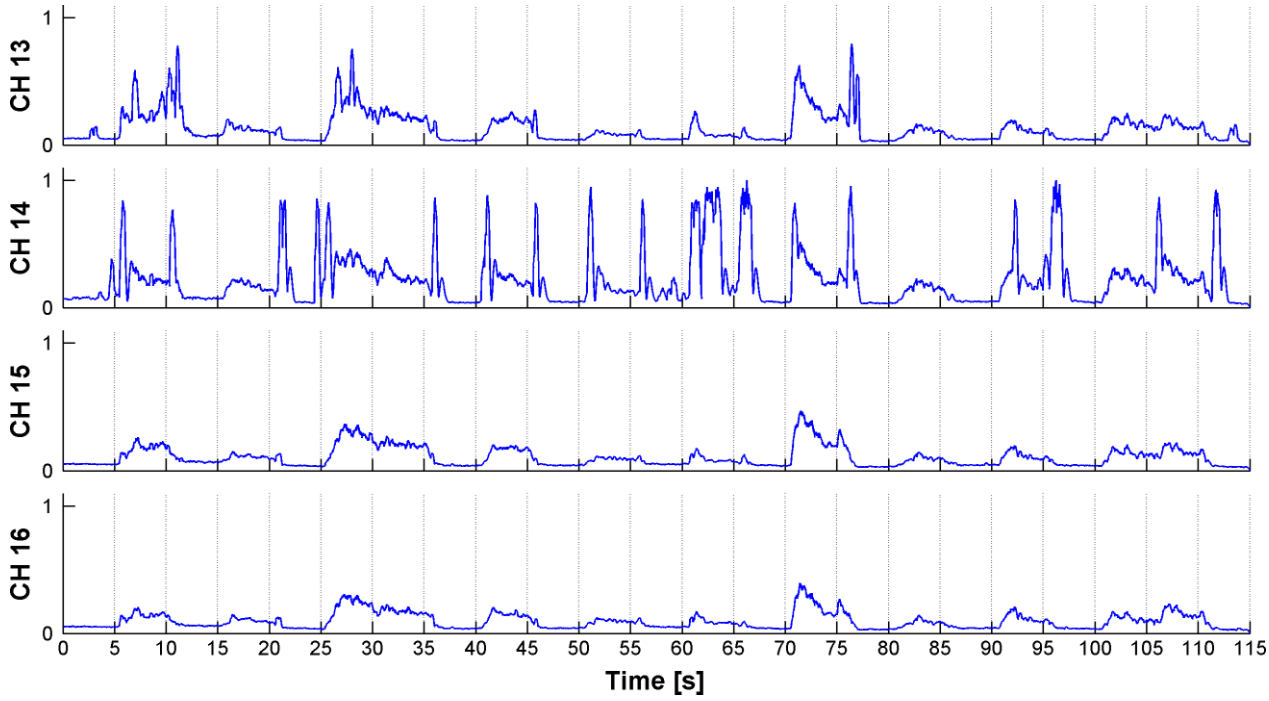

Figure 6.3 – Sample set of raw normalised EMG envelopes highlighting the adverse effects of outlier channels.

This sample dataset is from Participant 3, Timing 5s experiment, run 5 showing raw normalised EMG RMS filtered envelopes for channels 13-16. This contraction sequence follows the fixed MP with the movement name labels left out for brevity.

In comparison, channels 15 and 16 reflected as typical EMG signals, while channel 13 was not characteristic of EMG and was therefore removed from the dataset. The adverse effects of the artefacts present on channel 14 are clearly visible, the movement artefacts erroneously materialised as EMG bursts in the enveloped signal and therefore justified the removal of this channel from the dataset.

Another adverse effect of including these outlier channels is that they were found to reduce the relative amplitude of the other channels containing valid EMG activity when the entire dataset was normalised to the highest amplitude, which originated from an outlier channel containing a high erroneous signal spike.

[29] The SENIAM standard 250ms windowed root-mean-square (RMS) smoothing filter was applied to the raw EMG signals to compute the EMG envelopes that were subsequently normalised to lie between 0 and 1.

In the present study, the presence of EMG channel outliers required each raw EMG channel to be visually inspected to identify potential outliers. The outliers were then tabulated for each experimental run and subsequently removed in the raw data processing stage.

6.1.2 Raw Data Processing

Due to technical limitations of the EMG recording system, the raw datasets required several processing steps prior to ICA decomposition. The raw data processing steps are outlined in Figure 6.4 indicating the corrective steps implemented to address the limitations of the developed Data Acquisition System.

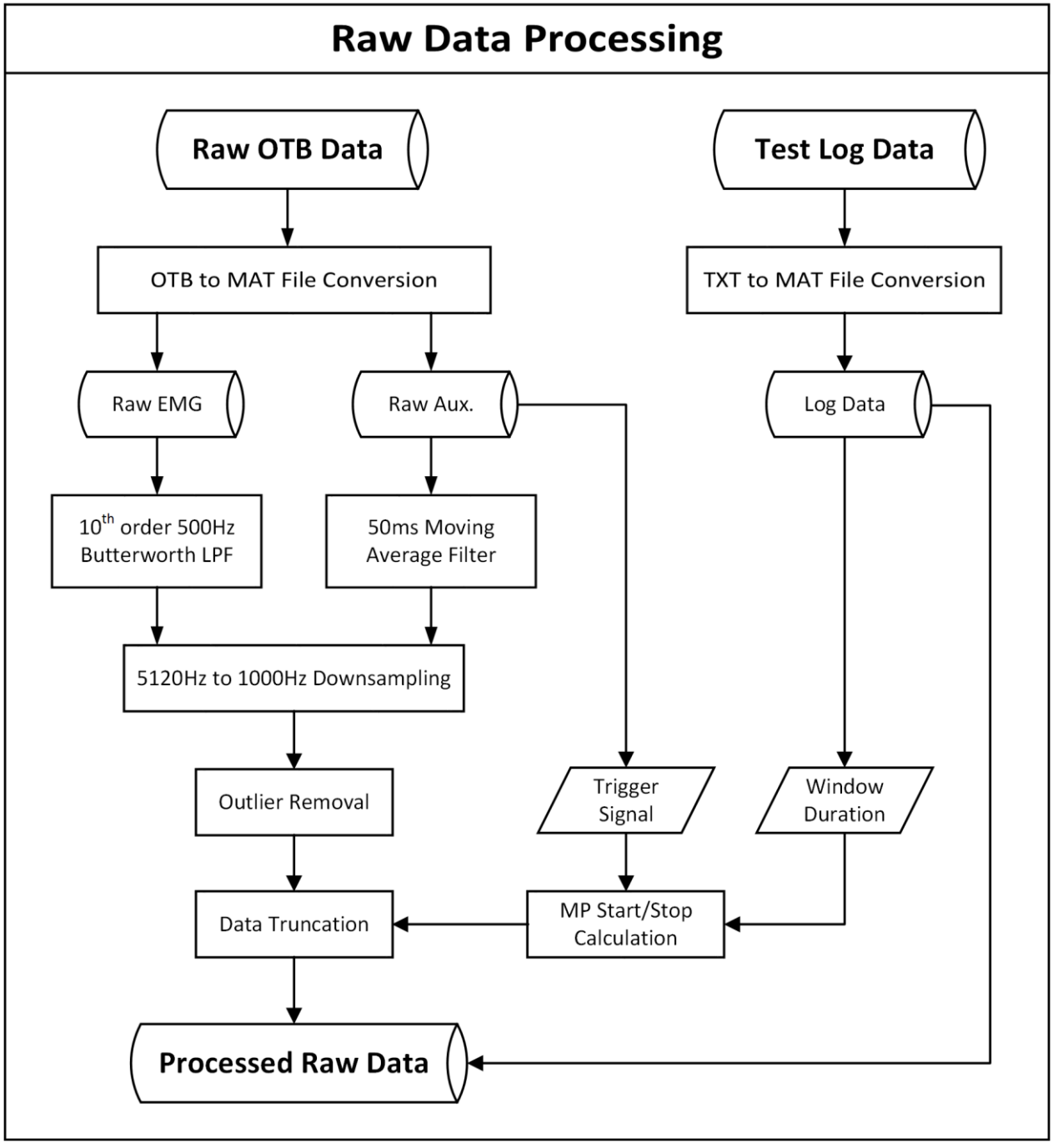

Figure 6.4 – Raw data software processing flowchart outlining the corrective processing steps implemented in the present study.

Due to a technical issue with the *OT Bioelettronica® EMG-USB2* amplifier, the only available sampling rate was 5120Hz. This introduced substantial high-frequency noise above the 400Hz EMG bandwidth[30] in spite of the 500Hz analog low-pass filter (LPF) implemented in the *EMG-USB2* amplifier. To correct for this, a digital 10th order 500Hz Butterworth LPF was applied to the raw data in the software processing pipeline. The raw data was filtered *before* down-sampling to prevent aliasing of the high-frequency noise (> 500Hz) into the resampled data. Due to the sheer volume of data, a lower sampling rate was needed for the EMG signal processing operations. The raw datasets were down-sampled to the commonly used 1000Hz sampling frequency which satisfies the Nyquist–Shannon sampling theorem for the sEMG signals.

The raw auxiliary data consisted of flex sensor data and the start trigger signal emitted from the Participant Instruction System developed in Section 4.3. While these are DC signals, they were coupled with high-frequency noise which was subsequently removed using a 50ms digital moving average filter. The start trigger signal from the auxiliary data was not filtered as this was a binary signal, therefore, a simple 50% ADC threshold was sufficient to detect the experimental run start time.

The test log data file was created in the Participant Instruction System and contained the MP sequence, movement window duration, timestamps, experimental run counters and other test parameters. In the Randomisation experiment, the MP sequence for each experimental run was needed to generate the run-specific predicted EMG waveforms which are discussed in Section 6.3.2.

The Randomisation and Anticipation experiments had a fixed movement window duration of 5 seconds, while the Timing experiments had varied movement window durations of 3, 5 and 7 seconds which resulted in different experimental run lengths. To account for this, the stop trigger time was calculated using the known 23 windows in an MP, the start trigger time from the auxiliary data, and the movement window duration from the test log data as illustrated in Figure 6.4. The start and stop trigger times were then used to truncate the data after the outlier channels were removed from the raw datasets.

6.1.3 ICA Decomposition

In the present study, ICA was used to separate mixed monopolar EMG signals into their statistically Independent Components (ICs). The MATLAB® *fastICA* package (Gävert et al., 2005) was implemented into the software pipeline to decompose the processed raw EMG data, which subsequently returned *up to N* ICs, where *N* was the number of input EMG signals *after* outlier removal.

The decomposed ICs were expected to reflect the *compound EMG source signals* which were further processed using standard EMG techniques consisting of signal rectification, RMS envelope filtering and normalisation. It should be noted that the amplitude scaling of the decomposed ICs is lost in the ICA algorithm, however, the relative amplitudes between ICs are retained, as discussed in Section 1.1.2. Consequently, the decomposed ICs were normalised in each dataset before further analysis was conducted.

Within the context of an sdEMG study, a *processed IC (pIC)* is defined as a decomposed IC that has been rectified, RMS envelope filtered and normalised to lie between 0 and 1. A sample set of raw normalised biphasic decomposed ICs is presented in Figure 6.5, and the corresponding pICs are shown in Figure 6.6. The pICs were subsequently compared against *predicted EMG (pEMG)* waveforms so as to identify *representative ICs* for each muscle investigated. The generation of the pEMG waveforms is discussed in Section 6.3.

[30] Surface EMG has an approximate signal bandwidth of 10-400Hz, and the SENIAM guidelines recommend a filtering bandwidth of 5-500Hz (Hermens et al., 1999).

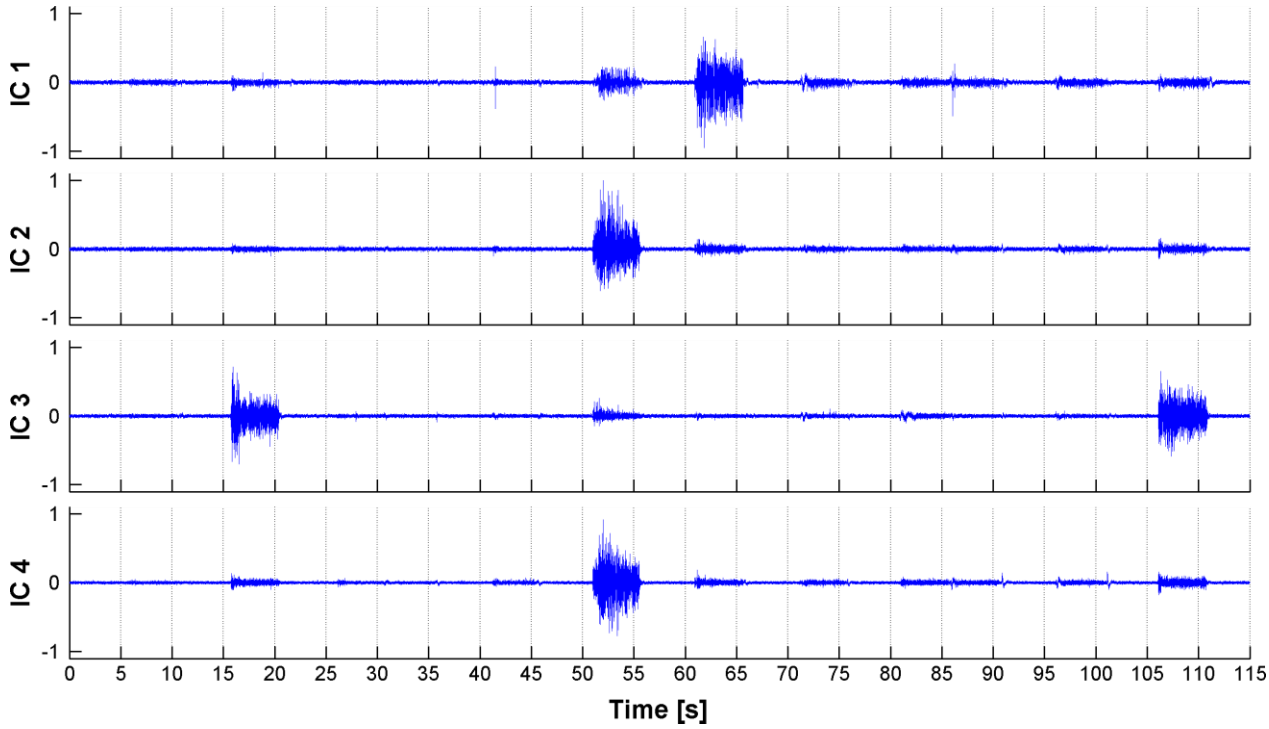

Figure 6.5 – Sample set of raw normalised biphasic decomposed Independent Components (ICs).

This sample dataset is from Participant 4, Randomisation experiment, run 5 showing the first four raw normalised biphasic ICs. This contraction sequence follows a randomised MP with the movement name labels left out for brevity. The ICs presented have been normalised to lie between -1 and +1 for visual purposes.

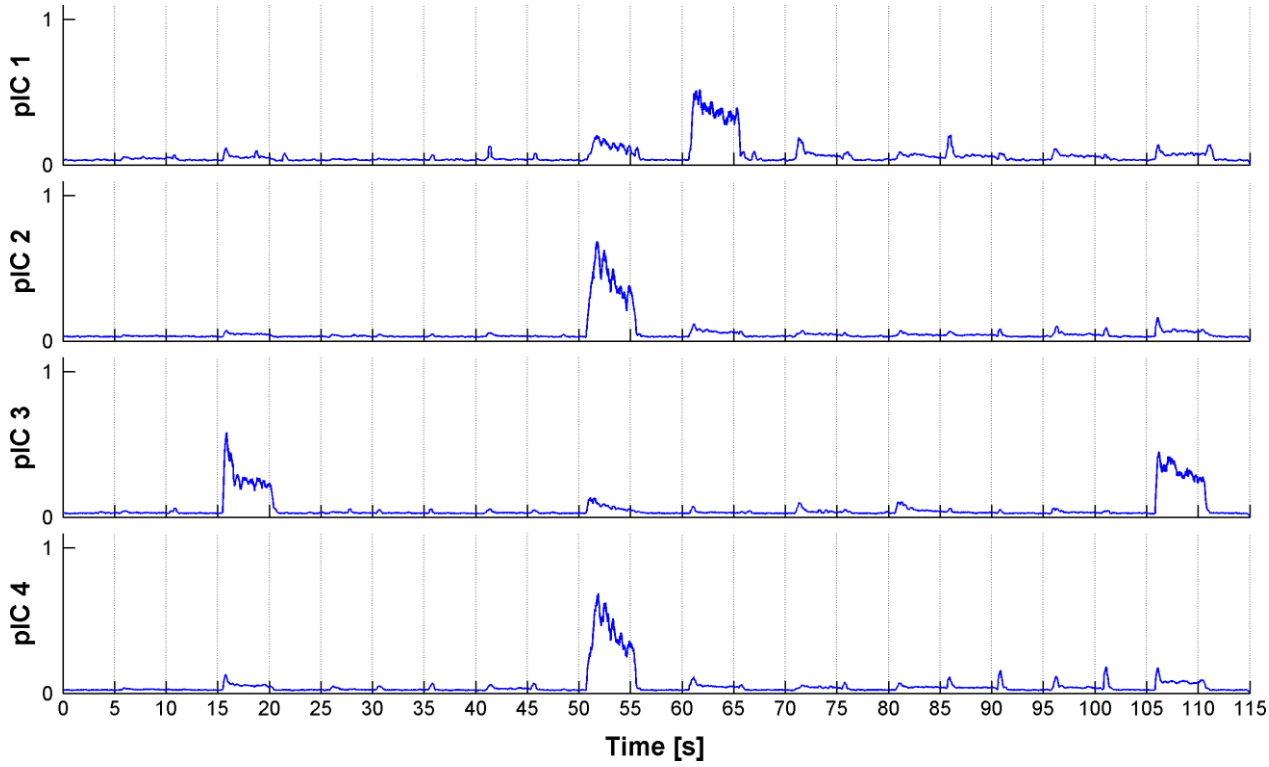

Figure 6.6 – Sample set of processed Independent Components (pICs).

This sample dataset is from Participant 4, Randomisation experiment, run 5 showing the first four processed ICs. This contraction sequence follows a randomised MP with the movement name labels left out for brevity.

6.2 Activation Timing Detection

The sdEMG technique compares *processed ICs* with *predicted EMG waveforms*, therefore the signals needed to be synchronised to align with the *actual contraction onset and offset times* in each experimental run. The processing steps required to generate the *activation timing masks (ATMs)* needed to synchronise the pEMG waveforms with the actual contraction timings is summarised in Figure 6.7.

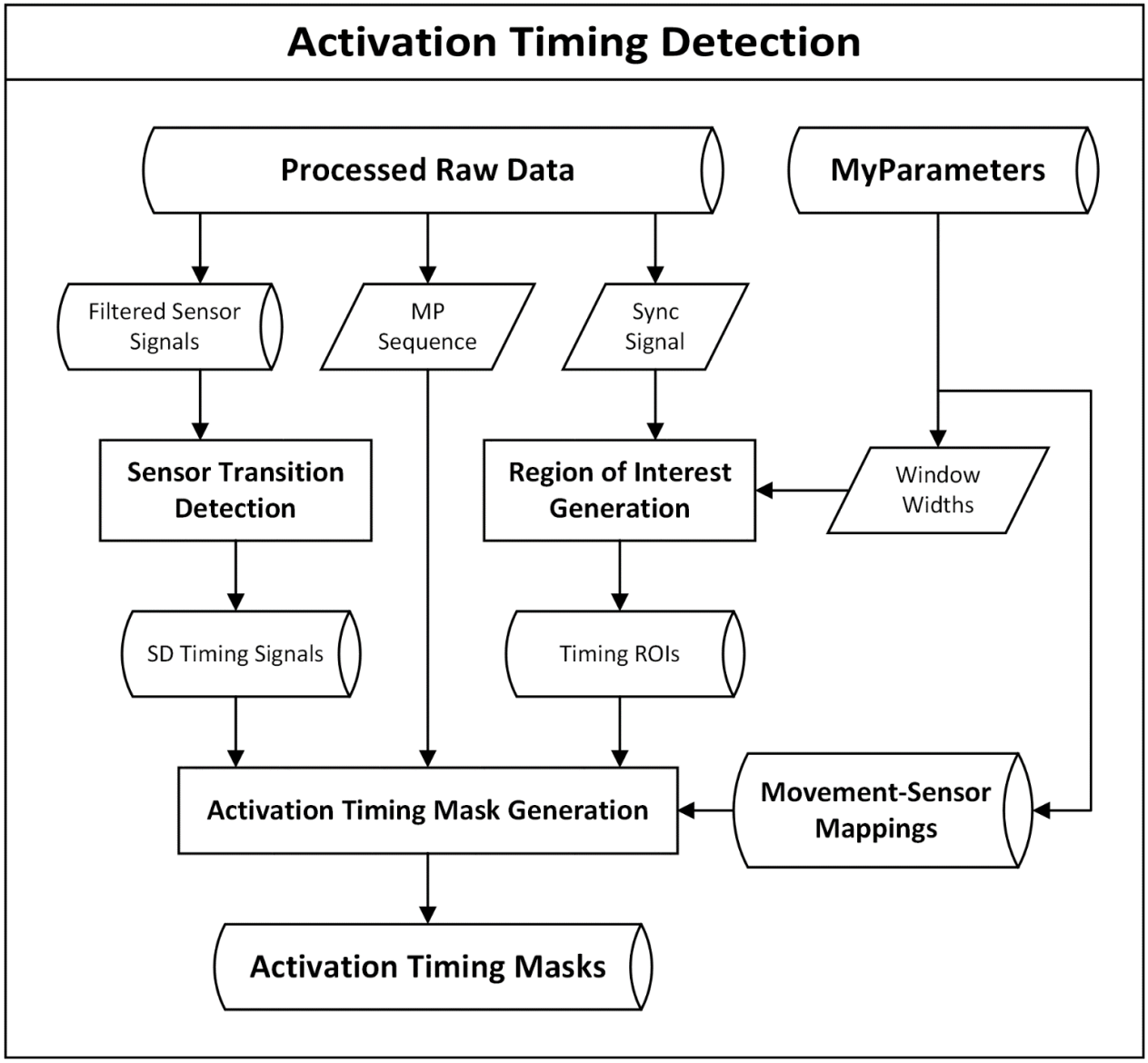

Figure 6.7 – Activation timing detection processing flowchart outlining the generation of activation timing masks.

SD – Standard deviation, ROI – Region of Interest.

6.2.1 Sensor Transition Detection

In order to identify the contraction onset and offset times of each movement window in the present study, a robust sensor transition detection algorithm was developed. The recorded flex sensor resting baselines were very inconsistent as a result of the participant's inability to consistently return to the same rest position as illustrated by flex sensor 1 (FS1) in Figure 6.8. Subsequently, due to the high-frequency noise coupled to

the flex sensor signals, a simple rise and fall trigger algorithm[31] was not feasible. Instead, a 75ms moving standard deviation (SD or σ) filter was developed to detect the contraction onset and offset times from the flex sensor signals. The developed detection algorithm identified regions of high variance (σ^2) that corresponded to *rapid signal transitions from the resting baseline*, irrespective of the signal direction or polarity. This method was robust to signal baseline inconsistencies and accurately identified signal transition points (contraction onset and offset times) from the flex sensor data as illustrated in Figure 6.8.

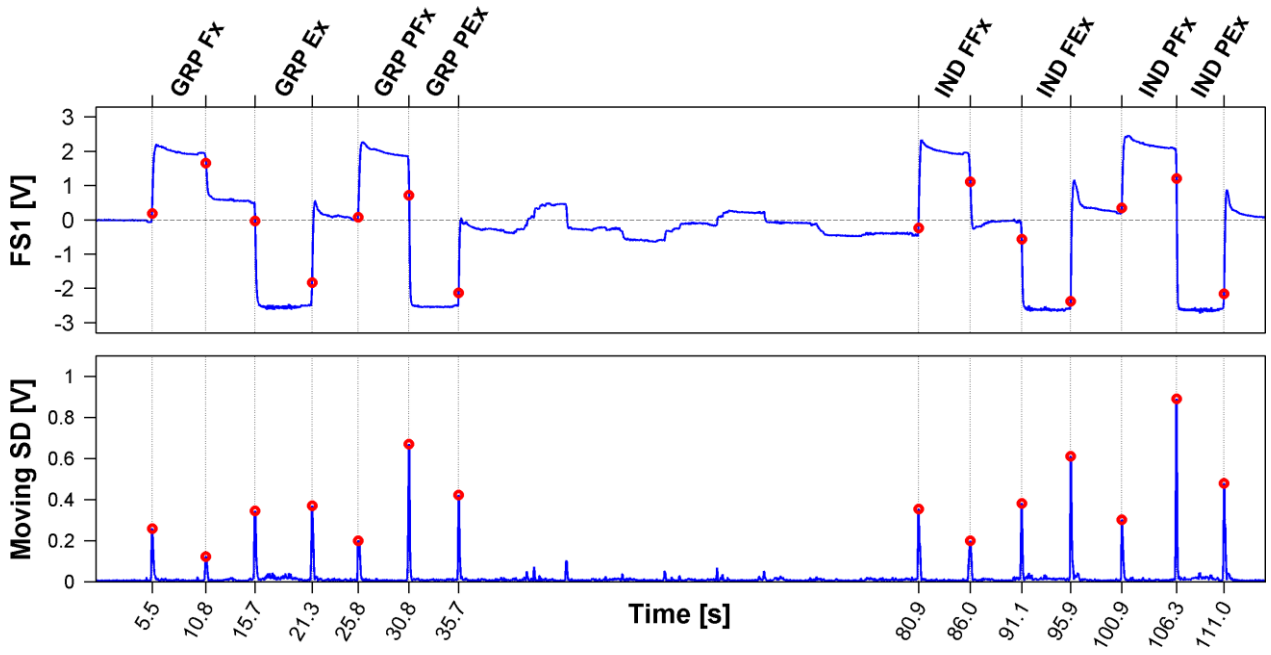

Figure 6.8 – Index PIP joint flex sensor (FS1) transition detection using a 75ms moving SD filter.

Fx – Flexion, Ex – Extension, GRP – Group, PFx – PIP flexion, PEx – PIP extension, FFx – full flexion, FEx – full extension.

This sample dataset is from Participant 4, Timing 5s experiment, run 3 showing FS1 corresponding to index PIP movement. This contraction sequence follows the fixed MP with the rest window labels and movements that do not activate the index PIP joint left out for clarity.

The identified contraction onset and offset times are indicated by red dots for movements activating index PIP joint.

The 50ms moving average smoothing filter implemented in Section 6.1.2 introduced a time delay which combined with the inherent SD filter delay. The combined delay could have been eliminated by introducing a negative time shift of equivalent length into the data, however, the delay was considered negligible for the purposes of the present sdEMG study which is robust to minor timing mismatches.

The SD filter was applied to all sensor signals and the resultant *SD timing signals* were combined with *regions of interest (ROIs)* and the *movement-sensor mappings* to form *ATMs* as outlined in Figure 6.4. Based on the movement performed, the corresponding joint flex sensor(s) were activated and the recorded signal(s) amplitudes increased for flexion and decreased for extension as indicated in Table 6-1. All movements except Group flexion and extension, as well as Index full flexion and extension, activated one flex sensor, therefore the contraction onset and offset times were extracted from a single sensor signal. Group flexion and extension activated flex sensors 1, 2 and 4, while Index full flexion and extension activated flex sensors 1 and 2 as indicated in Table 6-1 which required additional processing considerations during the ROI formations.

[31] A rise and fall trigger algorithm uses signal polarity, paired with a trigger threshold value to determine when a sensor was activated. This technique requires zero-mean signals with constant resting baselines and a user-defined threshold.

Table 6-1: Movement-sensor mappings indicating the flex sensor signal directions for the finger movements tested in the movement protocol.

		Finger movements											
		1	2	3	4	5	6	7	8	9	10	11	12
		Group Fx	Group Ex	Group PIP Fx	Group PIP Ex	Ring Group Fx	Ring Group Ex	Thumb IP Fx	Thumb IP Ex	Index full Fx	Index full Ex	Index PIP Fx	Index PIP Ex
Flex sensors	Index PIP (FS1)	↑	↓	↑	↓					↑	↓	↑	↓
	Index MCP (FS2)	↑	↓							↑	↓		
	Thumb IP (FS3)							↑	↓				
	Ring MCP (FS4)	↑	↓			↑	↓						

FS – Flex sensor, Fx – Flexion, Ex – Extension, PIP – Proximal interphalangeal (joint), MCP – Metacarpophalangeal (joint), IP – Interphalangeal (joint).

↑ – Increasing FS signal amplitude (green), ↓ – Decreasing FS signal amplitude (red).

6.2.2 Region of Interest Generation

Regions of interest (ROIs) refer to the time windows for identifying transition points in the sensor data, needed to extract the exact contraction onset and offset times. In the present study, the *ideal sync signal* reflected the exact times the participant was *instructed* to start or stop a movement. The rise and fall points of the ideal sync signal provided the reference times for constructing the ROIs using fixed start (α) and stop (β) window width parameters as illustrated in Figure 6.9.

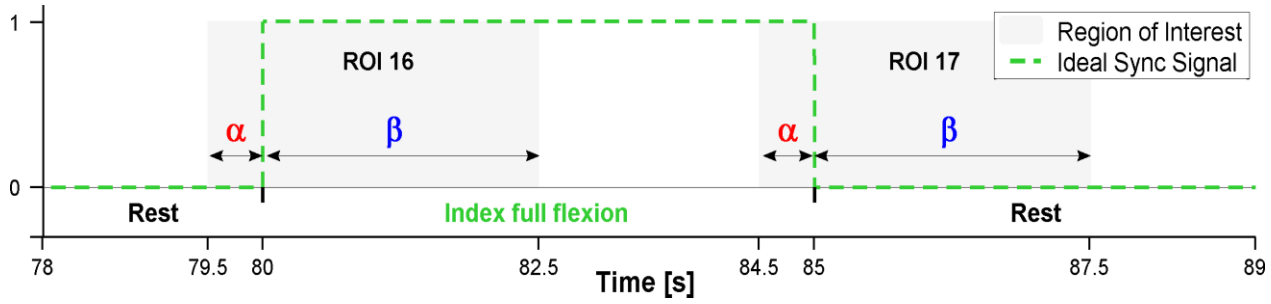

Figure 6.9 – Generation of regions of interest using fixed start (α) and stop (β) window widths.

α – Start window width, β – Stop window width.

It was assumed due to inherent participant reaction delays, the contraction onset time would *lead* the sync signal, therefore the start window width was kept short to prevent early triggers from the previous contraction stop time. Similarly, the stop window width was kept longer to account for the expected start delay, as well as the additional reaction delay from when the participant was instructed to stop a contraction. From experimentation, a 0.5s start window width and a 2.5s stop window width resulted in satisfactory contraction onset and offset selection accuracy across all participants and experiments. As an example, Figure 6.10 illustrates the ROIs (shaded in grey) required to extract the contraction onset and offset times for index full flexion, which activated the PIP (FS1) and MCP (FS2) joints simultaneously as indicated in Table 6-1.

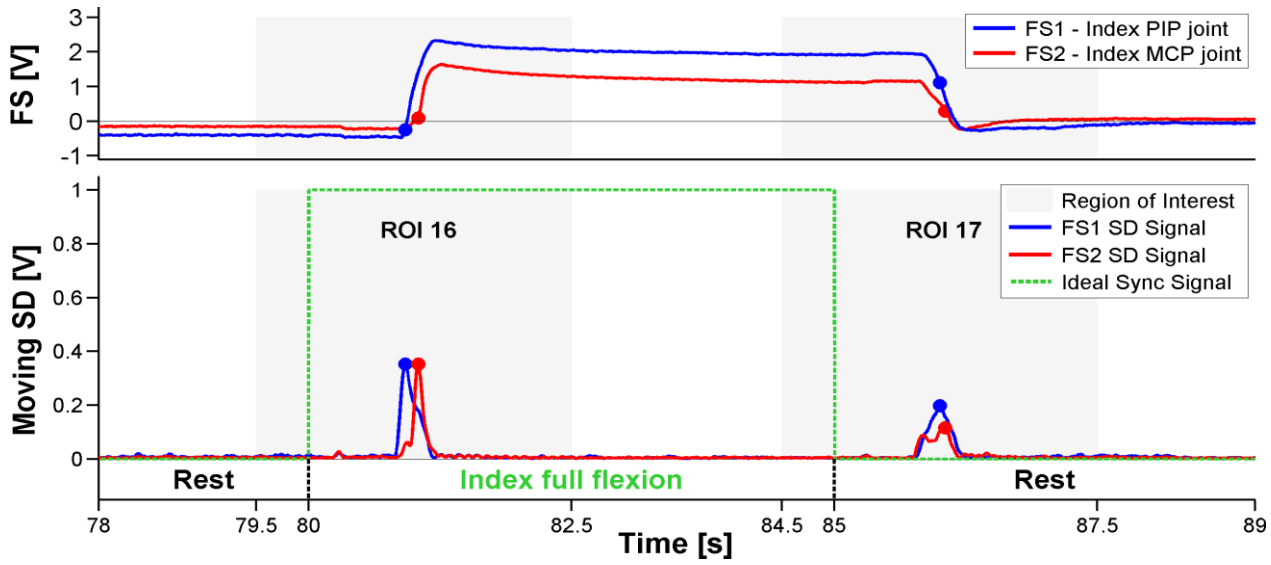

Figure 6.10 – Detection of the earliest onset and latest offset contraction times using the moving standard deviation filter technique.

This sample dataset is from Participant 4, Timing 5s experiment, run 3 showing FS1 and FS2 corresponding to index PIP and MCP movements. This contraction sequence follows the fixed MP.

In order to determine the contraction onset and offset times for these movements, the earliest onset and latest offset times were selected. This was performed as a precaution to ensure the predicted EMG movement window sufficiently covered the EMG bursts in the pICs. Figure 6.10 illustrates this concept for Index full flexion which activated FS1 and FS2, where the contraction onset time was informed by FS1 (blue dot) in ROI 16 and the offset time was informed by FS2 (red dot) in ROI 17.

6.2.3 Activation Timing Mask Generation

Activation timing masks (ATMs) are binary synchronisation signals needed to align the predicted EMG waveforms to the processed ICs. The fixed MP sequence used in the Timing and Anticipation experiments is shown in Table 6-1, beginning with Group flexion (Finger movement 1). In the Randomisation experiment, the columns of Table 6-1 were shuffled to obtain randomised MP sequences that maintained the same movement-sensor mappings required to generate the ATMs for each experimental run.

In the present study, each movement in an experimental run required a time-corrected ATM waveform reflecting the exact contraction onset and offset times, as informed by the flex sensor signals. The locations of the contractions were informed by the MP sequence and subsequently assigned a binary value of 1 in the ATM waveform. The process of generating ATM 1 corresponding to the first contraction window (Group flexion), as informed by the flex sensor SD timing signals (SD1, SD2 and SD4), is illustrated in Figure 6.11. The remaining ATMs for contractions 2 to 12 were produced in a similar fashion.

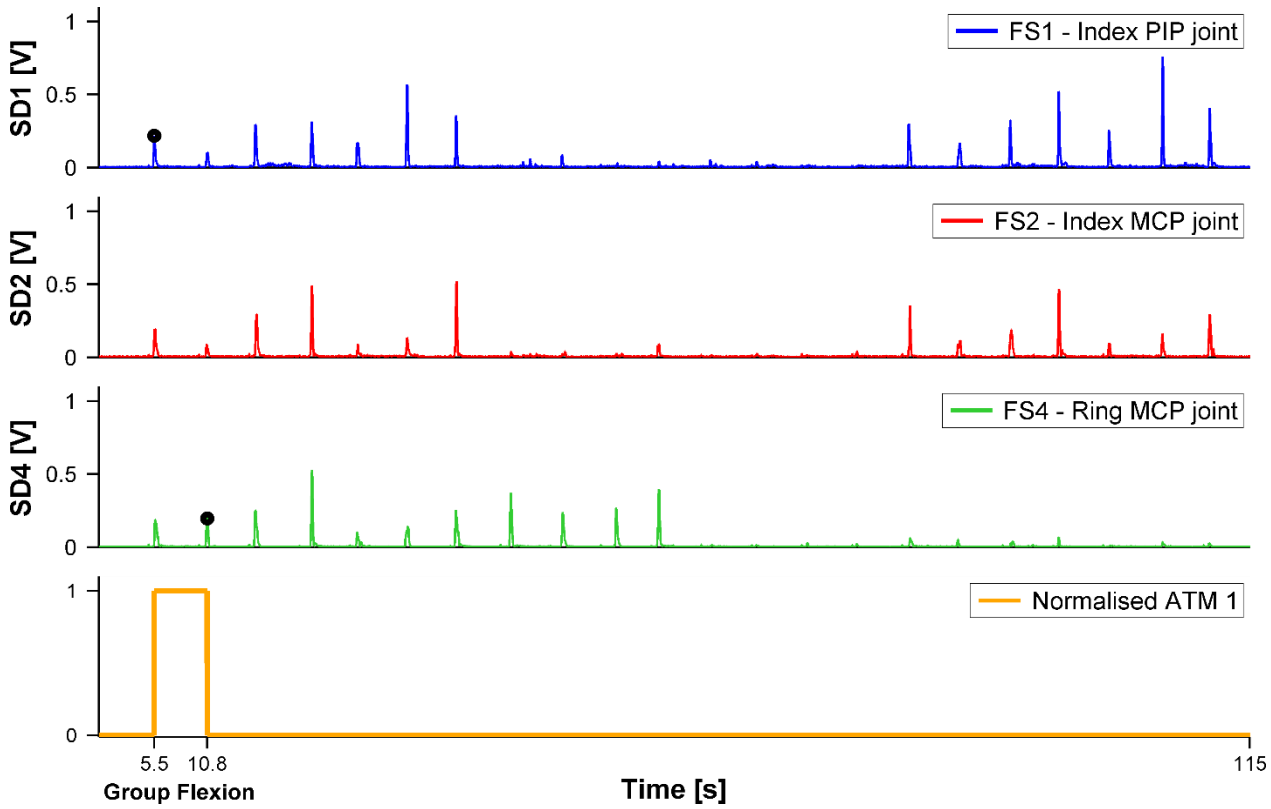

Figure 6.11 – Generation of activation timing mask 1 as informed by flex sensors 1, 2 and 4.

This sample dataset is from Participant 4, Timing 5s experiment, run 3 showing the moving standard deviation signals for FS1, FS2 and FS4. This contraction sequence follows the fixed MP with all the rest and other movement labels left out for clarity.

The black dots indicate the extracted earliest onset (informed by FS1) and latest offset time (informed by FS4) using the moving SD filter method for ATM 1.

6.3 Predicted EMG Activity

The next step in the implementation of an sdEMG system was to derive *literature-informed, predicted EMG waveforms* using the generated activation timing masks. A *literature-informed, predicted EMG (pEMG) waveform* is defined as a temporal signal that corresponds to the *anticipated EMG muscle activity* for a specific muscle during the movement protocol. The predicted EMG waveforms served as reference signals to be compared to the processed ICs, in order to select *representative ICs (rICs)* for each muscle investigated.

6.3.1 Literature Informed EMG Activity

The pEMG waveforms for the muscles under investigation were derived from the underlying musculature, biomechanics and unique muscle-movement mappings derived in Table 3-2. The muscle-movement mappings allowed for each muscle to be assigned an anticipated muscle activation waveform consisting of *full activation (fa), partial activation (pa) or inactive (0)* movement windows.

The muscle activations during fine motor finger movements were outlined in Table 3-2, which was expanded to include the *relative muscle activation contributions* expressed as *fa* and *pa* magnitudes. Functional anatomical literature was used to assign these levels in accordance with each muscle's relative contribution during the targeted contractions in the MP. Table 6-2 outlines the anticipated muscle activation contributions for the 12 unique movements implemented in the MP.

Table 6-2: Anticipated muscle activation contributions for each muscle during the finger movements tested in the movement protocol.

		Finger movements											
		1	2	3	4	5	6	7	8	9	10	11	12
		Group Fx	Group Ex	Group PIP Fx	Group PIP Ex	Ring Group Fx	Ring Group Ex	Thumb IP Fx	Thumb IP Ex	Index full Fx	Index full Ex	Index PIP Fx	Index PIP Ex
Deep muscles	Flexor pollicis longus							*fa*					
	Extensor pollicis longus								*fa*				
	FDP-Index Band	*fa*		*fa*						*fa*		*fa*	
	FDP-Ring Band	*fa*		*fa*		*fa*							
	Extensor indicis		*pa*		*pa*						*fa*		*fa*
Superficial muscles	FDS-Index Band	*fa*		*pa*						*fa*		*pa*	
	FDS-Ring Band	*fa*		*pa*		*fa*							
	Extensor digitorum		*fa*		*fa*		*fa*				*pa*		

Fx – flexion, Ex – Extension, fa – fully active (blue), pa – partial active (red).

Muscle activation contributions derived from Gilroy et al. (2012); Jenkins (2009); Schuenke et al. (2010).

6.3.2 Predicted EMG Generation

The muscle-specific predicted EMG waveforms were constructed by superimposing the required ATMs for each muscle and applying the corresponding movement activation amplitudes derived from the literature informed EMG activity outlined in Table 6-2. Subsequently, the pEMG waveforms underwent the same EMG processing steps (RMS envelope filtering) that was applied to the pICs before signal comparison was performed using Pearson's correlation (performed in Section 6.4.1). It should be noted that the RMS filtering introduced a 250ms delay to the pEMG waveforms, however, the pICs underwent the same filtering, therefore no further time correction was required as both waveforms had the same processing delay.

The predicted EMG generation process is illustrated in Figure 6.12 showing the construction of the FDS-Index Band predicted EMG waveform using the anticipated muscle activation sequence for FDS-Index Band presented in Table 6-2, and the corresponding ATMs for Group flexion (ATM 1), Group PIP flexion (ATM 3), Index full flexion (ATM 9) and Index PIP flexion (ATM 11). The ATM 1 presented below was generated in Figure 6.11 and ATMs 3, 9 and 11 for this experimental run were generated using the same method outlined in Section 6.2.3.

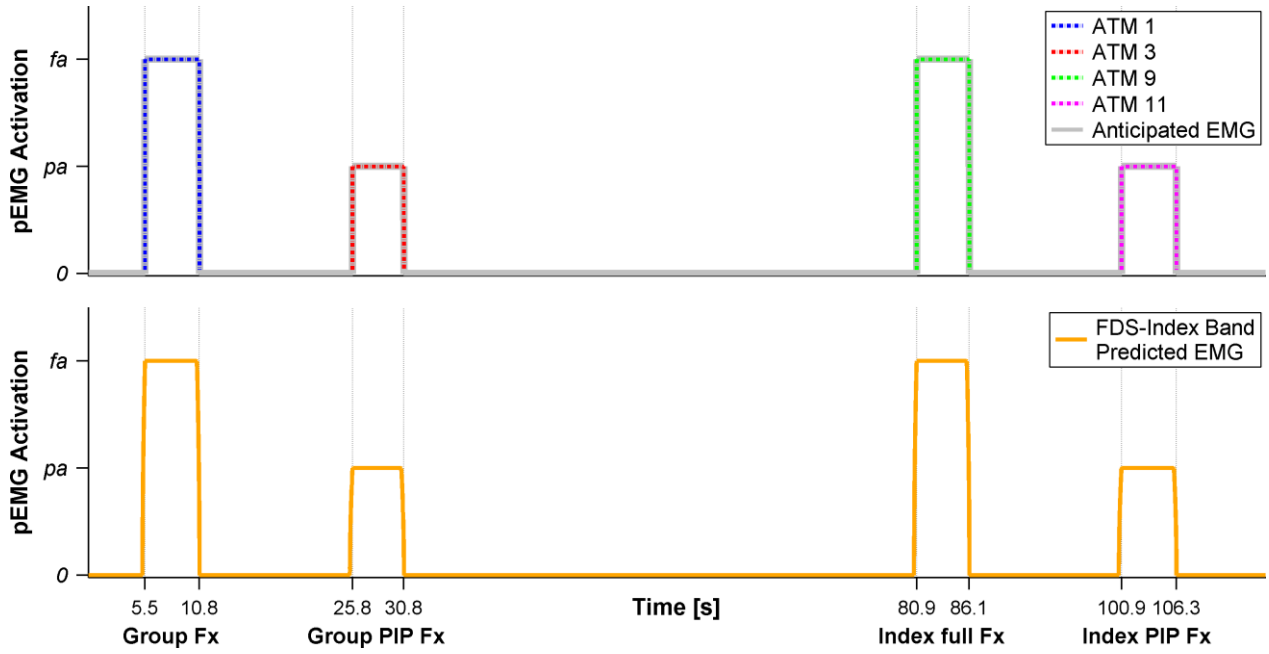

Figure 6.12 – Predicted EMG waveform generation for the FDS-Index Band muscle.

This sample dataset is from Participant 4, Timing 5s experiment, run 3 showing ATM 1, 3, 9 and 11. This contraction sequence follows the fixed MP with all rest and the other movement labels left out for clarity.

The superimposed ATMs create the anticipated EMG envelope waveform (shown in grey) which was then RMS envelope filtered to generate the predicted EMG waveform for the FDS-Index Band (shown in orange).

It should be noted that the anticipated EMG envelope waveform (grey signal) shown in Figure 6.12 has a *square profile* while the pEMG waveform (orange signal) is *rounded* at the vertices as a result of the 250ms RMS envelope filter. Additionally, the pEMG waveform does not align precisely with the time demarcations which highlights the introduced 250ms. The pEMG activation magnitudes, *fa* and *pa*, were set to 0.8 and 0.4, respectively, in accordance with previous sdEMG studies (Pitman, 2015; Swanepoel, 2017). The full activation value was selected below unity to account for large erroneous spikes found in some pICs which are not characteristic of EMG signals.

6.4 Representative IC Selection

One of the limitations of the ICA algorithm is that the decomposed ICs are output in an arbitrary order (see Section 1.1.2). Consequently, the output IC order has no relationship with the electrode placement locations. In order to associate the pICs with specific muscles, the pICs were compared to pEMG waveforms in the temporal domain. Since ICA preserves temporal relationships between ICs, the time-coding achieved using a timed targeted movement protocol allowed for the predicted EMG activity to be associated with pICs by considering the muscle-specific activation times of each movement in the MP.

In the present study, pICs were compared to muscle-specific pEMG waveforms in the temporal domain using Pearson's correlation coefficient (*r*) to determine *representative ICs (rICs)*. In each experimental run, the pIC with the highest *r* value for each muscle-specific pEMG waveform was selected to represent the EMG activity of that muscle. Additionally, the calculated Pearson's correlation coefficient values were also used to rank the *level of muscle isolation* for each rIC.

6.4.1 Pearson's Correlation Coefficient

Pearson's correlation coefficient (*r*) is a measure of the strength of association and linear conformity between two continuous-time signals (Belle, Fisher, Heagerty, & Lumley, 2004). The *r* value can be interpreted as an indicator of how similar the contours of two signals are. The *r* value is bound between -1 and +1 where; -1 indicates a strong negative linear relationship, 0 indicates no linear relationship and +1 indicates a strong positive linear relationship.

Previous sdEMG studies (Pitman, 2015; Swanepoel, 2017) used Pearson's correlation as the comparative method for rIC selection which produced favourable results, therefore it was also used to conform to the current implementation of the sdEMG technique. The MATLAB® *corrcoef* function was used to compute the *r* value between pICs and pEMG waveforms. The pEMG waveforms for the eight muscles were compared to all pICs (≤ 64) in each experimental run. The *r* values and pIC labels were stored for use in the rIC selection algorithm. Figure 6.13 shows an example of a pEMG waveform and a pIC for the FDP-Ring Band muscle, which when compared using Pearson's correlation produced an *r* value of 0.90.

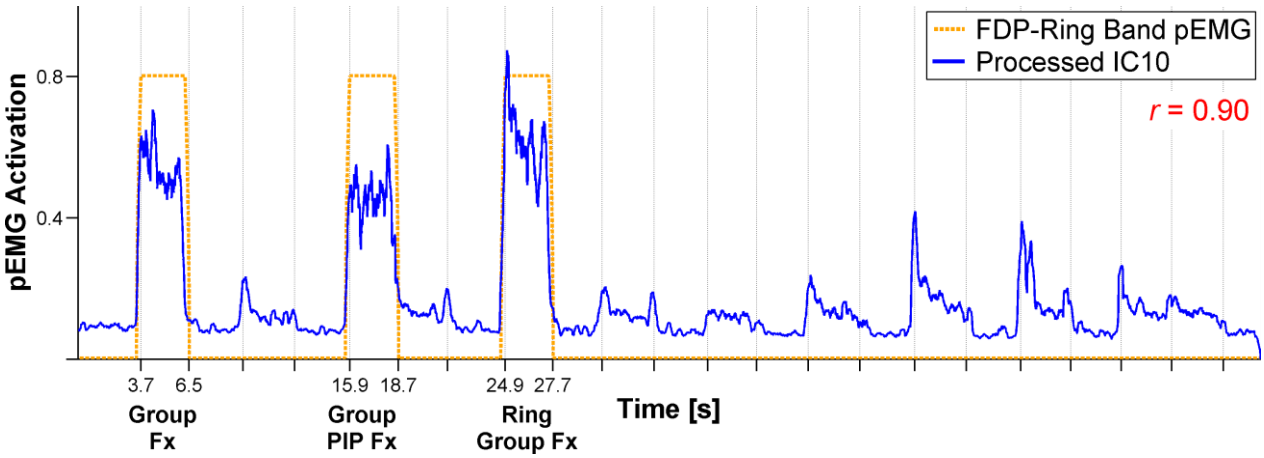

Figure 6.13 – Linear comparison of the predicted EMG waveform for FDP-Ring Band and a pIC.

This sample dataset is from Participant 4, Timing 3s experiment, run 1 showing the resultant Pearson's correlation coefficient for processed IC10.

This contraction sequence follows the fixed MP with all rest and the other movement labels left out for clarity.

The correlation coefficient analysis presented in the Case Study (Part D) focuses on the calculated *sample r values,* and how they describe the *mean population correlation values (ρ).*

Inherent to the definition of Pearson's correlation, the *r* distribution is *asymmetric* about the mean population correlation value as it is bound between -1 to +1, and is, therefore skewed towards zero[32] (Fisher, 1921). Due to this, averaged *r* values will *underestimate* the population mean as well as the standard error (SE) in the sense of being skewed closer to zero. Fisher first identified these inaccuracies were greatest in sample sizes N ≤ 30 (Fisher, 1915, 1921, 1924). To correct for this, Fisher proposed a set of transformation equations to compute an accurate *ρ* value, as well as an equation to correct the calculated standard error.

Fisher-corrected population means were calculated and reported in the correlation coefficient analysis presented in the Case Study (Part D). The method implemented to calculate the Fisher-corrected population means as well as the 95% confidence intervals (using Fisher's corrected SE equation) is outlined in Appendix D. Additionally, a three-tier ranking system was implemented from the guidelines outlined by Evans (1996) to interpret the sample and mean population correlation coefficient values.

The three correlation coefficient ranges used to rank the *level of muscle isolation* were defined as:

- Poor isolation: 0.00 – 0.59
- Moderate isolation: 0.60 – 0.79
- High isolation: 0.80 – 1.00

Using these definitions, comparisons were drawn across participants (*participant-level*) and across muscles (*muscle-level*) in the Case Study (Part D).

6.4.2 Representative IC Selection Algorithm

The calculated *r* values for each muscle in an experimental run were used to rank the pICs in descending order, where the highest ranked pIC was *initially* selected as the rIC for that muscle. One of the core principles of the sdEMG technique is that the muscles investigated are independent sources, therefore a single pIC cannot be representative of two muscles. However, due to the similarity of some of the pEMG waveforms, the same pIC was sometimes identified as the rIC for two different muscles. To resolve these conflicts, a lower ranked pIC was assigned to one of the muscles using a *unique rIC Selection Algorithm*. The algorithm recursively searched for a unique set of rICs for each experimental run as outlined in Figure 6.14.

[32] The direction of skewness is defined as the opposite direction in which the distribution is more concentrated. For example a positive mean *r* value skews the distribution in the negative direction (towards zero) and vice versa. Since the *r* distribution is bound between -1 and +1, the area below the probability density function (PDF) must remain equal to 1 thus the distribution becomes asymmetric and skewed inwards towards zero for non-zero mean *r* values. For a normal distribution, which is not bounded, the PDF simply shifts along the x-axis without skewing the distribution.

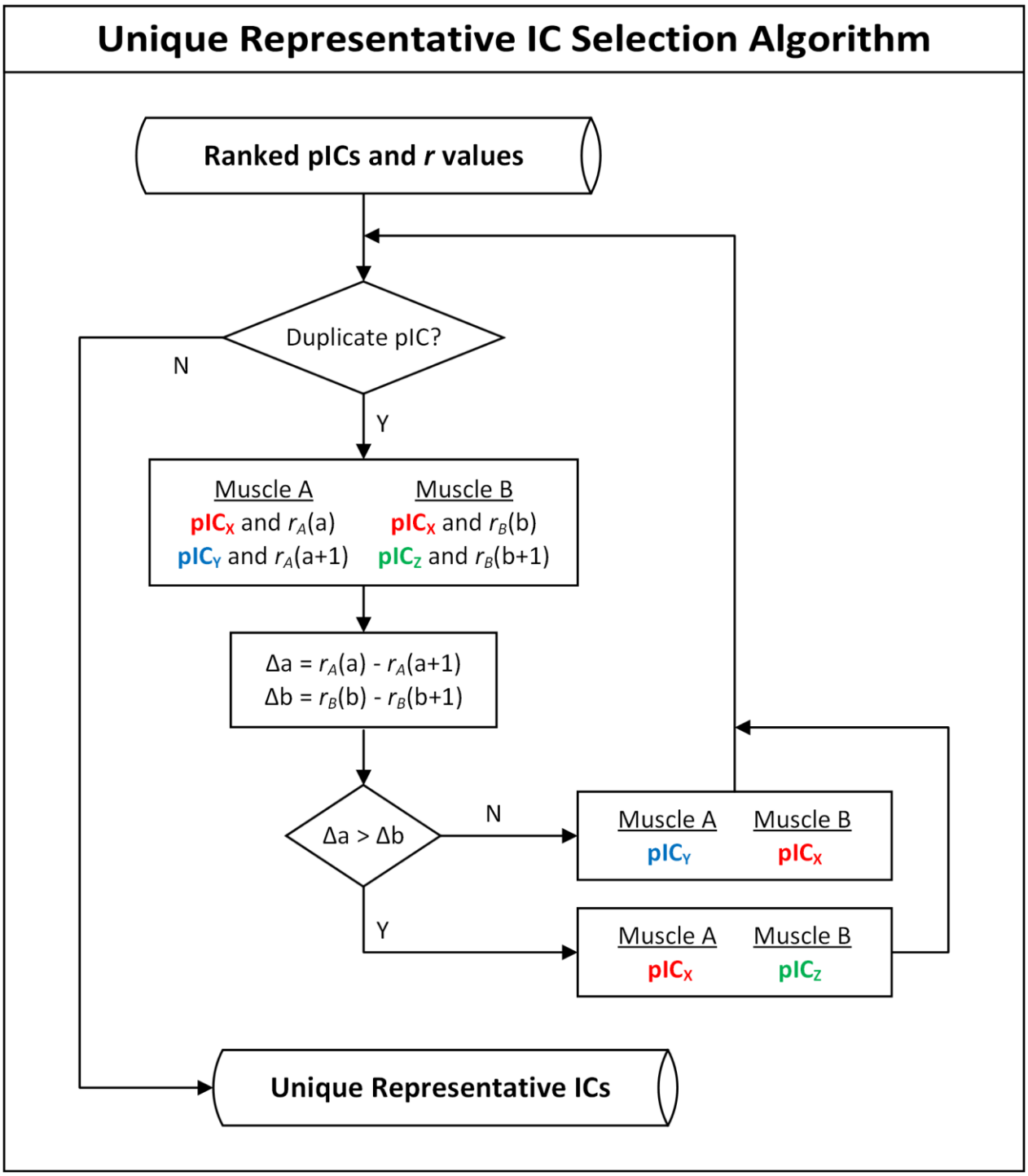

Figure 6.14 – Simplified flowchart outlining the Unique Representative IC Selection Algorithm.

As outlined in Figure 6.14, for the duplicate top ranked pIC_x; the algorithm compares the difference between the highest, and next highest *r* value for both muscles (Δa and Δb), and retains pIC_x for the muscle that has the largest change between successive *r* values. The method focuses on retaining pICs that have much *lower replacement r values*, and switch pICs that have *similar replacement r values*. The algorithm is further described using a sample dataset presented Table 6-3 which highlights two duplicate pIC cases, *pIC 5* and *pIC 14*.

Table 6-3: Sample set of top 5 r-ranked processed ICs (pICs) for the eight muscles investigated.

	Forearm muscles															
Rank	FPL		EPL		FDP-Index		FDP-Ring		EI		FDS-Index		FDS-Ring		ED	
	pIC	*r*	pIC	*r*	pIC	*r*	pIC	*r*	pIC	*r*	pIC	*r*	pIC	*r*	pIC	*r*
1	15	0.912	1	0.858	5	0.605	14	0.734	24	0.746	5	0.783	14	0.859	3	0.790
2	36	0.409	8	0.808	12	0.577	2	0.727	28	0.551	12	0.746	2	0.856	11	0.748
3	32	0.271	17	0.752	26	0.517	4	0.725	23	0.493	26	0.449	4	0.853	19	0.738
4	7	0.152	22	0.663	30	0.473	18	0.716	10	0.488	30	0.427	16	0.835	25	0.692
5	9	0.075	7	0.653	28	0.410	16	0.715	13	0.482	20	0.424	18	0.818	13	0.661

This sample dataset is from Participant 5, Timing 7s experiment, run 4 showing top 5 r ranked pICs.

Two sets of duplicate pICs are shown, pIC5 (highlighted in red) and pIC14 (highlighted in orange). The pICs that were selected to resolve the duplications are highlighted in green – pIC 12 for FDP-Index Band and pIC 2 for FDS-Ring Band.

In this dataset, pIC5 was ranked as the top pIC for FDP-Index Band and FDS-Index Band, as highlighted in red. Similarly, pIC14 was ranked as the top pIC for FDP-Ring Band and FDS-Ring Band, as highlighted in orange. These duplicates were resolved by examining the second highest pIC *r* values for each muscle.

Resolving duplicate pIC5:

The change in successive *r* values for FDP-Index Band was 0.028 while the corresponding change in FDS-Index Band was 0.037, therefore FDS-Index Band retained pIC5 and FDP-Index Band was reassigned to pIC12 (highlighted in green in Table 6-3).

Resolving duplicate pIC14:

The change in successive *r* values for FDP-Ring Band was 0.007 while the corresponding change in FDS-Ring Band was 0.003, therefore FDP-Ring Band retained pIC14 and FDS-Ring Band was reassigned to pIC2 (highlighted in green in Table 6-3).

This process was recursive to ensure a unique set of representative ICs was selected and the final results for this dataset are presented in Table 6-4, and the corresponding rIC plots are shown Figure 6.15.

Table 6-4: Final representative ICs (rICs) selected for Participant 5, Timing 7s experiment, run 4.

Forearm muscles																
FPL		EPL		FDP-Index		FDP-Ring		EI		FDS-Index		FDS-Ring		ED	
rIC	*r*	rIC	*r*	rIC	*r*	rIC	*r*	rIC	*r*	rIC	*r*	rIC	*r*	rIC	*r*
15	0.912	1	0.858	12	0.577	14	0.734	24	0.746	5	0.783	2	0.856	3	0.790

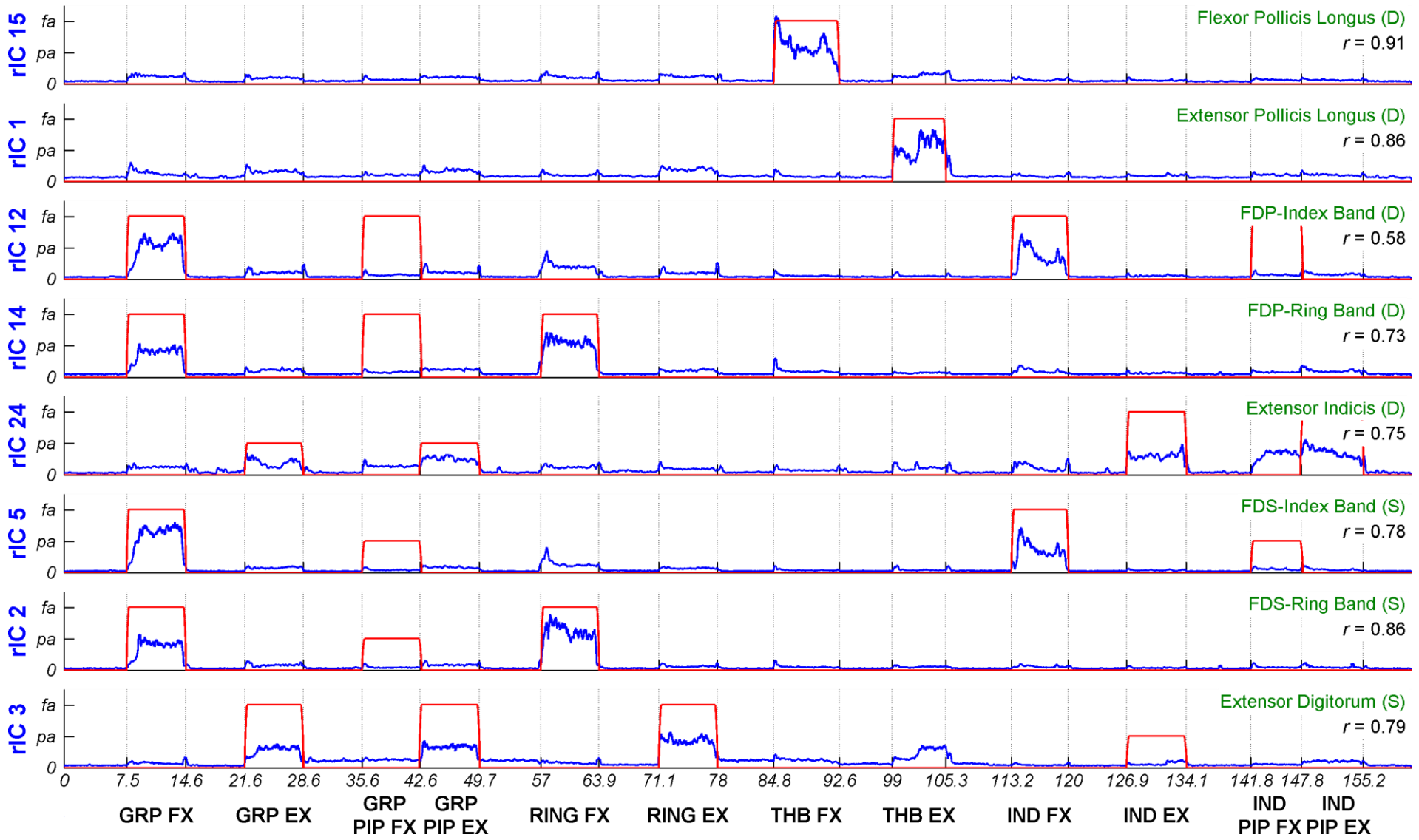

Figure 6.15 – Selected representative ICs (rICs) for Participant 5, Timing 7s (Experiment C, Run 4).

D – Deep muscle, S – Superficial muscle, FX – Flexion, EX – Extension, GRP – Group, THB – Thumb, IND – Index, PIP – Proximal interphalangeal (joint).

Full activation (fa) was set at 0.8 and Partial activation (pa) was set at 0.4. Rest labels are left out for brevity.

Figure 6.15 shows the selected rICs (blue lines) and the pEMG waveforms (red lines) for each forearm muscle investigated, as well as the corresponding *r* value indicating the *level of muscle isolation*. The rICs for flexor pollicis longus and extensor pollicis longus showed the highest *r* values of 0.91 and 0.86, respectively. Visual inspection of these waveforms indicates strong signal conformity between the rICs and pEMGs, where distinct EMG activity (near the *fa* and *pa* activation amplitudes) was seen during the expected active windows, and low EMG activity was seen during the expected inactive and rest windows. These two rIC cases serve as examples of where the sdEMG technique performed well.

However, this was not the case for all the muscles under investigation. There were instances where moderate[33] EMG activity was present in the expected inactive regions, for example, extensor digitorum (rIC 3) showed unexpected EMG activity during the thumb extension (THB EX) movement window. This type of signal mismatch was also observed in rICs 2, 3, 5, 12 and 14 where EMG activity was expected, but absent in the rIC.

These signal mismatches between the rICs and pEMG waveforms were found in most datasets and will be investigated further in Section 8.3 where potential causes are also proposed.

[33] Typically an EMG amplitude threshold is used to determine if EMG activity is present. There are several types of EMG activation thresholds such as a fixed percentage of MVC or standard deviation multipliers of the rest regions. In the present study, EMG activity between 0.1 and 0.2 (for a normalised amplitude) is considered *moderate activation*.

Part D – Case Study

Part D presents a case study exploring the experimental results. Chapter 7 primarily discusses the effects of the three movement protocol parameters investigated on the ability of the sdEMG technique to detect and isolate the extrinsic muscles of the hand. The global muscle performances are quantified and participant reaction delays are also explored.

Chapter 7 - Experimental Parameter Considerations

A case study consisting of five participants was conducted to develop sdEMG guidelines from experimental observations. Three parameters linked to the movement protocol (MP) were varied to evaluate the sdEMG technique and subsequently determine the effects of *timing*, *randomisation* and *anticipation* of movements on the ability of the sdEMG technique to detect and isolate deep and superficial muscle activity non-invasively.

The effects of the three experimental parameters were evaluated using the Fisher-corrected mean population correlation coefficients (ρ). A total of 122[34] experimental runs were recorded that produced 976 muscle rICs and sample r values which were evaluated at the *participant-level* (inter-participant population) and at the *muscle-level* (intra-participant population) across all experiments. The case study commences with a discussion on the individual experiments conducted followed by the participant-level and muscle-level analyses. The individual experiment findings are explored, thereafter an overview of the global muscle isolation performances are presented, and finally, participant reaction delay trends are considered.

7.1 Experiments Conducted

The case study investigated the effects of three movement protocol parameters on the identification of representative ICs for eight deep and superficial forearm muscles:

1. To investigate the effect of timing in the MP, three individual experiments A-C were designed to vary the movement window duration to 3, 5 and 7 seconds, respectively. Previous sdEMG studies implemented a 5 second movement window duration with favourable results, therefore the movement window duration was varied relative to this value to determine the effect of timing.
2. To investigate the effect of movement randomisation, the movement sequence in the MP was pseudo-randomised with the exception of the two sets of consecutive movements: Group PIP flexion and extension, and Index PIP flexion and extension. These consecutive movements were randomised as sets in the MP sequence. The Randomisation experiment is also referred to as Experiment D.
3. To investigate the effect of participant anticipation with respect to the upcoming movements in the MP sequence, the current movement instruction displayed on the GUI also showed the next movement to be performed as a watermarked image. The Anticipation experiment is also referred to as Experiment E.

The experiments conducted are summarised below and the results analysed in Sections 7.4, 7.5 and 7.6.

- **Experiment A** – Fixed MP sequence with 3s movement windows.
- **Experiment B** – Fixed MP sequence with 5s movement windows.
- **Experiment C** – Fixed MP sequence with 7s movement windows.
- **Experiment D** – Randomised MP sequence with 5s movement windows.
- **Experiment E** – Fixed MP sequence with anticipation GUI instructions and 5s movement windows.

[34] Three experimental runs were found to be incomplete or corrupt and had to be excluded from the study.

7.2 Participant-level Analysis

The participant-level groupings compared experiments across *participants*. Each experiment population consisted of all the muscle *r* values from *all* experimental runs from a *single participant*. For example, for a single participant, each experiment population consisted of 5 experimental runs where each run produced 8 muscle *r* values, resulting in a sample size of 40 *r* values. The distribution and variation of the sample *r* values are illustrated using box and whisker plots presented in Figure 7.1 which highlights the overall performance of each participant for each experiment by grouping the data for all muscles together.

To interpret the Pearson's correlation coefficient distributions plots, the following box and whisker plot parameters are specified:

- The height of each box represents the interquartile range (IQR) indicating the central 50% of the *r* values which is bound by the 25th percentile (first quartile, Q1) and the 75th percentile (third quartile, Q3).
- The width of the boxes are arbitrary and provides no information relating to the data.
- The median *r* values (50th percentile or second quartile, Q2) are shown by solid black lines in each box.
- The whiskers are shown by dashed black lines that extend to [1.5 x IQR][35] below Q1, and above Q3 which indicates the spread of ~99.3% of the data.
- Outliers are shown with black crosses outside the whisker boundaries.

As a simple measure of each participant's performance across all experiments, the medians[36] in Figure 7.1 showed that on average Participants 1 and 4 performed the best with all medians above 0.70. Of these two participants, Participant 4 performed the best as the central 50% of the *r* values (IQRs) and the data spread (estimated by the whisker ranges) for each experiment were on average more condensed than those of Participant 1, indicating less data variability within experimental runs.

Participants 2 and 5 performed similarly with medians in the range of 0.65 to 0.75, marginally lower than those of Participants 1 and 4. Participants 2 and 5 had more condensed IQRs compared to Participant 1 indicating less data variability within experimental runs.

Participant 3 had the lowest medians with very high data variation as seen by the large whisker ranges of 0.34 to 0.68 (*upper–lower* whiskers). While the IQRs for Participant 3 were more condensed than those of Participant 1, the Q3 levels for Participant 3 in experiments A, B, D and E were below 0.70. These Q3 levels show that on average only 25% of the data captured for these experiments lied above 0.70 which was the lowest performance of all the participants. By comparison, the Q3 levels for Participants 1, 4 and 5 were either above or close to 0.80, and always above 0.70 for Participant 2.

The participant-level findings were used to provide an initial analysis of the data and to assist in identifying poorly-performing participants.

[35] The 1.5 multiplier corresponds to approximately ±2.7σ for a normal distribution covering ~99.3% of the sample population (Krzywinski & Altman, 2014).

[36] For ease of reading 'median *r* values' will be shortened to 'medians'.

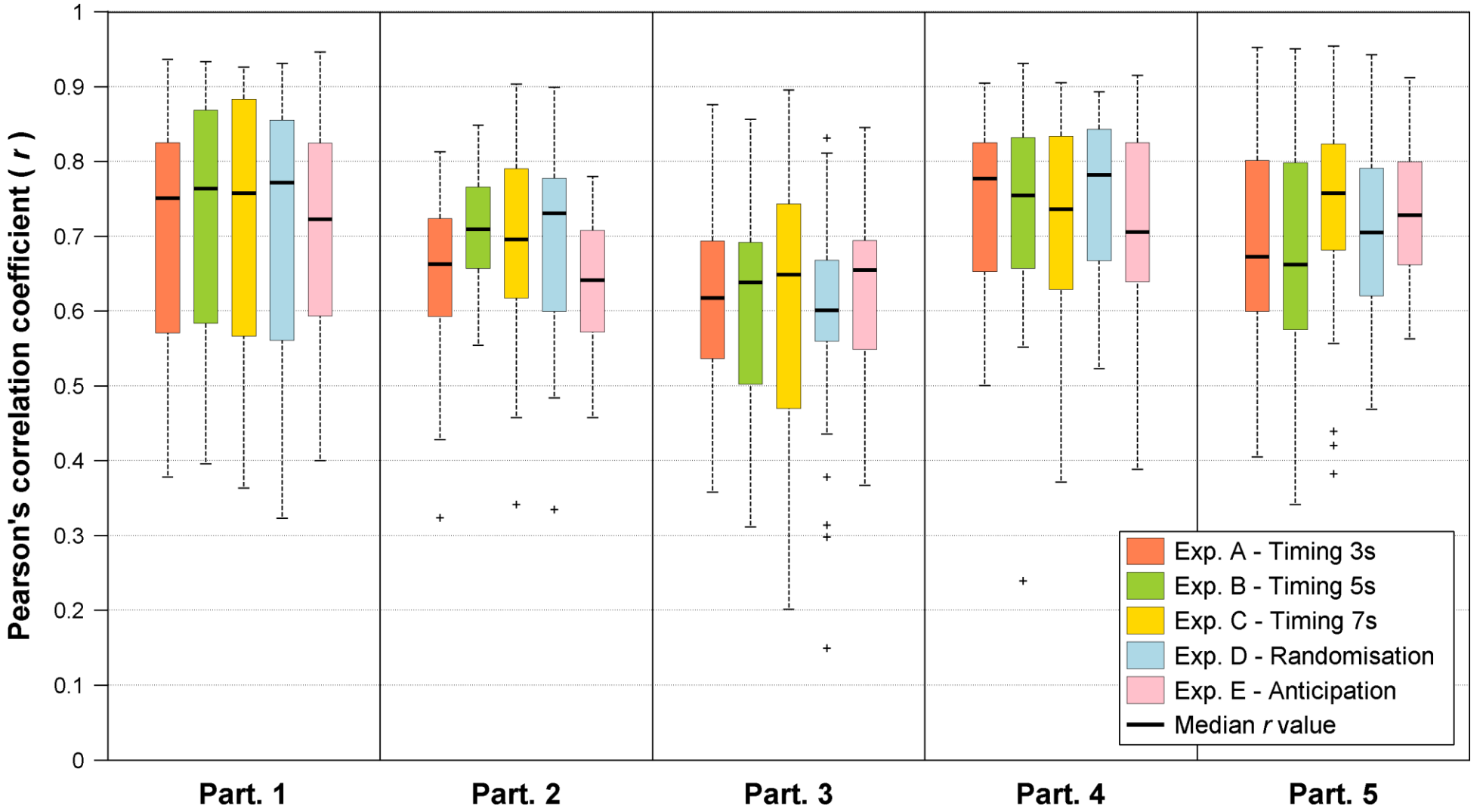

Figure 7.1 – Pearson's correlation coefficient (*r*) distributions for each experiment grouped by participants (participant-level results).

Each box and whisker plot reflects a single experiment population consisting of all the muscle r values grouped together from a single participant. For example, the leftmost red box and whisker plot consists of 5 runs of Experiment A which resulted in 8 r values per run (reflecting the eight muscles) which led to an experiment sample size of 40 r values.

7.3 Muscle-level Analysis

The primary objective of the sdEMG study was to determine how well each muscle was isolated. By assessing the levels of isolation for each muscle, conclusions regarding the experimental parameter variations could be made. To achieve this, muscle-level groupings of the data were formed which compared experiments across muscles, where the sample *r* values from all participants were combined for each muscle. For example, for a single muscle, an experiment grouping consisted of 5 runs from each participant resulting in a sample size of 25 *r* values. The Fisher-corrected mean population correlation values (ρ) and 95% confidence intervals (CIs), as described in Section 6.4.1, were then calculated using the method outlined in Appendix D. In Figure 7.2, the Pearson's correlation coefficient distributions are illustrated using grouped box and whisker plots, and the mean population correlation and 95% CIs are shown using grouped bar graphs.

7.3.1 Sample Distribution Observations

The median *r* values shown in Figure 7.2 served as an indication of *muscle isolation performance* across all participants. All muscles except FDP-Index Band, for Experiments A, C and D, were *moderately* isolated ($r > 0.60$). FPL was the only *highly* isolated muscle ($r > 0.80$) for Experiments B and D. All Q1 values were above 0.50 while only 23 out of 40 datasets had Q1 values above 0.60 indicating that 75% of all the muscle *r* values fell in the moderate isolation range. In general, the medians were closer to Q3 than Q2, and the upper whiskers were on average ~0.05 units above Q3 indicating that the upper 50% of the data was more densely grouped, while the lower 50% of the data was more spread out. This suggests that poor-performing participants may have pulled the sample distributions down as seen by the long Q1-Q2 ranges, as well as the long lower whiskers which are most pronounced for FPL, EI and FDS-Index Band which extend as low as 0.15.

A more detailed view of the influence of *individual participants* on muscle isolation performances is presented in Appendix E showing the sample distribution plots for each muscle and all experiments, grouped by *participants*. These distribution plots illustrate the inconsistency of participant performance across all experiments and muscles which accounts for the high variability seen in the lower 50% of the data.

7.3.2 Mean Population Observations

The Fisher-corrected mean population correlation results presented in Figure 7.2 indicate that for each muscle, the five experiments conducted did not show any distinct differences as evaluated by the ρ values. The 95% confidence intervals for all experiments showed very high variability with most intervals spanning ~0.45 units as a result of poor-performing participants and the low participant sample size. Nevertheless, the individual muscle isolation performances were examined to assist in the development of sdEMG guidelines, from which a number of trends were identified.

FPL, EPL and FDS-Ring Band had the highest ρ values (~0.80) indicating high muscle isolation. The results for FPL and EPL agreed with the postulation that *single muscle, single movement mappings* results in ideal muscle isolation using the sdEMG technique as discussed in Section 3.1. FDS-Ring Band was activated by three movements (see Table 6-2) which was the next lowest muscle-movement mapping in the movement protocols which further demonstrated that the sdEMG technique favours muscles with fewer functions. This was also supported by the results for FDP-Ring Band, which was also activated by three movements and had moderate isolation with ρ values of ~0.70, while the remaining muscles investigated were all activated by four movements and had comparatively lower ρ values across all experiments.

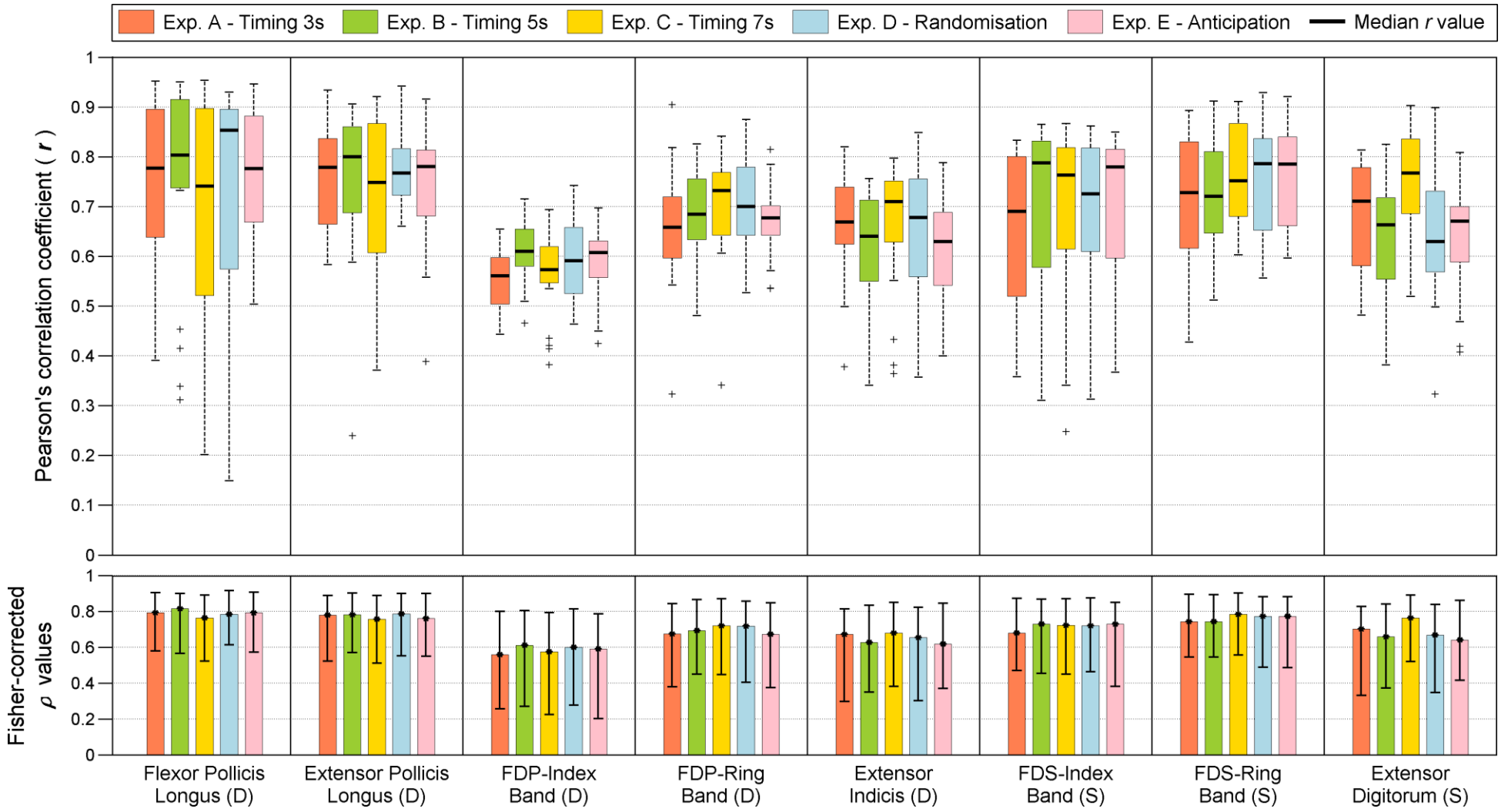

Figure 7.2 – Pearson's correlation coefficient (*r*) distributions and Fisher-corrected mean population correlation (*ρ*) results for each experiment grouped by the eight muscles investigated (muscle-level results).

Each box and whisker plot reflects a single experiment population consisting of all the r values from all participants grouped together for each muscle. For example, the leftmost red box and whisker plot consists of 25 r values calculated from all participants for flexor pollicis longus in Experiment A.

The bottom sets of bar graphs show the Fisher-corrected mean population correlation values (bar heights) and the corresponding 95% confidence intervals (solid error bars).

7.4 Timing Experiments

The movement timing parameter sets the muscle contraction and rest durations, which subsequently determines the length of each experimental run. Three movement window durations of 3, 5 and 7 seconds were investigated for the fixed MP sequence. The Fisher-corrected mean population correlation values for each muscle and experiment are summarised in Table 7-1 (the same results also appear in Figure 7.2 as the red, green and yellow bar graphs).

Table 7-1: Fisher-corrected mean correlation values (ρ) for the Timing experiments (A, B and C).

	Exp. A – Timing 3s		Exp. B – Timing 5s		Exp. C – Timing 7s		All Timings
Muscle	ρ	(95% CI)	ρ	(95% CI)	ρ	(95% CI)	$\rho_{max} - \rho_{min}$
Flexor Pollicis Longus (D)	0.79	(0.58, 0.90)	0.82	(0.57, 0.90)	0.76	(0.52, 0.89)	0.06
Extensor Pollicis Longus (D)	0.78	(0.52, 0.89)	0.78	(0.57, 0.90)	0.76	(0.51, 0.89)	0.02
FDP-Index Band (D)	0.56	(0.26, 0.80)	0.61	(0.27, 0.80)	0.58	(0.22, 0.79)	0.05
FDP-Ring Band (D)	0.68	(0.38, 0.84)	0.69	(0.45, 0.87)	0.72	(0.45, 0.87)	0.04
Extensor Indicis (D)	0.67	(0.30, 0.81)	0.63	(0.35, 0.83)	0.68	(0.38, 0.85)	0.05
FDS-Index Band (S)	0.68	(0.47, 0.87)	0.73	(0.45, 0.87)	0.72	(0.45, 0.87)	0.05
FDS-Ring Band (S)	0.74	(0.55, 0.90)	0.74	(0.54, 0.89)	0.78	(0.56, 0.90)	0.04
Extensor Digitorum (S)	0.70	(0.33, 0.83)	0.66	(0.37, 0.84)	0.76	(0.52, 0.89)	0.10

D – Deep muscle, S – Superficial muscle.

Comparisons were drawn across the three experiments for each muscle to determine the effect of timing in the movement protocol. For instance, flexor pollicis longus isolated with the highest ρ value (0.82) in the 5s experiment (shown in red text). The differences between the highest and lowest ρ values were also calculated and are shown in the last column of Table 7-1.

The 7s experiment had four muscles with the highest ρ values while the 5s experiment had three, and the 3s experiment had one. While the 7s experiment appears to outperform the 3s and 5s experiments it should be noted that the differences between the maximum and minimum ρ values are small, less than 0.06 for seven muscles and 0.10 for extensor digitorum which was considered negligible. In addition, the 95% confidence intervals for each Timing experiment overlapped and were relatively large with the smallest interval ($CI_{upper} - CI_{lower}$) being 0.33 (see red, green and yellow bar graphs in Figure 7.2).

The following conclusions were drawn from the Timing experiments:

1. The high variability seen in the data suggests that the sample population (no. of experimental runs) was too low, and was possibly influenced by poor-performing participants.
2. The experiments showed no discernible effect on the ability of the sdEMG technique to detect and isolate the deep and superficial muscles investigated.
3. No bias towards deep or superficial muscle isolation was evident, with both muscle groups resulting in similar ρ values with overlapping 95% confidence intervals.

7.5 Randomisation Experiment

For sdEMG studies with long movement protocols, it is suggested to randomise the movement sequence to reduce learning effects and movement specific muscle fatigue. While this has been implemented in previous studies (Mulligan, 2014; Pitman, 2015; Swanepoel, 2017), a Randomisation experiment was conducted to investigate if MP randomisation influenced the ability to isolate deep and superficial muscles when compared to a non-randomised MP sequence. The randomised MP (Exp. D) implemented a 5s movement window duration, therefore the results from the 5s Timing experiment (Exp. B) were used as the non-randomised control experiment. The randomised Fisher-corrected mean population correlation values are presented in Table 7-2 (the same results also appear in Figure 7.2 as the green and blue bar graphs).

Table 7-2: Fisher-corrected mean correlation values (ρ) for the Non-randomised and Randomised experiments (B and D).

	Exp. B – Non-randomised		Exp. D – Randomised		$\Delta\rho$
Muscle	ρ	**(95% CI)**	ρ	**(95% CI)**	$\rho_{non} - \rho_{rand}$
Flexor Pollicis Longus (D)	0.82	(0.57, 0.90)	0.79	(0.61, 0.92)	0.03
Extensor Pollicis Longus (D)	0.78	(0.57, 0.90)	0.79	(0.55, 0.90)	-0.01
FDP-Index Band (D)	0.61	(0.27, 0.80)	0.60	(0.28, 0.81)	0.01
FDP-Ring Band (D)	0.69	(0.45, 0.87)	0.72	(0.40, 0.86)	-0.02*
Extensor Indicis (D)	0.63	(0.35, 0.83)	0.65	(0.30, 0.82)	-0.03*
FDS-Index Band (S)	0.73	(0.45, 0.87)	0.72	(0.46, 0.88)	0.01
FDS-Ring Band (S)	0.74	(0.54, 0.89)	0.77	(0.49, 0.88)	-0.03
Extensor Digitorum (S)	0.66	(0.37, 0.84)	0.67	(0.35, 0.84)	-0.01

D – Deep muscle, S – Superficial muscle.

** The ρ values presented are rounded off to 2 decimal places while the difference calculation was performed on the full decimal ρ values (For example, FDP-Ring Band: 0.69411 – 0.71758 = -0.02347).*

Similar to the Timing experiments, there was little difference in the ρ values between the non-randomised MP sequence and randomised MP sequence experiments across all muscles as indicated in Table 7-2. The highest ρ values (shown in red text) for five muscles were found in the randomised experiment with the difference in ρ values between experiments being at most ± 0.03. Similar to the Timing experiments, the 95% CIs for the randomised dataset overlapped (see green and blue bar graphs in Figure 7.2) and were relatively large (≥ 0.30).

The same three conclusions found for the Timing experiments were drawn for the Randomisation experiment.

7.6 Anticipation Experiment

Visual cues are the most appropriate means to provide participants with instructions to complete an MP sequence in an experimental run. Watermarked instruction images were used to investigate the effect of anticipation of movements on the ability of the sdEMG technique to detect and isolate the deep and superficial muscles. See Table 5-3 and Table C-2 for the full set of watermarked images used.

The anticipated MP (Exp. E) implemented a 5s movement window duration, therefore the results from the 5s Timing experiment (Exp. B) were used as the non-anticipated control experiment. The same movement sequence was used in both experiments. The non-anticipated and anticipated Fisher-corrected mean population correlation values are presented in Table 7-3 (the same results also appear in Figure 7.2 as the green and pink bar graphs).

Table 7-3: Fisher-corrected mean correlation values (ρ) for the Non-anticipated and Anticipated experiments (B and E).

	Exp. B – Non-anticipated MP		Exp. E – Anticipated MP		$\Delta\rho$
Muscle	ρ	**(95% CI)**	ρ	**(95% CI)**	$\rho_{non-ant} - \rho_{ant}$
Flexor Pollicis Longus (D)	0.82	(0.57, 0.90)	0.79	(0.57, 0.91)	0.02*
Extensor Pollicis Longus (D)	0.78	(0.57, 0.90)	0.76	(0.55, 0.90)	0.02
FDP-Index Band (D)	0.61	(0.27, 0.80)	0.59	(0.20, 0.79)	0.02
FDP-Ring Band (D)	0.69	(0.45, 0.87)	0.67	(0.37, 0.85)	0.02
Extensor Indicis (D)	0.63	(0.35, 0.83)	0.62	(0.37, 0.85)	0.01
FDS-Index Band (S)	0.73	(0.45, 0.87)	0.73	(0.38, 0.85)	0.00
FDS-Ring Band (S)	0.74	(0.54, 0.89)	0.77	(0.49, 0.88)	-0.03
Extensor Digitorum (S)	0.66	(0.37, 0.84)	0.64	(0.42, 0.86)	0.02

D – Deep muscle, S – Superficial muscle.

** The ρ values presented are rounded off to 2 decimal places and the difference calculation was performed on the full decimal ρ values (For example, Flexor pollicis longus: 0.81568 – 0.79249 = 0.02319).*

Similar to the Timing and Randomisation experiments there was little difference in the ρ values between the non-anticipated MP sequence and anticipated MP sequence experiments across all muscles as indicated in Table 7-3. The non-anticipated MP sequence showed the highest ρ values (shown in red text) for seven muscles with small differences (± 0.03) in ρ values between experiments. Similar to the Timing and Randomisation experiments, the 95% CIs of the anticipation dataset overlapped (see pink bar graphs in Figure 7.2) and were relatively large (≥ 0.33).

The same three conclusions found for the Timing and Randomisation experiments were drawn for the Anticipation experiment.

7.7 Amalgamated Population Analysis

Due to the low variability seen between *experiments*, an amalgamated population was considered to provide a single measure of *individual muscle* isolation performances. The amalgamated muscle groupings consisted of the *r* values from all experiments, participants and experimental runs. The Fisher-corrected mean population correlation results for the muscle groupings are presented in Figure 7.3.

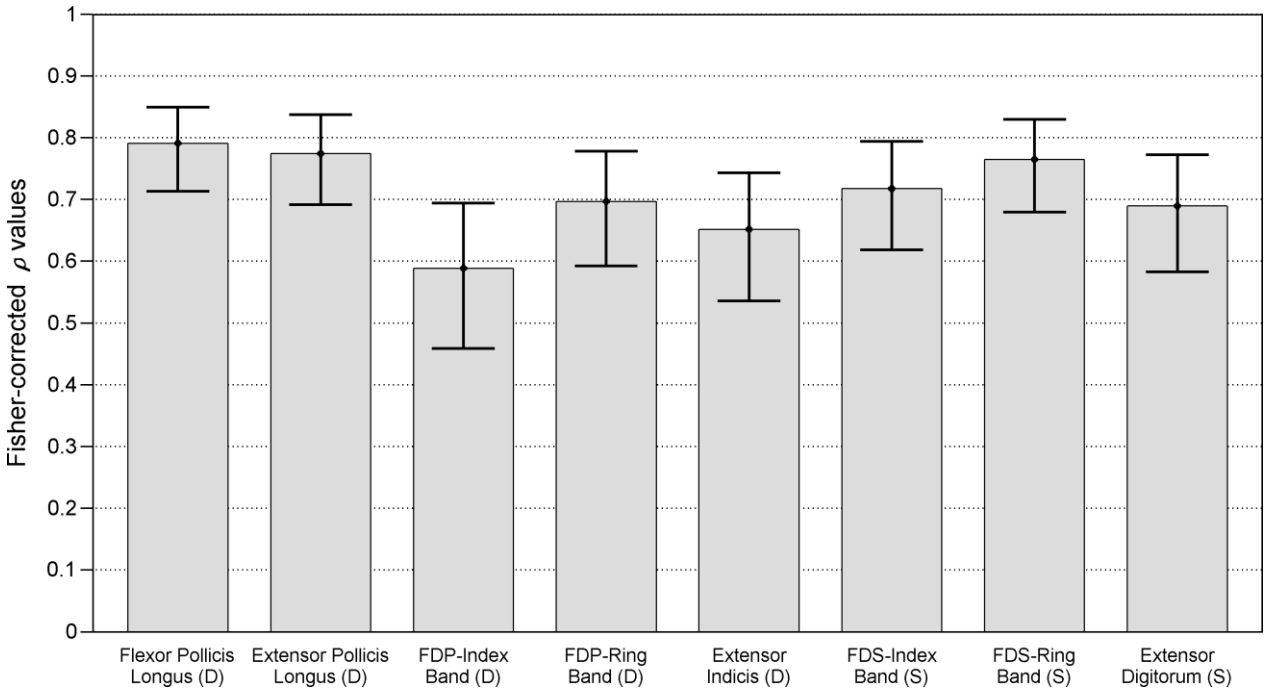

Figure 7.3 – Fisher-corrected mean correlation (*ρ*) results for the amalgamated dataset.

D – Deep muscle, S – Superficial muscle. The amalgamated dataset for each muscle consists of the 122 sample r values from all participants and all experiments. 95% confidence intervals are indicated by error bars.

Figure 7.3 shows that all muscles except FDP-Index Band were moderately isolated with *ρ* values greater than 0.65, while FDP-Index Band had a *ρ* value of 0.59. FPL and EPL were the best performing muscles with *ρ* values slightly below 0.80. FPL and EPL were almost completely encircled by the electrode arrays (see Figure 4.2), which was assumed to be the best placements to detect deep compound EMG activity and could account for the high *ρ* values.

FDS consists of more *well-defined* muscle bands than FDP (see Figure 3.1 (a)), therefore the relatively higher *ρ* values obtained for FDS agreed with the underlying anatomy. FDP-Index Band isolated with a *ρ* value of 0.59 while FDS-Index Band isolated with a *ρ* value of 0.72. Similarly, FDP-Ring Band isolated with a *ρ* value of 0.70 while FDS-Ring Band isolated with a *ρ* value of 0.76.

Extensor digitorum isolated with a *ρ* value of 0.69 and extensor indicis performed similarly with a *ρ* value of 0.65. This may be due to the pEMGs for both muscles having anticipated EMG activity in the same movement windows, albeit at different activation magnitudes (see Table 6-2).

From the amalgamated results it is evident that there are underlying anatomical mechanisms that influenced the ability of the sdEMG technique to isolate the tightly packed muscles of the forearm, which will be further discussed in Chapter 8.

7.8 Reaction Delays

Participant reaction delays were inspected to determine the influence Experiments A to E had on how well a participant was able to execute the movement protocol. Each experiment modified the movement protocol and subsequently the presentation of visual cues to the participant. Inspecting the reaction delays provided a quantitative view of the difficulty experienced by participants in executing the experiments in a consistent manner.

The calculation of the start and stop reaction delays is illustrated in Figure 7.4. The start reaction delay (α) for each movement in the MP was calculated as the difference between the time the start instruction was displayed on the GUI and the contraction onset time from the activation timing masks (ATMs, discussed in Section 6.2.3). Similarly, the stop reaction delay (β) was calculated as the difference between the stop instruction time and contraction offset time from the activation timing masks.

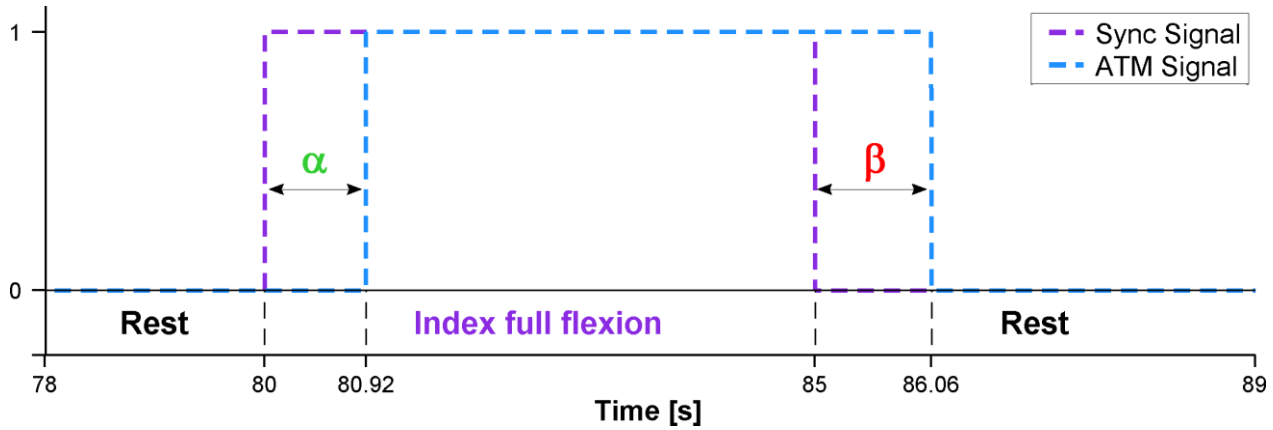

Figure 7.4 – Calculation of the start (α) and stop (β) participant reaction delays.

The Sync signal indicates when the start and stop instructions were displayed on the GUI.

The ATM signal indicates the contraction onset and offset times extracted from the flex sensor timing signals.

The mean reaction delays for each movement window across all experiments are shown in Figure 7.5. It is clear that for all experiments, the mean start and stop reaction delays were comparable within each movement window. In general the start reaction delays were slightly longer than the stop reaction delays, however, this was considered negligible since all the standard deviation error ranges overlapped.

The Timing and Randomisation experiments showed that the mean reaction delays were consistent throughout the MP at approximately 1 ± 0.5 seconds for all movement windows which indicated that participants were able to repeatedly execute the Timing and Randomisation experiments with consistency.

In contrast, the mean reaction delays for the Anticipation experiment showed a steadily increasing trend across the first 10 movements, originating at approximately 1 ± 0.25 seconds, and increasing linearly to approximately 3.5 ± 0.25 seconds. Thereafter the reaction delays show a decreasing trend, dropping to approximately 3.25 ± 2 seconds. These findings suggest that participants struggled with the anticipated movement protocol, and the reaction delays got progressively worse throughout each experimental run. These observations could indicate that the manner in which the anticipated visual cues were presented was too complex and possibly confused participants, resulting in the inconsistent execution of the movement protocol.

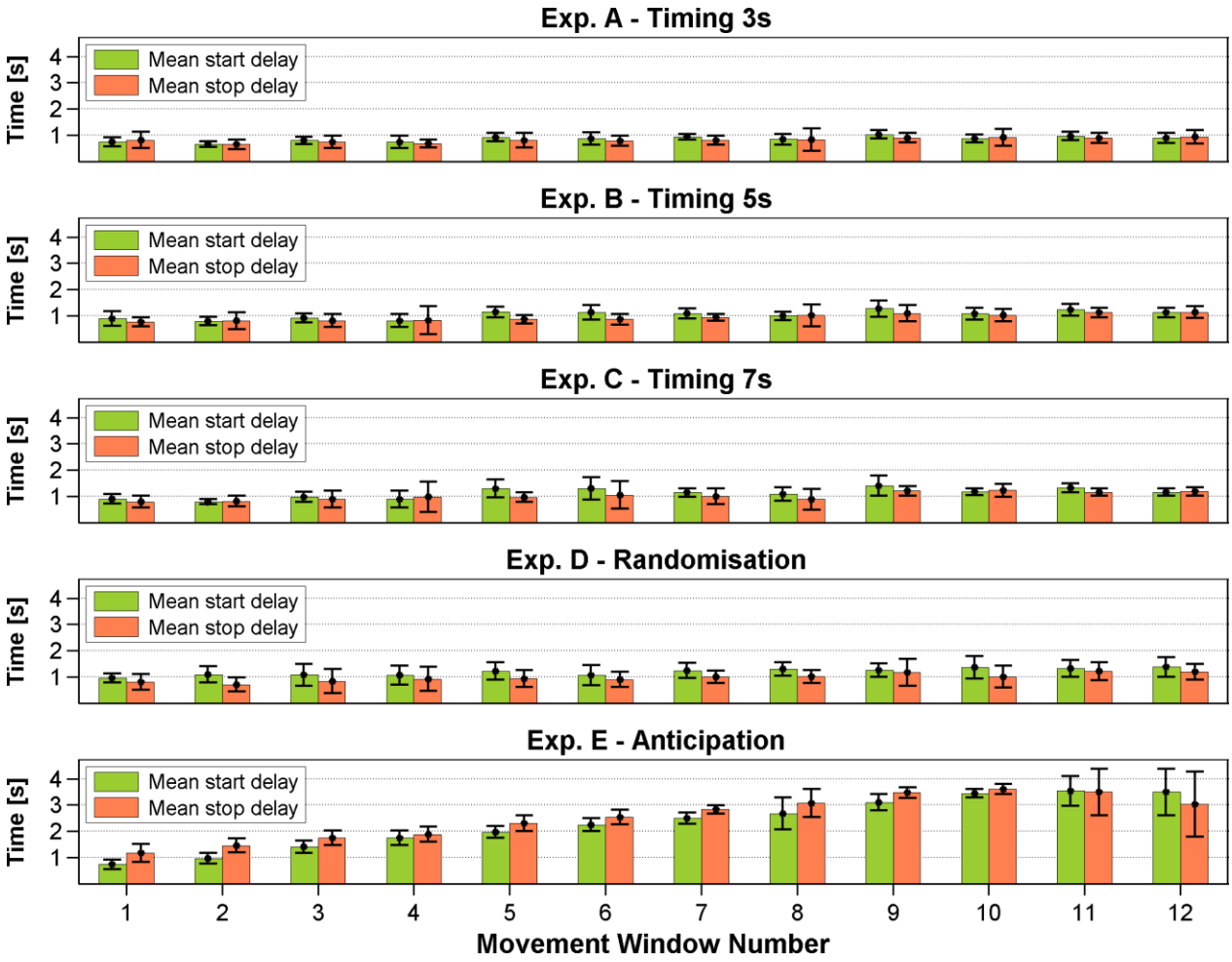

Figure 7.5 – Movement window mean start and stop reaction delays for Experiments A to E.

The movement window numbers correspond to the consecutive contractions performed during the movement protocols. Sample size per experiment is ≤ 25 experimental runs. The error bars indicate 1 standard deviation.

It should be noted that these reaction delays did not negatively impact the outcome of the sdEMG technique since the generation of the pEMG waveforms incorporated time synchronisation to ensure that the pICs and pEMGs aligned before calculating the correlation coefficient values. The reaction delay data for the Anticipation experiment does suggest that there are other factors that need to be considered when developing an sdEMG system, in particular, the manner in which movement instructions are presented.

Part E – Discussions and Conclusions

Part E presents the main findings and discusses the non-ideal observations identified throughout the analyses in Chapter 8. Proposed future work is outlined in Chapter 9 and a list of concise sdEMG guidelines is presented in Chapter 10.

Chapter 8 - Discussion

The case study highlighted several shortcomings in the implementation of the developed sdEMG system. This chapter discusses possible causes for the observed results with reference to the developed apparatus that could account for the non-ideal observations, as well as potential flaws in the methodology of the sdEMG technique. Furthermore, the possible causal links between the data processing methods and outcome measures of the technique are explored with an emphasis on guidance for future sdEMG research.

8.1 Summary of Main Findings

The deep and superficial extrinsic hand muscles of five healthy participants were successfully detected and isolated using the sdEMG technique. Using an amalgamated population of all participants combined (see Section 7.7), the eight muscles investigated were isolated with Fisher-corrected mean correlation coefficient (ρ) values greater than 0.65 indicating *moderate*[37] isolation, with the exception of FDP-Index Band which was *poorly* isolated with a ρ value of 0.59. The deep muscles FPL and EPL showed the best isolation performance with ρ values of 0.79 and 0.77, respectively. Furthermore, the results obtained indicated no clear bias between the ability to isolate deep or superficial muscles which was a trend identified in the previous forearm sdEMG study by Pitman (2015).

The *Timing*, *Randomisation* and *Anticipation* experiments showed *no* discernible effects across all participants on the ability of the sdEMG technique to detect and isolate the deep and superficial forearm muscles investigated. The data did, however, show high variability in all experiments indicating that the sample population was too small and was possibly influenced by poor performing participants. The Anticipation experiment also showed that, on average, the participant reaction delays increased steadily during each experimental run suggesting the anticipated visual cues were too complex and potentially confused participants. This, however, did not impact the performance of the sdEMG technique as the predicted EMG (pEMG) waveforms were synchronised to match the exact onset and offset of each movement in an experimental run.

8.2 Muscle Isolation Performances

In Section 7.7 an amalgamated population was constructed to provide a single measure of individual muscle isolation performance for *all* participants. Similarly, amalgamated populations were constructed for *each* participant to investigate the influence of participant fitness levels, relative muscle sizes and muscle bundle separability. These combined population results are presented in Table 8-1 where the muscles are ranked in descending order of muscle isolation performances (first row, from left to right) as determined by the Fisher-corrected mean ρ_{all} values.

The top four performing muscles, as determined by their ρ_{all} values, were FPL (0.79), EPL (0.77), FDS-Ring Band (0.76) and FDS-Index Band (0.72). It is suggested these muscles performed the best as they are anatomically *well-defined* and a *large portion* of each muscle belly (irrespective of the relative muscle size) lies within the *forearm window* which is where the electrode bands encircled the limb. Furthermore, the top two performing muscles, FPL and EPL, have *single muscle, single movement mappings* which is consistent

[37] As defined in the three-tier ranking system presented in Section 6.4.1: Poor isolation 0.00 – 0.59, moderate isolation 0.60 – 0.79 and high isolation 0.80 – 1.00.

with the postulation that the sdEMG technique is more effective on muscles that are easily targeted with a single movement.

Table 8-1: Mean amalgamated population correlation results for all experiments and participants, ranked in descending order of muscle isolation (first row, from left to right).

	FPL (D)	EPL (D)	FDS-Ring Band (S)	FDS-Index Band (S)	FDP-Ring Band (D)	ED (S)	EI (D)	FDP-Index Band (D)
All Parts.	0.79	0.77	0.76	0.72	0.70	0.69	0.65	0.59
Part. 1	0.86	0.86	0.87	0.79	0.77	0.54	0.47	0.58
Part. 2	0.64	0.68	0.70	0.74	0.65	0.80	0.69	0.59
Part. 3	0.53	0.78	0.64	0.44	0.64	0.69	0.68	0.56
Part. 4	0.86	0.73	0.81	0.83	0.74	0.69	0.64	0.65
Part. 5	0.90	0.78	0.75	0.69	0.67	0.68	0.74	0.56

Parts. – Participants, D – Deep muscle, S – Superficial muscle. 95% confidence intervals left out for brevity.

8.2.1 Participant Fitness Levels

As discussed in Section 7.2, Participants 1 and 4 were considered the best overall performing participants based on the *participant-level* results which compared experiments between participants, not muscles. These findings are consistent with the amalgamated population results presented in Table 8-1 where Participant 4 is still considered the best overall performing participant with *moderate* and *high* isolation levels across all muscles.

The findings presented also align with the fitness levels of participants, where Participants 1 and 4 were noted as bodybuilders with well-toned forearm muscles, while Participants 2, 3 and 5 were of average fitness. The selection of participants for the present study was limited and it is advised that future studies recruit participants of similar fitness levels to produce more comparable results.

8.2.2 Relative Muscle Sizes

The results show that there was no definitive link found between *muscle size* and *muscle isolation performance*. For example, consider FPL and EPL, these are two of the smallest muscles investigated (see Figure 3.1 and Figure 3.2 for relative muscle sizes) however they had the highest isolation performances. In contrast, ED which is one of the larger muscles was found to have lower isolation performances than FDS-Index Band which is a substantially smaller muscle. While the sample size of five participants was small, it is suggested that the results support the argument that there was no causal relationship found between muscle size and muscle isolation performance using the sdEMG technique.

The present study implemented a dynamic movement protocol with '*no-load*' conditions which resulted in very low muscle contraction levels (as a percentage of MVC). The raw EMG recordings showed mean *peak* EMG amplitudes of approximately 0.4mV which is considerably low for surface EMG. At these low levels, it is unknown whether the EMG activity originating from the deep muscle bellies, that were not fully within the forearm window, sufficiently propagated to the electrodes by means of volume conduction to contribute to the measured potentials and allowed for adequate source signal demixing.

8.2.3 Muscle Bundle Separation

In the development of the movement protocol (MP) described in Section 3.2, FDS and FDP were shown to have closely related functions that result in co-contraction during finger flexion movements. In order to isolate these muscles using the sdEMG technique, the muscles were split into *muscle bands* that would effectively function as *independent muscle sources*.

FDS has four *very* distinct muscle and tendon bundles that begin to branch out at the common tendon origin point and thus can effectively be split into individual muscle bands (see Figure 3.1 (a)). The amalgamated results presented in Table 8-1 agree with this postulation where the FDS-Ring Band and FDS-Index Band were well isolated with ρ_{all} values of 0.76 and 0.72, respectively.

Similar to FDS, FDP branches into four distinct muscle and tendon bundles however they are not as defined as FDS and only begin to branch out at approximately the midpoint of the FDP muscle belly (see Figure 3.1 (b)). This anatomical arrangement indicates that co-contractions are more prominent in the FDP than in FDS due to the shared motor unit innervation amongst the FDP muscle bundles. Nevertheless, the FDP bundles are separated in the vicinity of the forearm window, and so it was assumed that these bundles would be able to function as independent muscle sources.

Splitting FDP into FDP-Ring and FDP-Index bands was a reasonable proposition, however, the results attained did not support this. In particular, FDP-Index Band was the worst performing muscle with all participants showing poor isolation (ρ < 0.60) with the exception of Participant 4 (ρ = 0.65), as shown in Table 8-1. While FDP-Ring Band was the fifth best performing muscle (ρ_{all} = 0.70), it should be noted that FDP-Ring Band consists of *three* muscle bands acting as one therefore the resultant EMG activity detected would be more pronounced than FDP-Index Band (a single muscle bundle) and could have contributed to the higher isolation performance.

The high isolation performances of the FDS bands indicate that FDS is well-suited for muscle bundle separation when using the sdEMG technique. In contrast, FDP is not advised for muscle bundle separation however if required, a resistive load should be applied to increase muscle contraction levels (higher percentage of MVC) thereby increasing the likelihood of detecting sufficient EMG activity from these less distinct deep muscle bundles.

8.3 Signal Compliance

The sample set of representative ICs (rICs) presented in Figure 6.15 highlighted several non-ideal observations in the compliance between the best-selected rICs and the pEMG signals. A perfect match between rIC and pEMG signals is improbable given the stochastic nature of EMG signals as well as the idealised rectangular waveform model used to generate the pEMG waveforms. In the present study, minor signal mismatches such as misaligned pEMG windows were typical, however more pronounced mismatches such as unexpected EMG activity were sometimes observed. These phenomena were also noted in previous sdEMG studies (Pitman, 2015; Swanepoel, 2017) and appear to be a limitation of the current implementation of the sdEMG technique.

The two main types of signal mismatches identified in this study were: *EMG activity present but not expected*, and *EMG activity expected but absent*. Participant compliance also factored into the non-ideal observations and is considered in the proposed explanations for the signal mismatches.

8.3.1 Unexpected EMG Activity

The most common signal mismatch occurred when EMG activity was *present* in the rIC but was *unexpected* as informed by the pEMG waveform.

This signal mismatch is described with reference to a reduced dataset consisting of three muscle rICs presented in Figure 8.1 for a highly isolated experimental run.

FPL, FDS-Ring Band and FDS-Index Band muscle rICs along with the generated pEMG signals as well as the corresponding flex sensor (FS) signals are presented in Figure 8.1. The pIC selected to represent FDS-Ring Band (rIC 20) shows high correlation (0.80) with the corresponding pEMG signal, however there is a distinct EMG burst present that aligns with the *Index flexion window (IND FX)* as highlighted by ellipse A. In the movement protocol, Ring Group flexion is not instructed concurrently with index flexion, therefore no EMG activity is expected in the FDS-Ring Band rIC within this window. Furthermore, the Ring Group MCP flex sensor (FS4) shows no changes within this window as highlighted by ellipse B, which indicates that the participant did *not* incorrectly perform Ring Group flexion which could have accounted for the mismatch observed in the FDS-Ring Band rIC. Similarly, during the *Ring Group flexion window (RING FX)*, unexpected EMG activity is present on the FPL rIC as highlighted by ellipse D, however, thumb flexion was not detected by the thumb IP flex sensor (FS3), as highlighted by ellipse E that could have accounted for this mismatch.

Several factors influencing either the rIC signals or the pEMG waveforms could contribute to the observed mismatches. The most likely cause of the unexpected EMG activity mismatching is the inability of ICA to *fully* separate the mixed EMG signals into independent muscle sources. In the examples provided, the unexpected EMG activity observed is not anatomically linked to the movement being performed therefore the mismatch must lie with the rIC and not the pEMG. For example, thumb flexion activates FPL which has no shared musculature or motor unit innervation to FDS that could account for the activity found on the FPL rIC during Ring Group flexion – which only activates the FDS-Ring Band and FDP-Ring Band (not shown Figure 8.1).

In addition to the inability of ICA to fully decompose the underlying muscle sources, ICA could have also struggled to separate signal crosstalk between channels. Signal crosstalk is a common occurrence in monopolar surface EMG and given the large quantity of electrodes (64) and close inter-electrode distances (mean ± SD; IED: 7.6 ± 0.5 mm) used in this study, the mutual information shared between adjacent electrodes is high, thus making the signal separation task more challenging. Crosstalk is, however, a fundamental basis for the sdEMG technique in that the measured potentials at electrodes represent a mixture of compound EMG from different muscles, therefore it is inevitable that some latent EMG activity will be found on other rICs. For example, the rIC selected for FDS-Index Band in Figure 8.1 shows strong signal separation with very little EMG activity in the expected inactive regions however latent EMG activity is still present in the Ring Group flexion window which is indicative of signal crosstalk.

The processed ICs (pICs) were ranked based on their calculated *r* values and the highest ranked pICs were selected to represent the EMG activity for each muscle. In the case of duplicate rIC assignments, lower ranked pICs were assigned recursively until a unique set of rICs was found. The switching of pICs could be responsible for some of the observed signal mismatches, however, visual inspections generally showed that often the difference in *r* values were minor ($\Delta r < 0.05$) and the pICs had similar spatial profiles.

The examples provided in Figure 8.1 show highly isolated muscles ($\rho > 0.80$) however most datasets did not show such clear muscle isolation as highlighted by the mean population correlation results presented in Table 8-1.

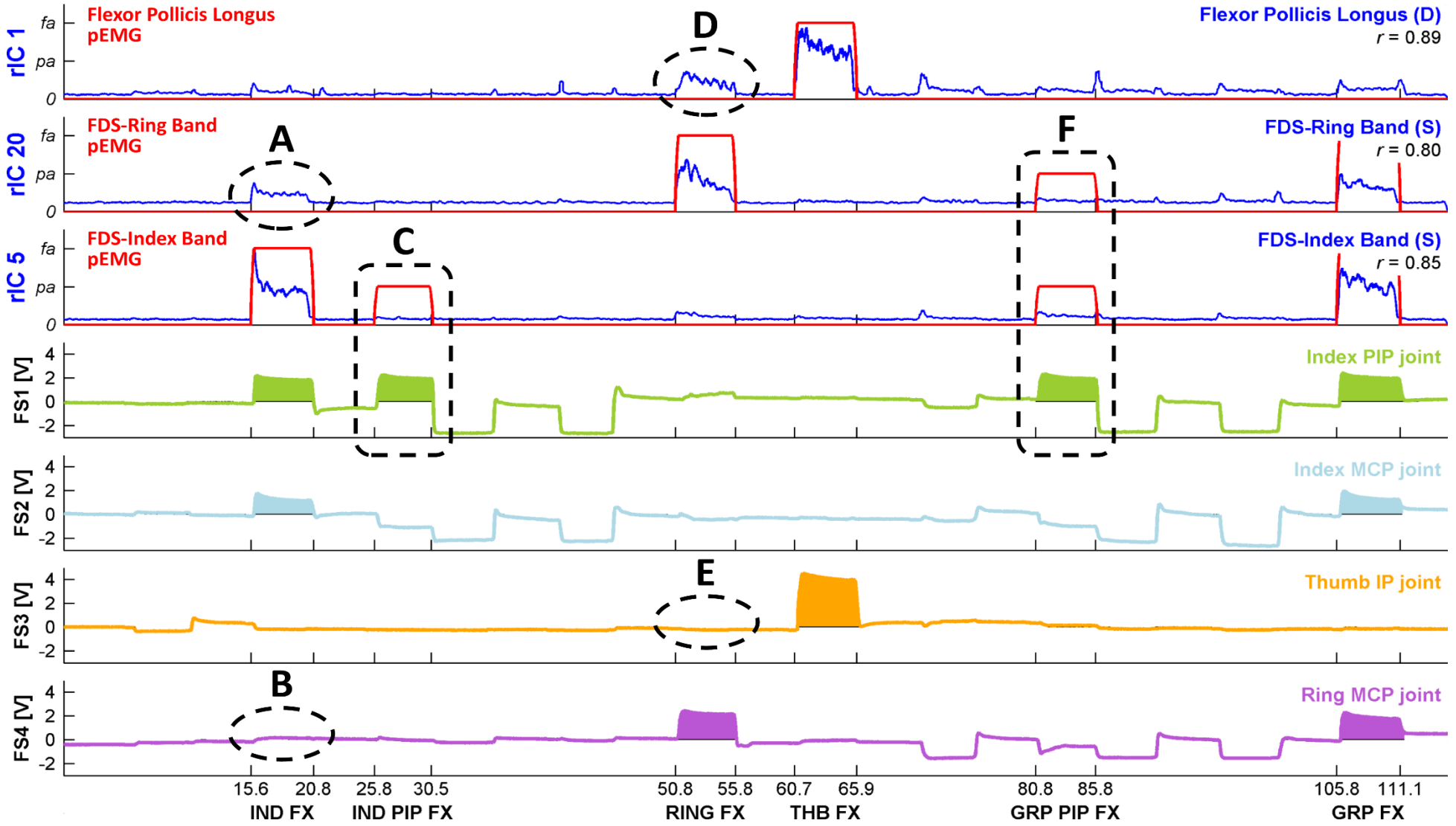

Figure 8.1 – Identified representative IC (rIC), predicted EMG (pEMG) signal mismatches and the corresponding flex sensor (FS) signals (Set A).

A sample set of pEMG waveforms (red signals) and rICs (blue signals) are shown. The shaded flex sensor signals indicate when finger movement was detected (positive changes indicate flexion and negative changes indicate extension). The ellipses show examples of where EMG activity was present (A and D) but not expected (pEMG inactive region) or movement detected (B and E). The rectangles indicate examples where EMG activity was expected (pEMG active regions and correct movements were detected) but not present.

8.3.2 Absent EMG Activity

Another common signal mismatch occurred when EMG activity was *expected*, as informed by the pEMG waveform, but was *absent* in the rIC.

This signal mismatch is described with reference to a reduced dataset consisting of three muscle rICs presented in Figure 8.1 for a highly isolated experimental run.

Two examples of this type of signal mismatch are highlighted by rectangles C and F where partial EMG activity (*pa*) was expected in the FDS-Index and FDS-Ring bands, however, no distinct EMG activity was present in the corresponding rICs. These instances occur during *Index PIP flexion (IND PIP FX)* and *Group PIP flexion (GRP PIP FX)* which both activate the index PIP joints as highlighted by the positive changes in FS1 (green shaded areas) which indicate that the participant did indeed perform the correct instructed movement.

It should be noted this phenomenon was not widely observed in the previous forearm (Pitman, 2015) and lower leg (Swanepoel, 2017) sdEMG studies. These studies implemented static movement protocols requiring sustained 30% and 40% MVC levels which activate substantially more motor units than the dynamic 'no-load' movements implemented in the present study. The regions of absent yet expected EMG activity observed in the present study could potentially be due to insufficient contraction levels during the dynamic movements. A further look at the complete dataset for Figure 8.1 presented in Appendix F shows that little EMG activity was present across all rICs during the Index PIP flexion and Group PIP flexion movement windows. It should be noted that a common trend was also observed in many datasets regarding the Index PIP flexion and Group PIP flexion movements where little activity was found in the rICs. While this observation has not been quantified, it does suggest that the PIP finger flexion movements did not sufficiently activate the FDS or FDP Index Band muscles when using the developed dynamic 'no-load' movement protocol. Furthermore, there are no intrinsic hand muscles that activate the digital PIP joints, thus only FDS and FDP are responsible for PIP flexion further supporting the argument that the contraction levels were too low.

An alternative explanation for the absence of EMG activity when expected is that the biomechanical models used to develop the muscle-movement mappings needed to generate the pEMG waveforms were incorrect. In order to target and isolate closely related muscles such as FDS-Index and FDP-Index bands, partial activation windows were required. It was assumed based on the underlying anatomy and biomechanics that these muscles were activated at different activation levels (*fa* or *pa*) during the common movements (see Table 6-2). This assumption allowed for a means to target muscles with similar functions, however, if this was not anatomically possible, then these muscles are not suitable for *isolation* using the sdEMG technique – in spite of the detected EMG activity.

In general, the pEMG full activation (*fa*) windows usually showed activity in the selected rICs while the partial activation windows often did not. This could be as a result of the way Pearson's correlation compares rICs and pEMG waveforms. For instance, the higher amplitude *fa* windows could influence the *r* value more than *pa* windows do. The complexity of developed movement protocol, which consisted of 23 movement windows could have also factored into the outcome of the Pearson's correlation comparison. A few experimental observations pertaining to the effectiveness of Pearson's correlation coefficient as a method for rIC selection will be explored further in Section 8.4.

As discussed in Section 8.3.1, the inability of ICA to fully separate the mixed monopolar EMG signals into independent muscle sources could also factor into the phenomenon of absent, yet expected EMG activity in selected rICs.

8.3.3 Participant Compliance

Participants were instructed to perform dynamic finger movements in response to visual cues however there were instances found where multiple *uninstructed* movements were performed concurrently. This phenomenon is known as co-contraction which is sometimes unavoidable with muscles having similar functions, however, participant errors can also be the underlying cause. Given the large volume of datasets in the present study, these cases were not searched for and possibly considered outliers. Figure 8.2 presents a reduced dataset consisting of the rICs for EPL, FDS-Ring and FDS-Index bands from a poorly isolated experimental run highlighting muscle co-contractions due to participant error.

The rICs show moderate isolation with EMG activity present in *all* movement windows suggesting the mixed raw EMG signals were not fully separated by ICA. Additionally the resting baseline is at a higher amplitude than the *well isolated* rICs presented in Figure 8.1, however, the resting baseline is still low enough to distinguish partial activation from rest.

The flex sensor data reveals that the participant made several movement errors as indicated by the red crosses. For instance, during Ring Group flexion the index finger was instructed to be in the rest position however rectangle A indicates that Index PIP flexion was performed simultaneously (as seen by the green shaded area in the FS1 signal). It is proposed that the large (near full activation) unexpected EMG burst present on the FDS-Index Band during the Ring Group flexion window was due to the uninstructed Index PIP flexion movement. Similarly during Ring Group extension, the uninstructed extension of the index PIP and thumb IP joints was found as highlighted by rectangle C and ellipse D. It is proposed that the EMG activity found on the EPL and FDS-Index Band was as a result of these unwanted co-contractions as highlighted in rectangle C and ellipse B.

While it is difficult to ascertain the exact reasons for the signal mismatches observed in Figure 8.2, it is proposed that poor signal separation and the noted participant errors are the most probable causes. Furthermore, the low isolation performances found for some muscles shown in Table 8-1 could be as a result of participant errors and it is advised that future studies consider this in light of low muscle isolation performances.

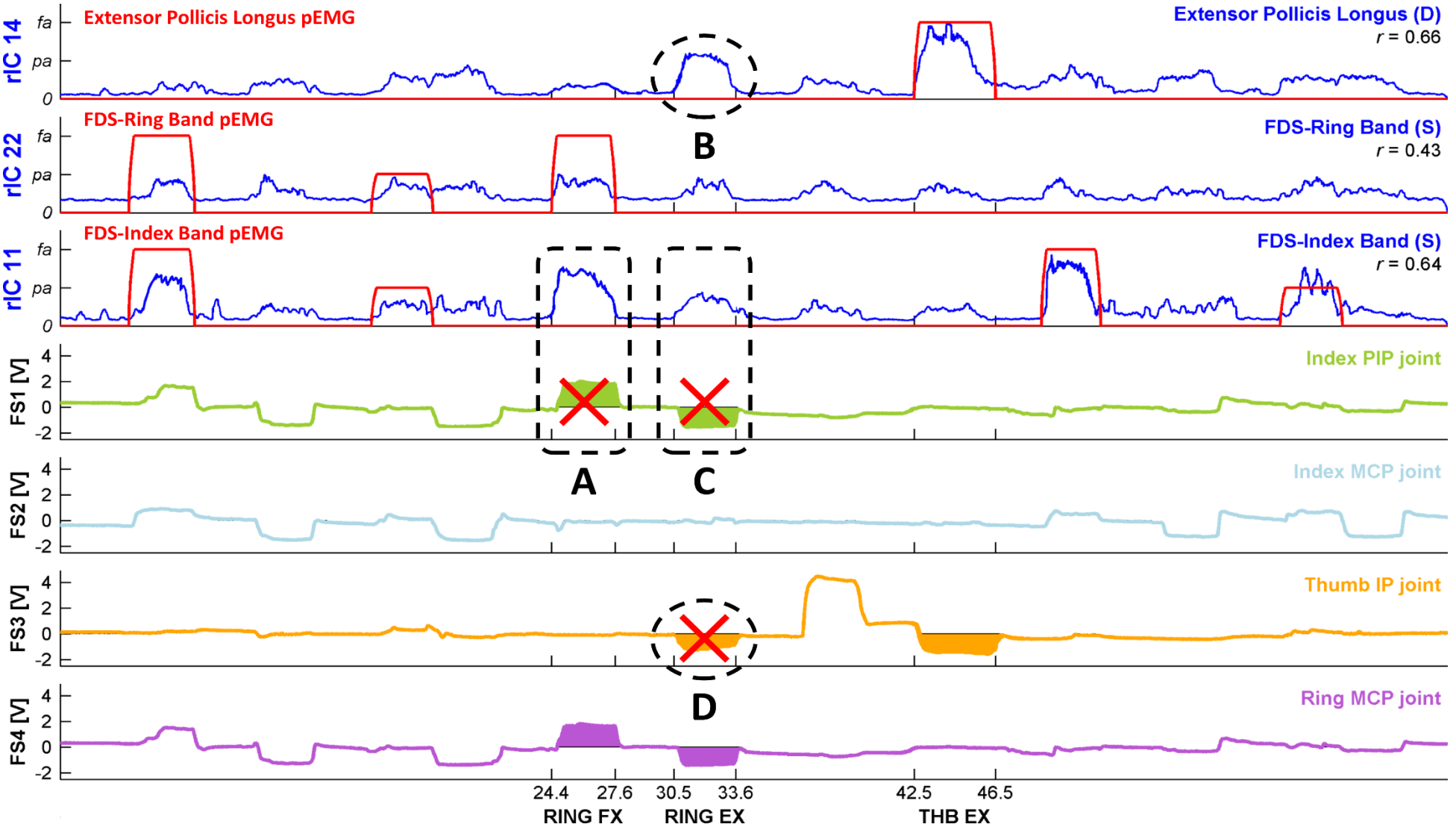

Figure 8.2 – Identified representative IC (rIC), predicted EMG (pEMG) signal mismatches and the corresponding flex sensor (FS) signals (Set B).

A sample set of pEMG waveforms (red signals) and rICs (blue signals) are shown. The shaded flex sensor signals indicate when finger movement was detected (positive changes indicate flexion and negative changes indicate extension). The red crosses indicate participant errors where uninstructed movements were performed concurrently with the instructed movement in the MP. The rectangles and ellipses indicate where incorrect movements resulted in co-contractions that manifested as unexpected EMG activity.

8.4 Limitations of Pearson's Correlation

The use of Pearson's correlation as the method to compare pICs to pEMGs, as well as to quantify the signal compliance in the present study was to adhere to the previous sdEMG conventions discussed in Section 1.2. This allowed for experimental guidelines to be developed that are applicable to the *current implementation* of the sdEMG technique. Pearson's correlation coefficient provides a simple metric that was used to rank the level of compliance between pICs and pEMGs which was needed to autonomously select rICs for the muscles investigated. The results show that Pearson's correlation coefficient is an adequate metric however several ambiguities have been noted that suggest an alternative metric may provide improved rIC selection.

To explore the efficacy of implementing Pearson's correlation in the sdEMG technique, a simulation was conducted to investigate the effects *spatially similar pICs* have on the calculated *r* values. Five pICs were synthesised consisting of five movement windows (A to E) with varied sets of mean EMG amplitudes (as relative percentages), illustrated in Figure 8.3. The simulation results highlight the inconsistent performance of Pearson's correlation signal comparisons between spatially similar pICs and the corresponding pEMGs.

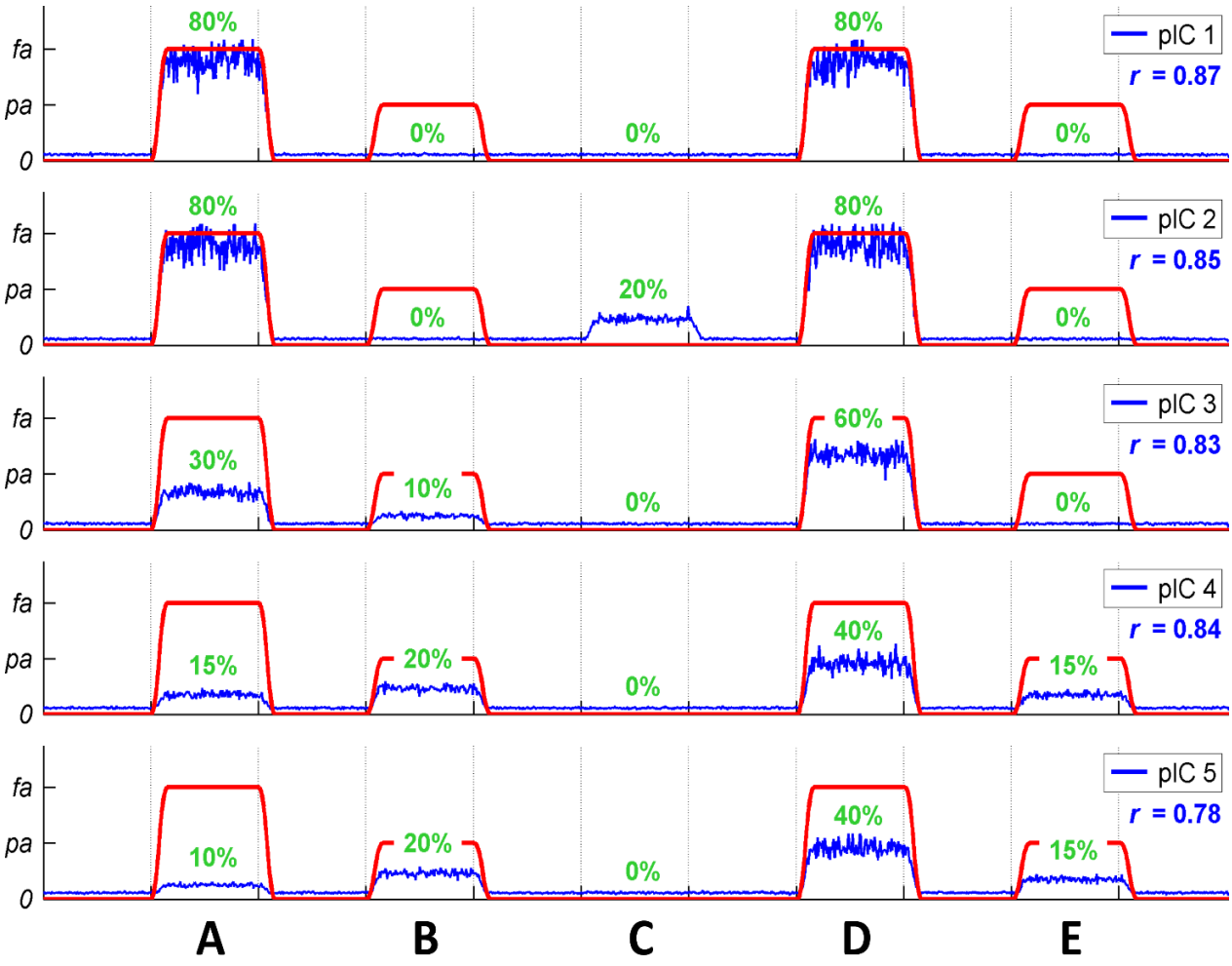

Figure 8.3 – Simulation results investigating the effects of processed IC (pIC) signal variation on the calculated Pearson's correlation coefficient (*r*) value.

Five pICs (1 to 5) were simulated consisting of five movement windows (A to E) interleaved with rest periods. The pIC mean EMG amplitudes (as relative percentages) are shown in green text. The predicted EMG signals are shown by the red lines and the calculated Pearson's correlation coefficient (r) value is indicated below the figure legend.

The partial activation (pa) level was set at 40% and the full activation (fa) level was set at 80% in accordance with the values used in the case study. The time axis and rest labels are omitted for brevity.

Several observations regarding the effectiveness of Pearson's correlation as a method to compare pICs to pEMGs are made with reference to Figure 8.3.

The highest *r* values were found for pIC 1 (0.87) and pIC 2 (0.85) suggesting that the *ideal matching*[38] of the full activation windows (A and D) was influential in the high *r* values, in spite of the absence of EMG activity in the partial activation windows (B and E). The absence of the expected partial EMG activity also indicates that pICs 1 and 2 are not *fully representative* of the muscle, under the assumption that the pEMG waveform is correct. Furthermore, the introduction of an *unexpected* EMG burst in pIC 2 (window C) only decreased the *r* value by 0.02 units suggesting that the ideal matching of the full activation windows (A and D) had more influence in the correlation calculation than the absent activity in the partial activation windows (B and E).

The simulation results show that pICs 3 and 4 performed slightly lower than pICs 1 and 2 with *r* values of 0.83 and 0.84, respectively. While the differences in *r* values are relatively small (≤ 0.04 units), these are considered *more* representative of the muscle since activity was present in three (pIC 3) and four (pIC 4) of the movement windows, albeit at lower amplitudes (≤ 60%). In the simulation, pIC 5 had the same set of mean EMG amplitudes as pIC 4 with the exception of window A where the mean EMG amplitude was decreased by 5%. The resultant *r* value for pIC 5 was 0.78 which was 0.06 units lower than that of pIC 4 (0.84). This is considered a significant difference given that the variation in the signals was a meagre 5% decrease in *expected* EMG activity in only *one* movement window. In contrast, the 20% addition of *unexpected* EMG activity in pIC 2 showed a much lower decrease of 0.02 units from that of pIC 1.

These are important findings that highlight the irregularity of Pearson's correlation coefficient as a measure of compliance between pIC and pEMG signals. Additionally, the irregularities found in muscle isolation performance could factor into the effectiveness of the pIC ranking system for sdEMG applications such as advanced prosthetic control, which requires accurate thresholds to determine the course of action to take.

Furthermore, the *manual* selection of a pIC to best represent the EMG activity for a particular muscle is highly subjective, hence the need for an autonomous rIC selection algorithm. It is however at the researcher's discretion to determine how the signal characteristics[39] in a pIC should be weighted in order to make a rIC selection. Pearson's correlation has been used to date, however, it is highly recommended that an alternative metric or an advanced rIC selection algorithm be implemented to more accurately select rICs in future studies.

[38] Pearson's correlation is a *linear comparison* of two signals therefore the actual amplitude of windows A and D (80%) is irrelevant as scalar multiples of the signal will yield the exact same *r* value. It should be noted that this refers to scalar multiples of the *exact same signal*, similar rIC signals (coupled with noise) with the *same proportions* of active and inactive windows would result in very similar *r* values.

[39] A typical signal characteristic that is considered is the relative signal amplitudes in the inactive, partially active and fully active movement windows. The shape of EMG bursts, number of unexpected EMG bursts and the number of absent EMG bursts can also factor into the selection criteria, further illustrating the subjectivity of the rIC selection task.

8.5 sdEMG System Performance

The developed sdEMG system was successfully implemented to detect and isolate the investigated extrinsic hand muscles with varying isolation performances. Several factors have been put forward relating aspects of the sdEMG technique to the results obtained, however, there are also technical limitations of the developed sdEMG system that may have contributed to the results obtained. In particular, the movement protocol parameters are revisited as well as apparent limitations of the electrode configuration used in the present study.

8.5.1 Movement Protocol Parameters

The developed dynamic 'no-load' movement protocol performed adequately to target the muscles investigated, however, the results suggest that some movements did not sufficiently isolate muscle activity as anticipated[40]. In particular, the *Index PIP flexion* and *Group PIP flexion* movements showed little EMG activity across most experimental runs which was speculated to be as a result of the low muscle contraction levels in the MP. The choice between static and dynamic movements is largely application based however future studies should consider introducing moderate resistance to dynamic movements in order to increase muscle contraction levels. It should be noted that ICA assumption (II) in Section 1.1.2 (requiring non-Gaussian sources) needs to be fulfilled therefore the level of contraction must be sufficiently low enough to preserve a super-Gaussian distribution while maintaining sufficient contraction levels from the target muscles that can be detected in the monopolar EMG signals.

The MP developed in the present study consisted of 12 movements compared to 6 implemented in previous studies (Pitman, 2015; Swanepoel, 2017), however, participants were still able to complete the MP without reported *muscle fatigue*. The 7s Timing experiment was reported by participants to be slightly too long to keep concentration indicating *mental fatigue* could have affected the results. Nevertheless, the outcome of the Timing experiments showed no substantial differences in muscle isolation performances between experiments, therefore, it is proposed that 7s is still a reasonable movement window duration for a long MP (~12 movements). The movement window duration value should be selected to match the sdEMG application and MP complexity, where the shortest duration is generally preferred.

The Randomisation experiment showed no noticeable differences compared to a non-randomised MP, therefore, it is advised that randomisation is incorporated in future studies to reduce standard sampling error and possible movement bias during experimental runs. Furthermore, the Anticipation experiment showed no substantial differences compared to the non-anticipated experiment, however increasing reaction delays were observed. Due to this, it is advised to not provide participants with feedforward visual cues as this proved to be confusing and participants struggled to perform the instructed movements in a timely manner.

[40] This is under the assumption that the pEMG waveform models were correct.

8.5.2 Electrode Sizes

As described in Section 2.1.5, volume conduction leads to higher attenuation of deep muscle MUAPs compared to superficial muscles, therefore it was hypothesised that measuring surface EMG from *more locations* would pool together sufficient compound EMG activity to *detect* the deep FPL, EPL and EI muscles along with the larger FDS, FDP and ED muscles. Additionally, the smaller rectangular electrode size (dimensions: 10×3x0.5mm, surface area: 30mm^2) used was expected to lessen the spatial filtering effect (due to volume conduction) of MUAPs from deep muscle fibres as well as reduce the pick-up of external noise. Pitman (2015) used circular electrodes (Ø10mm, surface area ~79mm^2) and Swanepoel (2017) used rectangular electrodes (LxW: 15×3mm, surface area: 45mm^2) which showed sufficient EMG detection, however poor signal-to-noise ratios were found in both studies suggesting the electrode size used in the present study was adequate for the sdEMG implementation.

It is suspected the absent yet expected EMG activity during the *Index PIP flexion* and *Group PIP flexion* movements discussed in Section 8.3.2 was most likely due to weak contraction levels, however, the small electrode EMG pick-up surface area could also account for this trend. Nevertheless, for a dynamic 'no-load' movement protocol it is advised that the electrode shape, size and quantity be investigated in a pilot study to determine an optimal EMG recording configuration.

8.5.3 Electrode Band Placement

The electrode bands were strategically placed to focus primarily on the small FPL, EPL and EI deep muscles which determined the location of the *forearm window*. The larger FDS, FDP and ED muscle bellies were partially located within the forearm window, however, the electrode bands were not optimally placed to measure EMG activity from these muscles. The poor results for FDP and ED suggest that the electrode bands should have been spread out across the forearm to record more direct EMG activity from these muscles which are located in the middle and proximal thirds of the forearm. As discussed in Section 8.5.2, a pilot study is recommended to investigate the optimal EMG recording configuration which should also include determining the optimal electrode band placements to sufficiently detect EMG activity from all the muscles under investigation.

Chapter 9 - Proposed Future Work

The outcome of an sdEMG study is dependent on the accuracy of the developed pEMG waveforms, the demixing performance of the implemented BSS technique, and the method of associating pICs to best represent the EMG activity for each muscle. Furthermore, the efficacy of the sdEMG technique can only be determined by comparison with intramuscular EMG techniques for measuring deep muscle activity. The following proposed future work aims to address shortcomings identified in the present study that have hindered the performance of the sdEMG technique.

9.1 Predicted EMG Verification

The literature-informed, pEMG waveforms developed in the present study were established by assessing the underlying forearm musculature, hand biomechanics and the developed MP to form unique muscle-movement mappings. These mappings correspond to idealised waveforms (rectangular EMG bursts) indicating the anticipated EMG activity from a single muscle during each movement window in the MP. The selection of rICs is dependent *solely* on the signal compliance between the pEMG and each pIC, therefore it is essential that the accuracy of the pEMG waveform be verified to ensure reputable results.

For dynamic movements the relationships between muscle and movements are well established, however, the *relative muscle activation contributions* (expressed currently as partial or full activation) from different muscles in the case of co-contracting muscles is unknown. In the present study, FDS and FDP, as well as EI and ED, were pairs of co-contracting muscles where the relative muscle activation contributions were estimated in the development of the pEMG waveforms. As described in Section 6.3.2, the pEMG activation levels implemented were defined as fully active (*fa* = 0.8), partially active (*pa* = 0.4) and inactive (0). Future work should investigate these muscles using intramuscular EMG for the deep FDP and EI muscles, in conjunction with surface or intramuscular EMG for the superficial FDS and ED muscles to determine the relative muscle activation contributions during various finger movements. These findings will lead to more accurate pEMG waveforms and subsequently improve the reliability of the sdEMG technique to detect and isolate these muscles.

9.2 Blind Source Separation Evaluation

The use of ICA as the BSS in the present study was to conform to the previous sdEMG conventions discussed in Section 1.2 in order to develop experimental guidelines that apply to the *current implementation* of the sdEMG technique. ICA has been shown in previous works, as well as the present study, to provide sufficient source signal separation needed to isolate deep and superficial muscles. While the results attained in this study are promising, several non-ideal observations found in the rICs suggest that ICA was unable to fully separate the mixed monopolar EMG recordings into the independent muscle sources.

The primary reason proposed for incomplete signal demixing is centred on whether the current implementation of the sdEMG technique satisfies the fundamental ICA assumptions and requirements discussed in Section 1.1.2. A pilot study is recommended to investigate both static and dynamic movement protocols with varying levels of contractions (as a percentage of MVC) in order to identify at what contraction level the measured monopolar EMG signals violate the assumptions and requirements of ICA. In particular,

the study should determine the contraction levels at which the PDFs of the monopolar EMG signals become Gaussian, as well as the linearity of the volume conductor mixing model in the limb investigated.

Future studies should also implement other suitable BSS algorithms, which could be considered as an alternative to ICA. In particular the research put forward by Holobar et al. (2016) provides a novel application of Convolution Kernel Compensation, a Blind Source Separation (BSS) algorithm which was used to decompose EMG signals into their constituent sources. This method as well as the K-means Clustering and Convolution Kernel Compensation BSS method implemented by Ning et al. (2015) could potentially be investigated as a BSS algorithm for the sdEMG technique. The performance achieved with the various algorithms can then be compared to determine the most effective algorithm for the sdEMG technique, assuming the pEMG waveforms have been verified as outlined in Section 9.1.

9.3 Association of pICs with EMG activity

Pearson's correlation has been shown to be an adequate comparative method to quantify the signal compliance between pEMGs and pICs needed for autonomous rIC selection. The results from the simulation investigating Pearson's correlation, described in Section 8.4, has outlined irregularities that demonstrate that minor spatial differences in pICs can drastically affect the *r* values and subsequently the selection of rICs to best represent the underlying EMG activity. Due to these discrepancies, an alternative method for quantifying signal compliance should be investigated and implemented in future studies to better associate pICs with EMG activity. As an initial guide, correlation metrics such as Kendall's rank coefficient and Spearman's rank coefficient should be investigated before considering using more complex rIC selection algorithms.

From observations made during the data processing, it appears that an algorithm that weights the importance of expected full and partial activation windows may be suitable. For instance in Figure 8.3, pICs 4 and 5 were considered more representative than pICs 1, 2 and 3 which all appeared to favour *full activation signal compliance*. For muscles with partial activation windows, a balance between full and partial EMG activity present in the pIC is preferred as these signals are considered more representative of the muscle's functionality. Similarly, a method that implements *windowed* correlation comparisons may be useful in finding pICs that show activity in *all* the expected windows instead of the pICs that show the overall highest *r* value, which appears to mainly be linked to the full activation windows.

Alternatively, a weighted sum of the *area under the curve* for each movement window could prove to be a powerful fuzzy logic orientated rIC selection algorithm. A more complex approach would be the introduction of wavelet analysis which is capable of providing spatio-temporal as well as frequency information that could be incorporated into a rIC selection algorithm.

9.4 Deep Muscle Intramuscular EMG Verification

The present study, as well as previous works, have shown that the sdEMG technique is able to non-invasively detect and isolate EMG activity from some of the deep muscles of the forearm and lower leg. While the results offer merit to the technique, it still does not definitively prove the findings are indeed originating from the deep muscles investigated. In order to show clinical efficacy, a concurrent surface and intramuscular sdEMG study needs to be conducted to verify that the detected and isolated deep muscle EMG activity aligns with the corresponding measured intramuscular EMG activity.

Chapter 10 - sdEMG Guidelines

Throughout this dissertation, experimental guidelines pertaining to the development and implementation of an sdEMG system have been provided. In particular, the finer technical and experimental aspects of the current sdEMG technique implementation have been explored in a broad manner to develop experimental guidelines that are applicable to all future studies. The case study investigated three experimental parameters linked to the movement protocol that were expected to influence the performance of the sdEMG technique however the findings indicated that the technique is quite robust to variations in the *timing*, *randomisation* and *anticipation of movements*. The discussions also highlighted several other factors that could contribute to the performance of the sdEMG technique.

The following guidelines are considered to be the most influential in the outcomes of an sdEMG study.

- Ideal ICA-based muscle isolation occurs when there is a one-to-one muscle-movement mapping. When setting up an sdEMG study it is advised to select muscles that can be independently activated. If that is not possible, then the muscles should be selected to minimise the number of shared functions so as to realise the least amount of co-contractions.
- A static, moderate resistance movement protocol is preferred over a dynamic 'no-load' movement protocol. If a dynamic MP is required, a low resistive load should be applied which can be determined through a pilot study. If ICA is used as the BSS, it is imperative when designing the MP to satisfy the ICA assumption requiring non-Gaussian sources. The extent to which monopolar EMG signals adheres to this assumption is related to muscle contraction levels, where low contractions result in super-Gaussian muscle sources.
- The MP should be designed with as few movements as possible that sufficiently target the muscles under investigation. A short MP is preferred as it allows for more experimental runs to be conducted in a single participant testing session. Furthermore, short MPs minimise muscle fatigue and maintain participant concentration levels, and subsequently MP adherence.
- Participants of similar fitness levels should be selected to provide comparable results where anthropometric data such as limb circumferences and body fat indexes can be used to determine suitable participants. Thick skin and fat layers attenuate EMG signals drastically which may reduce the performance of the sdEMG technique to detect and isolate the muscles of interest.
- The movement window duration should be selected in accordance with the investigated musculature to ensure that distinct muscle contractions can be detected. In the present study, participants found 3 seconds to be too quick and 7 seconds indicated possible mental fatigue. An initial movement window duration of 5 seconds is recommended for long MPs, such as the one developed in the present study consisting of 23 movement windows.
- The choice of electrode size, shape, quantity and placement should be investigated in a pilot study to determine an optimal EMG recording configuration for the desired application and the specific musculature investigated. Previous works, as well as the present study, have been successful using 40 and 64 electrodes arranged in four and three electrode arrays which can be used as an initial guideline in addition to the convention of using at least twice as many electrodes as there are muscles in the investigated body region.

- Activation timing detection is an important aspect of the sdEMG technique, therefore the developed experimental apparatus must account for contraction detection to ensure movement synchronisation between pEMG and pIC signals (in the case of an ICA-based study).
- Flex sensors have been shown to provide accurate *dynamic* contraction detection. Flex sensors are easily incorporated into experimental apparatus with little discomfort experienced by participants, and with only minimal obstruction of movements. Additionally, strain gauge force sensors are also easily implemented and have been successful in moderate resistance *static* movement protocols and are recommended over more complex force sensors.
- A suitable testing platform should be constructed to support the limb under investigation while restricting unwanted movements. Electrode cables should also be fastened to the testing platform and to the participant in an attempt to reduce cable movement artefacts in the raw EMG recordings.
- A visual participant instruction system should be implemented with easy to understand movement cues, as well as contraction feedback, possibly illustrated using intuitive needle gauges or progress bars.
- Standard surface EMG preparation must be followed in lieu of the SENIAM guidelines including thorough skin preparation, skin-electrode impedance checking and the use of EMG conductive paste.
- Recording equipment pre-testing, as well as real-time signal monitoring, should be conducted to assess the measured EMG amplitudes, baseline signal noise and possible signal artefact contaminations.
- The raw EMG data must be pre-processed to check for corrupt or incomplete files as well as potential outlier signals before the BSS algorithm is applied.

While the non-invasive superficial and deep muscle electromyography experimental technique is still in its infancy, the present study has shown it is a robust technique that has the potential to broaden the field of deep muscle sEMG. The technique was successfully applied to the forearm and further extended from the previous forearm study to include the deep extensor indicis muscle. Concise guidelines have been developed from experimental observations and it is hoped that future sdEMG studies will benefit from the research presented in this dissertation.

References

Belle, G. Van, Fisher, L. D., Heagerty, P. J., & Lumley, T. (2004). *Biostatistics: A Methodology for the Health Sciences, Second Edition* (2nd ed.). Hoboken: John Wiley & Sons, Inc. http://doi.org/10.1002/0471602396

Blok, J. H., Stegeman, D. F., & van Oosterom, A. (2002). Three-Layer Volume Conductor Model and Software Package for Applications in Surface Electromyography. *Annals of Biomedical Engineering*, *30*(4), 566–577. http://doi.org/10.1114/1.1475345

Clayton Silver, N., & P. Dunlap, W. (1987). Averaging Correlation Coefficients: Should Fisher's z Transformation Be Used? *Journal of Applied Psychology*, *72*, 146–148. http://doi.org/10.1037/0021-9010.72.1.146

Corey, D. M., Dunlap, W. P., & Burke, M. J. (1998). Averaging Correlations: Expected Values and Bias in Combined Pearson rs and Fisher's z Transformations. *The Journal of General Psychology*, *125*(3), 245–261. http://doi.org/10.1080/00221309809595548

Daube, J. R., & Rubin, D. I. (2009). Needle electromyography. *Muscle & Nerve*, *39*(2), 244–70. http://doi.org/10.1002/mus.21180

Day, S. (2002). *Important Factors in surface EMG measurement*. Calgary. Retrieved from http://health.uottawa.ca/biomech/courses/apa4311/semg.pdf

De Luca, C. J., & Basmajian, J. V. (1985). *Muscles Alive: Their Functions Revealed by Electromyography* (5th ed.). Ann Arbor: Williams & Wilkins.

Delorme, A. (2002). Independent Component Analysis for dummies. Retrieved from http://arnauddelorme.com/ica_for_dummies/

Delorme, A., Sejnowski, T., & Makeig, S. (2007). Enhanced detection of artifacts in EEG data using higher-order statistics and independent component analysis. *NeuroImage*, *34*(4), 1443–1449. http://doi.org/10.1016/j.neuroimage.2006.11.004

Djuwari, D., Kumar, D. K., & Palaniswami, M. (2005). Limitations of ICA for Artefact Removal. In *2005 IEEE Engineering in Medicine and Biology 27th Annual Conference* (pp. 4685–4688). Shanghai: IEEE. http://doi.org/10.1109/IEMBS.2005.1615516

Evans, J. D. (1996). *Straightforward statistics for the behavioral sciences*. Pacific Grove: Brooks/Cole Pub. Co.

Fisher, R. A. (1915). Frequency Distribution of the Values of the Correlation Coefficient in Samples from an Indefinitely Large Population. *Biometrika*, *10*(4), 507–521. http://doi.org/10.2307/2331838

Fisher, R. A. (1921). On the probable error of a coefficient of correlation deduced from a small sample. *Metron*, *1*, 3–32. Retrieved from citeulike-article-id:2346712

Fisher, R. A. (1924). The Distribution of the Partial Correlation Coefficient. *Metron*, *3*, 329–332. Retrieved from https://digital.library.adelaide.edu.au/dspace/handle/2440/15182

Gävert, H., Hurri, J., Särelä, J., & Hyvärinen, A. (2005). FastICA MATLAB Package. Retrieved from https://research.ics.aalto.fi/ica/fastica/code/FastICA_2.5.zip

Gilroy, A. M., MacPherson, B. R., & Ross, L. M. (Eds.). (2012). *Atlas of Anatomy* (2nd ed.). New York: Thieme.

Gorsuch, R. L., & Lehmann, C. S. (2010). Correlation Coefficients : Mean Bias and Confidence Interval Distortions, *1*(2), 52–65.

Guyton, A. C., & Hall, J. E. (2006). *Textbook of Medical Physiology* (11th ed.). Philadelphia: Elsevier Inc.

Guyton, A. C., & Hall, J. E. (2011). *Textbook of Medical Physiology* (12th ed.). Philadelphia: Elsevier Inc.

Hermens, H. J., Freriks, B., Disselhorst-Klug, C., & Rau, G. (2000). Development of recommendations for SEMG sensors and sensor placement procedures. *Journal of Electromyography and Kinesiology*, *10*(5).

Hermens, H. J., Freriks, B., Merletti, R., Stegeman, D., Blok, J., Rau, G., … Hägg, G. (1999). *SENIAM - European Recommendations for Surface ElectroMyoGraphy*. *Roessingh Research and Development* (2nd ed.). Netherlands: Roessingh Research and Development. Retrieved from http://www.seniam.org/

Hodgkin, A. L., & Huxley, A. F. (1952). A quantitative description of membrane current and its application to conduction and excitation in nerve. *The Journal of Physiology*, *117*(4), 500–544. Retrieved from http://www.ncbi.nlm.nih.gov/pmc/articles/PMC1392413/

Holobar, A., Chen, M., Zhang, X., Zhou,P. (2016). Progressive FastICA Peel-Off and Convolution Kernel Compensation Demonstrate High Agreement for High Density Surface EMG Decomposition. *The Journal of Neural Plasticity*, ID *3489540*, 1-5.

Hyvärinen, A., & Oja, E. (2000). Independent component analysis: algorithms and applications. *Neural Networks : The Official Journal of the International Neural Network Society*, *13*(4–5), 411–30. http://doi.org/10.1016/S0893-6080(00)00026-5

ICH. (2015). *Integrated Addendum to ICH E6 (R1): Guideline for Good Clinical Practice*. Retrieved from http://www.ich.org/home.html

James, C. J., & Hesse, C. W. (2005). Independent component analysis for biomedical signals. *Physiological Measurement*, *26*(1), 15–39. http://doi.org/10.1088/0967-3334/26/1/R02

Jenkins, D. B. (2009). *Hollinshead's functional anatomy of the limbs and back*. St. Louis, Mo.: Saunders/Elsevier.

John, L. R. (2010). Non-invasive deep muscle electromyography. USA, Europe, China, Japan, South Africa: World Intellectual Property Organization (WIPO). Retrieved from https://patentscope.wipo.int/search/en/detail.jsf?docId=WO2011012988

Jung, T. P., Makeig, S., McKeown, M. J., Bell, A. J., Lee, T. W., & Sejnowski, T. J. (2001). Imaging brain dynamics using independent component analysis. *Proceedings of the IEEE*, *89*(7), 1107–1122. http://doi.org/10.1109/5.939827

Konrad, P. (2005). *The ABC of EMG: A Practical Introduction to Kinesiological Electromyography* (1st ed.). Scottsdale: Noraxon Inc.USA.

Krzywinski, M., & Altman, N. (2014). Points of Significance: Visualizing samples with box plots. *Nature Methods*, *11*(2), 119–120. http://doi.org/10.1038/nmeth.2813

Kumar, S., & Mital, A. (1996). *Electromyography In Ergonomics*. Padstow: Taylor & Francis.

Makino, S. (2003). Blind Source Separation of Convolutive Mixtures of Speech. In J. Benesty & Y. Huang (Eds.), *Adaptive Signal Processing* (1st ed., pp. 195–225). Berlin: Springer. http://doi.org/10.1007/978-3-662-11028-7_7

Marieb, E. N. (Ed.). (2001). *Human Anatomy & Physiology* (5th ed.). San Francisco: Benjamin Cummings.

Merletti, R., & Parker, P. J. (Eds.). (2004). *Electromyography: Physiology, Engineering, and Non-Invasive Applications* (1st ed.). Hoboken: John Wiley & Sons, Inc.

Merlo, E. (2011). *OT Bioelettronica EMG-USB2 [ENG] User Manual*. Retrieved from http://www.otbioelettronica.it/attachments/article/70/EMG-USB2 ENG.pdf

Moroaswi, S., & John, L. R. (2010). *The measurement of deep brachialis muscle activity using surface electromyography. (Unpublished Results)*. University of Cape Town.

Mulligan, S. R. (2014). *A Comparison of ICA versus genetic algorithm optimized ICA for use in non-invasive muscle tissue EMG (Master's Dissertation)*. Department of Electrical Engineering, University of Cape Town.

Naik, G. R., & Kumar, D. K. (2011). Estimation of independent and dependent components of non-invasive EMG using fast ICA: validation in recognising complex gestures. *Computer Methods in Biomechanics and Biomedical Engineering*, *14*(12), 1105–11. http://doi.org/10.1080/10255842.2010.515211

Naik, G. R., Yina Guo, & Hung Nguyen. (2013). A new approach to improve the quality of biosensor signals using Fast Independent Component Analysis: Feasibility study using EMG recordings. In *2013 35th Annual International Conference of the IEEE Engineering in Medicine and Biology Society (EMBC)* (pp. 1927–1929). Osaka: IEEE. http://doi.org/10.1109/EMBC.2013.6609903

Nazarpour, K., Al-Timemy, A. H., Bugmann, G., & Jackson, A. (2013). A note on the probability distribution function of the surface electromyogram signal. *Brain Research Bulletin*, *90*, 88–91. http://doi.org/10.1016/j.brainresbull.2012.09.012

Ning, Y., Zhu, X., Zhu, S., & Zhang, Y. (2015). Surface EMG Decomposition Based on K-means Clustering and Convolution Kernel Compensation. IEEE Journal of Biomedical and Health Informatics, 19(2), 471–477. http://doi.org/10.1109/JBHI.2014.2328497

Roeleveld, K., Stegeman, D. F., Vingerhoets, H. M., & Oosterom, A. Van. (1997). The motor unit potential distribution over the skin surface and its use in estimating the motor unit location. *Acta Physiologica Scandinavica*, *161*(4), 465–472. http://doi.org/10.1046/j.1365-201X.1997.00247.x

Rutkove, S. B. (2007). Introduction to Volume Conduction. In A. S. Blum & S. B. Rutkove (Eds.), *The Clinical Neurophysiology Primer* (pp. 43–53). Totowa, NJ: Humana Press. http://doi.org/10.1007/978-1-59745-271-7_4

Sayed, A., Albertus-Kajee, Y., Schwellnus, M., & John, L. R. (2012). *The use of surface electromyography to measure electrical activity from a deep calf muscle (Tibialis Posterior Muscle). (Unpublished Results)*. University of Cape Town.

Schuenke, M., Schulte, E., & Schumacher, U. (2010). *Atlas of Anatomy - General Anatomy and the Musculoskeletal System*. (L. M. Ross & E. D. Lamperti, Eds.) (1st ed.). New York: Thieme.

Sé, D. C. da, Mello, J. M. de, Scalon, J. D., Muniz, J. A., Oliveira, M. S. de, & Scolforo, J. R. S. (2013). Use of the correlation coefficient between plots in order to improve the accuracy of forest inventories. *CERNE*, *19*, 575–580.

Seeley, R. R., Stephens, T. D., & Tate, P. (2007). *Essentials of Anatomy and Physiology* (6th ed.). Boston: McGraw-Hill.

Strommen, J. a, & Daube, J. R. (2001). Determinants of pain in needle electromyography. *Clinical Neurophysiology : Official Journal of the International Federation of Clinical Neurophysiology*, *112*(8), 1414–8.

Swanepoel, C. (2017). *Non-invasive Deep Muscle Electromyography: Measurement of Extrinsic Foot Muscle Activity (Master's Dissertation)*. Department of Human Biology, University of Cape Town.

Syed, A., Taj, Z., Agasbal, H., Melligeri, T., & Gudur, B. (2012). Flex Sensor Based Robotic Arm Controller Using Micro Controller. *Journal of Software Engineering and Applications*, *5*, 364–366. http://doi.org/10.4236/jsea.2012.55042

WMA. (2013). World medical association declaration of Helsinki: Ethical principles for medical research involving human subjects. *JAMA*, *310*(20), 2191–2194. Retrieved from http://dx.doi.org/10.1001/jama.2013.281053

Zimmerman, D. W., Zumbo, B. D., & Williams, R. H. (2003). Bias in Estimation and Hypothesis Testing of Correlation. *Psicológica*, *24*, 133–158.

Appendix A: Monopolar EMG Distributions

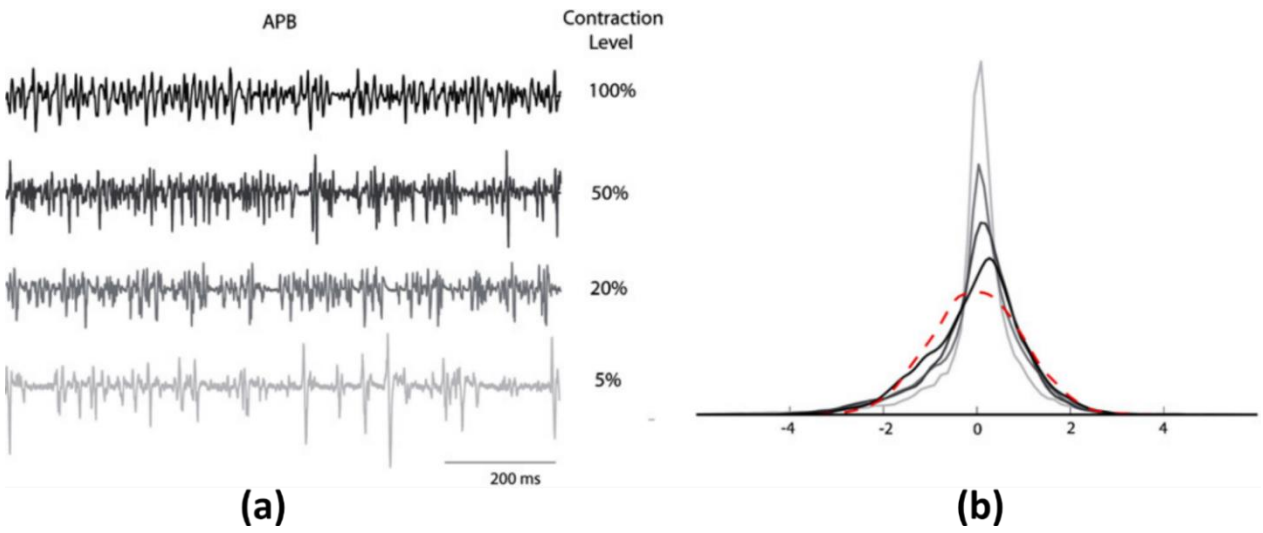

Figure A-1: Monopolar EMG recordings for abductor pollicis longus (APB) at various percentages of MVC (a) and the corresponding probability density functions (b) from the study by Nazarpour et al. (2013).

A Gaussian distribution with a zero mean and unit variance is shown by the dashed red line in (b). The peakedness of the PDFs in (b) show inverse relationships to EMG contraction levels (as a percentage of MVC). At low contraction levels, the monopolar EMG distribution is sufficiently peaked to be considered super-Gaussian and is suitable for ICA decomposition (fulfils the ICA non-Gaussian requirement).

Image reproduced from Nazarpour et al. (2013).

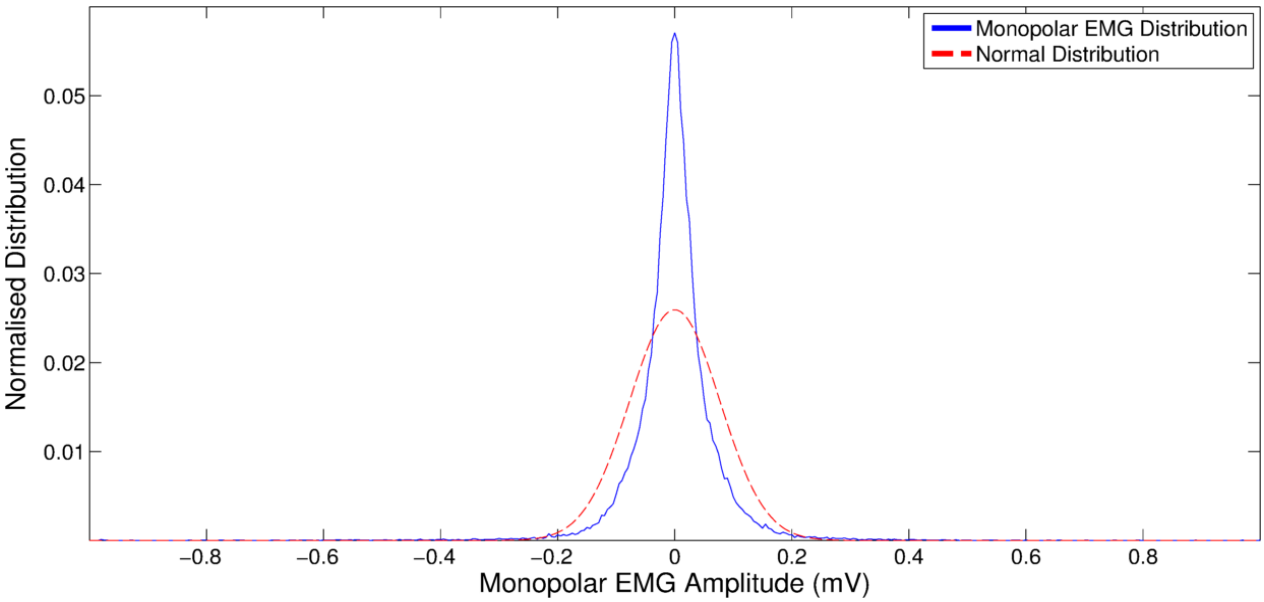

Figure A-2: Probability density function of a typical monopolar EMG signal corresponding to ~40% MVC level from the study by Swanepoel (2017).

The monopolar EMG PDF (solid blue line) shows sufficient peakedness to fulfil the non-Gaussian distribution requirement. The PDF of a Gaussian distributed variable with the same mean and standard deviation is depicted by the dashed red line.

Image reproduced from Swanepoel (2017).

Appendix B: OT Bioelettronica EMG-USB2 Specifications

The complete list of device specifications can be found in the *User Manual* available at:

http://www.otbioelettronica.it/attachments/article/70/EMG-USB2%20ENG.pdf

Parameter	Available options	Description
MODE	Chained Diff.	It is a single differential mode. Each channel amplify the difference between a subsequent signals of each input . The last channel of each input is obtained as difference between the last signal of the same input and the first signal of the subsequent input. For example, in this mode, the channel 16 is obtained as difference between the signal 16 (last signal of IN 1) and the signal 17 (first signal of IN 2). This mode have to be used when connecting an electrode matrix or an array to several input.
	Looped Diff.	It is a single differential mode. Each channel amplify the difference between a signal and the subsequent one. The last channel of each input is obtained as difference between the last signal and the first signal of the same input. For example, in this mode, the channel 16 is obtained as difference between the signal 16 (last signal of IN 1) and the signal 1 (first signal of IN 1). This mode have to be used when connecting a rectal probe.
	Float. Monop.	All the channel makes the difference between the corresponding input signal and the signal at the *DRL IN* connector. The DRL IN must be connected, by means of a ground strip to a point on the body patient without bioelectrica activity. This is a monopolar detection since all the channels are referred to the same potential present at DRL IN. This mode can be used with standard adapters to detect signals in monopolar mode.
	Refer. Monop.	All the channel makes the difference between the corresponding input signal and the reference point of the amplifier. This mode can be used jointly with adapter with suffix M5. This kind of adapters are specially designed to reduce interferences in monopolar detection.
	Bipolar	This modality require special adapters that allow the signals detection from electrode pairs as standard bipolar EMG.
	Hybrid	This mode can be used when different type of adapters are used together. In this condition the detection mode in not forced by the instrument but depend on the type of adapter used.

Figure B-1: EMG-USB2 recording modalities.

Image reproduced from OT Bioelettronica® EMG-USB2 User manual (Merlo, 2011).

Amplification channels (IN1÷4 and MULTIPLE IN 1÷3)	
Selectable gain	OFF, 100, 200, 500, 1000, 2000, 5000, 10000 V/V
Selectable bandwidth	High pass filter: 3, 10, 100, 200 Hz Low pass filter: 130, 500, 900, 4400Hz
Maximum input range	50 mV_{PP}
Noise level referred to input	< 4 μV_{RMS}
Input impedance	> 10^{11} Ω
CMRR	> 95 dB
Output range	0 ÷ 5 V
Insulation voltage	4.000 V_{DC}
Auxiliary channels (AUX-IN 1÷16)	
Input range	± 5 V
Bandwidth	Channels are not filtered
Gain	0.5 V/V
Input impedance	200 kΩ
A/D converter input dynamics	0 ÷ 5 V
Data conversion	
A/D converter resolution	12 bit
Data transfer to PC	USB2 interface
Selectable sample frequency	512, 2048, 4096, 10240 Hz

Figure B-2: EMG-USB2 instrumentation amplifier specifications.

Image reproduced from OT Bioelettronica® EMG-USB2 User manual (Merlo, 2011).

Parameter	Available options	Description
HP Filter	3 Hz	All the signals related to the corresponding input are high pass filtered and low pass filtered with the 3 dB cut off frequency displayed. It is up to the user to select the correct filters value for the conditioning of the desired signals. OT BioLab, in any case provide a warning when the cut off frequencies do not respect standard values for a given type of signal. Refer to the OT BioLab user manual for further details.
	10 Hz	
	100 Hz	
	200 Hz	
LP Filter	130 Hz	
	500 Hz	
	900 Hz	
	4.4 kHz	

Figure B-3: EMG-USB2 analog filter specifications.

Image reproduced from OT Bioelettronica® EMG-USB2 User manual (Merlo, 2011).

Appendix C: Movement Visual Cues

Table C-1: Visual cues implemented in the Timing and Randomisation experiment MPs.

1	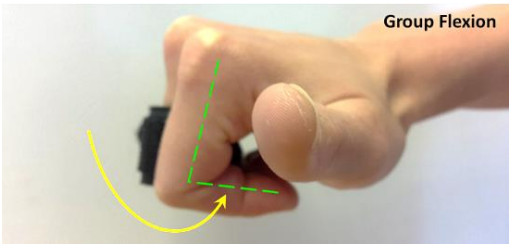	7	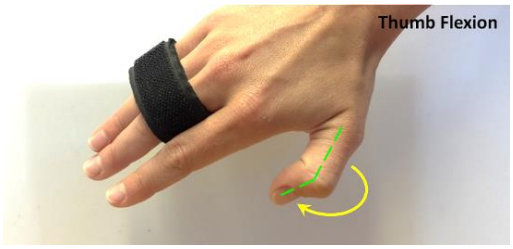
2	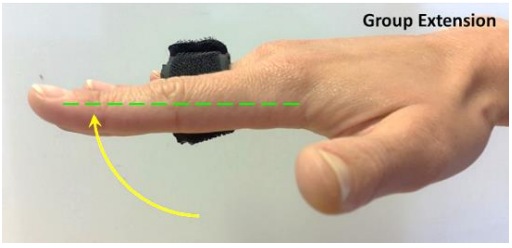	8	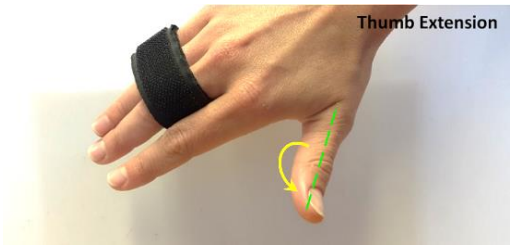
3	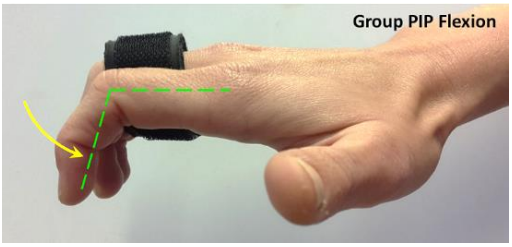	9	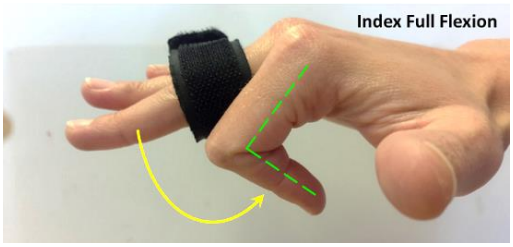
4	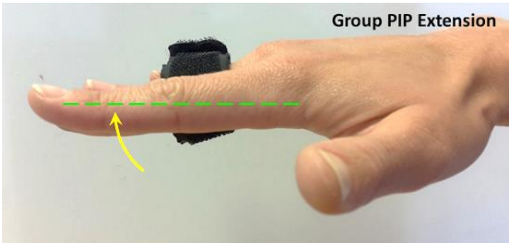	10	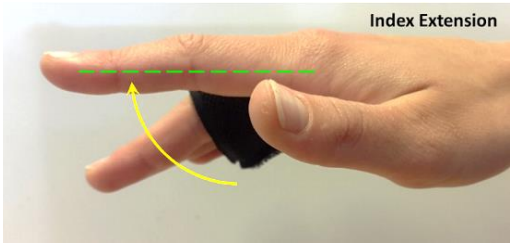
5	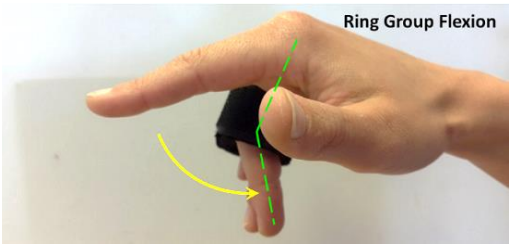	11	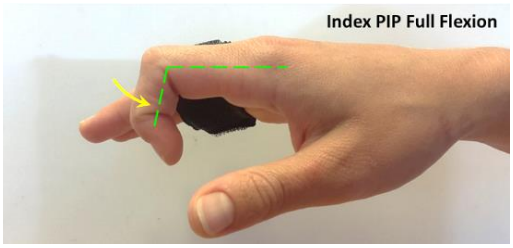
6	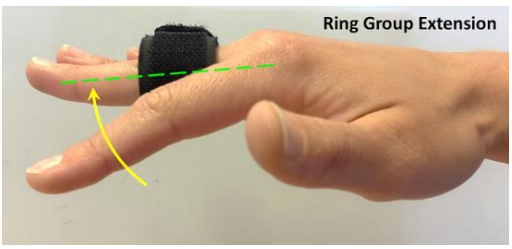	12	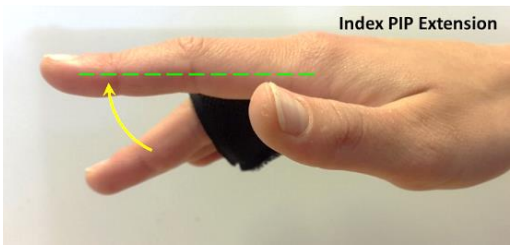

Table C-2: Watermarked visual cues implemented in the Anticipation experiment MP.

1		7	
2		8	
3	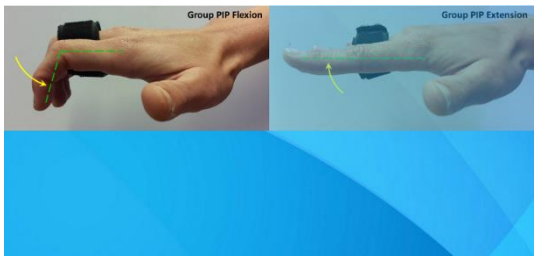	9	
4	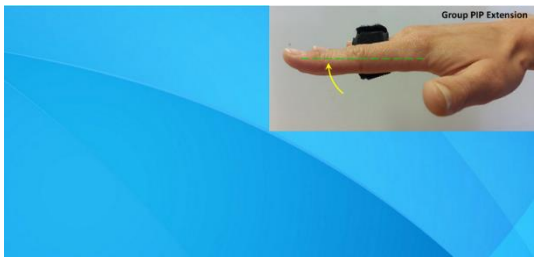	10	
5		11	
6		12	

Appendix D: Fisher Correlation Coefficient Correction

Fisher proposed a set of transformation equations known as the Fisher's *z*-transformation (Equation E-1) and the inverse *z*-transformation (Equation E-2) that are used to calculate the Fisher-corrected *ρ* value from the sample *r* values (Fisher, 1924).

$$z = \frac{1}{2}\ln\left(\frac{1+r}{1-r}\right) \qquad \textbf{Equation E-1}$$

$$r = \frac{e^{2z-1}}{e^{2z+1}} \qquad \textbf{Equation E-2}$$

In the present study, a *ρ* value was calculated for the eight muscles and for the five experiments resulting in a total of 40 *ρ* values. The generalised process of calculating the Fisher-corrected *ρ* value is described below.

For a population of *N r* values, the Fisher-corrected *ρ* value was calculated in three steps:

I. Transform the *N r* values using Equation E-1 to *N z* values.
II. Calculate the z mean value ($\overline{z}$) of the *N z* values.
III. Inverse transform $\overline{z}$ using Equation E-2 resulting in $\overline{r}$*, i.e. the ρ* value.

To further describe the population results, a Fisher-corrected 95% confidence interval (CI) was calculated for each *ρ* value. Several studies (Clayton Silver & P. Dunlap, 1987; Corey, Dunlap, & Burke, 1998; Sé et al., 2013; Zimmerman, Zumbo, & Williams, 2003) have investigated ways to correct the CI (due to the skewed *r* distribution) by including the Fisher transformations into the standard CI equation (Equation E-3).

Gorsuch & Lehmann (2010) report for a 95% CI, an *a* value of 1.96 (determined *z*-table of critical values) is sufficient correction and it was used in the present study. In the study by Gorsuch & Lehmann (2010), the Fisher's proposed correction equation for the standard error (SE) was used which is independent of the *r* value and subsequently the transformed *z* value of the SE provided more accurate results. Fisher's SE equation is presented in Equation E-4 and the Fisher transformed 95% CI upper and lower limits are described by Equation E-5 and Equation E-6, respectively. The corresponding 95% upper and lower limits in the *r* domain are calculated by applying the inverse Fisher z-transform (Equation E-2) to get r_u and r_l.

$$CI_x = \overline{x} \pm a \times SE_x \qquad \textbf{Equation E-3}$$

$$SE_z = \frac{1}{\sqrt{(N-3)}} \qquad \textbf{Equation E-4}$$

$$z_u = \overline{z} + 1.96 \times SE_z \qquad \textbf{Equation E-5}$$

$$z_l = \overline{z} - 1.96 \times SE_z \qquad \textbf{Equation E-6}$$

In the present study, a Fisher-corrected 95% CI was preferred over a standard deviation CI range to describe the population variation as it indicates an asymmetric range that has a *95% probability* of including the actual *ρ* value. An sdEMG study includes an *r* threshold value (r_{th}) selected by the researcher that determines if a muscle has been successfully isolated, i.e. $\mathrm{r} \geq r_{th}$. In the present study the, lowest *r* or *ρ* threshold value was set at 0.60, where any *r* or *ρ* value below this was considered *poorly isolated.*

Appendix E: Muscle-level Distribution Scatter Plots

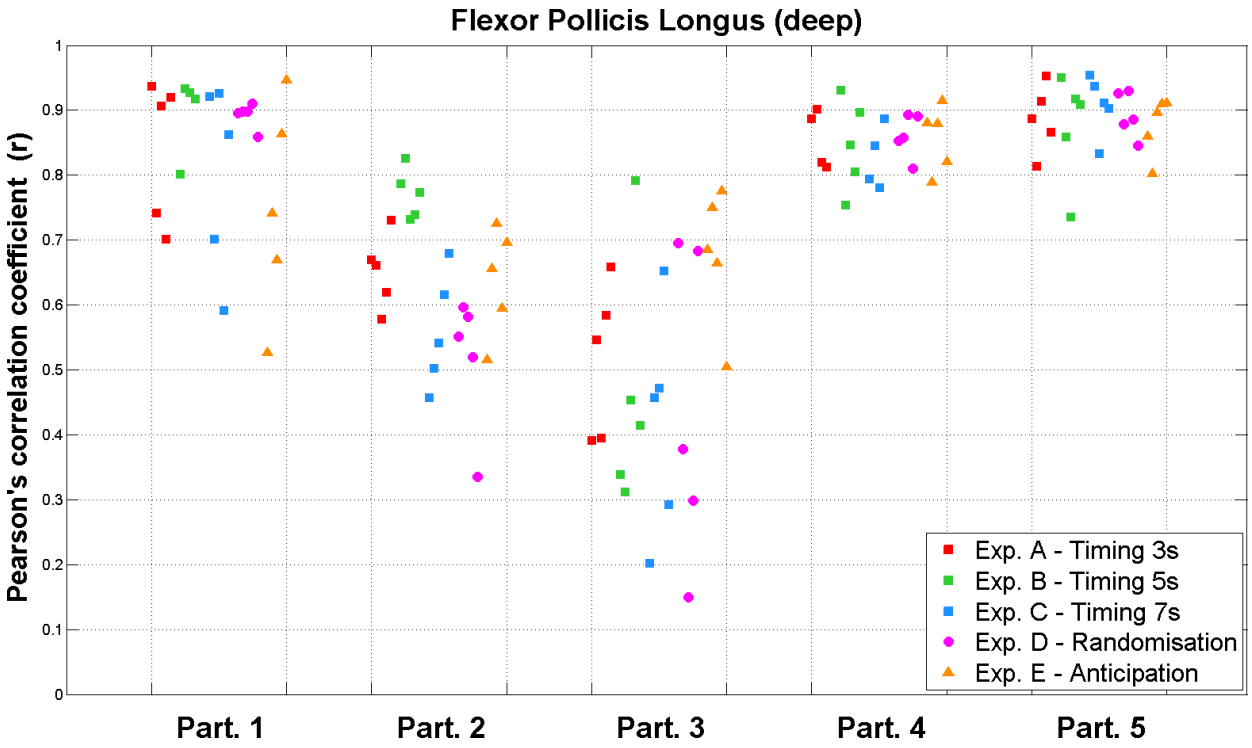

Figure E-1: Scatter plots of the correlation coefficients (*r*) for each experiment grouped by participants for flexor pollicis longus.

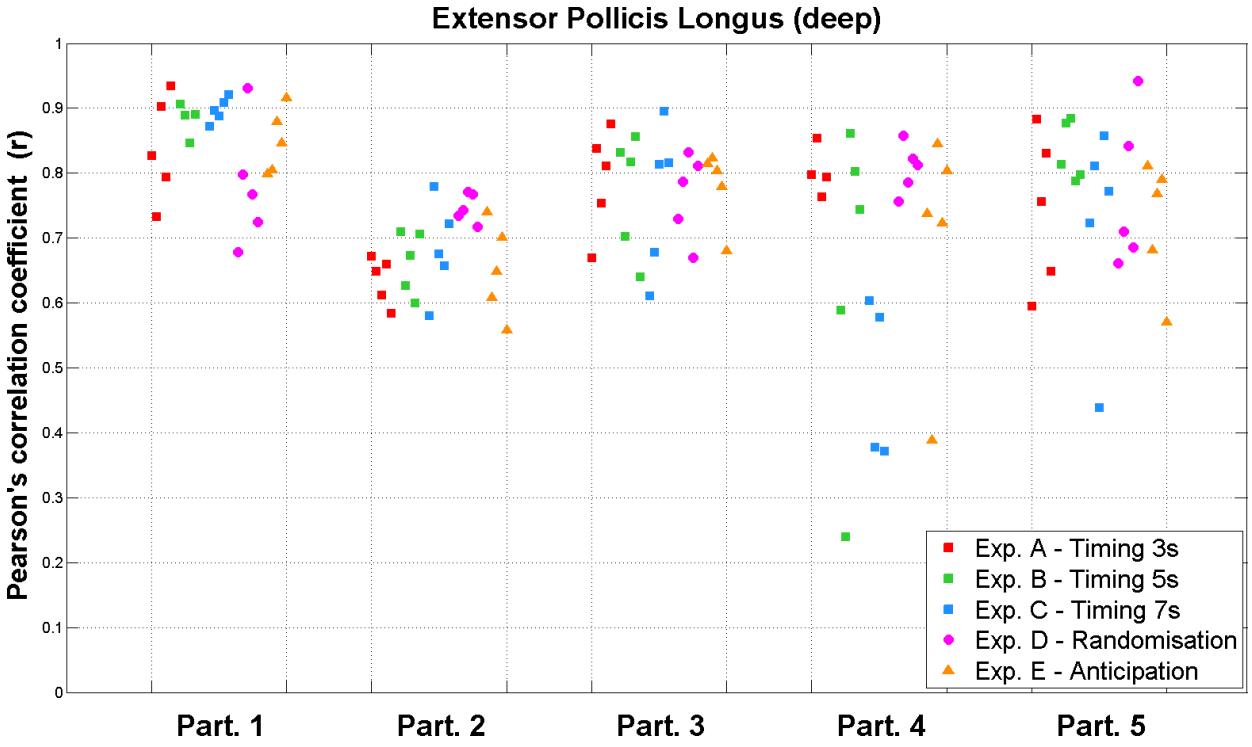

Figure E-2: Scatter plots of the correlation coefficients (*r*) for each experiment grouped by participants for extensor pollicis longus.

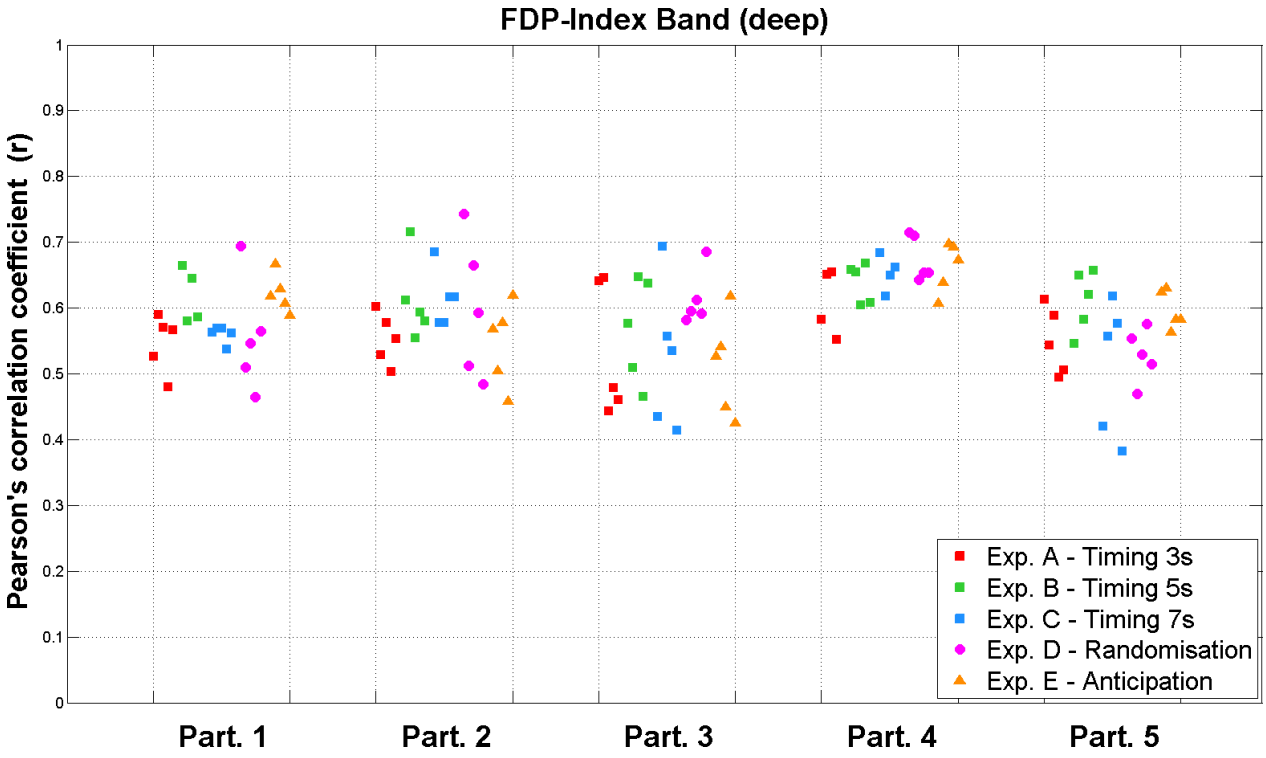

Figure E-3: Scatter plots of the correlation coefficients (*r*) for each experiment grouped by participants for flexor digitorum profundus index band.

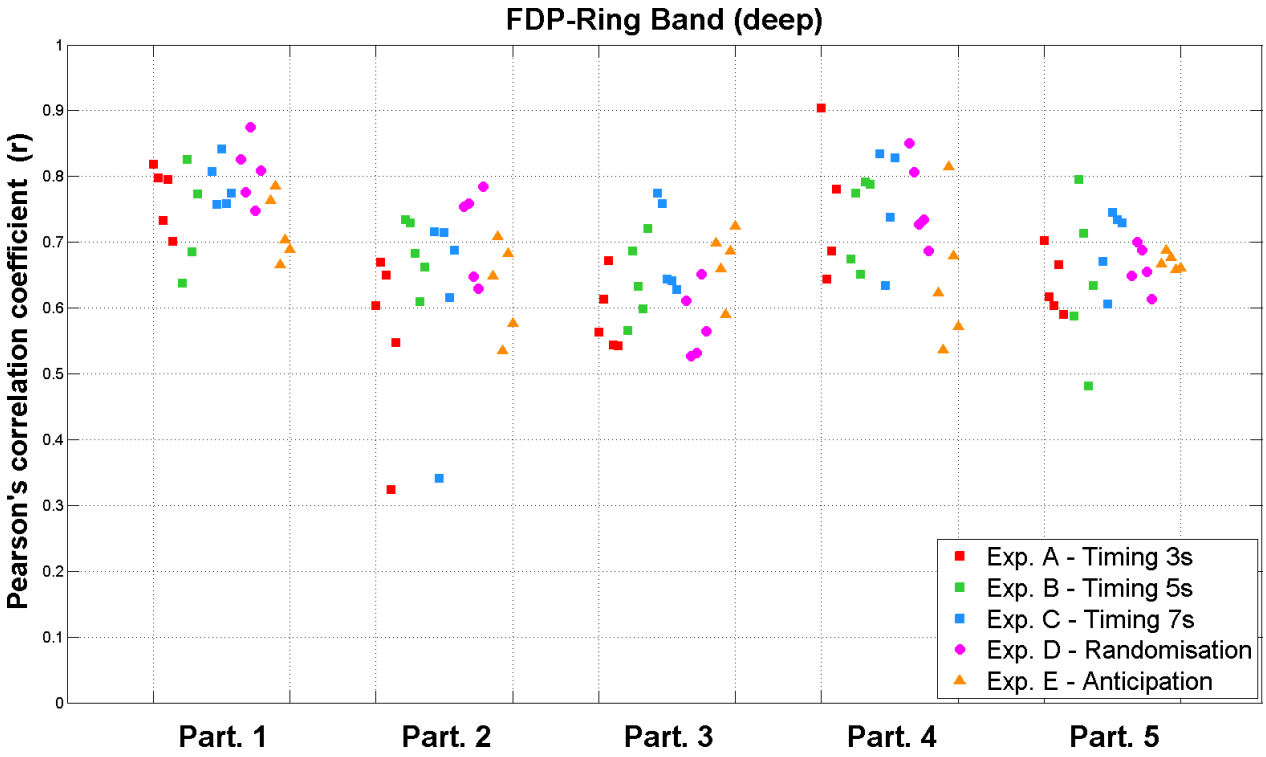

Figure E-4: Scatter plots of the correlation coefficients (*r*) for each experiment grouped by participants for flexor digitorum profundus Ring Group band.

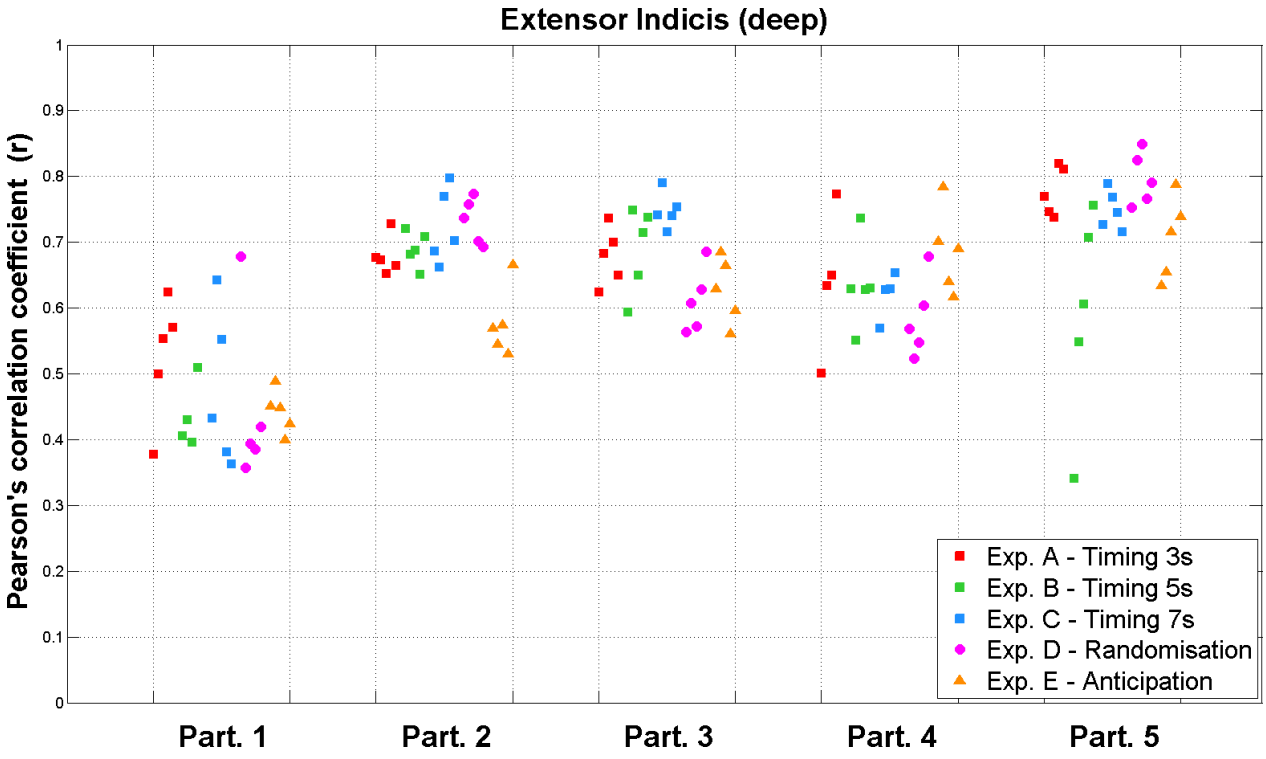

Figure E-5: Scatter plots of the correlation coefficients (*r*) for each experiment grouped by participants for extensor indicis.

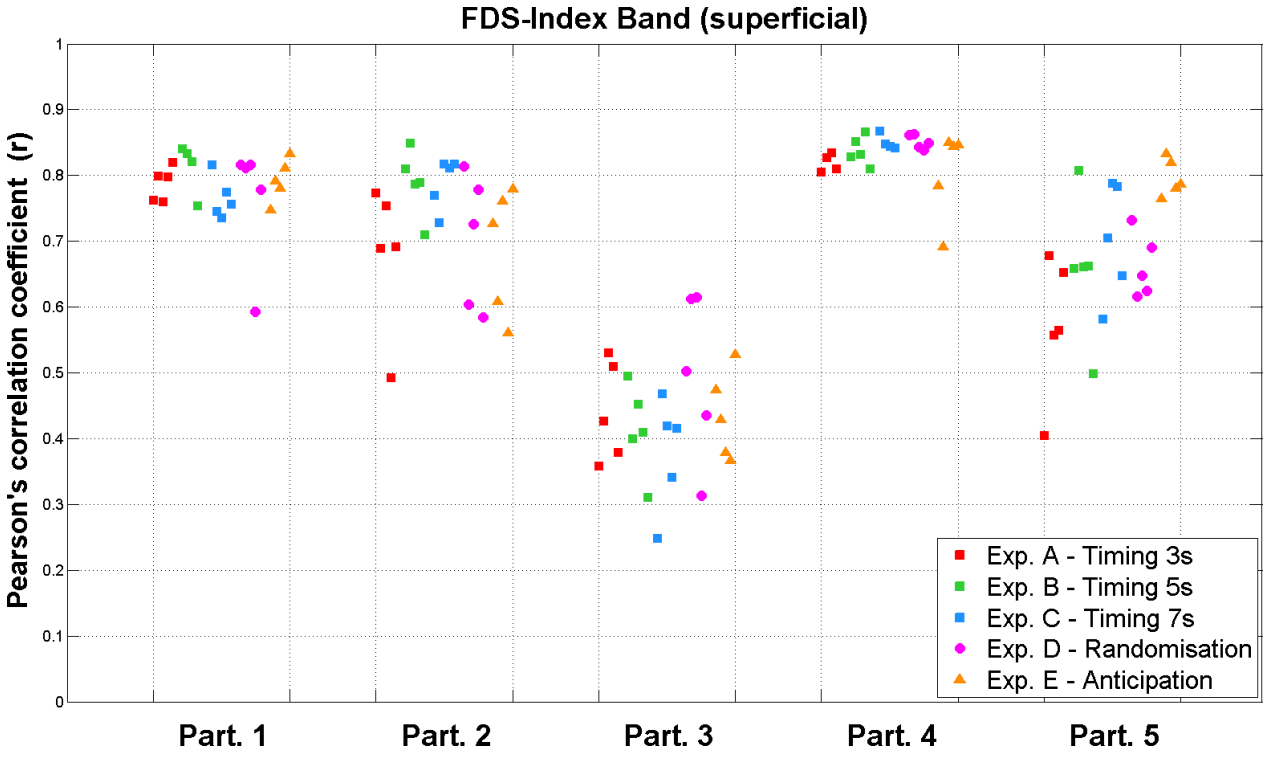

Figure E-6: Scatter plots of the correlation coefficients (*r*) for each experiment grouped by participants for flexor superficialis digitorum index band.

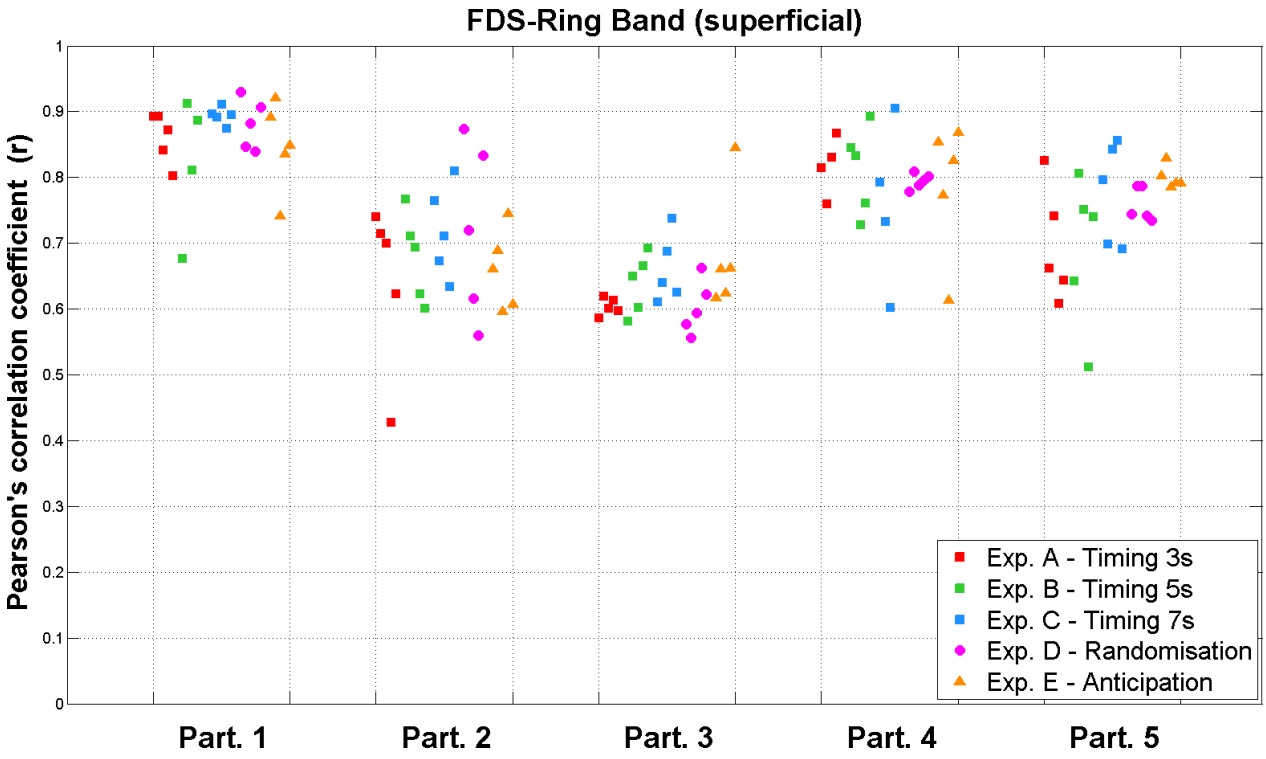

Figure E-7: Scatter plots of the correlation coefficients (*r*) for each experiment grouped by participants for flexor superficialis digitorum Ring Group band.

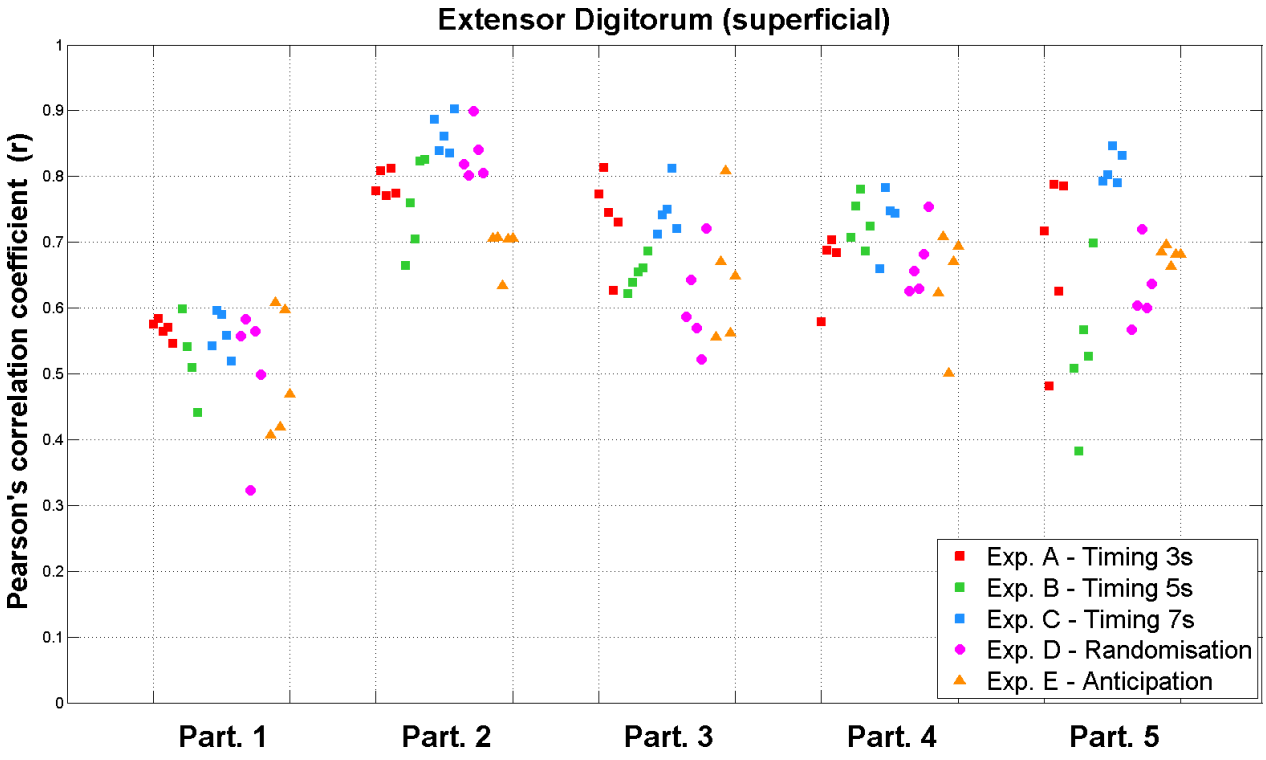

Figure E-8: Scatter plots of the correlation coefficients (*r*) for each experiment grouped by participants for extensor digitorum.

Appendix F: Additional Representative IC Dataset

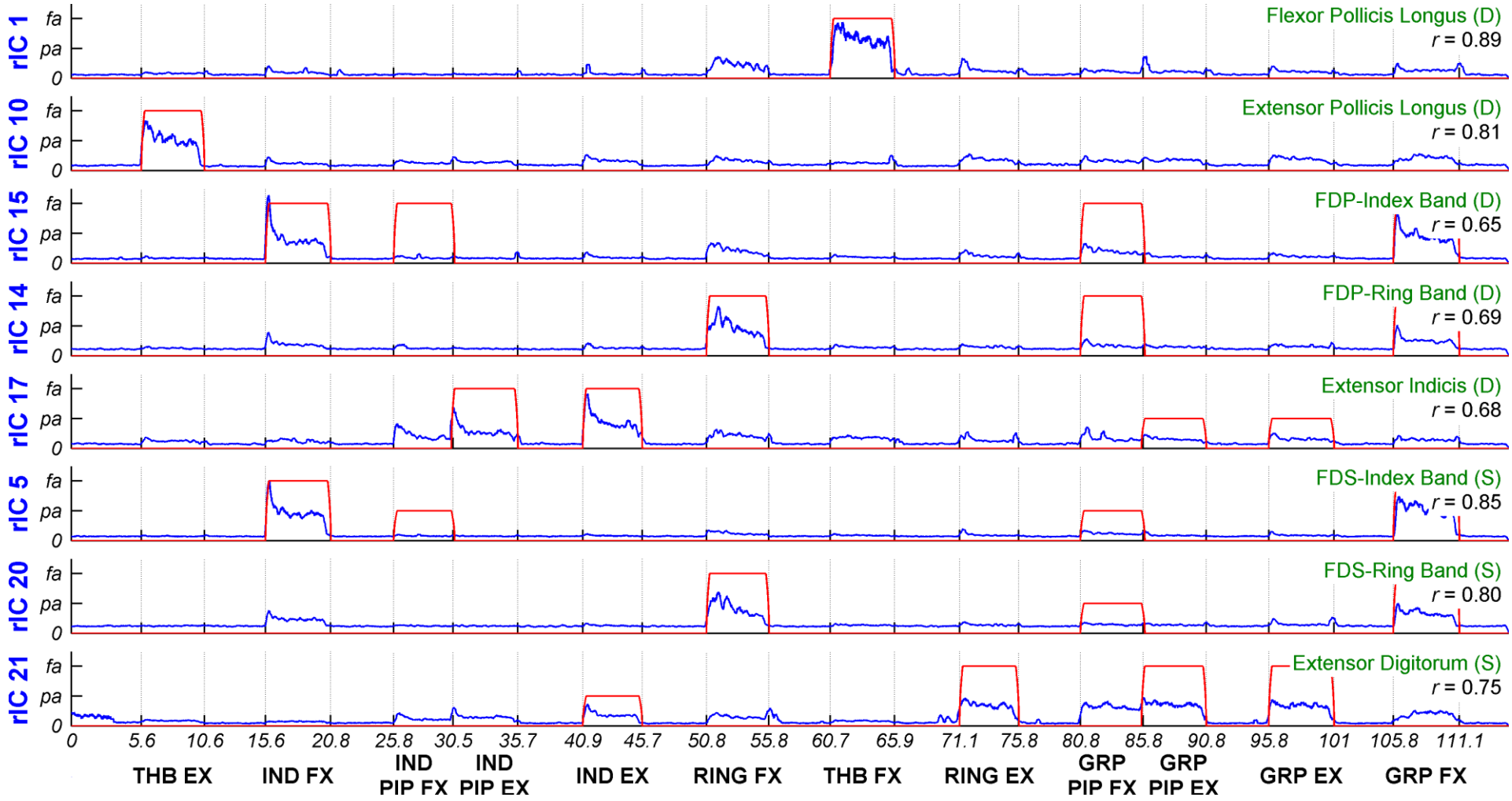

Figure F-1: Representative ICs for Participant 4, randomisation (Exp. D, Run 5) highlighting limited activity during index and Group PIP windows.

D – Deep muscle, S – Superficial muscle, FX – Flexion, EX – Extension, GRP – Group, THB – Thumb, IND – Index, PIP – Proximal interphalangeal (joint). Full activation (fa) was set at 0.8 and Partial activation (pa) was set at 0.4. Rest labels are left out for brevity.